Otrzymywanie celowanych radiofarmaceutyków bazujących na antagonistach receptora NK-1 do diagnostyki i terapii patologii onkologicznych

Rozprawa doktorska

Mgr farm. Paweł Krzysztof Halik

Promotor pracy: dr hab. Ewa Gniazdowska, prof. IChTJ

Instytut Chemii i Techniki Jądrowej

Ko-promotor pracy: prof. dr hab. n. farm. Grażyna Nowicka

Wydział Farmaceutyczny Warszawskiego Uniwersytetu Medycznego

Praca złożona w

Instytucie Chemii i Techniki Jądrowej w Warszawie

Warszawa, 2022

Podziękowania

Dziękuję serdecznie wszystkim, który byli dla mnie wsparciem w ciągu trwania i realizacji mojej pracy doktorskiej, a zatem przyczynili się do pomyślnego ukończenia istotnego etapu mojego życia.

Przede wszystkim szczególne podziękowania kieruję wobec **dr hab. Ewy Gniazdowskiej, prof. IChTJ** za przyjęcie mnie pod swoją opiekę, możliwość zrobienia doktoratu z chemii radiofarmaceutycznej w ramach projektu RadFarm w Instytucie Chemii i Techniki Jądrowej w Warszawie, za ogrom zdobytej wiedzy i doświadczenia oraz za poświęcony czas, którego zawsze brakuje, i za niespotykane zaangażowanie w edukację młodego naukowca i człowieka.

Dziękuję także **dr Przemkowi Koźmińskiemu** za nieocenioną pomoc w pracy laboratoryjnej oraz za naukowe inspiracje i wsparcie w rozwoju kariery naukowej.

Obydwojgu dziękuję również za zaufanie, jakim mnie obdarzyli jako członka zespołu, za wsparcie i opinie w tworzeniu tej pracy, a poza tym wszystkich publikacji, wykładów naukowych i plakatów. Dziękuję również za wsparcie możliwość uczestniczenia w kongresach krajowych i międzynarodowych, a także niesamowicie wartościowych zagranicznych kursach dokształcających.

Kolejno, dziękuję **prof. dr hab. n. farm. Grażynie Nowickiej** za serdeczność i poświęcony czas oraz wszystkie istotne rady i wskazówki w kluczowych kwestiach przygotowania tej pracy.

Dziękuję wszystkim koleżankom, kolegom i pracownikom naukowym grupy badawczej Pracowni Syntezy i Badań Radiofarmaceutyków, głównie **Kasi Masłowskiej, Kindze Żelechowskiej-Matysiak, Kamilowi Wawrowiczowi, dr Rafałowi Walczakowi, dr hab. Agnieszcze Majkowskiej-Pilip, dr hab. Markowi Pruszyńskiemu i prof. dr hab. Aleksandrowi Bilewiczowi,** za Waszą serdeczność, za współpracę w badaniach naukowych, za wspólne rozwiązywanie problemów, za Wasze nieocenione doświadczenie i wartościowe spojrzenie na kwestie naukowe, za Wasze wsparcie, dostępność dla mnie i owocne dyskusje naukowe.

Dziękuję współpracownikom projektu OPUS z Instytutu Medycyny Doświadczalnej i Klinicznej PAN, **Kasi Kosińskiej, dr Joannie Matalinskiej, dr hab. Piotrowi Lipińskiemu oraz prof. dr hab. Aleksandrze Misickiej-Kęsik** za współpracę podczas składania i realizacji projektów NCN, przygotowanie

doniesień naukowych oraz wszystkich zagadnień badawczych, nad którymi mieliśmy okazję współpracować.

Panu **Jackowi Olędzkiemu** z Instytutu Biologii i Biofizyki PAN dziękuję za niesamowitą serdeczność i wsparcie przy analizach MS.

Kluczowe podziękowania z serca dla **mojej żony Patrycji i członków mojej rodziny**, którzy przez lata mnie wspierali, motywowali i wierzyli we mnie oraz dzielnie znosili trud mojego poświęcenia pracy naukowej.

Niniejsza praca doktorska była prowadzona pod kierownictwem dr hab. Ewy Gniazdowskiej, prof. IChTJ w ramach projektu NCBiR Nr POWR.03.02.00-00-I009/17 Radiofarmaceutyki dla ukierunkowanej molekularnie diagnostyki i terapii medycznej (RadFarm) oraz projektu NCN Nr 2017/25/B/NZ7/01896 w Centrum Radiochemii i Chemii Jądrowej, w Pracowni Syntezy i Badań Radiofarmaceutyków, Instytutu Chemii i Techniki Jądrowej w Warszawie. Wyniki badań zgromadzone na poczet tej pracy zostały opublikowane oraz zaprezentowane i nagrodzone na wystawach i konferencjach krajowych i międzynarodowych. Niniejsza praca doktorska została przygotowana bazując na następujących artykułach opublikowanych w recenzowanych zagranicznych czasopismach naukowych:

I. Majkowska-Pilip, A.; **Halik, P.K.;** Gniazdowska, E. The Significance of NK1 Receptor Ligands and Their Application in Targeted Radionuclide Tumour Therapy. *Pharmaceutics* **2019**, *11*, 443. (IF (2019) = 4,421; pkt. MNiSW (2022) = 100)

II. **Halik, P.K.;** Lipiński, P.F.J.; Matalińska, J.; Koźmiński, P.; Misicka, A.; Gniazdowska, E. Radiochemical Synthesis and Evaluation of Novel Radioconjugates of Neurokinin 1 Receptor Antagonist Aprepitant Dedicated for NK1R-Positive Tumors. *Molecules* **2020**, *25*, 3756. (IF (2020) = 4,412; pkt. MNiSW (2022) = 140)

III. Matalińska, J.; Kosińska, K.; **Halik, P.K.;** Koźmiński, P.; Lipiński, P.F.J.; Gniazdowska, E.; Misicka, A. Novel NK1R-Targeted ^{68}Ga-/^{177}Lu-Radioconjugates with Potential Application against Glioblastoma Multiforme: Preliminary Exploration of Structure–Activity Relationships. *Int. J. Mol. Sci.* **2022**, *23*, 1214. (IF (2020) = 5,924; pkt. MNiSW (2022) = 140)

IV. **Halik, P.K.;** Koźmiński, P.; Matalińska, J.; Lipiński, P.F.J.; Misicka, A.; Gniazdowska, E. In Vitro Biological Evaluation of Aprepitant Based ^{177}Lu-Radioconjugates. *Pharmaceutics* **2022**, *14*, 607. (IF (2020) = 6,321; pkt. MNiSW (2022) = 100)

oraz monografii naukowej opublikowanej w recenzowanym wydawnictwie IChTJ:

Halik, P.K.; Gniazdowska, E.; Koźmiński, P.; Majkowska-Pilip, A. ^{68}Ga- and ^{177}Lu-radiopharmaceuticals based on neurokinin-1 receptor antagonist SPANTIDE I (5-11) peptide for glioblastoma multiforme treatment. *INCT Annual Report 2017* **2017**, 25. (pkt. MNiSW (2022) = 80)

Ponadto wybrany fragment tematyki mojej pracy doktorskiej był treścią komunikatu konferencyjnego przedstawionego podczas Międzynarodowego Sympozjum na temat Trendów w Radiofarmaceutykach (*ISTR 2019*, *Vienna*):

> **Halik, P.;** Gniazdowska, E.; Koźmiński, P.; Lipiński, P.; Matalińska, J. In vitro NK1R affinity evaluation of novel radioconjugates based on peptide antagonist SPANTIDE I and Ga-68/Lu-177 theranostic like isotopes for glioma cancer. Podczas *Trends in Radiopharmaceuticals (ISTR-2019*). Materiały z międzynarodowego sympozjum. Program i streszczenia.

Jednocześnie, prace badawcze na temat radiokoniugatów aprepitantu zostały objęte ochroną patentową przez Urząd Patentowy Rzeczypospolitej Polskiej:

> Patent Nr 238401 na wynalazek pt.: Zmodyfikowana cząsteczka substancji leczniczej, sposób jej wytwarzania, diagnostyczny lub terapeutyczny radiofarmaceutyk receptorowy oparty na tej cząsteczce, oraz jego zastosowanie. (od dnia 21-05-2019, uzyskany 23-08-2021).

oraz wyróżnione podczas krajowej i dwóch zagranicznych wystaw naukowych:

I. **Halik, P.K.;** Gniazdowska, E.; Koźmiński, P. Zmodyfikowana cząsteczka substancji leczniczej, sposób jej wytwarzania, diagnostyczny lub terapeutyczny radiofarmaceutyk receptorowy oparty na tej cząsteczce, oraz jego zastosowanie. Nagrodzony złotym medalem podczas IWIS 2020 w Warszawie, Polska.

II. **Halik, P.K.;** Gniazdowska, E.; Koźmiński, P. The modified drug substance molecule, method of its production, diagnostic or therapeutic receptor radiopharmaceutical based on this molecule, method of its production and its application. Nagrodzony złotym medalem podczas 13th EUROINVENT 2021 w Iasi, Rumunia.

III. **Halik, P.K.;** Gniazdowska, E.; Koźmiński, P. The modified drug substance molecule, method of its production, diagnostic or therapeutic receptor radiopharmaceutical based on this molecule, method of its production and its application. Nagrodzony srebrnym medalem podczas iENA 2021 w Norymbergii, Niemcy.

Spis treści

Streszczenie

Celowania terapia radionuklidowa (*targeted radionuclide therapy*, TRT, rozdział 1.1.), zaliczana do technik radioterapii wewnętrznej, jest jedną z najszybciej rozwijających się dziedzin we współczesnej onkologii. W przeciwieństwie do chemioterapii i radioterapii zewnętrznej, TRT jest metodą wysoce selektywną wobec konkretnego celu lub markera molekularnego (głównie receptora, enzymu lub innej struktury białkowej), który jest ściśle specyficzny dla komórek nowotworowych lub określonego procesu patologicznego. Celowana terapia radionuklidowa bazuje na zastosowaniu radiofarmaceutyków, to jest znakowanych promieniotwórczo cząsteczek zdolnych do wiązania się z wysokim powinowactwem jedynie do preferencyjnych (swoistych) celów molekularnych. Tym samym, zaprojektowanie i uzyskanie radiofarmaceutyku zdolnego do osiągnięcia zamierzonego celu wydaje się być istotą powodzenia celowanej terapii radionuklidowej (rozdział 1.3.).

Obiecującym potencjałem użyteczności w przeciwnowotworowej strategii terapeutycznej cechuje się dobrze znany receptor neurokininy 1 (receptor NK1, NK1R, rozdział 2.1.)[1]. Jest to receptor o ograniczonej abundancji w organizmie ludzkim, występujący głównie w ośrodkowym i obwodowym układzie nerwowym, swoisty dla endogennego neuropeptydu Substancja P (SP) o działaniu mitotycznym (rozdział 2.1.1.). Do tej pory opracowano już pierwsze wysoce selektywne ligandy receptora NK1 o znaczeniu klinicznym (rozdział 2.2.), w tym także pierwszy radiofarmaceutyk stosowany w eksperymentalnej TRT NK1R-pozytywnego glejaka wielopostaciowego (rozdział 2.1.3.)[1], niemniej wciąż istnieje potrzeba poszukiwania nowych wysoce efektywnych radiofarmaceutyków do celów onkologicznych.

W prezentowanej rozprawie przedstawiłem sposób w jaki otrzymałem potencjalne radiofarmaceutyki dedykowane do celowanej diagnostyki i terapii patologii NK1R-dodatnich (rozdział III)[2-5]. Podczas realizacji tego celu skupiłem swoją uwagę na dwóch grupach antagonistów NK1R, peptydowych antagonistach receptora cechujących się pełną stabilnością *in vivo*, mianowicie SPANTIDE I oraz SPANTIDE I (5-11), oraz wysoce specyficznych i wysoce selektywnych antagonistach niepeptydowych, mianowicie L732,138 i aprepitancie. W przypadku aprepitantu, zaproponowałem dwie metody modyfikacji cząsteczki otrzymując dwie serie pochodnych aprepitantu [3]. Seria pochodnych L732,138 zsyntezowana została w ramach wspólnego projektu w Zakładzie Neuropeptydów Instytutu Medycyny

Doświadczalnej i Klinicznej PAN [4]. Dwa peptydomimetyki SPANTIDE I zakupiłem w formie nieacetylowanej na *N*-końcu. Wszystkie związki poddałem funkcjonalizacji umożliwiającej znakowanie promieniotwórcze powszechnie dostępnymi radionuklidami pary teranostycznej, ^{68}Ga i ^{177}Lu, w sposób pozwalający na zachowanie celowalności do NK1R [2-5].

W kolejnym kroku otrzymałem pary ^{68}Ga-/^{177}Lu-radiokoniugatów dwóch peptydomimetyków SPANTIDE I, jednej serii pochodnych L732,138 oraz obydwu serii pochodnych aprepitantu, dla których wykonałem badania właściwości fizykochemicznych pod kątem użyteczności otrzymanych radiokoniugatów do celów TRT.

Następnie wykonałem badania charakterystyki wiązania (powinowactwa receptorowego i pojemności wiązania radiokoniugatu do celu molekularnego) wszystkich otrzymanych ^{177}Lu-radiokoniugatów pochodnych L732,138 i aprepitantu na komórkowym modelu NK1R-pozytywnym [4,5]. Dla ^{177}Lu-radiokoniugatów opartych na peptydomimetykach SPANTIDE I nie udało mi się zaobserwować bezpośredniego wiązania radiokoniugatów do żadnej z analizowanych linii komórkowych. Dodatkowo przeprowadziłem te same badania *in vitro* dla ^{177}Lu-radiokoniugatu opartego na pochodnej SP obecnie stosowanej w medycynie nuklearnej, w celu oceny konkurencyjności otrzymanych przeze mnie radiokoniugatów.

Podsumowując, w tej rozprawie zademonstrowałem sposoby otrzymywania oraz możliwości nowych radiokoniugatów o wysokiej specyficzności wobec linii komórkowych z nadekspresją NK1R oraz ich przewagę we właściwościach wiązania receptorowego nad radiofarmaceutykiem pochodnej SP. Wyniki przeprowadzonych przeze mnie badań są pierwszym porównaniem dwóch grup antagonistów NK1R ze wskazaniem kierunku dla dalszych badań w radiofarmacji oraz precyzują nową użyteczność aprepitantu do poszukiwania nowych terapii onkologicznych niepeptydowymi antagonistami receptora NK1.

Spis skrótów

2-PMPA	kwas 2-(fosfonometylo)pentadiowy
6E59	kod struktury krystalicznej ludzkiego receptora NK1 w bazie *Protein Data Bank*
α	cząstka lub rozpad alfa
AC	cyklaza adenylowa
ADME	*administration, distribution, metabolism, excretion* - podanie, dystrybucja, metabolizm, wydalanie
A_m	*molar activity* - radioaktywność molowa
Arg	arginina
A_s	*specific activity* - radioaktywność właściwa
β^-	elektron lub rozpad beta minus
β^+	pozyton lub rozpad beta plus
$^{biol.}T_{1/2}$	biologiczny czas połowicznego zaniku
B_{MAX}	parametr wiązania maksymalnego
Bn	grupa benzylowa
Bq (GBq, MBq)	*bequerel* - bekerel (gigabekerel, megabekerel)
CA153	antygen nowotworowy 153
cAMP	cykliczny adenozyno-monofosforan
CD20	antygen błonowy limfocytów B
CHO	linia komórkowa jajnika chomika chińskiego
CT	*computed tomography* - tomografia komputerowa
CYP3A4	izoenzym 3A4 cytochromu P450
DAG	diacyloglicerol
DFO	*deferoxamine* - deferoksamina
DNA	kwas deoksyrybonukleinowy
DOTA	*1,4,7,10-tetraazacyclododecane-1,4,7,10-tetraacetic acid*
DOTAGA	*1,4,7,10-tetraazacyclododecane4,7,10-triacetic acid-1-[2-glutaric acid]*
DTPA	kwas dietyleno-triamino-pentaoctowy
EC	*electron capture* - wychwyt elektronu
EDDA	*ethylenediamine-N,N'-diacetic acid*
$^{efekt.}T_{1/2}$	efektywny czas połowiczny
eV (keV, MeV)	elektronowolt (kiloelektronowolt, megaelektronowolt)
FAPI-04	wektor radiofarmaceutyku [^{68}Ga]Ga-FAPI-04
[^{18}F]FDG	2-deoksy-2-[^{18}F]fluoro-*D*-glukoza
$^{fiz.}T_{1/2}$	fizyczny czas połowicznego rozpadu
Gln	glutamina
Glu	kwas glutaminowy
Gly	glicyna
GPCR	*G-protein coupled receptor* - receptor związany z białkiem G
Gy	*gray* - grej, jednostka dawki pochłoniętej
IC_{100}	stężenie wywołujące całkowitą inhibicje
IC_{50}	stężenie wywołujące połowiczną inhibicje
IP_3	trifosforan inozytolu

IT	*isomeric transition* - przejście izomeryczne
K_i	*inhibition constant* - stała inhibicji
LET	*linear energy transfer* - liniowy transfer energii
Leu	leucyna
logD ($logP_{7.4}$)	logarytm dziesiętny współczynnika dystrybucji (podziału w pH = 7,4) związku pomiędzy fazy *n*-oktanolu i PBS
Lys	lizyna
Met	metionina
Met(O_2)	sulfon metioniny
MLC	*myosin light chains* - lekkie łańcuchy miozyny
MRI	*magnetic resonance imaging* - tomografia rezonansu magnetycznego
NF-κB	jądrowy czynnik *kappa* aktywowanych komórek B
NHS	*N*-hydroksysukcynoimid
NK1R	receptor neurokininy 1, receptor NK1
NK1R-Fl	izoforma pełnej długości receptora neurokininy 1
NK1R-Tr	izoforma skróconej długości receptora neurokininy 1
P450	nazwa monooksygenaz absorbujących światło przy długości fali 450 nm
PAN	Polska Akademia Nauk
PBS	*phosphate buffered saline* - sól fizjologiczna buforowana fosforanami
PET	*positron emission tomography* - tomografia pozytonowa
pH	ujemny logarytm ze stężenia jonów wodorowych
Phe	fenyloalanina
PKA	kinaza białkowa A
PKC	kinaza białkowa C
PLA_2	fosfolipaza A_2
PLC	fosfolipaza C
Pro	prolina
PSA	*prostate specific antigen* - swoisty antygen sterczowy
PSMA	*prostate specific membrane antigen* – swoisty, błonowy antygen sterczowy
RCY	*radiochemical yield* - wydajność radiochemiczna
ROCK	Rho-zależna kinaza białkowa
SCN	grupa izotiocyjanowa
SNNMI	*Society of Nuclear Medicine and Molecular Imaging* - Towarzystwa Medycyny Nuklearnej i Obrazowania Molekularnego
SP	Substancja P
SPECT	*single-photon emission computed tomography* - tomografia pojedynczego fotonu
SSTR2	receptor somatostatyny 2
TACR1	gen ludzkiego receptora NK1
Thi	tienyloalanina
TRT	*targeted radionuclide therapy* - celowana terapia radionuklidowa
TXA_2	tromboksan A_2
urea	mocznik
US FDA	*United States Food and Drug Administration* - Amerykańska Agencja Żywności i Leków

I. HIPOTEZY I CELE BADAWCZE PRACY

Nadrzędnym celem opublikowanych poniżej badań zebranych w niniejszej pracy było otrzymanie stabilnych (w symulowanych warunkach *in vivo*) radiofarmaceutyków o wysokim powinowactwie do receptora NK1, dedykowanych do diagnostyki i terapii patologii onkologicznych cechujących się nadekspresją receptora NK1, radiofarmaceutyków opartych na dobrze znanych antagonistach tego receptora.

Sygnalizacja komórkowa poszczególnych receptorów metabotropowych (w tym receptora NK1) bywa wykorzystywana do propagacji rozwoju zmian nowotworowych. Równolegle, w patologiach onkologicznych znaczącej eskalacji ulega ilość danego receptora określanego mianem markera molekularnego. Zastosowanie wybiórczych antagonistów tych receptorów umożliwia skuteczne celowanie w miejsce nadmiernej ekspresji markera oraz selektywną funkcjonalność, taką jak zahamowanie progresji nowotworowej. Niemniej zahamowanie wzrostu zmiany nowotworowej z reguły przynosi jedynie czasowy rezultat oraz niezadowalający efekt kliniczny. Proponowanym rozwiązaniem jest zastosowanie wysoce cytotoksycznych radiofarmaceutyków receptorowych bazujących na selektywnych antagonistach receptorów nadmiernie eksprymowanych na powierzchni komórek nowotworowych.

Powyższy paradygmat posłużył do postawienia hipotezy, że możliwe jest zastosowanie selektywnych antagonistów receptora NK1 jako wektora radiofarmaceutyku receptorowego do celowania wybraną funkcjonalnością (diagnostyczną lub terapeutyczną) w NK1R-pozytywne zmiany nowotworowe. Cel nadrzędny pracy został określony w celu weryfikacji postawionej hipotezy.

Po otrzymaniu potencjalnych radiofarmaceutyków receptorowych, kolejnym etapem było wykazanie na komórkowych modelach *in vitro* konkurencyjności otrzymanych przeze mnie radiokoniugatów wobec radiofarmaceutyku opartego na pochodnej Substancji P (SP), obecnie stosowanej w eksperymentalnej terapii glejaka wielopostaciowego. Wyniki prowadzonych przeze mnie badań okazały się istotnym wskazaniem dla dalszych poszukiwań nowych rozwiązań w radiofarmacji i onkologii klinicznej. Przede wszystkim zademonstrowałem możliwości konstruowania i zastosowania nowych radiokoniugatów o wysokiej specyficzności wobec linii komórkowych z nadekspresją NK1R oraz jednocześnie wskazałem nową użyteczność aprepitantu i kierunek rozwoju terapii antagonistami NK1R.

II. CZĘŚĆ TEORETYCZNA

1. Medycyna nuklearna i radiofarmacja

Medycyna nuklearna to specjalność medyczna wykorzystująca substancje promieniotwórcze do oceny funkcjonowania organizmu, diagnostyki obrazowej oraz leczenia patologii o wystarczająco poznanej etiologii molekularnej. W procedurach medycyny nuklearnej stosowane są radioaktywne znaczniki zwane radiofarmaceutykami, to jest związki chemiczne posiadające w swojej strukturze izotopy promieniotwórcze (radionuklidy). Idea stosowania radiofarmaceutyków zakłada, że stosowany u pacjenta znacznik radioaktywny umożliwi selektywną wizualizację danych funkcji komórkowych albo procesu (pato)fizjologicznego na poziomie molekularnym lub wywoła miejscowy efekt cytotoksyczny [6]. Określenie lokalizacji i gromadzenia się podanego radiofarmaceutyku w organizmie pacjenta możliwe jest dzięki rozpadom promieniotwórczym określonych radionuklidów, skutkującym emisją wysoce przenikliwego (poza ciało pacjenta) promieniowania jonizującego. To promieniowanie rejestrowane przez czułe detektory tomografów obrazowych (zlokalizowanych wokół ciała pacjenta) umożliwia wizualizację w czasie rzeczywistym rozkładu przestrzennego sygnałów emisji promieniowania jednoznacznie wynikających z obecności radiofarmaceutyku. Tym samym, medycyna nuklearna nazywana jest radiologią wewnętrzną, gdyż źródło promieniowania jonizującego wykorzystywane do diagnostyki lub terapii znajduje się wewnątrz ciała pacjenta, nie zaś na zewnątrz jego ciała, jak ma to miejsce w klasycznej radiologii zewnętrznej [7].

Przeważająca większość zastosowań radiofarmaceutyków skierowana jest ku diagnostyce i ocenie parametrów metabolicznych, zaś w niewielkim stopniu celom terapeutycznym. Radiofarmaceutyki jako narzędzia diagnostyczne *a posteriori* nie wywołują działania farmakologicznego [8], gdyż stosowane są w ilościach submikromolarnych, oddziałując na procesy biochemiczne w organizmie na poziomie cząsteczkowym. Dzięki identyfikacji dysfunkcji komórkowych (lokalnych lub obecnych w całym organizmie) możliwe staje się bardzo dokładne (miejscowe) i wczesne wykrycie tworzących się jednostek chorobowych i patologii tkankowych *de facto* przed pojawieniem się zewnętrznych objawów fizycznych danego schorzenia [9]. Jednocześnie medycyna nuklearna dostarcza celowanych rozwiązań dla znacznej części patologii molekularnych (głównie w onkologii) w postaci radiofarmaceutyków terapeutycznych [10]. Kluczowym aspektem terapii (jak również diagnostyki) przy użyciu preparatów radiofarmaceutycznych jest niewątpliwie zapewnienie bezpieczeństwa podczas ich stosowania.

Produkty lecznicze stosowane u ludzi podlegają ścisłym środkom kontroli jakości [11], a w przypadku radiofarmaceutyków warunki kontrolne dotyczą aspektów farmaceutycznych oraz aspektów jądrowych.

Radiofarmacja (farmacja jądrowa) to dział farmacji, który zajmuje się przygotowaniem, charakterystyką i ewaluacją jakości materiałów promieniotwórczych do stosowania w procedurach medycyny nuklearnej. Poza bezpośrednim zainteresowaniem radiofarmaceutykami, obszar zagadnień radiofarmacji obejmuje także kontrolę i licencjonowanie obiektów, procedur produkcji, użytkowania i przechowywania radiofarmaceutyków, oraz także kwestie transportu i ochrony radiologicznej, czyli szeroko pojętego bezpieczeństwa podczas kontaktu z materiałem promieniotwórczym [12]. Jednocześnie pociąga to za sobą potrzebę szerokiej znajomości prawa, zarówno w obszarze przepisów dotyczących preparatów farmaceutycznych (Ustawa „Prawo Farmaceutyczne" i inne), czy przepisów dotyczącymi materiałów radioaktywnych (Ustawa „Prawo Atomowe" i inne) na poziomie krajowym oraz międzynarodowym.

Radiofarmaceutyki to unikalne preparaty medyczne zawierające radionuklidy, które wykorzystywane są w głównych obszarach klinicznych do diagnostyki i/lub terapii. Europejska Farmakopea poświęca radiofarmaceutykom osobną monografię (*Radiopharmaceutical preparations, General Monograph 0125* [13]), gdzie definiuje: *„Preparat radiofarmaceutyczny lub radiofarmaceutyk jest produktem leczniczym, który gotowy do użycia zawiera jeden lub więcej radionuklidów (izotopów promieniotwórczych) do celów medycznych."* Dalej monografia podkreśla, że powyższa definicja produktów leczniczych obejmuje także:

- Generatory radionuklidowe: każdy układ zawierający utrwalony (unieruchomiony) radionuklid macierzysty (o długim okresie połowicznego rozpadu), z którego wytwarzany jest radionuklid potomny (o krótkim okresie połowicznego rozpadu), otrzymywany poprzez elucję lub jakąkolwiek inną metodą i stosowany do produkcji preparatu radiofarmaceutycznego;
- Gotowe zestawy do sporządzenia preparatu radiofarmaceutycznego (tzw. kity): każdy preparat (najczęściej w postaci liofilizatu), który ma zostać odtworzony lub połączony z radionuklidem w końcowym preparacie radiofarmaceutycznym przed jego podaniem;
- Prekursory radionuklidowe: każdy radionuklid wyprodukowany do znakowania promieniotwórczego innej substancji przed jej podaniem.

W każdym z powyższych przypadków, celem jest otrzymanie preparatu radiofarmaceutycznego gotowego do użytku klinicznego.

Radiofarmaceutyk jako substancja chemiczna (cząsteczka, związek kompleksowy czy nanocząstka) posiada w swojej strukturze dwie składowe, część radioaktywną i część biologiczno-chemiczną. Wyjątkiem są najprostsze postacie jonów lub cząsteczek chemicznych takich jak, przykładowo, anion jodkowy $[^{131}I]I^-$, anion kwasu technetowego (VII) $[^{99m}Tc]TcO_4^-$, atom ksenonu ^{133}Xe, czy cząsteczka wody $[^{15}O]H_2O$, w których trudno o podział na części składowe.

Integralną częścią radiofarmaceutyku jest izotop promieniotwórczy, który definiuje użyteczność oraz możliwości zastosowania preparatu [14,15]. Wybór radionuklidu *de facto* jest wyborem pożądanej charakterystyki rozpadu promieniotwórczego, a dokładniej czasu połowicznego rozpadu oraz typu promieniowania emitowanego podczas rozpadu. Do zastosowań diagnostycznych dedykowane są stosunkowo krótkożyciowe izotopy (o stosunkowo krótkim okresie połowicznego rozpadu rzędu od kilku minut do kilku godzin) emitujące wysoce przenikliwe promieniowanie gamma czy beta o niskim współczynniku liniowego transport energii (*linear energy transfer*, LET, rozdział 1.3.2.). Do celów terapeutycznych najskuteczniejsze są radionuklidy o stosunkowo dłuższym okresie połowicznego rozpadu (od kilku godzin do kilku dni) oraz emitujące wysokoenergetyczne (wysoce jonizujące) cząstki alfa lub elektrony Auger o krótkim zasięgu transferu energii [16]. Dodatkowo radionuklidy tego samego pierwiastka, które ulegają rozpadowi promieniotwórczemu poprzez różne ścieżki rozpadu, mogą być rozpatrywane jako izotopy teranostyczne, to jest radionuklidy tego samego pierwiastka użyteczne jednocześnie do terapii i obrazowania jej przebiegu oraz skuteczności (przykładowo radionuklidy skandu $^{43}Sc/^{47}Sc$, miedzi $^{64}Cu/^{67}Cu$, jodu $^{124}I/^{131}I$, czy terbu $^{149}Tb/^{152}Tb/^{161}Tb$)[17].

Drugą częścią radiofarmaceutyku jest część biologiczno-chemiczna zwana również częścią wektorową [14,15]. Odpowiada ona przede wszystkim za specyficzność (celowalność) radiofarmaceutyku, to jest jego zdolność do oddziaływania ze swoistym celem molekularnym. Poza tym, część wektorowa definiuje także szeroko pojęty charakter farmakologiczny radiofarmaceutyku, w tym stabilność *in vivo* oraz każdy z farmakokinetycznych aspektów systemu ADME (*administration, distribution, metabolism, excretion* – podanie, dystrybucja, metabolizm, wydalanie). Projektowanie części biologiczno-chemicznej jest etapem dopasowywania działania radiofarmaceutyku do wybranego procesu biochemicznego lub celu molekularnego. Jest to złożony proces empiryczny wymagający podejścia multidyscyplinarnego.

W zależności od wyboru sposobu przyłączenia izotopu do pozostałej części radiofarmaceutyku (metody znakowania promieniotwórczego) dostosować należy budowę jego wektorowej części. Najprostszy podział metod znakowania rozróżnia sposoby znakowania bezpośredniego, to jest przyłączenia radionuklidu bezpośrednio do cząsteczki prekursora radiofarmaceutyku (za sprawą reakcji kompleksowania, reakcji wymiany izotopowej, lub „wbudowania" radionuklidu do pierwotnej struktury wektora radiofarmaceutyku), lub znakowania pośredniego, obejmujące wszystkie sposoby pośredniego przyłączenia radionuklidu do pierwotnej struktury wektora radiofarmaceutyku (Obraz 1.)[18]. Wybór metody znakowania w głównej mierze zależy od stosowanego radionuklidu, aczkolwiek znane są przypadki, gdy wybrany radionuklid może być przyłączony do prekursorów radiofarmaceutycznych zarówno przy pomocy metod znakowania pośredniego jak i bezpośredniego. Tym samym do składowych części wektorowej radiofarmaceutyku należą:

- wektor właściwy, to jest cząsteczka lub jej fragment o wysokim i selektywnym powinowactwie wobec pożądanego procesu biochemicznego lub celu molekularnego. Funkcję wektora może pełnić dowolna substancja o aktywności biologicznej (rozdział 1.3.1.). Niekiedy w jednym radiofarmaceutyku stosowana jest większa ilość cząsteczek wektora lub kilka różnych wektorów jednocześnie [19,20];
- łącznik (*linker*), czyli fragment cząsteczki umożliwiający kowalencyjne przyłączenie radionuklidu lub chelatora z radionuklidem do pierwotnej struktury wektora, oraz wektorów między sobą lub wektora z nośnikiem radiofarmaceutyku (przykładowo glikole polietylenowe, ω-aminokwasy, terminalne diaminy);
- chelator radionuklidu będący makrocząsteczkowym ugrupowaniem kompleksującym radionuklid (przykładowo cykliczny chelator DOTA lub acykliczny chelator DTPA);
- nośnik radiofarmaceutyku (jeśli występuje), to jest indywiduum chemiczne spełniające funkcję nośną substancji (przykładowo nanocząstki, micele, polisacharydy).

Osobną grupą radiofarmaceutyków są te bazujące na zastosowaniu nośników w ich budowie. Najpowszechniejszymi przykładami tego typu radiofarmaceutyków są znakowane promieniotwórczo nanocząstki (metaliczne, lipidowe lub węglowe [21]), które radionuklid posiadają osadzony na swojej powierzchni lub wewnątrz rdzenia, oraz endogenne komórki krwi (pochodzące od pacjenta) we wnętrzu

których kompleksowany jest radionuklid (przykładowo leukocyty znakowane ^{18}F, ^{99m}Tc, ^{111}In, [22] lub erytrocyty znakowane różnymi radionuklidami [23]).

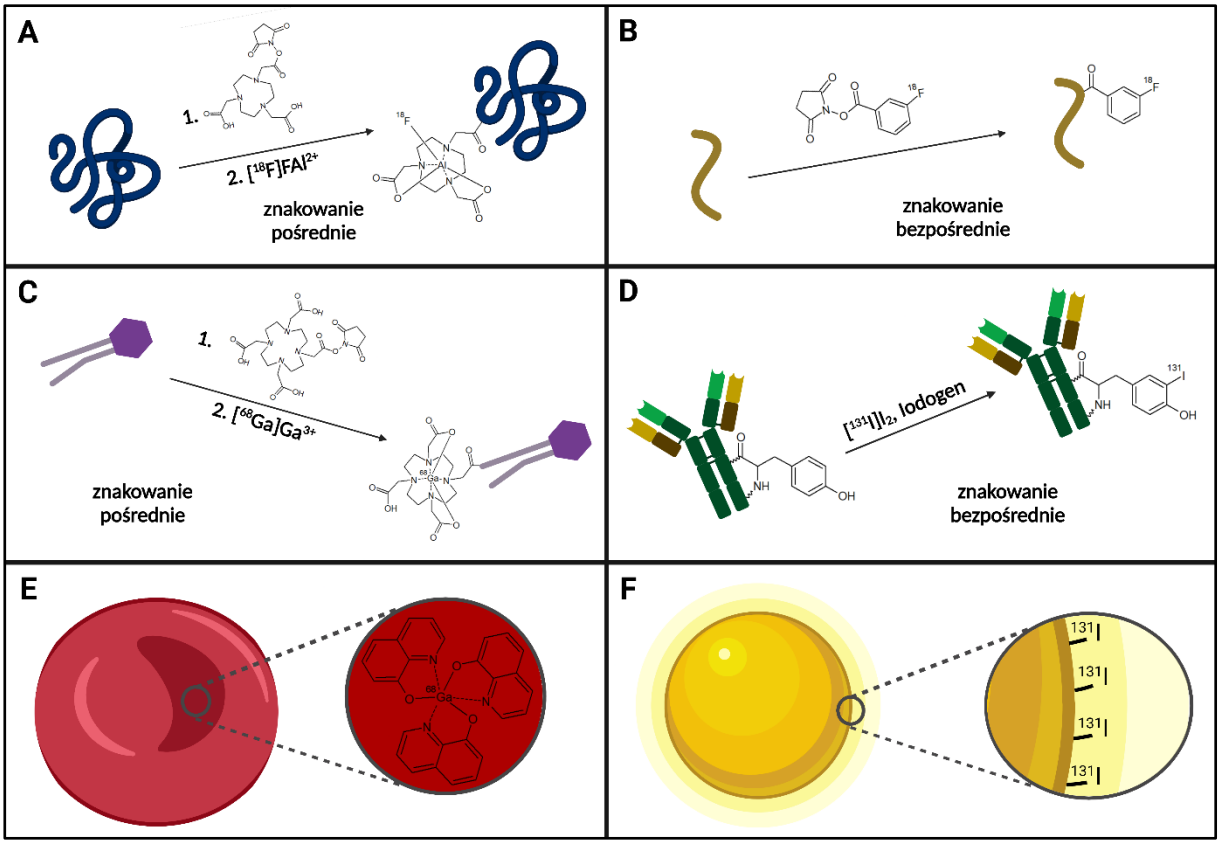

Obraz 1. Schematyczne przedstawienie przykładowych metod pośredniego i bezpośredniego znakowania wektorów o aktywności biologicznej, komórek oraz nanocząstek. Znakowania pośrednie przy użyciu chelatorów makrocyklicznych radionuklidami ^{18}F (**A**) oraz ^{68}Ga (**C**); znakowania bezpośrednie przy użyciu grupy prostetycznej zawierającej radionuklid ^{131}I (**B**) lub bezpośredniej substytucja radionuklidu ^{131}I do specyficznych aminokwasów (**D**), wychwytu ^{68}Ga-kompleksów przez erytrocyt (**E**) oraz adsorpcja jonów radionuklidu ^{131}I na powierzchni nanocząstek złota (**F**).

Zasadniczo, preparat radiofarmaceutyczny musi mieć także określoną postać leku. *Gros* preparatów radiofarmaceutycznych przygotowywanych jest w najprostszej postaci jako roztwór wodny do iniekcji w podaniu dożylnym lub miejscowym. Sporadyczne przypadki innych postaci obejmują kapsułki (przykładowo kapsułki z [^{131}I]NaI [24]), miksturę radiofarmaceutyku z jedzeniem (przykładowo ugotowane kurze jajko z koloidalną siarką znakowaną ^{99m}Tc [25]), zawiesiny do iniekcji (przykładowo szklane mikrosfery Therasphere z wbudowanym ^{90}Y lub ludzkie makroalbuminy znakowane ^{99m}Tc [26]), gazy i aerosole (przykładowo aerosole kompleksów ^{99m}Tc [27] oraz gazowy ^{133}Xe [28]). Wymienione formy aplikacyjne leku cechuje (niemal) maksymalna biodostępność substancji czynnych lub miejscowe działanie danej formy leku, wymagane ze względów bezpieczeństwa terapii przy stosowaniu substancji promieniotwórczych.

1.1. Celowana terapia radionuklidowa

Nieustanny rozwój badań naukowych prowadzący do poznania molekularnych podstaw rozwoju i przebiegu różnych procesów patologicznych, skutkujących pojawianiem się określonych chorób, stymuluje postęp naukowy w kierunku konstruowania bardziej celowanych metod terapeutycznych. [29]. Jednocześnie, za tym postępem podąża rozwój technologiczny i zrozumienie znaczenia zastosowań radioizotopów w naukach medycznych. Nieustannie rosnąca dostępność wybranych radionuklidów o pożądanych charakterystykach rozpadu (mianowicie rodzaju emitowanego promieniowania, LET, czasu połowicznego rozpadu) pozwoliła jeszcze przychylniej spoglądać na oferowane możliwości nowoczesnych, celowanych terapii radionuklidowych (*targeted radionuclide therapy*, TRT)[14,30-32]. Skutkiem tego na przestrzeni ostatnich dekad można zaobserwować rosnące zastosowanie kliniczne radiofarmaceutyków zarówno diagnostycznych (Obraz 2.)[33] jak i terapeutycznych, których największą grupą beneficjentów stanowią pacjenci onkologiczni. Dane kliniczne pokazują, że TRT stanowi jedynie niewielki procent całkowitej liczby przeprowadzanych terapii onkologicznych [30], mimo że aż około połowa wszystkich pacjentów onkologicznych kierowana jest do leczenia przy użyciu promieniowania jonizującego (metodami radiologii zewnętrznej lub brachyterapii), i najczęściej ma to miejsce w skojarzeniu z leczeniem operacyjnym i/lub chemioterapią [34].

TRT to unikalny koncept medyczny bazujący na zastosowaniu radiofarmaceutyków terapeutycznych, które zostały zaprojektowane w sposób umożliwiający im samoistnie celowanie do (i akumulację wewnątrz) wybranej zmiany nowotworowej, dzięki wysokiemu powinowactwu wobec specyficznych szlaków biochemicznych lub markerów molekularnych (takich jak receptory, enzymy lub antygeny) towarzyszących danej patologii. Umożliwia to dostarczanie źródeł promieniowania jonizującego w kontrolowany i ukierunkowany sposób wywołując silną cytotoksyczność selektywnie wobec komórek nowotworowych bez nadmiernego uszkadzania zdrowych tkanek. To wysoce ukierunkowane działanie sprawia, że TRT cechuje się wysokim indeksem terapeutycznym, umożliwiając wysoką skuteczność przy minimalnej liczbie skutków ubocznych [32]. Tym samym, szczególnie widoczny staje się kontrast możliwości terapii celowanych wobec zabiegów stosowanych w metodach konwencjonalnej terapii onkologicznej. Interwencja terapeutyczna TRT skierowana jest wybiórczo na określone grupy komórek (Obraz 2.), dzięki czemu, co istotne, umożliwia leczenie zarówno litych guzów już zlokalizowanych jak i licznych, drobnych zamian przerzutowych

niewidocznych w badaniach morfologicznych [33,35]. Niemałą zaletą TRT jest również stosunkowo duży komfort pacjenta podczas podawania radiofarmaceutyku poprzez prostą iniekcję (dożylnie lub domiejscowo) lub podanie doustne.

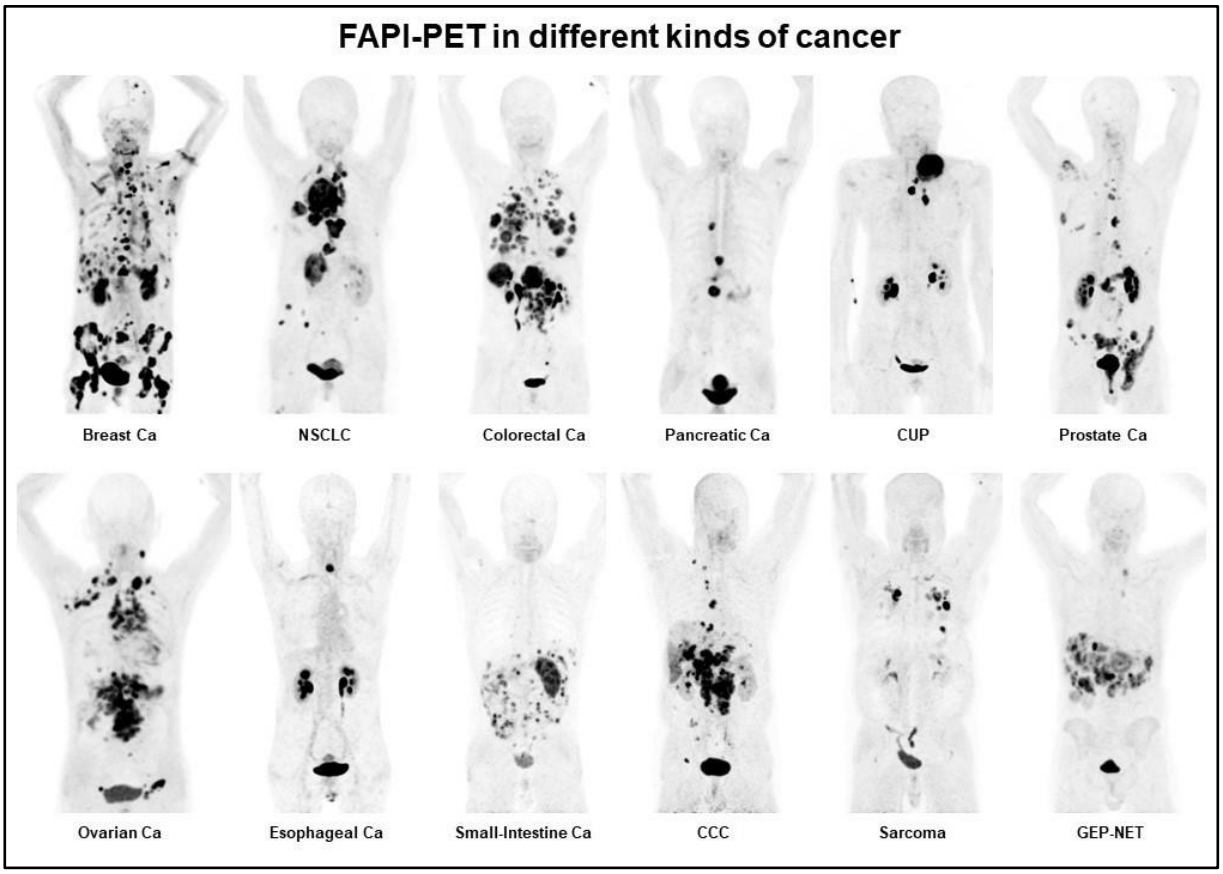

Obraz 2. Obraz roku 2019 według Towarzystwa Medycyny Nuklearnej i Obrazowania Molekularnego (*Society of Nuclear Medicine and Molecular Imaging*, SNMMI) przedstawiający wyniki obrazowania PET/CT (tomografii pozytonowej sprzężonej z tomografią komputerową) dwunastu pacjentów onkologicznych wykazujących odmienne jednostki nowotworowe przy użyciu tego samego radiofarmaceutyku [^{68}Ga]Ga-FAPI-04 w Uniwersyteckim Szpitalu w Heidelbergu w Niemczech [33]. Radiofarmaceutyk ten celuje w nadeksprymowane białko aktywacji fibroblastów, umożliwiając obrazowanie zmian nowotworowych w niespełna trzydziestu typach różnych nowotworów złośliwych. Kolejne przypisy pod obrazami tomografii: nowotwór piersi, niedrobnokomórkowy rak płuc, rak jelita grubego, rak trzustki, rak nieznanego pochodzenia, rak prostaty, rak jajnika, rak przełyku, rak jelita cienkiego, rak dróg żółciowych, mięsak i guz neuroendokrynny przewodu pokarmowego.

W przeciwieństwie do powyższych klasyczna chirurgia i radioterapia obejmują swoim działaniem fragment lub całość narządu, często wraz z dużym marginesem prawidłowej tkanki wokół patologicznej zmiany. Co więcej, jeden zabieg chirurgiczny lub sesja naświetlania nie wykazuje działania globalnego, lecz obejmuje jedynie ograniczony rejon ciała pacjenta. Wiąże się to ze znacznym obniżeniem bezpieczeństwa i komfortu terapii dla pacjenta, często również

z długotrwałą rekonwalescencją i rehabilitacją po zabiegach resekcji. Podobnie niespecyficzną terapią jest klasyczna chemioterapia, która powszechnie kojarzona jest z wysoką toksycznością z uwagi na wąski indeks terapeutyczny [36,37]. Leki cytostatyczne w niej stosowane nie eliminują komórek nowotworowych, a jedynie zatrzymują ich cykl podziału, przy jednoczesnym oddziaływaniu na materiał genetyczny wszystkich komórek w organizmie (w szczególności wrażliwych komórek szpiku kostnego, gamety czy dojrzewające komórki hematopoetyczne) znacznie redukując zdolność organizmu do autonomicznej remisji choroby po terapii.

Pomimo zauważalnych korzyści TRT ponad klasycznymi metodami terapii onkologicznej, zastosowanie tej pierwszej w praktyce klinicznej wciąż dotyczy jedynie wybranych schorzeń, tych najbardziej wrażliwych na cytotoksyczny efekt promieniowania jonizującego. Przegląd zarejestrowanych przez US FDA (Amerykańską Agencję Żywności i Leków) strategii TRT dostępnych do użytku klinicznego zebrany jest w Tabeli 1. [38-40].

Tabela 1. Radiofarmaceutyki dedykowane do celowanej strategii radionuklidowej wybrane spośród aktualnie zarejestrowanych radiofarmaceutyków zatwierdzonych przez US FDA.

Wskazanie kliniczne	**Radiofarmaceutyki terapeutyczne (nazwa handlowa)**
SSTR-pozytywne nowotwory neuroendokrynne	[^{177}Lu]Lu-DOTATATE (Lutathera)
PSMA-pozytywny przerzutowy rak prostaty oporny na kastrację	[^{177}Lu]Lu-vipivotide tetraxetan, [^{177}Lu]Lu-PSMA-617 (Pluvicto)
Nowotwory i nadczynność tarczycy	[^{131}I]NaI (Hicon)
CD20-pozytywna postać grudkowego B-komórkowego chłoniaka nieziarniczego	[^{90}Y]Y-ibritumomab tiuksetanu (Zevalin) [^{131}I]I-tositumomab (Bexxar)[a]
Przyzwojak (*paraganglioma*) Guz chromochłonny (*pheochromocytoma*)	*meta*-[^{131}I]jodo-benzyloguanidyna (Azedra)
Nieoperacyjne guzy raka wątrobowokomórkowego	Mikrosfery zawierające ^{90}Y (TheraSphere)[b]
Przerzutowy ból kostny	[^{223}Ra]$RaCl_2$ (Xofigo) [^{153}Sm]Samaru leksydronam (Quadramet) [^{89}Sr]$SrCl_2$ (Metastron)

[a] Preparat wycofany z użytku przez sponsora; [b] Preparat zarejestrowany jako wyrób medyczny.

Spektakularnym przykładem możliwości TRT jest wyjątkowo efektywna terapia PSMA-pozytywnego raka gruczołu krokowego opornego na kastrację i cechującego się przerzutowością (do węzłów chłonnych i kości) przy zastosowaniu [^{177}Lu]Lu-PSMA-617 (Obraz 3.)[40,41]. Wektorem radiofarmaceutyku jest motyw peptydowy Glu-urea-Lys (kwas glutaminowy-mocznik-lizyna) o wyjątkowo wysokim powinowactwie do swoistego antygenu błonowego prostaty (*prostate specific membrane antygen*, PSMA) – enzymu występującego w istotnej nadekspresji na powierzchni komórek raka prostaty w porównaniu do pozostałych komórek w organizmie ludzkim. Za sprawą tej dysproporcji terapia przy użyciu [^{177}Lu]Lu-PSMA-617 (oraz [^{225}Ac]Ac-PSMA-617) przynosi ponadprzeciętne rezultaty przedstawione na Obrazie 3. [40-44].

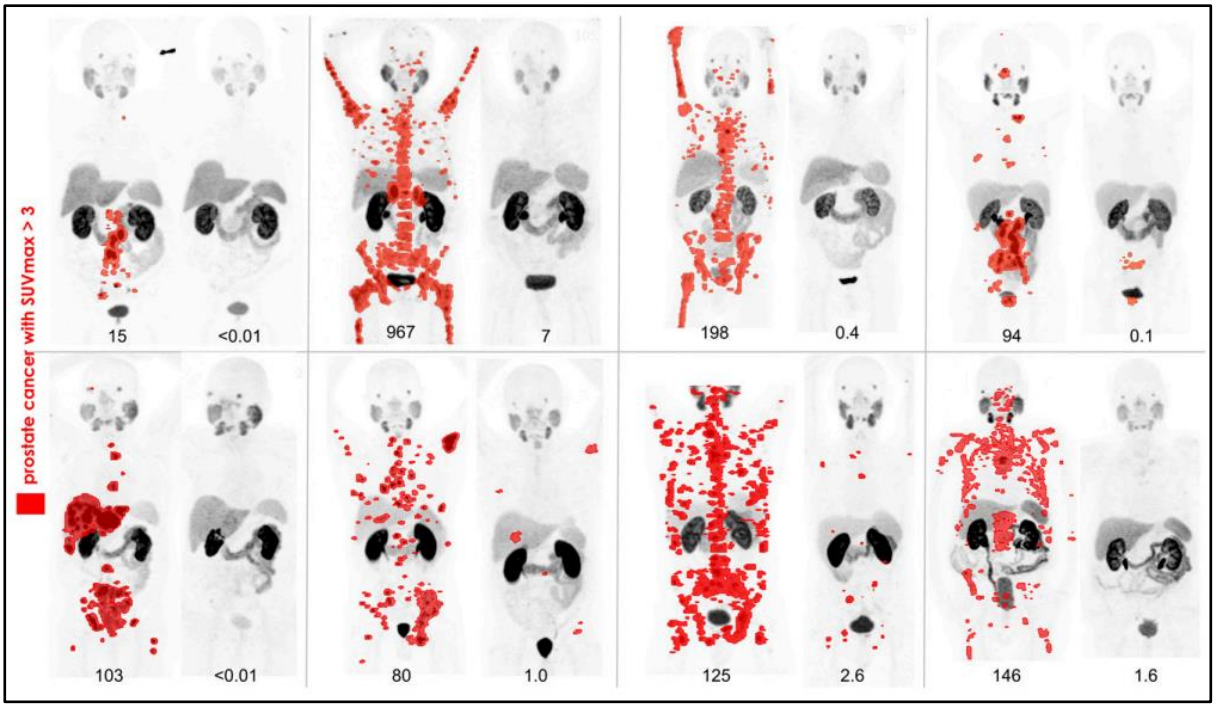

Obraz 3. Obraz roku 2018 według SNMMI przedstawiający wyniki obrazowania PET przy użyciu [^{68}Ga]Ga-PSMA-11 u wybranych ośmiu pacjentów przed (każdorazowo z lewej) i po (z prawej) terapii przerzutowego raka prostaty przy użyciu [^{177}Lu]Lu-PSMA-617 [44]. U przedstawionych pacjentów zarejestrowano spadek na poziomie ponad 98% markera zmiany nowotworowej PSA (*prostate specific antygen*) (wartości podane pod każdym obrazem) i spektakularną remisję zmian przerzutowych (zaznaczone jako czerwone punkty), mimo że pacjenci nie odpowiadali wcześniej na standardowe leczenie [41]. Przedstawione wyniki ilustrują również koncept celowanej terapii radionuklidowej realizowany w podejściu pary radiofarmaceutyków teranostycznych.

1.2. Radionuklidy medyczne stosowane w medycynie nuklearnej

Radionuklidy stosowane w radiofarmacji są dostarczane z jednego z trzech wymienionych źródeł: reaktora jądrowego, cyklotronu lub generatora radionuklidowego. Skutkiem tego bywają one nazywane potocznie od źródła ich wytwarzania (radionuklidy reaktorowe, cyklotronowe lub generatorowe), podobnie jak ma to miejsce dla nazewnictwa odnoszącego się do ich zastosowania (radionuklidy diagnostyczne, terapeutyczne lub teranostyczne).

Radionuklidy reaktorowe wytwarzane są dwojaki sposób, mianowicie w wyniku aktywacji neutronowej stabilnych izotopów (napromieniowania materiału tarczowego wiązką neuronów emitowaną z paliwa reaktora jądrowego), lub jako produkty rozszczepienia ciężkich radionuklidów paliwowych (głównie ^{235}U)[45,46]. Pozyskiwane tą drogą radionuklidy to przeważnie średnio- lub długożyciowe emitery beta lub alfa dedykowane do zastosowań terapeutycznych oraz długożyciowe izotopy promieniotwórcze wykorzystywane kolejno do produkcji generatorów radionuklidowych (Tabela 2. i 3.).

Radionuklidy cyklotronowe wytwarzane są w cyklotronach lub akceleratorach cząstek w procesie napromieniania stabilnych nuklidów materiału tarczowego wysoko energetycznym źródłem cząstek naładowanych ($^{1}H^{-}$, $^{1}H^{1}H^{+}$ $^{2}H^{-}$, $^{4}He^{2+}$ lub cięższymi jądrami) [46,47]. Powstałe w ten sposób radionuklidy to najczęściej krótkożyciowe emitery promieniowania beta plus i gamma do zastosowań diagnostycznych, ale także emitery promieniowania alfa i radionuklidy do wytwarzania generatorów radionuklidowych (Tabela 2. i 3.).

Generator radionuklidowy to układ radiochemiczny, zawierający zaadsorbowany (unieruchomiony), długożyciowy radionuklid macierzysty ulegający rozpadowi promieniotwórczemu do krótkożyciowego radionuklidu potomnego, podatnego na prostą elucję lub ekstrakcję ze złoża kolumny wewnątrz generatora. Generator jest regularnie odnawialnym źródłem izotopu potomnego i stanowi najbardziej preferowany układ pozyskiwania prekursora radionuklidowego do zastosowań w laboratoriach szpitalnych [48].

Rozróżnia się pięć procesów rozpadu promieniotwórczego, którym ulegają medyczne izotopy promieniotwórcze, mianowicie rozpad alfa, rozpad beta, rozpad beta plus, wychwyt elektronów oraz przejście izomeryczne [46], przy czym dany izotop może podlegać rozpadowi tylko jednego typu lub jednocześnie kombinacji

kilku typów z powyżej wymienionych. Pierwszym trzem rozpadom towarzyszy emisja cząstek naładowanych (są to odpowiednio cząstki alfa (jądra $^{4}He^{2+}$), cząstki beta (elektrony) i cząstki beta plus (pozytony)), zaś dwa ostatnie rozpady to procesy emisji kwantów gamma (fotonów). Jednocześnie deekscytacja jądra na drodze przejścia izomerycznego jest częstym następstwem wyżej wymienionych rozpadów z emisją naładowanej cząstki [46]. Izotopy rozpadające się poprzez wychwyt elektronów mają niekiedy zdolność (w zależności od energii emitowanych kwantów gamma) do wtórnej emisji elektronów określanych mianem elektronów Augera, to jest elektronów wybitych z zewnętrznych powłok elektronowych na skutek absorpcji kwantu gamma emitowanego z jądra po jego pierwotnym rozpadzie. Wykaz powszechnie stosowanych radionuklidów w medycynie nuklearnej przedstawiono w Tabeli 2. i Tabeli 3.

Tabela 2. Wybrane radionuklidy diagnostyczne, ich właściwości rozpadu oraz źródła wytwarzania dla potrzeb medycyny nuklearnej (dane dotyczące rozpadów promieniotwórczych zaczerpnięte z bazy danych IAEA [49])

Nuklid	Czas połowicznego rozpadu	Typ rozpadu[a] (średnia energia cząstki)[b]	Główne źródło wytwarzania
^{11}C	20,4 min	β^+ (385,7 keV)	cyklotron
^{15}O	122,2 s	β^+ (735,3 keV)	cyklotron
^{18}F	109,8 min	β^+ (249,8 keV)	cyklotron
^{43}Sc	3,9 h	β^+ (508,1 i 344,5 keV) EC (372,9 keV)	cyklotron
^{44}Sc	4,0 h	β^+ (632,0 keV) EC (1157,0 keV)	cyklotron
^{64}Cu	12,7 h	β^+ 61,5% (278,0 keV) β^- 38,5% (579,6 keV)[c]	cyklotron
^{67}Ga	3,3 d	EC (93,3, 184,6 i 300,2 keV)	cyklotron
^{68}Ga	67,7 min	β^+ (836,0 keV)	generator
^{89}Zr	78,4 h	EC (909,2 keV) β^+ (395,5 keV)	cyklotron
^{99m}Tc	6,0 h	IT (140,5 keV)	generator
^{111}In	2,8 d	EC (245,4 i 171,3 keV)	cyklotron
^{123}I	13,2 h	EC (159,0 keV)	cyklotron
^{124}I	4,2 d	EC (602,73, 1691,0 i 722,8 keV) β^+ (687,0 i 974,7 keV)	cyklotron
^{201}Tl	3,0 d	EC (70,8, 68,9 i 167,4 keV)	cyklotron

[a]EC- wychwyt elektronu; β^+- rozpad beta plus; β^-- rozpad beta minus; IT- przejście izomeryczne.

[b]Wartości średnich energii podane w kolejności malejącej intensywności, do wartości powyżej 10% intensywności i powyżej 50 keV.

[c]Dla elektronów podano wartość maksymalnej energii cząstek.

Tabela 3. Wybrane radionuklidy terapeutyczne, ich właściwości rozpadu oraz źródła wytwarzania dla potrzeb medycyny nuklearnej (dane dotyczące rozpadów promieniotwórczych zaczerpnięte z bazy danych IAEA [49]).

Nuklid	Czas połowicznego rozpadu	Typ rozpadu[a] (energia cząstki)[b]	Główne źródło wytwarzania
^{47}Sc	3,3 d	β^- (439,0 i 600,3 keV) IT (159,4 keV)	generator
^{67}Cu	61,8 h	β^- (377,1, 468,4 i 561,7 keV) IT (184,6 i 93,3 keV)	cyklotron
^{90}Y	64,1 h	β^- (932,4 keV)	reaktor, generator
^{131}I	8,0 d	β^- (606,3 keV) IT (364,5 keV)	reaktor
^{153}Sm	46,3 h	β^- (704,3 i 807,5 keV) IT (103,2 keV)	cyklotron
^{177}Lu	6,6 d	β^- (496,8 i 175,5 keV) IT (208,4 keV)	reaktor
^{188}Re	17,0 h	β^- (2120,4 i 1965,4 keV) IT (155,0 keV)	reaktor, generator
^{211}At	7,2 h	EC 58,2% (785,0 keV) IT (79,3 i 76,9 keV) α 41,8% (5,87 MeV)	cyklotron
^{213}Bi	45,6 min	β^- 97,9% (1422, 982 keV) IT (440,5 keV) α 2,1% (5,88 MeV)	generator
^{223}Ra	11,4 d	α (5,71 i 5,61MeV) IT (83,8 i 81,1 keV)	cyklotron
^{225}Ac	9,9 d	α (5,83 i 5,79 MeV)	generator

[a] β^-- rozpad beta minus; IT - przejście izomeryczne; EC- wychwyt elektronu; α - rozpad alfa.
[b] Dla fotonów podano średnie wartości energii cząstek, zaś dla elektronów i cząstek alfa maksymalne wartości energii cząstek. Wartości energii podane są w kolejności malejącej intensywności, do wartości powyżej 10% intensywności i powyżej 50 keV.

Użyteczność danego radionuklidu do zastosowań diagnostycznych lub terapeutycznych ilościowo charakteryzuje parametr LET dla danej cząstki emitowanej podczas rozpadu promieniotwórczego [50]. LET wyraża gęstość jonizacji otoczenia wzdłuż toru emitowanej cząstki i określa średnią stratę energii cząstki (lub średnią ilość energii zdeponowanej w otoczeniu) w jednostce długości drogi pokonanej przez tę cząstkę. Przestrzenny rozkład jonizacji ma istotny wpływ na powstawanie cytotoksycznych uszkodzeń DNA (na drodze pierwotnych

lub wtórnych uszkodzeń) w pojedynczych komórkach oraz tkankach organizmów żywych [50,51], z tego względu w medycynie nuklearnej parametr LET pozwala oszacować efekt cytotoksyczny danego promieniowania. Wartości LET mogą oscylować od około 0,1 keV/μm dla wysokoenergetycznych promieni gamma do 50 keV/μm (a nawet powyżej 200 keV/μm) dla cząstek alfa i protonów o umiarkowanych energiach poniżej 5 MeV [52]. Skutkiem tego promieniowanie radionuklidów diagnostycznych powinno wykazywać jak najmniejsze wartości LET, zaś promieniowanie radionuklidów terapeutycznych optymalnie duże (powyżej 10 keV/μm). Skuteczność biologiczna cytotoksycznego działania promieniowania jest odmienna dla poszczególnych typów cząstek (o różnych wartościach LET), co ilustruje poniższy schemat (Obraz 4.)[30,50-52].

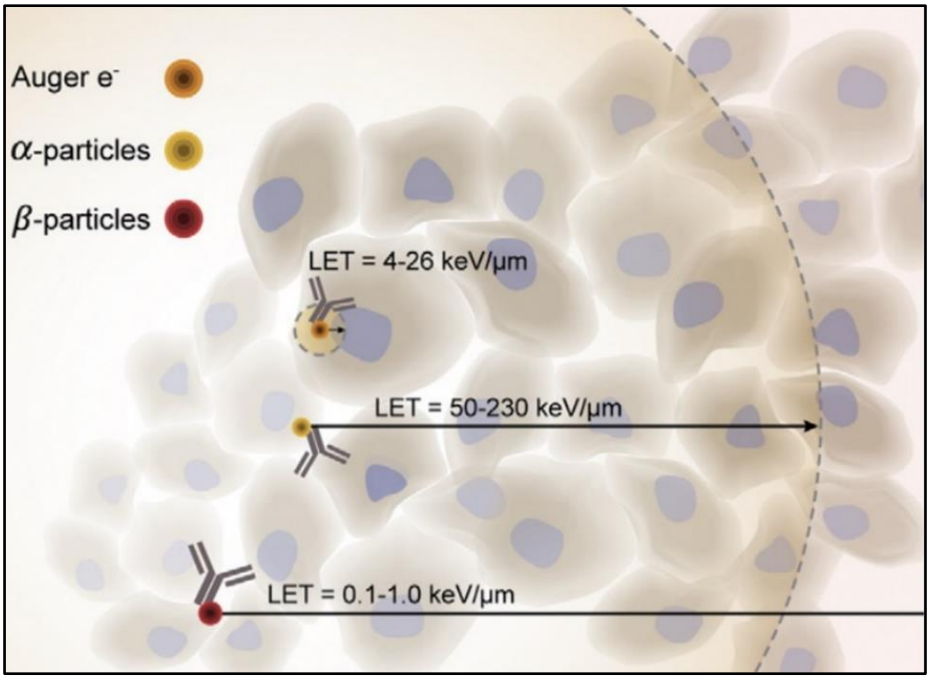

Obraz 4. Schemat ilustrujący LET dla cząstek α, β i elektronów Augera emitowanych w miejsce zmiany nowotworowej. Specyficznie dostarczone emitery cząstek α i elektronów Augera w pobliżu komórek rakowych skutecznie wywołują efekt cytotoksyczny za sprawą bardzo wysokiej zdolność jonizacji najbliższego otoczenia. Emitery cząstek β poprzez znacznie dalszy zasięg jonizacji otoczenia dedykowane są do endoradioterapii największych guzów nowotworowych. Obraz zapożyczony z pracy przeglądowej [52].

1.3. Projektowanie idealnego radiofarmaceutyku

Na obecnym etapie rozwoju technologicznego oraz w obecnym statusie prawnym dotyczącym stosowania preparatów medycznych u ludzi, projektowanie radiofarmaceutyków powinno opierać się o realistyczne założenia produkcyjne, ekonomiczne, infrastrukturalne oraz kliniczne. Cały koncept musi być ze sobą spójny i logiczny, aby umożliwić regularną produkcję w sposób spełniający rygorystyczne normy jakości preparatu dotyczące bezpieczeństwa (personelu medycznego i pacjentów) oraz skuteczności działania dla wskazanego zastosowania klinicznego. Nie jest możliwe przedstawienie jednej, idealnej charakterystyki dla wszystkich radiofarmaceutyków, gdyż odmienne preparaty dedykowane są do wykonywania różnych funkcji (diagnostyka i/lub terapia), przez co należy je rozpatrywać osobno. Mimo to są pewne istotne aspekty procesu projektowania preparatów radionuklidowych do regularnego użytku medycznego dotyczące wszystkich radiofarmaceutyków bez wyjątku.

1.3.1. Wybór wektora

Głównym aspektem przy wyborze wektora radiofarmaceutyku jest zdefiniowanie konkretnego procesu lub celu molekularnego wymagającego interwencji medycznej. Funkcję wektora może pełnić dowolna substancja o wysoce swoistej aktywności biologicznej, miedzy innymi syntetyczna cząsteczka organiczna, aminokwas, peptyd, oligonukleotyd, przeciwciało monoklonalne, czy cukier (Tabela 4.)[15,36,53-55]. Zaprojektowany wektor będzie pełnił funkcję kierującą do obranego systemu biologicznego i pożądane jest, aby wykonywał to działanie jak najszybciej i z maksymalną wydajnością. Projektowany wektor bezkompromisowo musi cechować się wysokim powinowactwem, wysoką selektywnością oraz wysoką stabilnością oddziaływania molekularnego wobec obranego celu. Zbiór tych cech radiofarmaceutyku określa parametr biodystrybucji definiowany jako stosunek radioaktywności obecnej w rejonie docelowym do radioaktywności poza nim (*target-to-nontarget radioactivity ratio*) i w największym stopniu przekłada się na jakość obrazowania przy użyciu radioznacznika diagnostycznego [56] oraz bezpieczeństwo terapii z wykorzystaniem radiofarmaceutyku terapeutycznego [57].

Tabela 4. Zestawienie podziału wektorów radiofarmaceutyków celowanych, różnic w ich biologicznym czasie połowicznego zaniku oraz zastosowaniu klinicznym.

Typ wektora	Rząd wielkości biologicznego czasu połowicznego zaniku[a]	Przykład radiofarmaceutyku	Zastosowanie kliniczne
Cukry	minuty	[^{18}F]FDG, [^{18}F]fluorodeoksyglukoza	Obrazowanie metabolizmu komórkowego
Aminokwasy	minuty-godziny	*L*-[*metylo*-^{11}C]metionina	
Drobne cząsteczki organiczne	minuty-godziny-dni	[^{123}I]Ioflupan	Celowana diagnostyka neurologiczna i onkologiczna (rzadko terapia)
Peptydy i peptydomimetyki	minuty-godziny	[^{177}Lu]Lu-DOTATATE	Celowana diagnostyka i terapia nowotworowa
Oligonukleotydy (aptamery, optimery itd.)	godziny	[58]	
Mimetyki i fragmenty przeciwciał monoklonalnych	dni-tygodnie	[56,59]	
Przeciwciała monoklonalne	tygodnie-miesiące	[^{89}Zr]Zr-DFO-Bevacizumab	

[a]Podane wartości rzędu wielkości biologicznego czasu połowicznego zaniku odnoszą się do nieznakowanych promieniotwórczo substancji.

Niestety, w praktyce większość radiofarmaceutyków chwilowo lokalizuje się również w niepreferencyjnych organach ciała, między innymi w wątrobie, nerkach lub pęcherzu moczowym, z uwagi na proces eliminacji ksenobiotyku. Skutkuje to zjawiskami pogorszenia jakości (osłabianiem lub przysłanianiem) wizualizacji pożądanych regionów ciała pacjenta oraz narażenia niedocelowych narządów na pochłonięcie zbędnej dawki promieniowania. Ilość otrzymanej dawki promieniowania bezpośrednio skorelowana jest z czasem eskpozycji organu na radiofarmaceutyk, ten zaś uwarunkowany jest od charakterystyki farmakokinetycznej zaprojektowanego radiofarmaceutyku. Celem projektowania całej części wektorowej radiofarmaceutyku jest dobór i optymalizacja parametrów fizykochemicznych cząsteczki warunkujących rozprowadzanie radiofarmaceutyku w obrębie organizmu. Mowa tu o parametrach takich jak lipofilowość (lipofilność), masa cząsteczkowa oraz ładunek wypadkowy cząsteczki, siła wiązania z białkami osocza lub tkanek, zdolność i szybkość transportu (biernego lub aktywnego)

przez błony biologiczne oraz podatność na biotransformację *in vivo* [55,60,61]. Optymalizacja powyższych parametrów umożliwia dopasowanie biodystrybucji radiofarmaceutyku (tempo dystrybucji i metabolizmu oraz sposób eliminacji z organizmu) do potrzeb interwencji medycznej, co bezpośrednio przekłada się na użyteczność zastosowania radiofarmaceutyku.

1.3.2. Wybór radionuklidu

Poza fundamentalnymi wymaganiami celowalności, kluczowym kryterium regularnej produkcji radiofarmaceutyku jest prostota wytwarzania i/lub łatwa dostępność produktu medycznego. Radiofarmaceutyk powinien być otrzymywany w nietrudny, powtarzalny i niedrogi sposób, *ergo* powinien charakteryzować się szeroką dostępnością dla maksymalnej ilości zakładów klinicznych [48,62]. Najdogodniej, aby finalny etap produkcji radiofarmaceutyku, to jest znakowania promieniotwórczego, odbywał się w laboratorium szpitalnym przy użyciu generatora radionuklidowego, zaś wytworzony w ten sposób preparat radiofarmaceutyczny był zdatny do bezpośredniej aplikacji.

Zasadniczym kryterium wyboru radionuklidu jest kompatybilność charakterystyki jego rozpadu promieniotwórczego i właściwości farmakokinetycznych wybranego wektora oraz przeznaczenia radiofarmaceutyku. Dotyczy to przede wszystkim doboru porównywalnych wartości okresu połowicznego rozpadu izotopu promieniotwórczego oraz czasu połowicznego zaniku ksenobiotyku z organizmu [55]. Ten pierwszy parametr to statystyczny czas potrzebny do rozpadu połowy danej ilości atomów promieniotwórczych w jednostce czasu, zaś w radiofarmacji parametr ten bywa nazywany także fizycznym czasem połowicznym. Biologiczny czas połowiczny to statystyczny czas potrzebny do eliminacji lub wydalenia połowy danej ilości substancji z organizmu. Obydwa te czasy bezpośrednio określają efektywny (rzeczywisty) czas połowiczego zaniku radiofarmaceutyku (na skutek rozpadu promieniotwórczego i eliminacji z organizmu) według przedstawionego poniżej wzoru [61]:

$$^{efekt.}T_{1/2} = \frac{^{fiz.}T_{1/2} \times {}^{biol.}T_{1/2}}{^{fiz.}T_{1/2} + {}^{biol.}T_{1/2}}, \text{ gdzie}$$

$^{efekt.}T_{1/2}$ – efektywny czas połowiczny radiofarmaceutyku, $^{fiz.}T_{1/2}$ – fizyczny czas połowicznego rozpadu, $^{biol.}T_{1/2}$ – biologiczny czas połowicznego zaniku.

Wnioski płynące w powyższej zależności to w szczególności fakt, że efektywny czas połowiczny jest zawsze wartością mniejszą niż obydwie jego

składowe. W przypadku znaczącej różnicy pomiędzy wartościami składowymi efektywnego czasu połowicznego, ten ostatni przyjmie wartość zbliżoną do mniejszej z jego składowych, zaś największą wartość efektywnego czasu połowicznego uzyskuje się, gdy fizyczny i biologiczny czas połowiczny niewiele się od siebie różnią, a efektywny czas połowiczny przyjmie wówczas wartość zbliżoną do połowy średniej z jego składowych. Finalnie, dąży się do tego, aby składowe czasy połowiczne były porównywalne, a efektywny czas połowiczny radiofarmaceutyku był współmiernie długi do potrzeb przeprowadzenia skutecznej i wiarygodnej procedury medycznej (protokołu obrazowania lub jednostki cyklu terapeutycznego), jednocześnie mając na względzie pryncypialne dążenie do zminimalizowania dawki (i czasu) promieniowania pochłoniętego przez pacjenta. Ponadto warto zauważyć, że chociaż fizyczny okres połowiczny jest dokładnie określoną stałą, wartość biologicznego okresu połowicznego wektora radiofarmaceutyku może ulec znacznemu odchyleniu pod wpływem modyfikacji wektora do postaci radiofarmaceutyku oraz nade wszystko w warunkach patologicznej fizjologii *in vivo*, wobec czego zaleca się dobór stosunkowo krótkiego czasu rozpadu fizycznego kierując się bezpieczeństwem pacjenta.

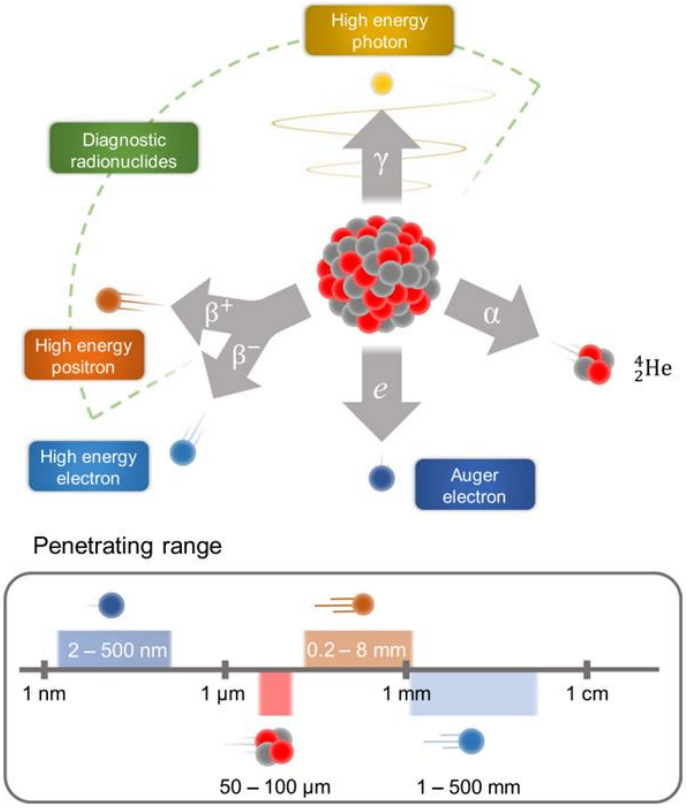

Obraz 5. Schemat typów rozpadów promieniotwórczych wykorzystywanych w medycynie nuklearnej (z wyróżnieniem typów rozpadów odpowiadającym radionuklidom diagnostycznym). W ramce pokazano zakresy zasięgu wymienionych cząstek w tkankach miękkich. Obraz zapożyczony z pracy przeglądowej [63].

Zgodność wyboru radionuklidu z przeznaczeniem radiofarmaceutyku wymaga także doboru typu i energii emitowanych cząstek podczas rozpadu promieniotwórczego [14,46]. Do celów diagnostycznych dedykowane są radionuklidy emitujące wysoce przenikliwe promieniowanie gamma o określonym zakresie energetycznym (Obraz 5.). Jednocześnie, przeznaczone do tego celu izotopy powinny ulegać w maksymalnym stopniu rozpadom promieniotwórczym na skutek wychwytu elektronu, przejścia izomerycznego lub rozpadu beta plus. Pozytony emitowane podczas rozpadów beta plus to jedyne naładowane cząstki, które są preferowane (i bardzo efektywne) do celów obrazowych [64,65]. Niepożądane jest, aby radionuklidy diagnostyczne wykazywały emisję innych naładowanych cząstek, cząstek alfa i elektronów. W przeszłości wiele badań diagnostycznych bazowało na wykorzystaniu emiterów elektronów, jednakże wynikało to z braku dostępności bardziej odpowiednich radionuklidów diagnostycznych. Do tych celów preferowana jest emisja kwantów gamma o energii rzędu 30-250 keV, gdyż mniej energetyczne promieniowanie zostanie zaabsorbowane przez tkanki pacjenta, i tym samym naraża pacjenta na zbędną dawkę promieniowania, zaś to o wyższej energii nie zostanie efektywnie zarejestrowane przez powszechnie stosowane detektory urządzeń obrazujących [66]. Niemniej do detekcji koincydencji kwantów gamma o energii 511 keV powstałych w wyniku anihilacji pozytonów po rozpadzie beta plus stosowane są wysoko rozdzielcze detektory tomografów PET (rozdział 1.4.)[64].

Inaczej wyglądają wymagania wobec radionuklidów terapeutycznych. W tym przypadku izotopy powinny ulegać rozpadom promieniotwórczym, którym towarzyszy emisja naładowanych cząstek o wysokim LET, to jest cząstek alfa, elektronów Augera, rzadziej cząstek beta minus (jedynie w przypadku największych guzów) (Obrazy 4 i 6.)[16,46,50,52]. Innymi słowy, do zastosowań terapeutycznych preferowane są izotopy, które emitują cząstki deponujące wysoką porcję energii jedynie w ściśle ograniczonym pobliżu źródła promieniotwórczego wywołując efekt cytotoksyczny. Dodatkowa obecność promieniowania gamma w nielicznych przypadkach umożliwia jednoczesne obrazowanie akumulacji radiofarmaceutyku podczas terapii [41,57], dzięki czemu proces terapeutyczny może być monitorowany i znacznie lepiej kontrolowany.

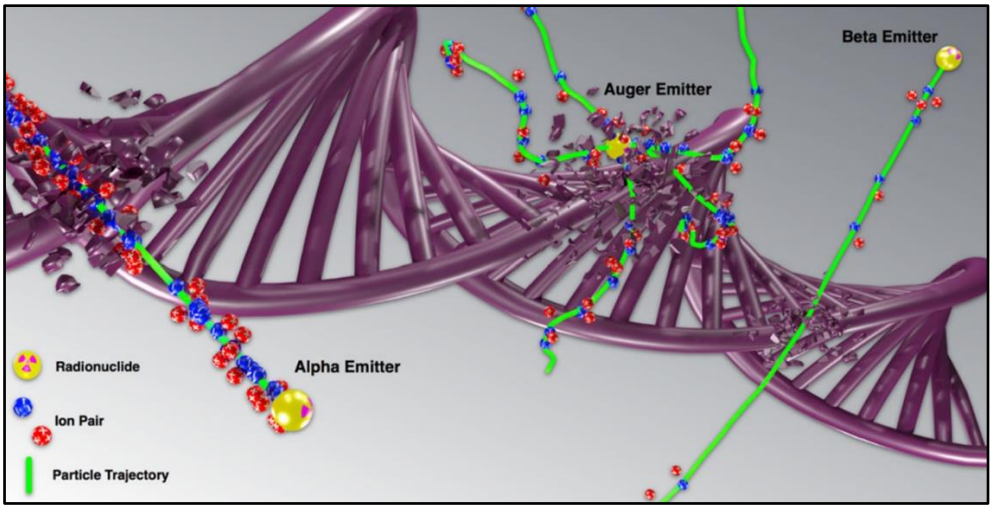

Obraz 6. Schemat gęstości jonizacji wzdłuż toru cząstek α, β i elektronów Augera oraz uszkodzenia DNA wynikające ze zjawisk emisji tych cząstek. Warto zauważyć, że emitery elektronów Augera zdolne są często do emisji więcej niż jednej cząstki naładowanej podczas pojedynczego rozpadu. Obraz zapożyczony z pracy przeglądowej [67].

Z praktycznego punktu widzenia, nie mniej istotnym aspektem wyboru radionuklidu jest możliwość jego zastosowania w medycynie za sprawą efektywnego przyłączenia do struktury części wektorowej przyszłego radiofarmaceutyku. Pomimo stosunkowo dobrze zdefiniowanej gamy niespełna trzech tysięcy izotopów promieniotwórczych, jedynie niewielki procent z nich dostępny jest do stosowania w radiofarmacji i medycynie nuklearnej [68]; ponadto raptem kilka z nich jest pierwiastkami o znaczeniu biologicznym (^{3}H, ^{11}C, ^{13}N, ^{15}O, ^{18}F, ^{32}P, ^{35}S, $^{123/131}$I)[69], którymi można zastąpić stabilne nuklidy tych samych pierwiastków. Pozostała większość radionuklidów medycznych to pierwiastki sztucznie wprowadzane do substancji biologicznie aktywnych, w celu nadania im właściwości radioznacznikowych. Są to głównie metale o różnorodnych właściwościach, aktywności chemicznej i zdolności do tworzenia wiązań chemicznych [14,65,70]. Skutkuje to potrzebą opracowania metod znakowania dla konkretnej grupy lub wręcz pojedynczego pierwiastka, w dodatku dopasowanych do pożądanego wektora projektowanego radiofarmaceutyku.

Jedynym z największych sukcesów w tej tematyce było wprowadzenie do radiofarmacji radionuklidu o wybitnie użytecznej charakterystyce rozpadu promieniotwórczego technetu-99m, izotopu pierwiastka, który nie posiada stabilnych form izotopowych, przez co nie znalazł innych praktycznych zastosowań poza diagnostyką obrazową. Obecnie, ^{99m}Tc jest najpowszechniej eksploatowanym radionuklidem medycznym na świecie, za sprawą odkrycia i zagospodarowania do użytku radiofarmaceutycznego jego bardzo bogatej chemii koordynacyjnej [71,72], dzięki czemu znakowanie tym radionuklidem wręcz dowolnych substancji

jest w dzisiejszych czasach niezwykle przystępne. Podobnie, dzięki dokonanym odkryciom w dziedzinie chemii koordynacyjnej opracowano także wiele cząsteczek makrocyklicznych o zdefiniowanych właściwościach chelatujących, dedykowanych do tworzenia trwałych kompleksów z poszczególnymi grupami metali [15,73-75]. Otworzyło to szereg nowych możliwości projektowania radiofarmaceutyków zawierających metaliczne radionuklidy przyłączone do wręcz dowolnych wektorów biologicznych (przykłady tego typu radiofarmaceutyków znajdują się w Tabeli 1.).

1.3.3. Optymalizacja finalnej formy radiofarmaceutyku

Efektywność radiofarmaceutyku, a zarazem jego użyteczność, wynika z obserwowanej biodystrybucji leku *in vivo*. Praktycznie największy wpływ na charakterystykę biodystrybucji tuż po wyborze wektora radiofarmaceutyku ma finalna postać preparatu radiofarmaceutycznego [8,76], od której zależy czy zaprojektowana substancja biologicznie czynna (część wektorowa z dołączonym radionuklidem) będzie w stanie spełnić swoją funkcję w organizmie. Wymagania bezpieczeństwa terapii i diagnostyki radionuklidowej niemalże narzucają stosowanie preparatów radiofarmaceutycznych w postaciach umożliwiających maksymalną (natychmiastową) biodostępność substancji czynnych (w podaniu dożylnym), lub ograniczających obecność radiofarmaceutyku jedynie do wybranych tkanek lub organów (w podaniu miejscowym). Najwłaściwiej umożliwiają to iniekcje wodnych roztworów lub zawiesin oraz, w wybranych przypadkach, preparaty w postaci kapsułek doustnych lub aerozoli do inhalacji. Należy pamiętać, że warunkiem *a priori* dla iniekcyjnych postaci preparatów radiofarmaceutycznych jest oczywiście zachowanie sterylności (czystości mikrobiologicznej) i apirogenności (braku endotoksyn bakteryjnych) oraz inne wymagania stawiane ciekłym postaciom leku podawanym dożylnie [13,77-79].

Ponadto, wyróżniającą cechą radiofarmaceutyków w kontekście skutecznej formulacji i wymaganej jakości leku są wymogi wysokiej wydajności radiochemicznej reakcji znakowania, wysokiej stabilności produktu znakowania, oraz wysokiej radioaktywności właściwej preparatu [13]. Wydajność radiochemiczna reakcji znakowania (*radiochemical yield*, RCY) [80] określa procent aktywności promieniotwórczej prekursora radionuklidowego użytego do znakowania zawartej w pożądanej formie radiofarmaceutyku. Tym samym RCY określa stopień związania użytego do reakcji radionuklidu w określoną formę radiochemiczną. Reakcje znakowania radionuklidowego wymagają przestrzegania ścisłych

warunków prowadzenia reakcji, w tym wysokiej czystości chemicznej środowiska reakcji (brak związków kompleksujących, oraz stabilnych pierwiastków konkurujących z radionuklidem o udział w reakcji znakowania)[81-83], gdyż celem reakcji jest jak najszybsze i w jak największym stopniu wprowadzenie radionuklidu do prekursora radiofarmaceutyku przy jednoczesnym zachowaniu aktywności biologicznej wektora.

Stabilność produktu znakowania wyrażana jest jako procent aktywności promieniotwórczej niezmienionej (początkowej) formy otrzymanego w reakcji znakowania radiofarmaceutyku oznaczany po określonym czasie. Ogólnie pojęta stabilność, w tym trwałość metaboliczna, dotyczy wszystkich ksenobiotyków, jednakże radiofarmaceutyki podatne są także na dodatkowe zjawiska braku stabilności wynikające z ich natury, a mianowicie odłączenie izotopu od reszty cząsteczki (wymianę izotopową pierwiastka lub transchelatację radiometalu z kompleksu)[84,85] oraz autoradiolizę preparatu (degradację radiofarmaceutyku w wyniku adsorpcji promieniowania lub w wyniki reakcji z produktami radiolizy wody)[86-88]. Aby zapobiec tym zjawiskom, preparaty radiofarmaceutyczne uzupełniane są o stabilizatory kompleksów radionuklidowych (przykładowo trycyna i EDDA), przeciwutleniacze (przykładowo *L*-cysteina lub kwas askorbinowy), związki redukujące (najczęściej chlorek cyny (II)), dodatki utrzymujące pożądane pH (przykładowo bufor węglanowy lub wodorotlenek sodu) oraz ciśnienie osmotyczne roztworu (najczęściej chlorek sodu lub dekstroza), ale także substancje powierzchniowo czynne (przykładowo glicerol), stabilizatory zawiesin (przykładowo powidon lub żelatyna) i konserwanty (przykładowo alkohol benzylowy)[89].

Radioaktywność właściwa (*specific activity*, A_s)[80] to określenie ilości aktywności promieniotwórczej radiofarmaceutyku wyrażona na jednostkę masy substancji, mierzona w GBq/mg lub MBq/μg. Pokrewnym parametrem jest radioaktywność molowa (*molar activity*, A_m)[80], definiowana jako ilość radioaktywności na jednostkę liczby moli substancji, wyrażana w GBq/mmol lub MBq/μmol. Obydwa te parametry kontroli jakości radiofarmaceutyku określają czystość chemiczną preparatu i efektywność procesu znakowania promieniotwórczego. Tym samym jedynie te radiofarmaceutyki, które zostały otrzymane o (możliwie maksymalnie) wysokiej A_s, mogą cechować się pożądaną skutecznością farmakologiczną [81]. W tym celu do syntezy radiochemicznej zaleca się stosować prekursory radionuklidowe o odpowiednio wysokiej czystości radiochemicznej (zawartości pożądanej formy chemicznej danego

radioizotopu) i czystości radionuklidowej (zawartości pożądanego radionuklidu). Preparaty o stosunkowo niskiej radioaktywności właściwej zawierają znaczący udział niewyznakowanych prekursorów radiofarmaceutyku lub pochodnych radiofarmaceutyku, które konkurują i blokują pożądanym cząsteczkom wyznakowanym dostęp do celu molekularnego *in vivo* [90], przez co mogą obniżać skuteczność radiofarmaceutyku (fałszować wynik obrazowania lub osłabiać działanie terapeutyczne).

Znane są także przypadki, gdy niekorzystna biodystrybucja radiofarmaceutyku powoduje obniżenie indeksu terapeutycznego leku, a redukcję działań niepożądanych z niej wynikających można osiągnąć poprzez skojarzenie radiofarmaceutyku z tak zwanym blokerem organu niepreferencyjnego [91]. W tym przypadku substancja kompetycyjna (współzawodnicząca, bloker) dla radiofarmaceutyku powinna być selektywna jedynie wobec zajmowanego (blokowanego) regionu organizmu, w którym występowałaby niepożądana nadmierna kumulacja radiofarmaceutyku. Podanie blokera może mieć miejsce równocześnie z preparatem radiofarmaceutycznym, lecz najczęściej preparat blokujący podaje się przed aplikacją radiofarmaceutyku (metoda wstępnego blokowania)[91]. Przykładami tego typu skojarzonych preparatów blokujących są roztwory aminokwasów [92] lub metforminy [93] do blokowania wychwytu kłębuszkowego w nerkach radiofarmaceutyków peptydowych, lub stosowanie radiofarmaceutyku oraz fragmentów lub analogów wektora o powinowactwie do tego samego celu molekularnego, lecz o odmiennych charakterystykach dystrybucji narządowej (przykładowo 2-PMPA lub glutaminian sodu wobec radiofarmaceutyków [^{68}Ga]Ga-PSMA-11 lub [^{177}Lu]Lu-PSMA-617 [91,94,95]).

1.4. Techniki obrazowania molekularnego z użyciem radiofarmaceutyków

Obrazowanie molekularne to dyscyplina łącząca zagadnienia biologii molekularnej i obrazowania *in vivo*. W medycynie nuklearnej podstawowymi metodami do nieinwazyjnego obrazowania molekularnego procesów (pato)fizjologicznych *in vivo* są SPECT (*single photon emission computed tomography*, tomografia pojedynczego fotonu) i PET (*positron emission tomography*, tomografia pozytonowa)[9,64,66,96-98]. W porównaniu z innymi metodami obrazowania, takimi jak tomografia komputerowa (CT) czy rezonans magnetyczny (MRI), które dostarczają w wysokiej rozdzielczości przestrzennej informacji o cechach morfologicznych tkanek i narządów, przewaga PET i SPECT polega na ich zdolności

do wizualizacji procesów biochemicznych na poziomie komórkowym i molekularnym przy pomocy radiofarmaceutyków [96-98]. Kluczowym aspektem użyteczności tych technik jest ich bezkonkurencyjnie wysoka czułość, która pozwala na podawanie radioaktywnych związków obrazujących w wyjątkowo niskich stężeniach. Współczesne tomografy wykorzystywane do obrazowania to instrumenty multimodalne łączące obrazowanie morfologiczne CT lub MRI z funkcjonalnym obrazowaniem radiofarmaceutyków w połączonym obrazie. To podejście hybrydowe umożliwia osiąganie lepszej dokładności lokalizacji (rozdzielczości) radioznaczników [97,98] oraz zmniejszenie obciążenia pacjenta promieniowaniem.

Technika obrazowa SPECT wymaga stosowania radiofarmaceutyków zawierających radionuklidy emitujące promieniowanie gamma o energii w przedziale 30-250 keV, takie jak ^{67}Ga, ^{99m}Tc i ^{111}In (Tabela 2. i Obraz 7.)[98]. Emitowane fotony są pojedynczo rejestrowane przez detektory scyntylacyjne w głowicy lub głowicach gamma kamery obracającej się wokół osi pionowej pacjenta [66].

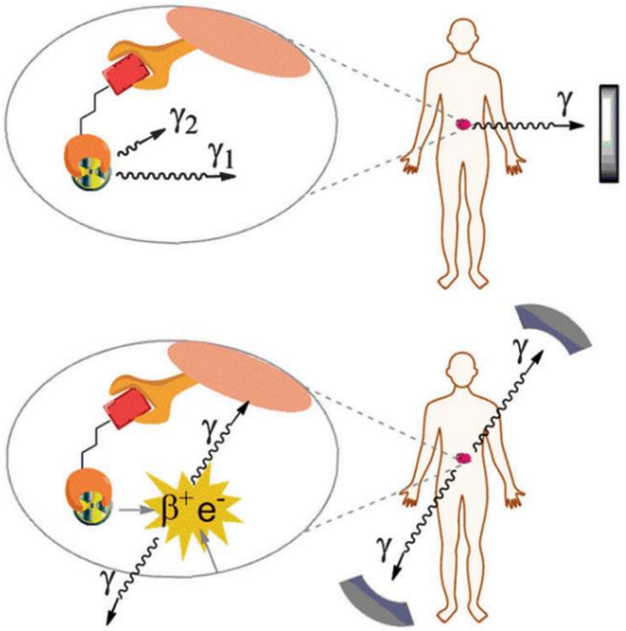

Obraz 7. Schemat zasady obrazowania metodą SPECT (powyżej) oraz obrazowania metodą PET (poniżej). Obraz zapożyczony z pracy przeglądowej [14].

Do techniki PET wykorzystuje się radiofarmaceutyki zawierające radionuklidy będące emiterami promieniowania β^+ o odpowiedniej energii, takie jak ^{11}C, ^{15}O, ^{18}F, ^{68}Ga i ^{89}Zr (Tabela 2. i Obraz 7.)[64,98]. Następstwem emisji pozytonu jest wytracanie energii przez cząstkę (minimalnie zasięgowe dla radionuklidów stosowanych w PET) oraz anihilacja pozytonu z napotkanym

w otaczającej materii elektronem, w wyniku czego dochodzi do jednoczesnej emisji dwóch przeciwbieżnych fotonów o energii 511 keV. Pomiar koincydencji dwóch fotonów umożliwia przestrzenne pozycjonowanie rozpadu radionuklidu, co jednoznacznie utożsamiane jest z określeniem lokalizacji radiofarmaceutyku w ciele pacjenta. Do generowania obrazów PET wykorzystuje się kamerę tomografu zbudowaną z koliście ułożonych gamma detektorów połączonych naprzeciwlegle dwójkami [64]. Technika PET za sprawą pomiaru koincydencji umożliwia detekcję o wyżej czułości i lepszej rozdzielczości przestrzennej (mniej rozproszone tło promieniowania) niż technika SPECT [97].

2. Znaczenie receptora NK1 w patologiach onkologicznych

2.1. Receptor neurokininy 1

Receptor neurokininy 1 zwany także receptorem tachykininy 1, należy do podrodziny receptorów tachykininowych, metabotropowych receptorów sprzężonych z białkiem G (*G-protein coupled receptors*, GPCRs)[99,100]. Receptor ten jest produktem translacji genu *TACR1*, przy czym występuje głównie w postaci dwóch izoform, NK1R-Fl, białka pełnej długości zawierającej 407 aminokwasów, oraz NK1R-Tr, skróconej izoformy pozbawionej 96 aminokwasów od wewnątrzkomórkowej strony *C*-końca [101-103] (struktura ludzkiego receptora NK1 dostępna jest w *Protein Data Bank* pod kodem 6E59 [104]). NK1R jest szeroko obecny zarówno w ośrodkowym jak i obwodowym układzie nerwowym, na powierzchni neuronów (szczególnie strukturach prążkowia)[105-109], w niewielkich ilościach na powierzchni neuronów wewnętrznego układu nerwowego oraz komórek układu odpornościowego [103,110]. Aktywacja receptora skutkuje przekazywaniem sygnałów stresu, bólu i regulowania stanu zapalnego oraz prowadzi do rozkurczu mięśni gładkich narządów obwodowych [103,108-112]. Jednocześnie nadekspresja receptora została powiązana z przebiegiem konkretnych patologii [109,113], co zainspirowało do opracowania wysoce selektywnych ligandów tego receptora o znaczeniu klinicznym.

2.1.1. Substancja P

Endogennym agonistą receptora NK1 u ludzi jest jedenastoczłonowy neuropeptyd z rodziny tachykinin zwany Substancją P (SP, Arg-Pro-Lys-Pro-Gln-Gln-Phe-Phe-Gly-Leu-Met-NH_2). Pełni on regulatorową funkcję dla procesów fizjologicznych w ośrodkowym i obwodowym układzie nerwowym poprzez preferencyjną interakcję ze swoim specyficznym białkiem błonowym NK1R.

Podobnie jak pozostałe tachykininy, SP posiada konserwatywną sekwencję pięciu aminokwasów na *C*-końcu, Phe-X-Gly-Leu-Met-NH_2 (gdzie X to dowolny aminokwas), która musi ulec amidowaniu terminalnej grupy aminowej w celu aktywacji biologicznej [114,115].

SP odgrywa istotną rolę peptydoergicznego neuromodulatora wybranych sygnałów nocyceptywnych [116-118] oraz w przebiegu (nasileniu) neurogennych stanów zapalnych [111,119,120]. Szczególnie widoczne jest to na poziomie obwodowym, gdzie w układzie naczyniowym SP powoduje rozszerzenie naczyń tętniczych, wynaczynienie białek osocza i adhezję leukocytów do komórek śródbłonka kapilarnych naczyń żylnych [111,121]. Ośrodkowo aktywność SP związana jest z kontrolą ośrodka wymiotów [122,123], regulacji nastroju, w tym zachowań i zaburzeń afektywnych (lęku i depresji) [112,124], dodatkowo SP wykazuje działanie neuroprotekcyjne (jako nieswoisty czynnik wzrostu tkanki nerwowej)[125-127] obserwowane między innymi w chorobach Alzheimera, Parkinsona. Nie mniej istotnym wydaje się być udział systemu SP-NK1R w rozwoju i progresji zmian nowotworowych [128,129].

Na poziomie komórkowym interakcja SP z błonowym receptorem NK1 indukuje wewnątrzkomórkowe ścieżki sygnalizacyjne zależne od sprzężonego z receptorem białka G (Obraz 8.)[100,130]. Obejmują one aktywację:

- fosfolipazy C (PLC) z wytworzeniem trifosforanu inozytolu (IP_3) i diacyloglicerolu (DAG), które aktywują wyrzut wewnątrzkomórkowych zapasów jonów Ca^{2+} oraz kinazę białkową C (PKC)[131,132];
- cyklazy adenylowej (AC) oraz następczą syntezę cAMP i aktywację kinazy białkowej A (PKA)[132];
- fosfolipazy A_2 (PLA_2), która katalizuje wytwarzanie kwasu arachidonowego, prekursora eikozanoidów (prostaglandyn, leukotrienów i tromboksanu A_2 (TXA_2))[133];
- Rho-zależnej kinazy białkowej (ROCK), która fosforyluje lekkie łańcuchy miozynowe (MLC)[134].

Prowadzi to do różnorodnych efektów, często specyficznych dla danego typu komórki, które obejmują proliferację i migrację komórkową, pobudzenie neuronalne, aktywację stanu zapalnego, oraz efekty przeciwapoptotyczne.

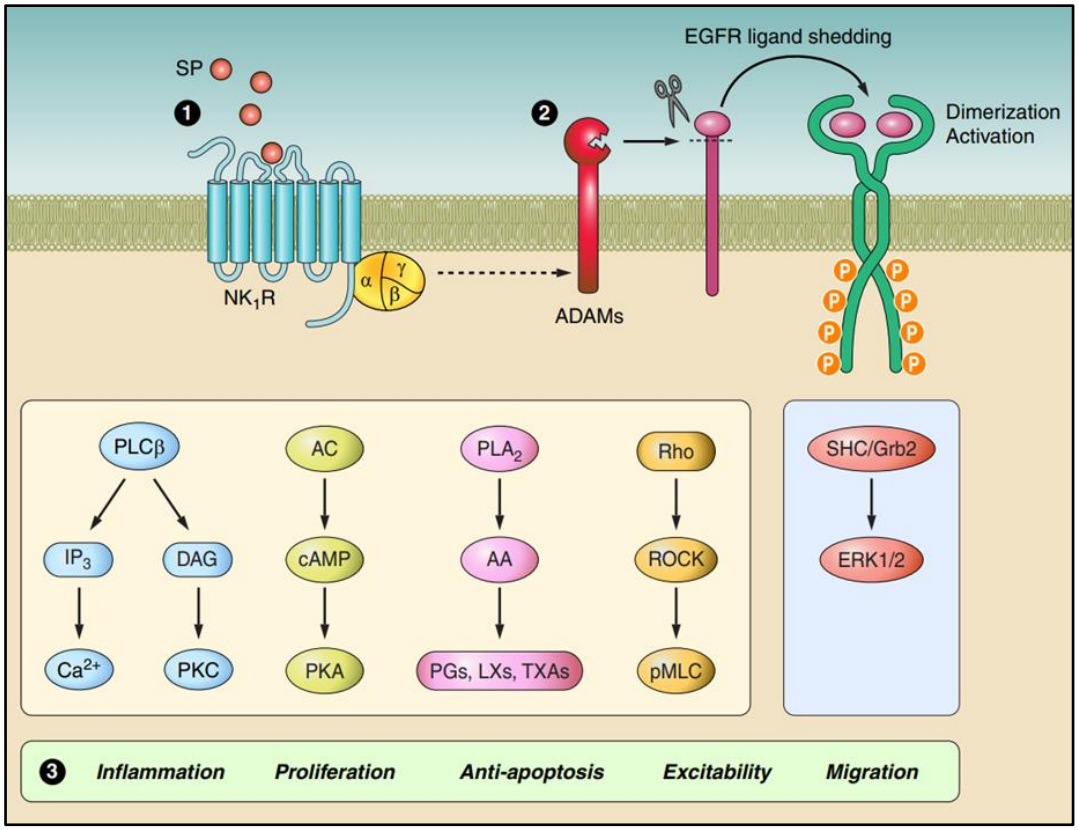

Obraz 8. Schemat agonistycznego działania SP poprzez aktywację receptora NK1, to jest indukcji wewnątrzkomórkowych ścieżek sygnalizacyjnych, prowadzących do wymienionych odpowiedzi komórkowych. Obraz zapożyczony z pracy przeglądowej [130].

Jednocześnie, skuteczność lub efekt stymulacji SP zależy od izoformy receptora, z którą łączy się ten agonista, mając na uwadze zjawisko około 10-krotnie wyższego powinowactwa neuropeptydu wobec izoformy pełnej długości receptora [101]. Izoforma receptora NK1 pełnej długości jest podatna na fosforylację w obrębie wewnątrzkomórkowego fragmentu *C*-końca, czego nie obserwuje się dla skróconej izoformy receptora posiadającej znacznie zredukowany fragment wewnątrzkomórkowy [135,136]. Fosforylacja umożliwia receptorowi oddziaływanie z β-arrestyną, która promuje komórkową sygnalizację endosomalną, endocytozę receptora oraz desensytyzację komórki na działanie agonistyczne SP (sprzężenie zwrotne ujemne)[137]. Skutkiem tego, skrócona izoforma NK1R z uwagi na zaburzone procesy internalizacji i desensytyzacji, wydaje się być zdolna do przedłużonej sygnalizacji wewnątrzkomórkowej po związaniu agonisty, aczkolwiek zdolność sygnalizacji komórkowej również ulega modyfikacji [135,136]. NK1R-Tr nie jest zdolna do silnej aktywacji wewnątrzkomórkowego wyrzutu Ca^{2+} i jądrowego czynnika NF-κB oraz hamuje fosforylację szlaku PKC i wydzielanie interleukiny 8. Ta odmienna komórkowa sygnalizacja endosomalna jest niezwykle istotna w sytuacjach patologicznych, w których występuje alternatywne

wytwarzanie receptora i niefizjologiczna nadekspresja skróconej izoformy receptora [138,139].

2.1.2. NK1R jako cel molekularny celowanej diagnostyki i terapii nowotworowej

Receptory GPCR stanowią największą i najbardziej zróżnicowaną rodzinę białek sygnalizacyjnych, zaś niespełna trzecia część obecnie stosowanych leków ukierunkowana jest wobec tych struktur molekularnych [140]. Wśród ligandów receptorowych wyróżnia się związki, które po związaniu się z receptorem indukują sygnalizację endosomalną (agonisty) lub te, które blokują miejsca wiążące receptora bez wywoływania odpowiedzi komórkowej (antagonisty), uniemożliwiając dostęp agonistom do receptora.

Bogata literatura naukowa wskazuje układ SP-NK1R jako znaczący cel molekularny o istotnej roli w pobudzaniu proliferacji i migracji komórek nowotworowych, zarówno guzów litych, jak i guzów tkanek miękkich [129,141-144]. Wiązanie się endogennego agonisty do receptora NK1 promuje mitozę komórek nowotworowych, ich migrację (proces inwazji i przerzutowania), działanie przeciwapoptotyczne oraz zwiększenie tempa glikolizy komórkowej (efekt Warburga)[128,145]. Co więcej, komórki nowotworowe zdolne są do własnej produkcji SP w guzie i stopniowo za pomocą mechanizmu wydzielania autokrynnego działanie stymulujące SP zostaje zapętlone [146], sprzyjając mechanizmom progresji złośliwości nowotworu. Równolegle, w sąsiadujących komórkach śródbłonka posiadających ekspresję NK1R, działanie SP również promuje proliferację tych komórek, indukując angiogenezę oraz rozwój guza [147]. Jednocześnie SP w komórkach nowotworowych wykazuje działanie regulatorowe czynników transkrypcyjnych i protoonkogenów [148]. Sprzyja to różnicowaniu się komórek guza, heterogeniczności metabolicznej, progresji cyklu komórkowego oraz syntezie cytokin prozapalnych, tworząc specyficzne mikrośrodowisko wokoło guza, utrudniające skuteczne działania układu odpornościowego.

Patologiczna ekspresja NK1R jest obserwowana w większym stopniu w mniej zróżnicowanych i bardziej zaawansowanych nowotworach [149-151]. Dodatkowo, na powierzchni komórek nowotworowych ekspresja skróconej izoformy NK1R-Tr jest wyższa niż izoformy pełnej długości NK1R-Fl [152-154]. Nadekspresja tej pierwszej koreluje ze złośliwym różnicowaniem się komórek nienowotworowych, zaś wzrost ekspresji NK1R-Fl koreluje z hamowaniem lub ograniczeniem nadmiernej proliferacji i migracji nowotworowej [155,156]. Tak więc propagacja proliferacji

komórek nowotworowych oraz wyłączenie mechanizmów apoptotycznych w tych komórkach sygnalizowane jest przez NK1R-Tr, zaś skuteczna blokada szczególnie skróconej izoformy NK1R prowadzi do śmierci komórek nowotworowych na drodze apoptozy.

Opisane powyżej dane wskazują, że nadekspresja NK1R na powierzchni komórek nowotworowych (a szczególnie skróconej izoformy receptora) może być wykorzystana jako potencjalny marker molekularny do diagnostyki oraz leczenia guzów NK1R-pozytywnych, zaś zahamowanie działania agonistycznego SP może być istotnym działaniem terapeutycznym [153]. Do tej pory nie potwierdzono tych doniesień w badaniach kohortowych, niemniej na wybranych grupach pacjentów onkologicznych zaobserwowano korelację nadmiernej eksprymacji NK1R-Tr lub zwiększoną obecność SP w surowicy wraz z rozwojem cech złośliwości guza i progresji choroby [157]. Przede wszystkim dotyczy to złośliwych nowotworów komórek glejowych, raka piersi, raka rdzeniastego tarczycy, raka jelita grubego i innych części przewodu pokarmowego, nowotworów złośliwych układu hematopoetycznego, raka szyi i głowy, endometrium, nerwiaka zarodkowego, czy raka nabłonkowego jamy ustnej [143,149-152,154-161]. Z drugiej strony, często obserwuje się, że nienowotworowe tkanki sąsiadujące ze zmianami nowotworowymi nie nasilają ekspresji tego markera [157], dzięki czemu uwidacznia się zróżnicowanie guza w organie lub danym rejonie ciała, działając na korzyść celowanych metod terapeutycznych.

2.1.3. Celowana terapia radionuklidowa przy zastosowaniu pochodnych SP

Obecnie, jedyna TRT skierowana wobec receptora NK1 stosowana jest w eksperymentalnej terapii pierwotnych guzów złośliwych tkanki glejowej oraz glejaków wielopostaciowych (wykazujących nadekspresję receptorów NK1) przy zastosowaniu radiofarmaceutyków pochodnych Substancji P [102,162-164].

Większość nowotworów ośrodkowego układu nerwowego to zmiany jednoogniskowe, o przenikliwym charakterze (bez dobrze zdefiniowanych granic guza), naciekające na sąsiadujące struktury nerwowe i zdolne do nawracania w miejscu ogniska [165]. W takich przypadkach podejście chirurgiczne jest wyjątkowo trudne i mało skuteczne, szczególnie we wrażliwym przeżyciowo obszarze mózgu, co sprawia, że najbardziej pożądanymi metodami są te wysoce ukierunkowane. Glejaki o niskim stopniu złośliwości są stosunkowo promieniowrażliwe oraz często wykazują zwiększoną ekspresję SSTR2 (receptor

somatostatyny drugi) [166,167]. Zastosowanie w podaniu miejscowym celowanego radiofarmaceutyku terapeutycznego [^{90}Y]Y-DOTATOC umożliwia zatrzymanie progresji guza oraz redukcję symptomów choroby i dawek przyjmowanych przeciwzapalnych leków sterydowych [168-170]. Jednakże ekspresja receptora SST2 zanika z postępem złośliwości glejaków, co wymusza wytypowanie innego, bardziej specyficznego markera molekularnego. Dodatkowo, rozwiązanie terapeutyczne powinno być wysoce cytotoksyczne, gdyż najbardziej złośliwe guzy tkanki glejowej charakteryzuje umiarkowana promienioczułość, heterogeniczność metaboliczna sprzyjająca skutecznej lekooporności oraz „zamknięte" mikrośrodowisko guza ograniczające dostęp leków z układu krwionośnego.

Do miana efektywnego celu molekularnego we wspomnianym zastosowaniu urasta receptor NK1, rejestrowany w nadekspresji na pierwotnych guzach złośliwych tkanki glejowej oraz glejaków wielopostaciowych [102,157,171], nowotworach o wysokim stopniu złośliwości, z bardzo niewielkim wskaźnikiem przeżywalności. Za sprawą zjawiska nadekspresji NK1R, wspomniane guzy wykazują zdolność do wybiórczej akumulacji znakowanych promieniotwórczo pochodnych SP po podaniu miejscowym do wewnątrzczaszkowej zmiany nowotworowej lub loży po resekcji guza [172]. Aplikacja radiofarmaceutyku przebiega przy użyciu uprzednio wszczepionego operacyjnie systemu portu cewnikowego umożliwiającego iniekcję roztworu preparatu radiofarmaceutycznego wewnątrzczaszkowo [173]. Takie rozwiązanie umożliwia nadzwyczaj korzystną celowalność radiofarmaceutyku w kierunku zmiany nowotworowej (przy ograniczonym unaczynieniu guza), skutkując znaczną redukcją ilości efektów ubocznych terapii w porównaniu do podania ogólnoustrojowego.

Pierwsze próby kliniczne przy użyciu prostego analogu SP, [^{111}In]In-DTPA-[Arg^{1}]-SP, miały miejsce na grupie 12 pacjentów do obrazowania patologicznych zmian grasicy [174]. Radiokoniugat wykazywał mało specyficzny wychwyt narządowy oraz krótki efektywny okres połowicznego zaniku, aczkolwiek umożliwiał obserwację istniejącej patologii. Mimo że niska specyficzność w tym przypadku była akceptowalna dla potrzeb obrazowania molekularnego, taki radiokoniugat nie spełniałby tym samym kluczowych aspektów bezpieczeństwa stawianych radiofarmaceutykom terapeutycznym.

Pierwszymi radiofarmaceutykami terapeutycznymi badanymi *in vivo* wobec glejaków różnych stadiów były najprostsze radiokoniugaty SP z makrocyklicznymi chelatorami DOTA lub DOTAGA, znakowane itrem-90, lutetem-177 lub bizmutem-213, stosowane w podaniu wewnątrzczaszkowym [172,173].

We wstępnych badaniach klinicznych wykazały one wysokie powinowactwo do komórek zmian nowotworowych i umożliwiły skuteczniejszą następczą resekcję chirurgiczną martwej masy guza w porównaniu do resekcji guza bez uprzedniej radioterapii wewnętrznej, lub po terapii przy użyciu [^{90}Y]Y-DOTATOC ukierunkowanej wobec receptorów somatostatyny. Niestety, zastosowane w badaniu radiokoniugaty pochodnych SP cechowały się nieakceptowalną stabilnością w obecności surowicy krwi ludzkiej, co uniemożliwiało stosowania tychże pochodnych jako wektorów radiofarmaceutyków w podaniu dożylnym, a także w niezagojonej, pooperacyjnej loży wewnątrzczaszkowej. Opracowanie pochodnej [Thi^{8},Met(O$_2$)^{11}]SP (zamiana fenyloalaniny na 3-tienyloalaninę w pozycji ósmej oraz utlenienie metioniny na *C*-końcu peptydu) [175-177], umożliwiło otrzymanie radiokoniugatów ([^{111}In]In-/[^{177}Lu]Lu-DOTA/DOTAGA-[Thi^{8},Met(O$_2$)^{11}]SP) o poprawionej stabilności metabolicznej oraz lepszym powinowactwie receptorowym w porównaniu do poprzednich radiokoniugatów pochodnych SP.

Obecnie badaniom klinicznym poddawany jest teranostyczny koncept alfa terapii glejaka wielopostaciowego przy użyciu [^{213}Bi]Bi- lub [^{225}Ac]Ac-DOTA-[Thi^{8},Met(O$_2$)^{11}]SP łącznie z [^{68}Ga]Ga-DOTA-[Thi^{8},Met(O$_2$)^{11}]SP w miejscowym podaniu mieszanki radiofarmaceutyków (Obraz 9.)[162-164,178-181]. Mimo że glejak wielopostaciowy charakteryzuje się niezwykłą agresywnością z minimalnym wskaźnikiem przeżycia, badacze uznają proponowane podejście terapeutyczne za obiecujące, dobrze tolerowane z jedynie łagodnymi i przemijającymi działaniami niepożądanymi [163]. Efekt terapeutyczny widoczny jest w wydłużeniu czasu bez progresji choroby (średnio 2,7 miesiąca dla terapii z ^{213}Bi oraz średnio 2,4 miesiąca dla terapii z ^{225}Ac), wydłużeniu średniej ogólnego czasu przeżycia (23,6 miesiąca od diagnozy i 10,9 miesiąca od nawrotu zmiany dla terapii z ^{213}Bi oraz 35 miesięcy od diagnozy i 13,2 miesiąca od nawrotu dla terapii z ^{225}Ac), oraz w poprawie jakości życia pacjentów. Procedura przygotowania preparatów radiofarmaceutycznych pary teranostycznej jest szybka, wydajna i możliwa do opracowania w postaci gotowych kitów (liofilizatów) do znakowania.

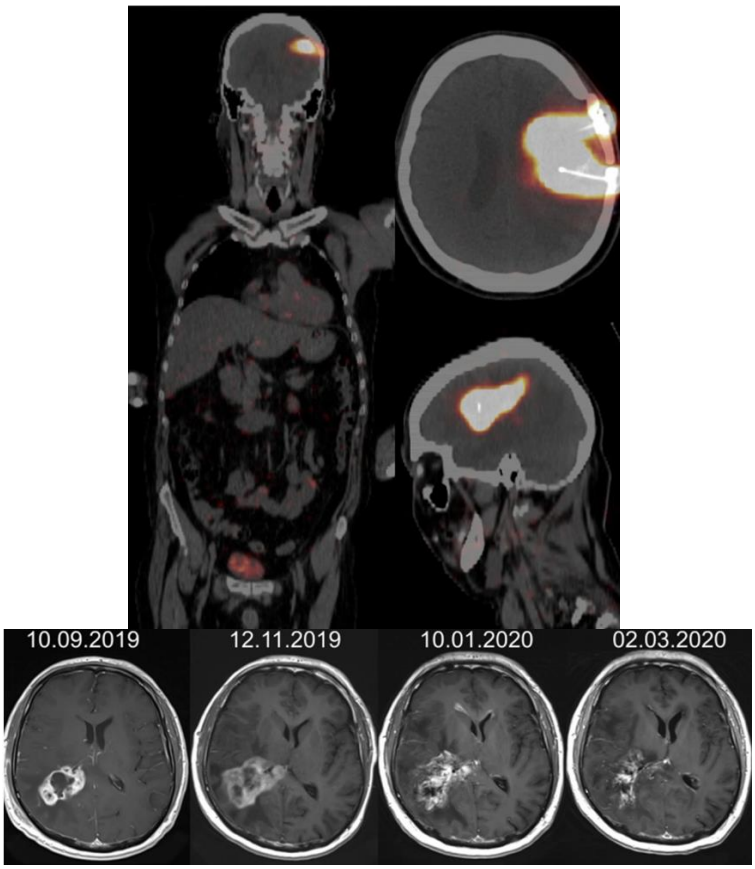

Obraz 9. Wyniki obrazowania PET/CT pacjenta we wszystkich trzech osiach po miejscowym podaniu doczaszkowym 10 MBq [^{68}Ga]Ga-DOTA-[Thi^{8},Met(O$_2$)^{11}]SP wraz z dawką terapeutyczną [^{225}Ac]Ac-DOTA-[Thi^{8},Met(O$_2$)^{11}]SP do loży po resekcji glejaka (obrazy powyżej), a także wyniki obrazowania MRI w płaszczyźnie poprzecznej pacjenta przed podaniem dawki 30 MBq [^{225}Ac]Ac-DOTA-[Thi^{8},Met(O$_2$)^{11}]SP (pierwsze trzy na dole) oraz po terapii (z prawej na dole). Obrazy zapożyczone z pracy przeglądowej [181].

Dane literaturowe wskazują też, że nadekspresja NK1R w glejakach zapewnia odpowiedni marker i cel molekularny, który pozwala na skuteczną terapię celowaną [102,157,172,178]. Stosowany radioterapeutyk powinien swobodnie dyfundować w obrębie guza i przenikać do strefy naciekowej, tak aby mógł dotrzeć nawet do pojedynczych komórek nowotworowych oraz efektywnie wywoływać apoptozę ich maksymalnej ilości. W tym miejscu pojawiają się wątpliwości co do terapii przy użyciu opisanych powyżej radiofarmaceutyków pochodnych SP, gdyż obserwowane efekty terapeutyczne wydają się być niewspółmiernie małe w porównaniu do osiągnięć innych TRT (patrz terapia glejaków SSTR-pozytywnych przy użyciu analogów somatostatyny [168-170] lub Obraz 3. [41,44]). Pierwszym zarzutem przeciwko powyższej terapii jest przede wszystkim ograniczona stabilność wektora radiofarmaceutyków ([Thi^{8},Met(O$_2$)^{11}]SP) w obecności peptydaz surowicy krwi ludzkiej [172,177,182,183], która może być obecna w loży wewnątrzczaszkowej po zabiegu chirurgicznym lub pojawić się

w wyniku dekompresji ciśnienia wewnątrzczaszkowego. Warto też zwrócić uwagę na fakt, że pacjenci z guzem mózgu cierpią na zwiększone ciśnienie wewnątrzczaszkowe (również po zabiegu resekcji), tym samym miejscowa iniekcja preparatu radiofarmaceutycznego jeszcze bardziej nasila ten efekt. Jednocześnie, wysokie ciśnienie mikrośrodowiska guza uniemożliwia efektywną dyfuzję radiofarmaceutyku do komórek nowotworowych oraz dotarcie do celu molekularnego. W przypadku tej terapii, na dyfuzję radiofarmaceutyku wpływ może mieć też lipofilowość substancji czynnej, która dla peptydowego wektora z chelatorem DOTA jest bardzo niska (przykładowo lipofilowość radiofarmaceutyku [^{177}Lu]Lu-DOTA-[Thi^{8},Met(O_2)^{11}]SP wynosi -5,28 [177]). Ostatnią kwestią jest powinowactwo stosowanych radiofarmaceutyków bazujących na pochodnych SP wobec konkretnych izoform receptora NK1R. Rozwojowi złośliwości nowotworu towarzyszy wzrost udziału skróconej izoformy w puli receptorów NK1, wobec której powinowactwo SP (więc także radiofarmaceutyku analogu SP), jest około 10-krotnie niższe niż wobec izoformy NK1R-Fl [102].

Powyższe wątpliwości wskazują, że preferowany radiofarmaceutyk do celowanej terapii NK1R-pozytywnych glejaków wielopostaciowych powinien cechować się pełną stabilnością w warunkach *in vivo* oraz wysokim powinowactwem receptorowym szczególnie wobec skróconej izoformy receptora NK1 [153]. Dodatkowo, powinien też cechować się wyższą lipofilowością niż radiokoniugaty bazujące na pochodnych SP, dzięki czemu dyfuzja substancji czynnej mogłaby być bardziej efektywna. Preferowana byłaby również dożylna aplikacja preparatu, w związku z czym pożądany radiofarmaceutyk powinien być zdolny do przekraczania bariery krew mózg [184], aby dotrzeć do komórek nowotworowych guza. Potencjalnymi wektorami radiofarmaceutyków o opisanych własnościach wydają się być drobnocząsteczkowe antagonisty receptora NK1, przedstawione w następnym rozdziale.

2.2. Niepeptydowe antagonisty receptora NK1

Pobudzający wpływ SP na proliferację nowotworów NK1R-pozytywnych można zahamować blokując dostęp agonisty do receptora przy użyciu antagonistów receptora NK1 [113,129,141]. Jednocześnie niepeptydowe antagonisty NK1R wykazują szerokie działanie przeciwnowotworowe wobec NK1R-pozytywnych linii komórkowych oraz indukują apoptozę tychże komórek nowotworowych [141]. Blokada receptora NK1 u szerokiej gamy komórek nowotworowych skutkuje działaniem antyproliferacyjnym, antyangiogennym oraz hamowaniem efektu

Warburga i migracji komórkowej [141,145]. Jednakże, przeniesienie tych efektów na pole kliniczne do zastosowań u pacjentów stawia wymagania wysoce ukierunkowanego działania oraz braku toksyczności ogólnoustrojowej wobec stosowanej substancji czynnej.

Wyróżnia się dwa rodzaje antagonistów receptora NK1, peptydowe, będące peptydomimetykami zmodyfikowanej cząsteczki SP, lub niepeptydowe, o syntetycznej budowie niepeptydowej. Peptydowe antagonisty NK1R (przykładowo peptydy SPANTIDE [185-187]), to jest analogi lub pochodne SP, zostały odkryte jako pierwsze, na drodze prostych modyfikacji struktury SP. Z uwagi na swoją budowę cechuje je ograniczona stabilność *in vivo* oraz hydrofilowy charakter, ponadto część z nich wykazuje niską selektywność receptorową oraz obserwowalną toksyczność ogólnoustrojową [186,188]. Jak opisano powyżej (rozdział 2.1.3.), wybrane pochodne znalazły zastosowanie w medycynie nuklearnej, aczkolwiek jedynie w ograniczonych warunkach użycia (doświadczalna terapia lokoregionalna).

Niepeptydowe antagonisty NK1R to bardzo liczna i zróżnicowana grupa syntetycznych związków o wysokim powinowactwie do swoistego receptora [189]. Z reguły są to związki o znacznym charakterze lipofilowym, dobrze rozpuszczalne w lipidach, zdolne do przekraczania barier biologicznych (typu bariera krew-mózg), oraz niewrażliwe na działanie peptydaz *in vivo* [189]. Dzięki tym właściwościom (odmiennym od peptydowych antagonistów), niepeptydowe antagonisty receptora NK1 wydają się być wyjątkowo interesujące pod kątem potencjału zastosowania klinicznego w onkologii. Opracowanie pierwszych związków z tej grupy umożliwiło istotne postępy w lepszym zrozumieniu fizjologicznego działania SP i patomechanizmów receptora NK1. Co więcej, część antagonistów wykazuje działanie plejotropowe w ośrodkowym układzie nerwowym (działanie przeciwbólowe, przeciwwymiotne, anksjolityczne, wspomagające przeciwko alkoholizmowi [190-193]) oraz obwodowo (działanie immunoprotekcyjne, przeciwwirusowe i przeciwświądowe [194-196]), aczkolwiek większość z tych efektów trudno przenieść do zastosowań klinicznych [197]. Wyjątkowo ciekawy jest fakt szerokiego działania przeciwnowotworowego *in vitro* tej grupy związków, gdyż wykazują one silną aktywność cytotoksyczną wobec wielu linii rakowych w stosunkowo bezpiecznym zakresie dawek dla nienowotworowych linii komórkowych [141].

Dotychczas opracowane niepeptydowe antagonisty receptora NK1 znalazły zastosowanie w farmakoterapii klinicznej w leczeniu nudności i wymiotów indukowanych chemioterapią lub powikłaniami zabiegów operacyjnych.

US FDA oraz Europejska Agencja Leków zarejestrowały pięć substancji czynnych (aprepitant i jego prolek fosaprepitant, netupitant i jego prolek fosnetupitnant, oraz rolapitant) z grupy antagonistów NK1R w powyższym wskazaniu [198], jednocześnie dostarczając rzetelne dane na temat bezpieczeństwa tych leków. I rzeczywiście, terapia przy użyciu antagonistów NK1R jest wysoce bezpieczna i bardzo dobrze tolerowana przez pacjentów onkologicznych [199,200]. Skojarzenie (i potwierdzenie) powyższych danych na temat bezpieczeństwa oraz plejotropowego działania dostępnych klinicznie antagonistów NK1R zrodziło hipotezę badawczą na temat możliwości przeprofilowania tej grupy związków do nowych zastosowań terapeutycznych ukierunkowanych na specyficzne dla nowotworu zaburzenia molekularne wybranego receptora. Pierwsze badania *in vivo* potwierdziły wspomniane wcześniej liczne działania przeciwnowotworowe niepeptydowych antagonistów NK1R przeciwko poszczególnym rodzajom raka [113,129,141]. *De facto* odkrycia te sugerują, że układ SP i NK1R może odgrywać ważną rolę w przebiegu choroby nowotworowej, a antagoniści receptora NK1 mogą działać jako celowane środki przeciwnowotworowe o szerokim spektrum działania.

W zbiorowej pracy przeglądowej zebrałem i przedstawiłem dane literaturowe na temat istniejących już znakowanych promieniotwórczo antagonistów NK1R, ich właściwości farmakokinetycznych oraz ich zdolności do wizualizacji gęstości receptora NK1 towarzyszącym schorzeniom neurologicznym [1]. Natomiast w niniejszej pracy badawczej położyłem nacisk na możliwości zastosowania antagonistów receptora NK1 w funkcji wektora radiofarmaceutyków umożliwiających celowanie w patologiczną nadekspresję nowotworową wspomnianego receptora. Poniżej zostaną przybliżone dane dotyczące tych spośród niepeptydowych antagonistów NK1R, które były wykorzystane do projektowania potencjalnych radiofarmaceutyków celowanych do zastosowań onkologicznych.

2.2.1. L733,060

L733,060 jest wyjątkowo silnym antagonistą NK1R z grupy pochodnych piperydyny (Obraz 10.). Charakteryzuje się jedną z najniższych wartości stałej inhibicji ludzkiego receptora NK1 (K_i = 0,2 nM)[201] i wartości wypierania SP z kompleksu z NK1R (IC_{50} = 0,87 nM)[189]. Jest jednym z pierwszych antagonistów NK1R zawierających kluczowy dla silnego oddziaływania pierścień *bis*(trifluorometylo)fenylowy, opracowanych przez firmę *Merck, Sharpe and Dohme Ltd.* (obecnie koncern *Merck*)[202]. Związek wykazuje wysoką lipofilowość, jest biodostępny po podaniu doustnym i przenika biologiczną barierę krew-mózg.

W badaniach laboratoryjnych na gryzoniach wykazano plejotropowe działanie L733,060 wynikające z blokowania działania agonistycznego SP, mianowicie działanie przeciwdepresyjne i anksjolityczne [201,203], działanie przeciwwymiotne, działanie przeciwzapalne, analgetyczne, immuno- i neuroprotekcyjne [195,204-207] oraz szerokie działanie przeciwnowotworowe obserwowane *in vitro* [141,153,208]. L733,060 stanowi modelowy związek spośród niepeptydowych antagonistów NK1R, który wraz z opisanymi poniżej L732,138 i aprepitantem, jest regularnie wykorzystywany do ewaluacji zdolności przeciwnowotworowych tej grupy związków.

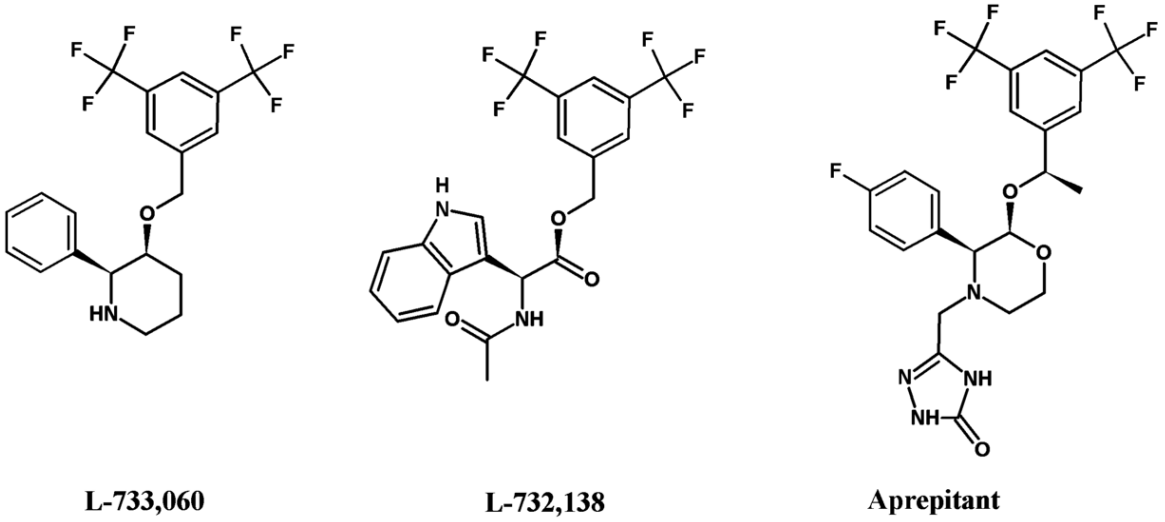

Obraz 10. Struktury wybranych antagonistów receptora NK1.

Dotychczas, L733,060 był wykorzystany jako wektor do otrzymania dwóch typów radiofarmaceutyków diagnostycznych dedykowanych do obrazowania nowotworów NK1R-pozytywnych [209,210]. W pierwszym doniesieniu, L733,060 został skoniugowany z cyklicznym chelatorem NOTA na eterowym łączniku i wyznakowany radionuklidami ^{64}Cu i ^{68}Ga z wysoką wydajnością i aktywnością właściwą. Otrzymany ^{64}Cu-radiokoniugat wykazał pełną stabilność po 30 minutach w mysiej krwi, niewielką lipofilowość (logP = 0,6) oraz wysoką zdolność wiązania *in vitro* do receptora NK1 wrażliwą na obecność blokera. W badaniu PET radiokoniugat L733,060 umożliwił wizualizację NK1R-pozytywnej zmiany nowotworowej, aczkolwiek jednoznaczna diagnostyka była możliwa dopiero po czasie 20 godzin od iniekcji, gdy g*ros* podanej radioaktywności niespecyficznie zgromadzonej w przewodzie pokarmowym i układzie moczowym zostało wydalone. Niemniej, wskazało to na obiecujące możliwości zastosowania radiokoniugatu antagonisty NK1R do celowania w zmianę nowotworową.

W drugim doniesieniu tej samej grupy badawczej [210], L733,060 został skoniugowany z chelatującym ugrupowaniem peptydowym na eterowym łączniku i wyznakowany radionuklidem ^{99m}Tc. W badaniu *in vitro* radiokoniugat zachował selektywne wiązanie do receptora NK1, zaś w badaniu *in vivo* już po 2 godzinach od podania zaobserwowano wyraźny wychwyt radioznacznika. Co istotne, podczas obrazowania SPECT/CT już po 4 godzinach od iniekcji możliwa była dogodna obserwacja zaszczepionego NK1R-pozytywnego guza, wskazując tym samym poprawioną dystrybucję przy użyciu hydrofilowego radiokoniugatu L733,060.

2.2.2. L732,138

L732,138 (Obraz 10.) to pochodna tryptofanu wykazująca silny i selektywny antagonizm wobec ludzkiego receptora NK1 (IC_{50} = 1,6 nM)[211]. Wykazuje ona również działanie analgetyczne neuroprotekcyjne i słabe działanie przeciwalergiczne [205,212-214] oraz szeroko obserwowane działanie przeciwnowotworowe (lecz zauważalnie słabsze niż L733,060 i aprepitantu)[141,153].

Do tej pory nie było w literaturze żadnego doniesienia na temat wykorzystania L732,138 jako wektora dla radiofarmaceutyków radiometalicznych, tym samym w swojej pracy otrzymałem pierwsze radiokoniugaty tego związku dedykowane do obrazowania nadekspresji NK1R oraz porównałem zdolności wiązania do receptora otrzymanych ^{177}Lu-radiokoniugatów tego antagonisty wobec peptydowego ^{177}Lu-radiokoniugatu wektora [Thi^{8},Met(O_2)^{11}]SP [4].

2.2.3. Aprepitant

Niepeptydowym antagonistą ludzkiego receptora NK1 o największej renomie jest aprepitant (MK-869, L754,030, Obraz 10.). Jest to silny, bardzo selektywny i długo działający antagonista NK1R (IC_{50} = 0,09 nM dla wypierania SP z kompleksu z NK1R [189] oraz K_i = 0,28 nM)[201,215]), będący jednocześnie substancją czynną leku Emend o wskazaniu w leczeniu nudności i wymiotów indukowanych chemioterapią lub powikłaniami pooperacyjnymi [216]. Aprepitant jest biodostępny po podaniu doustnym (zaś w formie ufosforylowanego proleku, fosaprepitnatu, biodostępny po podaniu dożylnym [217,218]) i zdolny do penetracji ośrodkowego układu nerwowego, gdzie w obszarze neuronów pola najdalszego (*area postrema*) blokuje odruch wymiotny [219]. Biologiczny okres połowicznego zaniku aprepitantu mieści się w przedziale 9-13 godzin, zaś metabolizm leku przebiega w wątrobie przy udziale enzymów cytochromowych P450, głównie izoenzymu CYP3A4 [200,220]. Struktura aprepitantu bazuje na pierścieniu morfoliny, co znacznie

wzmocniło powinowactwo receptorowe antagonisty NK1R w porównaniu do pochodnych piperydynowych, zaś modyfikacje chemiczne jak fluorowanie pierścienia fenylowego i metylacja pierścienia fenylowego (Obraz 10.) zminimalizowały podatność metaboliczną cząsteczki [221,222].

Poza działaniem przeciwwymiotnym aprepitant wykazuje działanie przeciwzapalne [223,224], przeciwwirusowe [195,225], przeciwkaszlowe [226], przeciwświądowe [196,227,228] i przeciwnowotworowe [141,153]. Podejrzewano także, że aprepitant może być skutecznym lekiem przeciwbólowym [229], przeciwdepresyjnym [112,192,230], aczkolwiek prowadzone badania kliniczne nie dostarczyły wystarczających ku temu dowodów. Co istotne, indeks terapeutyczny aprepitantu jest bardzo wysoki, a incydenty wykazujące działanie toksyczne na skutek przedawkowania leku są rzadko obserwowane. W badaniach klinicznych aprepitant w dawce 300 mg na dobę był dobrze tolerowany przez pacjentów bez istotnych statystycznie różnic w częstości występowania zdarzeń niepożądanych w porównaniu ze stosowaniem placebo [112,200,226]. Podobnie, dawki aprepitantu 1140 mg/dobę przez 45 dni [231], czy podanie dożylne fosaprepitantu w dawce 150 mg były dobrze tolerowane przez pacjentów [218]. Terapii aprepitantem towarzyszyć mogą najczęściej łagodne neurologiczne działania niepożądane, jak bóle i zawroty głowy, czkawka, czy senność po podaniu [200,223,225], aczkolwiek rejestrowano także występowanie mniej powszechnych, łagodnych działań niepożądanych ze strony układu pokarmowego.

Wskutek powyższych, aprepitant wydaje się być doskonałym kandydatem do repozycjonowania leku w procesie poszukiwania nowych strategii leczenia onkologicznego [232], gdyż jest to lek o potencjalnym działaniu przeciwnowotworowym, a jednocześnie stosowany klinicznie, zarejestrowany w innych wskazaniach, o dobrze znanym profilu bezpieczeństwa oraz charakterystyce farmakokinetycznej i metabolicznej [200,220]. Rzeczywiście, w wielu badaniach *in vivo* i *in vitro* aprepitant (i fosaprepitant) wykazał wspomniane wcześniej liczne działania przeciwnowotworowe zależne od dawki przeciwko różnym rodzajom raka poprzez mechanizmy indukowania apoptozy w komórkach nowotworowych [141-144,153,156,171,233]. Aprepitant indukuje apoptozę na drodze bezpośredniego działania antyproliferacyjnego (zmiany szybkości replikacji DNA oraz zatrzymanie cyklu komórkowego [155,234]; wyrzutu jonów wapnia z retikulum endoplazmatycznego do mitochondriów z następczą produkcją mitochondrialnych reaktywnych form tlenu [235]; aktywacji komórkowych mechanizmów apoptotycznych poprzez szlak

zależny od kaspaz [155,234]), hamowania angiogenezy w masie guza [147,153,157], oraz hamowania migracji komórek nowotworowych (w tym także przerzutowania)[134]. Pośrednio, jako antagonista NK1R, aprepitant eliminuje także silny sygnał mitotyczny indukowany przez SP, zaburzając równowagę przeżyciową komórek nowotworowych [153].

Jednocześnie, efekt cytotoksyczny aprepitantu jest wielokrotnie słabszy wobec komórek prawidłowych (bez patologicznej nadekspresji receptora NK1) niż ma to miejsce w przypadku szeregu analizowanych komórek nowotworowych. W badaniach *in vitro* stężenia IC_{100} dla wszystkich dotychczas badanych komórek nowotworowych wynosiły poniżej 80 μM [141,153,154,233], zaś wartości IC_{50} dla prawidłowych komórek kontrolnych zawsze były wyższe, często wielokrotnie wyższe, od wyznaczanych wartości IC_{100} dla komórek nowotworowych [141]. Niemniej dawki aprepitantu stosowane w leczeniu nudności i wymiotów indukowanych chemioterapią lub powikłaniami pooperacyjnymi są zbyt małe, a sama terapia zbyt krótka, aby wywołać skuteczne działanie przeciwnowotworowe [200,231]. Sugeruje się (na podstawie stężenia aprepitantu, które wykazuje działanie przeciwnowotworowe w doświadczeniach *in vitro*), że dawki leku, które mogłyby być skuteczne i jednocześnie bezpieczne w praktyce klinicznej, powinny wynosić 40-50 mg/kg/dzień [141]. Dodatkowo, aprepitant stosowany w skojarzeniu z licznymi chemoterapeutykami (cyklofosfamidem [236], temozolomidem [237], trójtlenkiem arsenu [238], etopozydem, doksorubicyną [239,240], arabinozydem cytozyny [241], cisplatyną [242]) i radioterapią [231,236] wykazuje synergistyczne działanie przeciwnowotworowe lub uwrażliwia na działanie cytotoksyczne umożliwiając optymalizację dawek pod kątem redukcji działań niepożądanych.

W następstwie powyższych danych, stopniowo pojawiają się doniesienia na temat pierwszych przypadków zastosowań klinicznych *off-label* aprepitantu u pacjentów onkologicznych. U pacjentki z inwazyjnym rakiem piersi stopnia drugiego, z przerzutami do mózgu, cierpiącej na nudności i wymioty ustępujące jedynie po zastosowaniu aprepitantu (80 mg/dobę), przedłużono terapię antagonistą NK1R (do 7 miesięcy) i zwiększono dawkę leku (do 120 mg co trzeci dzień)[243]. Dzięki tej terapii zaobserwowano poprawę stanu klinicznego pacjentki, dobrą kontrolę nudności i wymiotów oraz niespodziewaną poprawę poziomu markera nowotworowego CA153, przy braku zgłaszanych skutków ubocznych.

U pacjenta z pojedynczym guzem płaskonabłonkowego raka płuc (8 x 7 cm średnicy) zastosowano przez 45 dni skojarzoną radioterapię (25 sesji naświetlania dawką 50,4 Gy, następnie 8 dodatkowych sesji dawką 65 Gy) przy jednoczesnej

aplikacji 1140 mg/dzień aprepitantu [231]. Po sześciu miesiącach od rozpoczęcia terapii stan pacjenta wyraźnie się poprawił, zaobserwowano zanik obecności guza w badaniu CT oraz zdecydowany zanik wychwytu [^{18}F]FDG w miejscu guza w badaniu PET, przy braku działań niepożądanych ze strony antagonisty NK1R.

Opisy tych dwóch przypadków sugerują, że aprepitant może nie tylko odgrywać rolę środka przeciwwymiotnego w opiece paliatywnej, ale również może być obiecującym chemioterapeutykiem celowanym o szerokim spektrum działania. Antagonisty NK1R charakteryzują się wysoką cytotoksycznością wobec komórek nowotworowych wykazujących patologicznie wysoki poziom skróconej izoformy receptora NK1, izoformy która nie jest nadmiernie eksprymowana w warunkach fizjologicznych na powierzchni komórek prawidłowych [152-154,189,201]. Jednocześnie aprepitant jest wysoce specyficznym i selektywnym antagonistą NK1R, a mimo tego dotychczas nie ukazał się w literaturze żaden artykuł odnośnie zastosowania aprepitantu w formie wektora radiofarmaceutycznego celującego w NK1R-pozytywne zmiany nowotworowe. Z tego względu, w swojej pracy zastosowałem aprepitant jako wektor radiofarmaceutyku do zastosowań celowanych [3,5].

III. CZĘŚĆ PRAKTYCZNA

1. ZAKRES WYKONANYCH BADAŃ

1.1. Otrzymywanie i ewaluacja radiokoniugatów opartych na peptydomimetykach SPANTIDE I

Spośród peptydowych antagonistów NK1R wytypowałem peptydomimetyk SPANTIDE I, [*D*-Arg^{1},*D*-Trp^{7,9},Leu^{11}]SP, jako najbardziej obiecujący związek do zastosowań w formie wektora radiofarmaceutyku. Związek ten wykazuje kluczowe aspekty użyteczności dla wektora radiofarmaceutycznego, mianowicie, zgodnie z danymi literaturowymi korzystne i selektywne powinowactwo wobec receptora NK1 [185] oraz pełną stabilność *in vivo* u ssaków [187]. Jednocześnie zaproponowałem skrócony analog SPANTIDE I(5-11), [*D*-Trp^{7,9},Leu^{11}]SP(5-11), o potencjalnie lepszej zdolności do dyfuzji pomiędzy tkankami, wzorując się na doniesieniach na temat radiokoniugatów skróconego peptydu SP(5-11) [177].

Dla obydwóch peptydomimetyków zsyntezowałem z powodzeniem koniugaty z chelatorem DOTA przyłączonym poprzez *N*-terminalne grupy aminowe α. W przypadku peptydomimetyku pełnej długości otrzymany koniugat zawierał dwie cząsteczki chelatora DOTA przyłączone poprzez *N*-terminalną grupę aminową α oraz grupę aminową ε w łańcuchu bocznym lizyny. Następnie obydwa koniugaty wyznakowałem z wysoką wydajnością radionuklidami ^{68}Ga i ^{177}Lu, uzyskując cztery radiokoniugaty, dla których kolejno wyznaczyłem parametry lipofilowości (wyrażona jako logD, to znaczy logarytm dziesiętny współczynnika dystrybucji wobec fazy *n*-oktanolu i PBS) i stabilności w ludzkiej surowicy (Tabela 5.)[2,244]. Wykazałem pełną stabilność wszystkich czterech radiokoniugatów w trakcie prowadzenia badań, zaś dla obydwóch radiokoniugatów SPANTIDE I(5-11) określiłem także stopień wiązania związków do białkowych składników obecnych w ludzkiej surowicy.

Wyznaczone lipofilowości radiokoniugatów SPANTIDE I(5-11) przyjęły nieznacznie ujemne wartości [2], natomiast w przypadku radiokoniugatów SPANTIDE I, większa liczba aminokwasów w cząsteczce wektora oraz obecność dwóch chelatorów DOTA znacząco obniżyły wartości parametru lipofilowości w porównaniu z tymi wartościami dla radiokoniugatów SPANTIDE I(5-11)[244]. Jednakże te wartości są nadal znacząco wyższe w porównaniu z wartościami

parametrów lipofilowości radiokoniugatów pochodnych SP [177]; uzyskane rezultaty stanowią obiecującą informację z farmakokinetycznego punktu widzenia.

Tabela 5. Zestawienie wyników parametrów fizykochemicznych dla otrzymanych radiokoniugatów peptydomimetyków SPANTIDE I.

Radiokoniugat	Lipofilowość	Stabilność w surowicy
[^{68}Ga]Ga-DOTA- SPANTIDE(5-11)	-0,36 ± 0,02	99,4% po 4 h
([^{68}Ga]Ga-DOTA)$_2$- SPANTIDE	-1,67 ± 0,02	98,9% po 4 h
[^{177}Lu]Lu-DOTA-SPANTIDE(5-11)	-0,19 ± 0,01	99,6% po 14 d
([^{177}Lu]Lu-DOTA)$_2$-SPANTIDE	-1,83 ± 0,03	99,2% po 14 d

Następnie, podjąłem próby wyznaczenia bezpośredniego wiązania receptorowego obydwóch otrzymanych ^{177}Lu-radiokoniugatów do komórek dwóch linii glejaka (U87 MG i U373 MG) oraz linii CHO z transfekowanym genem *TACR1* wykazujących nadekspresję ludzkiego NK1R. Uzyskane wyniki dla obydwóch radiokoniugatów [244] były niepowtarzalne, niejednoznaczne i świadczyły o wątpliwej wiarygodności. Obserwacja ta jest poniekąd zgodna z doświadczeniami prezentowanymi w literaturze, gdzie ilekroć badane było powinowactwo peptydomimetyków SPANTIDE I, wykonywano to na drodze eksperymentów pośrednich (poprzez badanie kompetycyjne z ^{125}I-jodowaną pochodną SP [186] lub pomiar inhibicji wyrzutu jonów wapnia z retikulum endoplazmatycznego [187]), a nie wiązania bezpośredniego.

1.2. Otrzymywanie i ewaluacja radiokoniugatów opartych na L732,138

Równolegle z opracowywaniem radiokoniugatów bazujących na strukturze SPANTIDE I, podjąłem badania oceny zastosowania drobnocząsteczkowych niepeptydowych antagonistów NK1R, w tym L732,138 (Obraz 10.), jako wektora radiofarmaceutycznego [4]. Wybór tego antagonisty został podyktowany wysoką selektywnością i dogodnym powinowactwem L732,138 do ludzkiej formy NK1R oraz optymalną strukturą cząsteczki umożliwiającą funkcjonalizacje radiochemiczne (dołączenie łącznika i części chelatującej radionuklid bez ingerencji we fragment farmakoforowy odpowiedzialny za interakcję z receptorem).

W Zakładzie Neuropeptydów Instytutu Medycyny Doświadczalnej i Klinicznej PAN w ramach wspólnego projektu wykonano analizę modelowania molekularnego przy użyciu homologicznego modelu ludzkiego NK1R (badania wykonane jeszcze przed pojawieniem się dostępnych struktur krystalicznych receptora), co dostarczyło danych, iż ligand L732,138 wiązał się poprzez umiejscowienie się pierścienia 3,5-*bis*(trifluorometylo)fenylowego na samym dole kieszeni wiążącej receptora [4]. U wylotu miejsca wiązania znajdował się fragment *N*-acetylowy, który został wytypowany jako najbardziej dogodne miejsce do funkcjonalizacji i rozbudowy sterycznej liganda bez uszczerbku na powinowactwie receptorowym. Postawiono też hipotezę, że bezpośrednie przyłączenie dużego ugrupowania chelatującego (jak makrocykliczny chelator DOTA) w miejsce fragmentu *N*-acetylowego nie będzie tolerowane ze względu na zawadę steryczną chelatora we wnęce wiążącej receptora. W celu sprawdzenia słuszności postawionej hipotezy wykonana została funkcjonalizacja cząsteczki L732,138 bez użycia łącznika, a także z łącznikami o różnej długości i lipofilowości.

W ramach prac związanych z realizacją mojej pracy doktorskiej zsyntezowałem pięć koniugatów chelatora DOTA z otrzymanymi analogami L732,138 o łącznikach różnej długości [4]. Koniugaty pochodnych L732,138 poddałem znakowaniu radionuklidami ^{68}Ga i ^{177}Lu (dla których otrzymałem również związki referencyjne zawierające stabilny Ga) i dokonałem wyznaczenia właściwości fizykochemicznych i aktywności biologicznej. Otrzymane radiokoniugaty charakteryzowały się nieznaczną lipofilowością (wartości logD zawarte w przedziale od -0,5 do 0,9) oraz ograniczoną stabilnością w ludzkim osoczu (akceptowalną stabilnością do 2 h). Jak pokazuje przykład radiokoniugatów pochodnych SP (rozdział 2.1.3.), nie jest to jednoznacznie dyskwalifikujące, ponieważ potencjalne zastosowanie w terapii miejscowe NK1R-pozytywnego glejaka obejmuje podanie radiofarmaceutyku do loży pooperacyjnej, gdzie, podobnie jak w płynie mózgowo-rdzeniowym, aktywność enzymów surowicy jest bardzo niska [245].

Dalej, ^{177}Lu-radiokoniugaty poddałem ocenie powinowactwa receptorowego uzyskując odpowiedź, że dołączenie chelatora (nawet w sytuacji braku łącznika) nie wpływa negatywnie na zdolność radiokoniugatów do wiązania się z NK1R (rezultat ten został równolegle potwierdzony dla związków referencyjnych zawierających stabilny metal). Co więcej, wykazałem, że ^{177}Lu-radiokoniugaty w badaniu bezpośredniego wiązania komórkowego cechują się podobną lub lepszą charakterystyką wiązania do NK1R aniżeli referencyjny radiokoniugat [^{177}Lu]Lu-

DOTA-[Thi^{8},Met(O_2)^{11}]SP, wcześniej stosowany już eksperymentalnie w praktyce klinicznej. Szczególnie ciekawe okazały się wyniki pojemności wiązania (wartości B_{MAX}) wyższe dla niepeptydowych radiokoniugatów niż dla referencyjnego radiofarmaceutyku, co prawdopodobnie wynika z zastosowania lipofilowego wektora radiokoniugatu.

1.3. Otrzymywanie i ewaluacja radiokoniugatów opartych na aprepitancie

Jednym z najlepiej poznanych i szeroko przebadanych związków z grupy niepeptydowych antagonistów receptora NK1 jest aprepitant (Obraz 10.) będący substancją czynną zarejestrowanego leku Emend o działaniu antyemetogennym (przeciwwymiotnym), wysoce skutecznego leku o korzystnym profilu bezpieczeństwa.

Dla Nas, radiochemików i radiofarmaceutów, struktura APT wydała się interesującym wektorem do projektowania radiofarmaceutyków celowanych do guzów wykazujących nadekspresję NK1R. W tym celu dokonałem ewaluacji zależności pomiędzy aktywnością biologiczną (zdolnością do interakcji z NK1R) a strukturą cząsteczki aprepitantu oraz jego analogów [3]. Na podstawie doniesień literaturowych określiłem kluczowe fragmenty struktury aprepitantu pod względem wysokiego powinowactwa do swoistego receptora, na podstawie czego wybrałem pierścień triazolinonu jako najbardziej racjonalne miejsce w cząsteczce potencjalnie tolerujące określone modyfikacje bez znaczącej utraty powinowactwa receptorowego (moja ocena miejsca modyfikacji aprepitantu okazała się zgodna z później przeprowadzoną analizą modelowania molekularnego [3,5] po opublikowaniu modelu ludzkiego receptora NK1 dostępnego w bazie *Protein Data Bank* pod kodem 6E59 [104]).

Podczas prac laboratoryjnych skupiłem się pierwotnie na otrzymaniu koniugatów aprepitantu z wybranymi chelatorami radionuklidowymi, jednakże bezpośrednia koniugacja wydała się mało optymalnym rozwiązaniem z uwagi na bliskie sąsiedztwo hydrofilowego, masywnego fragmentu chelatora i lipofilowej cząsteczki aprepitantu, co mogłoby negatywnie wpłynąć na zachowanie powinowactwa do NK1R. W związku z tym, zaproponowałem nowatorskie rozwiązanie syntetyczne polegające na dołączeniu do pierścienia triazolinonu łącznika mającego na celu wzajemne odseparowanie przestrzenne wektora i chelatora. Funkcjonalizację cząsteczki zaproponowałem w dwojaki sposób,

poprzez zastosowanie łączników alifatycznych różnej długości posiadających pierwszorzędową grupę aminową na końcu [3,5] oraz zastosowanie łączników acetamidowych (acethydrazydu lub *N*-aminoetylo-acetamidu) również zakończonych pierwszorzędową grupą aminową [3], otrzymując w ten sposób dwie serie pochodnych aprepitantu. Następnie najkrótszą pochodną (aprepitantu z etyloaminą) poddałem koniugacji z czterema wybranymi dwufunkcyjnymi chelatorami radionuklidowymi (DOTA-NHS, DOTA-Bn-SCN, DOTAGA-Bn-SCN i bezwodnikiem DTPA) otrzymując pięć koniugatów najkrótszej pochodnej aprepitantu (w przypadku zastosowanego bezwodnika DTPA do cząsteczki chelatora dołączyłem jedną lub dwie cząsteczki pochodnej aprepitantu otrzymując dwa różne koniugaty). Z uwagi na obserwowaną w dalszych doświadczeniach stabilność wyłącznie dla radiokoniugatów z chelatorem DOTA, jedynie ten chelator zastosowałem do syntezy koniugatów w przypadku wszystkich pozostałych pochodnych aprepitantu. Obydwie serie otrzymanych przez mnie koniugatów wyznakowałem izotopami ^{68}Ga i ^{177}Lu (poza koniugatami DTPA wyznakowanymi jedynie ^{68}Ga). Na przykładzie koniugatu DOTA i pochodnej aprepitantu z oktyloaminą zoptymalizowałem warunki znakowania obydwoma radionuklidami, w celu uzyskania maksymalnej aktywności molowej produktów znakowania. Jednocześnie, stosując do syntezy metale niepromieniotwórcze, otrzymałem dla wszystkich radiokoniugatów związki referencyjne o analogicznej strukturze.

W kolejnym kroku, otrzymane radiokoniugaty wszystkich pochodnych aprepitantu poddałem badaniom fizykochemicznym, mianowicie wyznaczeniu parametru lipofilowości oraz parametru stabilności w surowicy krwi ludzkiej. Dla radiokoniugatów wykazujących pełną stabilność w surowicy krwi ludzkiej zakres lipofilowości obejmował wartości logD w przedziale od -1 do +2.

W celu ewaluacji, czy zaprojektowane radiokoniugaty zachowały wystarczająco wysokie powinowactwo do receptora NK1, wykonałem badanie bezpośredniego wiązania otrzymanych ^{177}Lu-radiokoniugatów aprepitantu na modelu linii komórkowej CHO transfekowanej genem ludzkiego receptora NK1 oraz porównanie charakterystyki wiązania otrzymanych przeze mnie radiokoniugatów wobec ^{177}Lu-radiokoniugatu pochodnej SP, [^{177}Lu]Lu-DOTA-[Thi^{8},Met(O$_2$)^{11}]SP, stosowanej obecnie w eksperymentalnej terapii glejaka wielopostaciowego [5]. Uzyskane wyniki powinowactwa receptorowego radiokoniugatów aprepitantu były równie dobre lub lepsze niż wartość powinowactwa radiokoniugatu [^{177}Lu]Lu-DOTA-[Thi^{8},Met(O$_2$)^{11}]SP, zaś pojemność

wiązania radiokoniugatów pochodnych aprepitantu była znacznie większa niż ten sam parametr radiokoniugatu pochodnej SP.

2. WNIOSKI I PODSUMOWANIE WYKONANYCH BADAŃ ORAZ DALSZE PERSPEKTYWY

W ramach mojej pracy doktorskiej podjąłem próby zaprojektowania i otrzymania odpowiedniego wektora radiofarmaceutycznego do zastosowania w TRT guzów NK1R-dodatnich. Wyniki eksperymentalne przedstawione w poniższych doniesieniach [2-5] jednoznacznie nadają kierunek ku projektowaniu małocząsteczkowych wektorów niepeptydowych kierujących do receptora NK1. Wciąż istnieje przestrzeń do projektowania i wprowadzania nowych rozwiązań klinicznych wobec patologii cechujących się nadekspresją NK1R, pomimo pierwszych sukcesów eksperymentalnego konceptu TRT przy użyciu pochodnych SP.

Otrzymane przez mnie nowe radiokoniugaty oparte na peptydowych antagonistach NK1R SPANTIDE I wykazują satysfakcjonujące właściwości fizykochemiczne do dalszego rozważenia jako potencjalne radiofarmaceutyki, lecz ograniczona możliwość bezpośredniej obserwacji ich wiązania się z receptorem, jednoznacznie podważa użyteczność tych związków w roli radiofarmaceutyków diagnostycznych.

Kolejno, małocząsteczkowy antagonista NK1R L732,138 może być dobrym wektorem radiokoniugatów celowanych, jednakże po rozwiązaniu kluczowej kwestii niestabilności *in vivo*. Mając na względzie przyszłe radiofarmaceutyki do stosowania systemowego, uważam, że należałoby zlokalizować fragment struktury pochodnych L732,138 podatny na działanie składników (peptydaz) surowicy krwi (najprawdopodobniej wiązanie estrowe) i dokonać odpowiednich modyfikacji strukturalnych (przykładowo poprzez zamianę izosteryczną). Dopiero wtedy będzie można wskazać potencjalną użyteczność tego antagonisty NK1R w roli wektora radiofarmaceutycznego do TRT glejaka wielopostaciowego.

Najbardziej perspektywiczne wyniki eksperymentalne otrzymałem dla nowo zaprojektowanych serii radiokoniugatów pochodnych aprepitantu. Wykonane przez mnie badania biologiczne potwierdzają nasze przypuszczenia o użyteczności aprepitantu jako wektora skutecznie celującego do receptora NK1. Nowo otrzymane radiokoniugaty pochodnych aprepitantu spełniają wiele istotnych aspektów dla potencjalnych radiofarmaceutyków, ściśle wymaganych z punktu widzenia

zastosowań klinicznych, mianowicie, wykazują szeroki zakres parametru lipofilowości (wartości znacznie wyższe niż w przypadku radiokoniugatów SP [177]), przy zachowaniu pełnej stabilności w surowicy krwi ludzkiej. Dodatkowo wykazują korzystniejszą charakterystykę wiązania do celu molekularnego *in vitro* w porównaniu do referencyjnego radiokoniugatupochodnej SP, obecnie stosowanej w eksperymentalnej terapii glejaka wielopostaciowego.

W swojej pracy przedstawiłem koncepcję projektowania radiofarmaceutyków na drodze wygodnych modyfikacji struktury aprepitantu, w sposób umożliwiający zachowanie powinowactwa receptorowego związku. Opracowałem koniugaty pochodnych aprepitantu z chelatorem DOTA i zoptymalizowałem znakowanie koniugatów radionuklidami pseudo-teranostycznej pary izotopów ^{68}Ga i ^{177}Lu z wysoką wydajnością radiochemiczną i radioaktywnością molową. Co więcej, zaproponowane modyfikacje struktury aprepitantu pozwalają na koniugacje nie tylko z innymi chelatorami radionuklidowymi (oraz jednocześnie znakowanie innymi radioizotopami), ale także grupami prostetycznymi, chromoforowymi lub fluoroforowymi. Moje wstępne badania nieopublikowanych prac w tym temacie wskazują na szeroki potencjał możliwości projektowania kolejnych związków diagnostycznych bazujących na strukturze aprepitantu.

W związku z tym, że udało mi się wykazać satysfakcjonujące możliwości celowania do NK1R *in vitro* przy użyciu radiokoniugatów opartych na strukturze aprepitantu, nawiązaliśmy współpracę z Zakładem Medycyny Nuklearnej Centralnego Szpitala Klinicznego Warszawskiego Uniwersytetu Medycznego pod kierownictwem prof. dr. hab. Leszka Królickiego, gdzie prowadzona jest eksperymentalna terapia celowana glejaka wielopostaciowego przy użyciu radiofarmaceutyków SP. Wspólnie przygotowujemy niezbędne dane (otrzymaliśmy już pozytywny rezultat badania nietoksyczności na modelu mysim dawki stukrotnie większej niż planowana dawka terapeutyczna) do podjęcia badań celowania do NK1R-pozytywnych zmian nowotworowych u gryzoni oraz pierwszego podania preparatu radiofarmaceutycznego u pacjentów onkologicznych.

3. OPUBLIKOWANE DONIESIENIA NAUKOWE

3.1. ^{68}Ga- and ^{177}Lu-radiopharmaceuticals based on neurokinin-1 receptor antagonist SPANTIDE I (5-11) peptide for glioblastoma multiforme treatment

Halik, P.K.; Gniazdowska, E.; Koźmiński, P.; Majkowska-Pilip, A. 68Ga- and 177Lu-radiopharmaceuticals based on neurokinin-1 receptor antagonist SPANTIDE I (5-11) peptide for glioblastoma multiforme treatment. *W INCT Annual Report 2017* **2017**, 25.

pkt. MNiSW (2022) = 80

Autorzy	Udział
Halik, P.K.	- wykonanie preparatyki syntetycznej; - wykonanie preparatyki radiosyntetycznej; - wykonanie analiz radiochemicznych; - przygotowanie manuskryptu;
Gniazdowska, E.	- koncepcja pracy; - pozyskanie finansowania; - praca nad manuskryptem (2. czytanie);
Koźmiński, P.	- zarządzanie pracą laboratoryjną; - praca nad manuskryptem (1. czytanie);
Majkowska-Pilip, A.	- koncepcja pracy; - praca nad manuskryptem (2. czytanie);

^{68}Ga- AND ^{177}Lu-RADIOPHARMACEUTICALS BASED ON NEUROKININ-1 RECEPTOR ANTAGONIST SPANTIDE I (5-11) PEPTIDE FOR GLIOBLASTOMA MULTIFORME TREATMENT

Paweł Krzysztof Halik, Ewa Gniazdowska, Przemysław Koźmiński, Agnieszka Majkowska-Pilip

Gliomas are extremely serious and aggressive brain tumours in adults. For patients with the most malignant glioma – glioblastoma multiforme (GBM, glioblastoma) the prognosis for survival is 9-12 months. All malignant gliomas are primary brain tumours associated with a high morbidity and mortality due to very difficult treatment regimes. It is caused by the fact that tumour cells are relatively resistant to chemo- and radiotherapy, which is highly damaging to healthy brain tissue. Moreover, an accurate surgical treatment is also ineffective and leads to cancer resumption due to the infiltrating and diffusive character of glioblastoma cells spreading beyond the primary tumour area [1]. Therefore, novel therapeutic strategies are needed for the effective management of GBM.

In the past two decades, targeted glioma therapy has become the subject of extensive scientific reflection and study. The development of biomolecular techniques has allowed the recognition of characteristic tumour cell markers, showing potential for treatment. Many published reports have indicated the participation of the Substance P (SP)-Neurokinin 1 receptor (NK-1R) system in the evolution and metastasis of various neoplasm, including malignant gliomas [2-4].

NK-1R is a seven transmembrane helix protein receptor belonging to the family of G-protein coupled receptors (GPCRs). Its endogenous ligands are tachykinins, from which Substance P shows the highest affinity to the receptor. SP is undeca-neuropeptide (sequence Arg-Pro-Lys-Pro--Gln-Gln-Phe-Phe-Gly-Leu-Met-NH_2) distributed mainly in the nervous system, but also in peripheral tissues. Both SP and NK-1R are responsible for cell proliferation, vasodilation, transmission of pain, endocrine secretion, immune system inflammatory response and modulation of neuronal sensory transmission related to stress, emesis and anxiety. SP is also a mitosis and haematopoiesis regulatory agent [5].

In pathological conditions the NK-1 receptor is upregulated. This fact makes SP with its receptor system a potential target for recognition and diagnosis of many diseases related with an excessive NK-1R stimulation. However, to date, clinical studies have confirmed application effectiveness of one NK-1R antagonist only against nausea and vomiting induced by chemotherapy. NK-1R overexpression is widely presented in a variety of tumour cell lines, also in glioma cancer lines [4, 6]. Preclinical trials proved the feasibility of targeted local radiotherapy based on the SP/NK-1R system. For GBM treatment, studies have been performed using a labelled SP derivative (^{213}Bi--DOTA-[Thi^8,Met$(O_2)^{11}$]-Substance P) proposed in 2010 by Cordier *et al.* [7]. Such treatments were also applied at the Department of Nuclear Medicine, Central Clinical Hospital, Warszawa, in cooperation with the Institute for Transuranium Elements (JRC-ITU, Karlsruhe), where ^{213}Bi/^{225}Ac-DOTA-[Thi^8,Met$(O_2)^{11}$]-Substance P radiopharmaceuticals were examined in patients diagnosed with recurrent critically located GBM. The results of this experiment showed good toleration of the preparation without acute or serious side effects. Although the disease was stabilized, applied radiobioconjugates showed poor migration into the marginal tumour area and instability in blood presence conditions.

To eliminate these disadvantages, we propose a change of biological vector in applied radiopharmaceuticals to the shorter peptide NK-1R antagonist, Spantide I (5-11), SPE (5-11), (sequence Gln--Gln-D-Trp-Phe-D-Trp-Leu-Leu-NH_2). Spantide I is a SP analogue, (D-Arg^1, D-Trp^{7,9}, Leu^{11})SP(1-11) with similar affinity to NK-1 receptor [8]. The shorter peptide was chosen according to our experience with fragments of SP [9], where the radiobioconjugate ^{177}Lu-DOTA-SP(5-11) has showed the highest log P value from analysed compounds. Moreover, Spantide I is more resistant to blood peptidases than SP, because of the replacement of L-amino acids with D-isomers.

In this work we have focused on the labelling of the peptide NK-1R antagonist Spantide I (5-11)

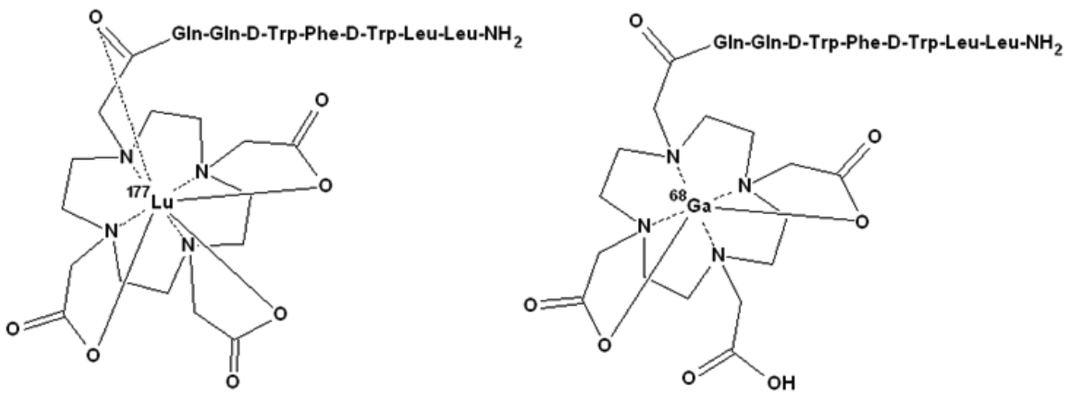

Fig. 1. Structures of the ^{177}Lu-DOTA-SPE (5-11) and ^{68}Ga-DOTA-SPE (5-11) radiobioconjugates.

Table 1. Physicochemical properties of ^{68}Ga-DOTA-SPE (5-11) and ^{177}Lu-DOTA-SPE (5-11) radiobioconjugates.

Radiobioconjugate	log P	Human serum stability [%] (after certain time)	Radiobioconjugate bound to the biomatrix components [%] (after certain time)		
^{68}Ga-DOTA-SPE (5-11)	-0.56 ± 0.02	> 99 (4 h)	8.7 (1 h)	-	11.9 (4 h)
^{177}Lu-DOTA-SPE (5-11)	-0.19 ± 0.03	> 99 (7 d)	5.3 (1 h)	8.3 (2 d)	9.1 (7 d)

with two radioisotopes – ^{68}Ga and ^{177}Lu (Fig. 1), using a macrocyclic chelator DOTA (1,4,7,10-tetraazacyclododecane-1,4,7,10-tetraacetic acid) in the form of active mono-N-hydroxysuccinimide ester (NHS) – DOTA-NHS (1,4,7,10- tetraazacyclododecane-1,4,7,10-tetraacetic acid mono-N-hydroxysuccinimide ester). Our aim was to obtain a novel peptide radiobioconjugate, elaborate on the conditions for effective labelling and examine the stability parameters of the obtained radiobioconjugates.

SPE (5-11) was coupled with DOTA-NHS with addition of Et_3N in DMF at 50°C over night (the molar ratios of reagents were 1 : 1.3 : 4, respectively). Crude DOTA-SPE (5-11) product was purified on a semi-preparative HPLC and lyophilized giving a yield of 60%. MS of DOTA-SPE (5-11): calculated – 1405.63 m/z, found – 1405.73 m/z [M+H$^+$]. The labelling reactions of the obtained bioconjugate were performed according to the following procedures: to the vial containing about 50 μg of lyophilized DOTA-SPE (5-11) in 300 μL of acetate buffer (pH = 5.0), about 100 μL of concentrated $^{68}GaCl_3$ solution (80-100 MBq) from ^{68}Ge/^{68}Ga generator or about 20 μL of $^{177}LuCl_3$ solution in 0.04 M HCl (10-15 MBq) were added. In the ^{68}Ga labelling reaction mixture pH was strictly set below 4.0. Both reactions were performed at 95°C for 30 min and 60 min, respectively, with progress HPLC verification. The radiochemical yield of the synthesized radiobioconjugates was higher than 97%.

The lipophilicity parameters for both radiobioconjugates were determined as the log P values, which are the logarithms of the partition coefficients of each molecule in a biphasic mixture of n-octanol and phosphate buffered saline (pH 7.40). Then the stability studies were performed, where the percentage of the unchanged form of each radiobioconjugate in certain time periods was determined. Experiments included analysis of the stability in human serum verified by the HPLC method with radiometric detection.

All examined radiobioconjugate parameters are presented in Table 1. The lipophilicity values of both molecules of interest are slightly negative (-0.56 and -0.19 for ^{68}Ga and ^{177}Lu, respectively). These values, compared to the lipophilicity parameters of radiobioconjugates based on SP and its fragments [9], are significantly higher; this is promising from a pharmacokinetic point of view. Moreover, the presented radiobioconjugates showed total stability in human serum for the entire duration of the experiments (4 h and 7 d for ^{68}Ga and ^{177}Lu, respectively), verified by the radiometric chromatograms (Fig. 2).

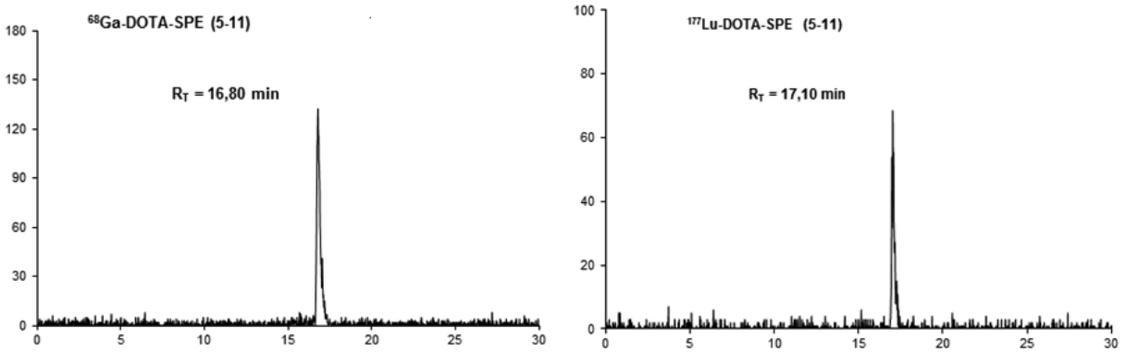

Fig. 2. Radiometric chromatograms of liquid phases of ^{68}Ga-DOTA-SPE (5-11) and ^{177}Lu-DOTA-SPE (5-11) radiobioconjugates in human serum solution after 4 h and 7 d, respectively. HPLC conditions: Phenomenex Jupiter Proteo semi-preparative column (4 μm, 90 Å, 250 mm × 10 mm), γ detection; elution conditions: solvent A – water with 0.1% TFA (v/v); solvent B – acetonitrile with 0.1% TFA (v/v); gradient: 0-20 min 20 to 80% of B, 20-35 min 80% solvent B; 2 ml/min.

Considering ligand exchange, reactions with amino acids or other strongly competing natural ligands present in human serum did not take place. In the case of stability studies in human serum, we have measured the radioactivity of precipitated matrix proteins (using ethyl alcohol) and the supernatant fractions. A few percent of ^{68}Ga/^{177}Lu-DOTA-SPE (5-11) molecules were shown to be bound by the biomatrix components, while the rest of the studied radiobioconjugates remained in the liquid phase in an unchanged form.

In conclusion, we have obtained novel ^{68}Ga- and ^{177}Lu-radiobioconjugates based on peptide antagonist of NK1 receptor. Both examined molecules showed promising physicochemical properties for further consideration as potential radiopharmaceuticals for glioblastoma multiforme treat-

ment, competitive to presently applied methods in oncology.

The presented work was financially supported by the statutory activity of the Institute of Nuclear Chemistry and Technology (INCT).

References

[1]. Ramirez, Y.P., Weatherbee, J.L., Wheelhouse, R.T., & Ross, A.H. (2013). Glioblastoma multiforme therapy and mechanisms of resistance. *Pharmaceuticals*, *6*, 1475-1506. DOI: 10.3390/ph6121475.

[2]. Palma, C., Nardelli, F., Manzini, S., & Maggi, C.A. (1999). Substance P activates responses correlated with tumour growth in human glioma cell lines bearing tachykinin NK1 receptors. *Br. J. Cancer*, *79*(2), 236-243. DOI: 10.1038/sj.bjc.6690039.

[3]. Munoz, M., Covenas, R., Esteban, F., & Redondo, M. (2015). The substance P/NK-1 receptor system: NK-1 receptor antagonists as anti-cancer drugs. *J. Biosci.*, *40*, 441-463. DOI: 10.1007/s12038-015-9530-8.

[4]. Palma, C., & Maggi, C.A. (2000). The role of tachykinins via NK_1 receptors in progression of human gliomas. *Life Sci.*, *67*, 985-1001. DOI: 10.1016/S0024--3205(00)00692-5.

[5]. Garcia-Recio, S., & Gascón, P. (2015). Biological and pharmacological aspects of the NK1-receptor. *BioMed Res. Int., 2015*, Article ID 495704. DOI: 10.1155/2015/495704.

[6]. Covenas, R., & Munoz, M. (2014). Cancer progression and substance P. *Histol. Histopathol.*, *29*, 881-890. DOI: 10.14670/HH-29.881.

[7]. Cordier, D., Forrer, F., Bruchertseifer, F., Morgenstern, A., Apostolidis, C., Good, S., Müller-Brand, J., Mäcke, H., Reubi, J.C., & Merlo, A. (2010). Targeted alpha--radionuclide therapy of functionally critically located gliomas with ^{213}Bi-DOTA-[Thi^{8},Met$(O_2)^{11}$]-substance P: a pilot trial. *Eur. J. Nuc.l Med. Mol. Imaging*, *37*(7), 1335-1344. DOI: 10.1007/s00259-010-1385-5.

[8]. Folkers, K., Hakanson, R., Horig, J., Jie-Cheng, X., & Leander, S. (1984). Biological evaluation of substance P antagonists. *Br. J. Pharmacol.*, *83*(2), 449-456. DOI: PMC1987101.

[9]. Majkowska-Pilip, A., Gniazdowska, E., Koźmiński, P., Wawrzynowska, A., Budlewski, T., & Kostkiewicz, B. (2016). On the syntheses and evaluation of substance P fragments labelled with ^{99m}Tc and ^{177}Lu as potential receptor radiopharmaceuticals in glioma treatment. In *INCT Annual Report 2016* (pp. 35-39). Warszawa: Institute of Nuclear Chemistry and Technology.

3.2. The Significance of NK1 Receptor Ligands and Their Application in Targeted Radionuclide Tumour Therapy

Majkowska-Pilip, A.; **Halik, P.K.;** Gniazdowska, E. The Significance of NK1 Receptor Ligands and Their Application in Targeted Radionuclide Tumour Therapy. *Pharmaceutics* **2019**, *11*, 443. DOI: 10.3390/pharmaceutics11090443

IF (2019) = 4,421; pkt. MNiSW (2022) = 100

Autorzy	Udział
Majkowska-Pilip, A.	- koncepcja pracy; - napisanie paragrafu 3.1. Radiolabelled NK1R Agonists for Targeted Radionuclide Tumour Diagnosis; - napisanie paragrafu 3.2. Radiolabelled NK1R Agonists for Targeted Radionuclide Tumour Therapy; - praca nad manuskryptem (1. czytanie);
Halik, P.K.	- napisanie paragrafu 2.2. Application of NK1R Antagonists; - napisanie paragrafu 3.3. Antagonist Radioligands of NK1R for Targeted Radionuclide Imaging; - przygotowanie Figur 3., 4., 5., 9.; - formatowanie tekstu; - praca nad manuskryptem (1. czytanie);
Gniazdowska, E.	- koncepcja pracy; - napisanie paragrafu 1. Introduction; - napisanie paragrafu 2.1. Significance of NK1R Agonists; - praca nad manuskryptem (2. czytanie);

pharmaceutics

MDPI

Review

The Significance of NK1 Receptor Ligands and Their Application in Targeted Radionuclide Tumour Therapy

Agnieszka Majkowska-Pilip *, Paweł Krzysztof Halik and Ewa Gniazdowska

Centre of Radiochemistry and Nuclear Chemistry, Institute of Nuclear Chemistry and Technology, Dorodna 16, 03-195 Warsaw, Poland

* Correspondence: a.majkowska@ichtj.waw.pl; Tel.: +48-22-504-10-11

Received: 7 June 2019; Accepted: 16 August 2019; Published: 1 September 2019

Abstract: To date, our understanding of the Substance P (SP) and neurokinin 1 receptor (NK1R) system shows intricate relations between human physiology and disease occurrence or progression. Within the oncological field, overexpression of NK1R and this SP/NK1R system have been implicated in cancer cell progression and poor overall prognosis. This review focuses on providing an update on the current state of knowledge around the wide spectrum of NK1R ligands and applications of radioligands as radiopharmaceuticals. In this review, data concerning both the chemical and biological aspects of peptide and nonpeptide ligands as agonists or antagonists in classical and nuclear medicine, are presented and discussed. However, the research presented here is primarily focused on NK1R nonpeptide antagonistic ligands and the potential application of SP/NK1R system in targeted radionuclide tumour therapy.

Keywords: neurokinin 1 receptor; Substance P; SP analogues; NK1R antagonists; targeted therapy; radioligands; tumour therapy; PET imaging

1. Introduction

Neurokinin 1 receptor (NK1R), also known as tachykinin receptor 1 (TACR1), belongs to the tachykinin receptor subfamily of G protein-coupled receptors (GPCRs), also called seven-transmembrane domain receptors (Figure 1) [1–3]. The human NK1 receptor structure [4] is available in Protein Data Bank (6E59). Tachykinins, widely distributed within the central (CNS) and peripheral (PNS) nervous system, are small bioactive neuropeptides which share a conserved C-terminal pentapeptide sequence, Phe-X-Gly-Leu-Met-NH_2. Examples of these neurotransmitters belonging to the tachykinin group include Substance P (SP), the first neuropeptide discovered in mammals [5], neurokinin A (NKA) and neurokinin B (NKB). These compounds listed above are the preferential ligands for NK1, NK2 and NK3 receptors, respectively, although they can bind additional NK receptors with varying affinity [6].

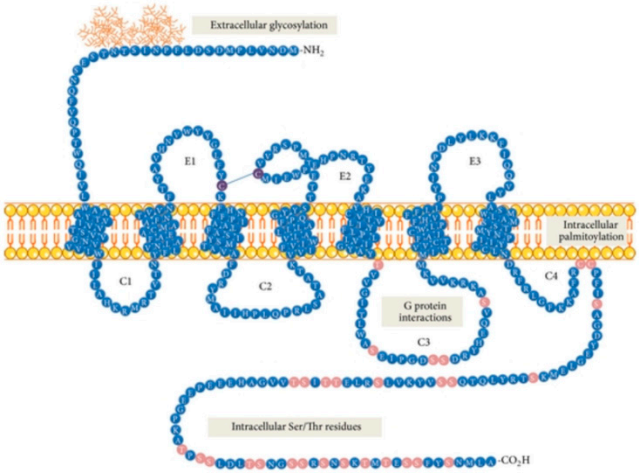

Figure 1. Schematic model of NK1 receptor of full length isoform (NK1R-Fl) [3].

Within the neurokinin receptor family, there are three pharmacologically distinct receptor subtypes: NK1R (TACR1, SPR), NK2R (TACR2) and NK3R (TACR3) [7–9]. NK1R is widely expressed in both the CNS and PNS, whereas NK2R is preferentially expressed in PNS [9]. NK1R contains 407 amino acids, and NK2R and NK3R (the longest one) consist of 398 and 465 amino acids, respectively [3]. NK1R exists in two isoforms, as a full-length peptide (NK1R-Fl, Figure 1) and in the truncated isoform (NK1R-Tr), containing 311 amino acids (96 amino acids less at the C-terminus) [3]. NK1R displays two nonstoichiometric binding sites, the more abundant NK-1M ("majority"—representing 80–85% of the total receptor population) and NK-1m ("minority"—so-called "septide sites" or "septide-sensitive") defined according to the different binding potencies of SP and its analogues [10–14]. NK1R contains an extracellular N-terminus, three extracellular loops (E1, E2 and E3), seven transmembrane domains, three intracellular loops (C1, C2 and C3, as well as a possible C4 loop) and an intracellular C-terminus.

The wide overexpression of NK1R in various human organs has led to successful development of highly selective agonists and antagonists of this receptor for the treatment of various diseases [8]. Some NK1R ligands, for example SP, its analogues and derivatives, have been investigated in preclinical and clinical studies. Moreover, based on high density of transmembrane NK1Rs on human cancer cells, new therapeutic approaches involve the use of radiolabelled NK1R ligands in targeted radionuclide tumour therapy [2,15–17].

The aim of this review is to discuss data from recent literature concerning the chemical and biological aspects of natural and synthetic NK1R ligands in classical and nuclear medicine, with a specific focus on targeted radionuclide therapy.

2. NK1R Ligands in Classical Medicine

2.1. Significance of NK1R Agonists

The endogenous peptide ligands of NK1R are tachykinins, a large family of neuropeptides produced by neuronal and glial cells [5,18]. These compounds play an important role in nociception, synaptic transmission (as excitatory neurotransmitters) and neuroimmunomodulation. They have a variety of effects on physiological and pathological conditions, as well as intrinsic neuroprotective and neurodegenerative properties [19]. The tachykinin family is characterized by a common C-terminal 5-amino-acid sequence Phe-X-Gly-Leu-Met-NH_2, where X is either an aromatic (Phe or Tyr) or a branched chain aliphatic (Val or Ile) amino acid residue [19–21].

The most widespread and tested agonistic peptide ligand of NK1R is human endogenous undecaneuropeptide Substance P (Arg-Pro-Lys-Pro-Gln-Gln-Phe-Phe-Gly-Leu-Met-NH_2, SP(1–11), SP, [Arg^1]SP, Figure 2). At physiological pH, SP characteristically holds a positive charge on N-terminal amino acid residues. The C-terminus contains hydrophobic residues providing the SP peptide with

an amphiphilic character [22]. The interaction between SP and NK1R results in internalisation of the membrane-bound complex, via a clathrin-dependent mechanism, to the acidified endosomes, where the complex disassociates [8,22–24].

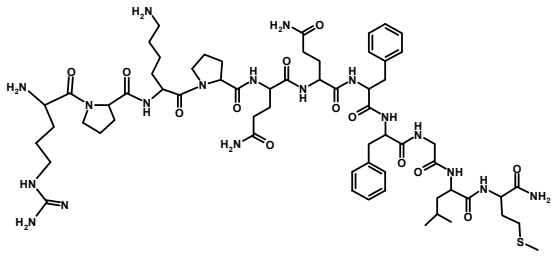

Figure 2. Structure of Substance P(1–11).

The SP fragment responsible for NK1R affinity is a five amino acid sequence, Phe^{7}–Phe^{8}–Gly^{9}–Leu^{10}–Met^{11}, located at the C-terminus of the peptide [21,25,26]. Tachykinins are degraded by neutral endopeptidases (NEPs) and the angiotensin-converting enzyme (ACE) [27]. The half-life of SP ranges from seconds to 1.5 h in blood and tissues, while in extracted plasma SP is stable for hours [22]. In the biodegradation process the SP metabolites, SP(1–4), SP(1–5), SP(1–6), SP(1–7), SP(8–9) and SP(10–11), can form as a results of enzymatic peptide cleavage at different sites [19,21,27–37]. Typical cleavage points are Lys–Arg, Arg–Arg and Arg–Lys doublets [19]. SP and NK1R are widely distributed in the CNS and PNS. SP mediates neural–immune/hematopoietic cross-talk [20] in the brain, and has specifically been isolated from the brain regions which regulate emotion (hypothalamus, amygdala and the periaqueductal gray) [19,28]. Additionally, SP plays an important role in the aetiology of many diseases [22]. It is thought that SP has a role in the regulation of depression and anxiety, emesis, pain, asthma, psoriasis, inflammatory bowel disease and in diseases of the CNS, including migraines and schizophrenia. The inhibition of NK1R stimulation via NK1R-specific secondary messenger pathways may be a useful in treatment in a variety of diseases. Concise information concerning the biological activity and the potential application of SP, its analogues and derivatives in medicine are presented in Table 1.

Multiple groups have recently published research concerning SP and its analogues or derivatives as agonistic or antagonistic peptide NK1R ligands [7,8,19,21,38–65]. New unnatural peptides are designed in order to improve their biological properties (e.g., half-life, receptor affinity and lipophilicity). Moreover, appropriate modifications can give peptides specific properties (e.g., photoactivation) or allow labelling with iodine radioisotopes or with other diagnostic/therapeutic radionuclides. NK1R has also been identified on various cancer cells, including astrocytoma, neuroblastoma, melanoma, and pancreatic cancer cells. NK1Rs have been implicated in tumour tissue growth and SP contributes to cancer volume increase, angiogenesis, proliferation and metastasis [5,49,50]. The authors of the patent "Radiolabeled conjugates based on substance P and the uses thereof" examined about ten different SP radiolabelled analogues (Table 2) in order to select optimal analogues in terms of stability and receptor affinity [53]. Endogenous SP is a potent vasodilator [54] and this action limits the application of SP-derived medical preparations.

Table 1. Substance P, its analogues and derivatives: biological activity and potential application in classical medicine.

NK1R ligands	Ligand Biological Properties and Applications	References
Mammalian NK1R ligands		
Substance P (SP, SP(1–11), [Arg^1]SP)	• Phosphatidylinositol signal pathway activation and intracellular calcium concentration increase; • Treatment of depression and associated anxiety; • Prevention of vomiting after anaesthesia or chemotherapy; • Increase of endothelial ion transport and permeability of vessels in tissue inflammation states; • Neuropathic pain modulation; • Liver cirrhosis biomarker; • Bone tissue metabolism modulator, especially of osteoblast activity at a later stage of bone formation;	[20] [38] [39,40] [41–44] [45] [46–48] [47,48]
Arg^1-Pro^2-Lys^3-Pro^4-Gln^5-Gln^6-Phe^7-Phe^8-Gly^9-Leu^{10}-Met^{11}-NH_2	• Cancer growth promotor (astrocytoma, melanoma, neuroblastoma, pancreatic cancer), angiogenesis, migration and metastasis;	[5,49,50]
(Figure 2)	• Study of the synergistic effect of SP and insulin-like growth factor 1 (IGF-1) on corneal epithelial wound healing – synergistic effect possible only in the presence of the SP fragment containing minimum C-terminus 4 amino acids, SP(8–11);	[51]
[Thi^8,$Met(O_2)^{11}$]SP Pro^4-Gln^5-Gln^6-Phe^7-Thi^8-Gly^9-Leu^{10}-$Met(O_2)^{11}$-NH_2	Treatment of recurrent and critically located glioblastoma multiforme;	[55]
[Sar^9,$Met(O_2)^{11}$]SP(1–11) and **(Sendide)** **[Tyr^6,D-Phe^7,D-His^9]SP(6–11)**	Studies of the role of NK1R in regulation and release of vasopressin peptide;	[56,57]
(X)Arg^1-Pro^2-Lys^3-Pro^4-Gln^5-Gln^6-Phe^7-Phe^8-Gly^9-Leu^{10}-Met^{11}-NH_2 (1) or Arg^1-Pro^2-(X)Lys^3-Pro^4-Gln^5-Gln^6-Phe^7-Phe^8-Gly^9-Leu^{10}-Met^{11}-NH_2 (1)	Studies of photoactivatable SP derivatives;	[59]
$Bapa^0$[(pBzl)PheX]SP (2) **$Bapa^0$[Pro^9,(pBzl)Hcy$(O_2)^{11}$]SP** (2) **$Bapa^0$[Hcy(ethylaminodansyl)^{11}]SP**	Studies of activation of different second messenger pathways as a result of ligand binding to various NK1Rs sites; studies of dual behaviour of the tested SP derivatives: as antagonists at the NK-1M binding site activating AC pathway or agonists at the NK-1m binding site activating PLC pathway;	[10]
Septide [$pGlu^6$,Pro^9]SP(6–11) $pGlu^6$-Phe^7-Phe^8-Pro^9-Leu^{10}-Met^{11}-NH_2	Agonist as potent as SP in eliciting smooth muscle contraction, however poor competitor of SP due to interaction with another binding site of NK1R (NK-1m, so-called 'septide-sensitive');	[7,60]
GR 73,632 $NH_2(CH_2)_4C(O)$-Phe^7-Phe^8-Pro^9-(Me)Leu^{10}-Met^{11}-NH_2	Approximately 200-fold more potent than SP in inducing the characteristic behavioural response in murine models.	[61]
Non-mammalian NK1R ligands		
Physalaemin Pyr^1-Ala^2-$Asp(OH)^3$-Pro^4-$Asp(NH_2)^5$-Lys^6-Phe^7-Tyr^8-Gly^9-Leu^{10}-Met^{11}-NH_2	Stimulation of extravascular smooth muscles, component of eye drops for Sjögren syndrome treatment and other forms of keratoconjunctivitis sicca;	[3,19,62,63]
Eledoisin $pGlu^1$-Pro^2-Ser^3-Lys^4-Asp^5-Ala^6-Phe^7-Ile^8-Gly^9-Leu^{10}-Met^{11}-NH_2	Similar biological activities as Physalaemin but slightly less active and more stable *in vivo*; clinical trials for limb arteriosclerosis treatment; component of eye drops for Sjögren syndrome;	[19,63]
Sialokinin I Asn^2-Thr^3-Gly^4-Asp^5-Lys^6-Phe^7-Tyr^8-Gly^9-Leu^{10}-Met^{11}-NH_2 **Sialokinin II**, Asp^2-Thr^3-Gly^4-Asp^5-Lys^6-Phe^7-Tyr^8-Gly^9-Leu^{10}-Met^{11}-NH_2	Vasodilation, effect on salivation, influence on the acinar cells of the submandibular glands.	[3,64,65]

(1) X = p-benzoylbenzoic moiety; (2) Bapa = biotinyl sulfone-5-aminopentanoic acid; Bzl = benzyl; Hcy = homocysteine; $HcyO_2$ = homocysteine sulfone.

Table 2. The IC_{50} values determined for SP and various radiobioconjugates based on SP analogues [53].

Substance	IC_{50} ± SEM [nM]
Substance P	2.7 ± 0.22
^{111}In-DOTAGA-Substance P	1.1
^{111}In-DOTAGA-[Met$(O_2)^{11}$]-Substance P	9.8 ± 1.00
^{111}In-DOTA-[Met$(O_2)^{11}$]-Substance P	3.55 ± 0.45
^{111}In-DOTA-[Sar^9]-Substance P	3.20 ± 0.30
^{111}In-DOTA-[Thi^8]-Substance P	7.30 ± 2.00
^{111}In-DOTA-[Thi^7]-Substance P	9.40 ± 1.60
^{111}In-DOTA-[Sar^9,Met$(O_2)^{11}$]-Substance P	2.00 ± 0.00
^{111}In-DOTA-[Thi^8,Met$(O_2)^{11}$]-Substance P	0.78 ± 0.03
^{111}In-DOTA-[Thi^8,Sar^9]-Substance P	3.40 ± 0.40
^{111}In-DOTA-[Thi^7,Thi^8]-Substance P	7.70 ± 0.70

The autoradiography studies carried out on tumour tissues expressing NK1Rs revealed that ^{111}In-DOTA-[Thi^8,Met$(O_2)^{11}$]SP radiobioconjugate exhibited the highest affinity to examined receptors, therefore the SP analogue [Thi^8,Met$(O_2)^{11}$]SP was used in further development for the synthesis of radiopharmaceuticals applied in medicinal experiments for recurrent, critically located glioblastoma multiforme (GBM) [55].

The SP derivatives agonistic ligand [Sar^9,Met$(O_2)^{11}$]SP(1–11) and antagonistic ligand [Tyr^6, D-Phe^7, D-His^9]SP(6–11) (Sendide), along with others, were recently used to examine the role of NK1R in regulation and release of vasopressin peptide (AVP) from neurohypophysis [56,57]. Notably, it has been reported that replacement of L-amino acid by D-amino acid in the peptide results in antagonizing effects [21,58]. Numerous SP analogues (Table 1) with agonistic or antagonistic properties towards SP have been designed based on results of structure activity relationship (SAR) studies.

There are also non-mammalian NK1R ligands belonging to the tachykinin family. These compounds have distinctly different structure from SP, however in COOH-terminal region they have similar pentapeptide sequence Phe-(Tyr/Ile)-Gly-Leu-Met-NH_2 (often referred as the "message domain") [8,19,62–65] (Table 1). The non-mammalian tachykinins display the same spectrum of activity as the mammalian tachykinins and bind to the same receptors.

Taking into account the above information, it can be concluded that the measurement of the level of NK1Rs agonists (SP and its analogues), may be used as a diagnostic probe to inform about disease state. Nevertheless, literature shows the results of using NK1R agonists in application as drug active substances [19] (Table 1). Despite the existence of several examples of the use of NK1R agonists in therapy, it is anticipated that antagonists will be much more effective therapeutics.

2.2. Application of NK1R Antagonists

Despite the wide expression of the NK1R and the implication of SP in physiological regulation, NK1R antagonists remain infrequent in clinical use. Among NK1R antagonists aprepitant (MK-869, L-754,030) has been used to prevent of chemotherapy-induced nausea and vomiting (CINV) and obtained market registration (Emend®, Merck) by United States Food and Drug Administration (US FDA) and European Medicines Agency (EMA) in 2003 [3,40,66]. Application in patients during moderate and acute emetogenic chemotherapy (e.g., cisplatin, doxorubicin or cyclophosphamide) was broadened by postoperative nausea and vomiting (PONV) indication two years after registration. In 2008, fosaprepitant (Ivemend®, Merck), an intravenous prodrug of aprepitant, obtained FDA and EMA approvals. Aprepitant regimen [67–69] shows significantly higher response rates in CINV patients than the standard therapy (5-HT_3R antagonist ondansetron combined with corticosteroid dexamethasone). The antiemetic effect of aprepitant was reported to be due to the inhibition of high density NK1R brainstem regions (the area postrema and the nucleus solitarius) involved in the vomiting reflex [3]. Although aprepitant treatment is well tolerated, there may occur some gastrointestinal track and CNS mild adverse effects. This NK1R antagonist, importantly, is an inhibitor and inductor of xenobiotic metabolism fundamental cytochromes CYP3A4 and CYP2C9, respectively [67,70]. It is

worth to keep in mind that aprepitant may affect the plasma concentration of many chemotherapeutics and dexamethasone (or other narrow therapeutic margin drugs like warfarin).

Additionally, in the CINV prevention, other NK1R antagonists have been evaluated, but only three obtained market authorization [71–75]. Rolapitant (Varubi® or Varuby®, Tesaro) received FDA and EMA approvals in human application, maropitant (Cerenia®, Zoetis and Prevomax®, Le Vet) received approval for the prevention of acute vomiting or vomiting due to motion sickness in veterinary clinics. Finally, netupitant, used in combination with the 5-HT_3R antagonist palonosetron, also received approval for human use (Akynzeo®, Helsinn Birex). Casopitant (Rezonic® or Zunrisa®, GlaxoSmithKline) nearly received approval, but GlaxoSmithKline withdrew its EMA authorization proposal following further safety assessments.

Many NK1R antagonists were explored as potentially therapeutic agents during early phase clinical trials [75–79]. A number of these were found ineffective or insignificantly useful in the treatment of major depressive disorder, depression, social anxiety, phobias, post-traumatic stress disorder, insomnia, schizophrenia, cannabis and opioid dependency, irritable bowel syndrome and overactive bladder, hot flashes, tinnitus and hearing loss, migraines, and painful diabetic polyneuropathy, and synergistically in antiviral HIV-1 therapy. Nevertheless, in a few studies of the NK1R antagonists, these compounds were revealed to be active in comparison to the placebo control. These successful reports refer to treatment of alcohol dependency (LY-686,017 case [80]) or chronic pruritus (aprepitant and serlopitant cases [81,82]).

On the other hand, great expectations are arising from the application of NK1R antagonists for the targeted treatment of malignant tumours. The antitumour action of NK1R antagonists (Table 3) was demonstrated in vitro on multiple human cell lines overexpressing NK1R as well as through in vivo research in xenograft murine models [2,16,17,83–98].

Table 3. Anticancer effects of three most studied NK1R antagonists.

NK1R Antagonists	Anticancer Effect	References
Aprepitant	Tumour cell growth inhibition	[2,16,17,83–98]
	Tumour cell migration and proliferation inhibition	[2,16,17,83–98]
L-733,060	Apoptotic action on cells	[2,16,17,85–98]
	Tumour size/volume decrease	[2,86,91,93–96]
L-732,138	Inflammation state inhibition	[2,93,95,96]
	Angiogenesis decrease	[2,16,86,91,93,95,96]
(Figure 3)	Antiproliferative effect	[2,16,86,91,93–96]
	Metastases prevention	[2,86,91,93,95,96]

Recent studies refer to high specific antagonist nonpeptide agents, which efficiently compete with the SP/NK1R pathway. Despite structural differences of the presented antagonists (Figure 3), all cause direct receptor blockage correlated with a broad spectrum of anticancer effects. This pleiotropic activity may be highly valuable in terms of tumour treatment. Several NK1R ligands are also effective antiemetic agents. This is the case with aprepitant, the most studied NK1R antagonist with well-known pharmacokinetic and safety characteristics [2,15,39,66–69,78,99]. Alternatively, NK1R peptide ligand cyclosporine A, a commonly used immunosuppressive drug, also shows antitumour activity by binding to NK1R, as was demonstrated on various cancer cell lines [100,101].

Taken together, these reports suggest that NK1R antagonists may exert a wide range of potential therapeutic actions which may expand their clinical application. Despite the fact that there have been no oncological clinical trials executed to date to verify reported data, NK1R antagonists may prove to be a significant advance in the development of specific targeted antitumour therapy.

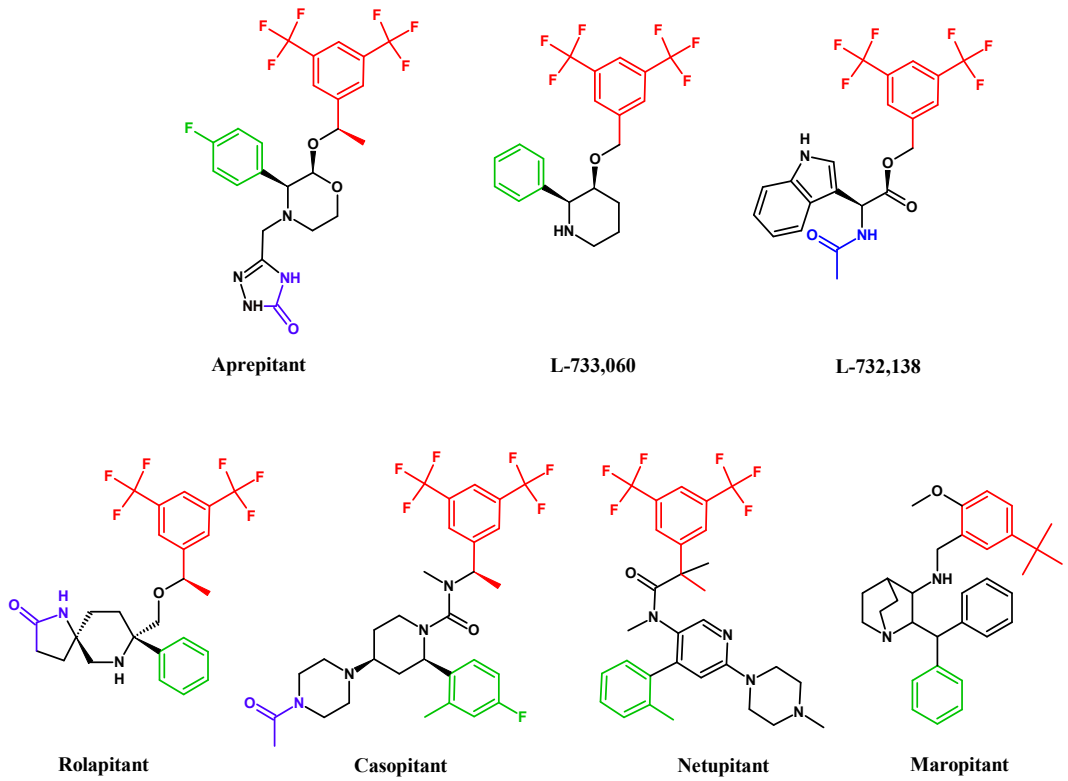

Figure 3. Colour visualisation of structure differences and similarities in the group of most antitumour evaluated NK1R antagonists (aprepitant, L-733,060 and L-732,138) and in group of CINV indicated NK1R antagonists (aprepitant, rolapinant, casopitant, netupitant and maropitant); the last presented, maropitant, despite the biggest structural distinction, showed high affinity to NK1R and sufficient clinical efficacy.

3. NK1R Radioligands in Nuclear Medicine

In nuclear medicine, ligands play the role of vectors leading medicine applied radionuclides to the target disease sites, which overexpress receptors for the implicated ligand. Radionuclide complexes are stable coordination compounds in which radionuclide cations are bonded by multidentate chelators (e.g., DOTA, NOTA, DOTAGA and DTPA). Syntheses of radioligands (radiopharmaceuticals) are performed according to the commonly known and described procedures, coupling reaction of ligand and bifunctional agent and labelling the obtained bioconjugate with the desired radionuclide.

3.1. Radiolabelled NK1R Agonists for Targeted Radionuclide Tumour Diagnosis

Diagnostic radiotracers (diagnostic radiopharmaceuticals) contain γ or β^+-emitting radionuclides for SPECT and PET imaging, respectively. Radiopharmaceuticals are administered in such small amounts (at the nanomolar level) that they do not induce any pharmacological responses. After patient administration, the measurement of emitted gamma ray intensity allows for determination of the localization of the radiopharmaceutical and definition of tissue and organ abnormalities in the patient. These diagnostic methods enable detection of the biochemical and molecular pathologies at early disease stages, much earlier than the symptoms may be detected by the standard methods.

There are numerous studies describing the application of SP and its analogues or derivatives, labelled with diagnostic radionuclides (e.g., ^{68}Ga, ^{99m}Tc, ^{111}In, ^{125}I) designed for targeted radionuclide tumour diagnosis [102,103]. Table 4 presents concise information about published studies.

Nuclear characteristics of applied diagnostic radionuclides: ^{3}H: emitter β^-, $t_{1/2}$ = 12.32 y, E_{max} = 18.59 keV; ^{68}Ga: emitter β^+, $t_{1/2}$ = 67.71 min, E_{mean} = 0.836 MeV; ^{99m}Tc: emitter γ, $t_{1/2}$ = 6.01 h,

E_{max} = 0.141 MeV; ^{111}In: EC decay, emitter γ, $t_{1/2}$ = 2.80 d, E_{max} = 0.245 and 0.171 MeV; ^{125}I: EC decay, emitter γ, $t_{1/2}$ = 59.41 d, E_{max} = 27.47, 27.20 and 35.49 keV.

Table 4. Structure and potential application of NK1R diagnostic radioligands based on SP and its analogues or derivatives.

NK1R Radioligand Molecules	Biological Properties and Potential Applications	References
[^{125}I]I-BH-[Tyr^{8}]SP	• Animal tests: high affinity to pancreatic acinar cells isolated from guinea pigs; • Animal or human tests: used as a radiotracer for determination of specific binding and/or internalisation in various organs, tissues and cells, namely in: ■ anterior pituitary cells ■ in rat thymus, spleen ■ brain ■ spinal cord ■ chicken small intestine ■ epithelial cells ■ mesencephalic primary cultures prepared from embryonic mouse brain ■ rat parotid membranes ■ human eyes;	[104] [104–106] [105–107] [108] [109,110] [111–115] [116] [117,118] [119] [120]
[^{3}H]H-SP	Animal tests: specificity for imaging of cat inflamed bladder tissue;	[121]
[^{111}In]In-DTPA-[Arg^{1}]SP	• Animal tests: imaging of SP receptor-positive (SPR+) immunologic disorders; high affinity to NK1R presented in parotid gland and brain cortex membranes; rapid enzymatic degradation; high uptake in pancreatic tumour (CA20948), salivary glands, kidneys and arthritic hind leg joints; unable to cross the intact blood–brain barrier; • Clinical trials: used in scintigraphy of immune-mediated diseases;	[122] [123]
[^{99m}Tc]Tc-IMB-SP [1]	Animal tests: significant uptake in the salivary glands;	[124]
[^{99m}Tc]Tc-Hynic-SP [2] [^{99m}Tc](NS$_3$)-Tc-CN-SP and [^{99m}Tc]((NS$_3$)-Tc-CN)$_2$-SP [3]	In vitro study: high stability in biological fluids; relationship between molecular structure and physicochemical properties;	[125]
[^{99m}Tc][Tc(N)(Cys-Cys-SP)(PCN)] [4] [^{188}Re][Re(N)(Cys-Cys-SP)(PCN)]	• In vitro study: application of theranostic pair ^{99m}Tc and ^{188}Re; affinity studies using U87MG cell line expressing NK1R and negative control cell line L-929; • Animal tests: accumulation in salivary glands, kidneys and thymus;	[126]
[^{111}In]In-DOTA-[Thi^{8},Met(O$_2$)^{11}]SP [^{68}Ga]Ga-DOTA-[Thi^{8},Met(O$_2$)^{11}]SP	Clinical trials: used for visualisation of NK1R expression and control of radiocompound distribution at the target site and whole body; administrated simultaneously with therapeutic radiopharmaceutical [^{213}Bi]Bi-DOTA-[Thi^{8},Met(O$_2$)^{11}]SP;	[55,127]
[^{99m}Tc][Tc-Hynic-[Tyr^{8},Met(O)^{11}]SP [5]	Animal tests: specific uptake in the tumour; stable in HS; internalisation studies on U373 MG astrocytoma cell line; significant accumulation in kidneys;	[128]
[^{3}H]H-[Pro^{9}]SP and [^{3}H]H-propionyl-[Met(O$_2$)^{11}]SP(7–11)	In vitro study: applied for the studies of different NK1R binding sites: NK-1M (majority) and NK-1m (minority);	[11]
[^{125}I]I-BH-[Sar^{9},Met(O$_2$)^{11}]SP	• Animal tests: comparison of uptake in submandibular gland and in several regions of rat brain of the tested radiocompound and [^{125}I]I-BH-SP; • In vitro study: comparison of physicochemical properties of the tested radiocompound and [^{125}I]I-BH-SP.	[129–131]

[1] IMB = bifunctional chelator 1-imino-4-mercaptobutyl; [2] labelling in the presence of EDDA and tricine as coligands; [3] CN = isocyanide group, NS_3 = 2,2′,2″-nitrilotriethanethiol; [4] PCN = tris(2-cyanoethyl)phosphine; [5] labelling in the presence of EDDA and tricine as coligands.

In order to label SP with the iodine-125 radionuclide, Phe in position 8 was replaced by Tyr. The [Tyr^{8}]SP was radioiodinated with ^{125}I by the Bolton–Hunter agent (3-(3-iodo-4-hydroxyphenyl)propionic acid *N*-hydroxysuccinimide ester, [^{125}I]I-BH). The experiments with radioligand [^{125}I]I-BH-[Tyr^{8}]SP showed specific, rapid and temperature-dependent binding of radiobiomolecules, as well as internalisation into pancreatic acinar cells derived from guinea pigs [104]. The same Bolton–Hunter iodinated SP derivative was used as a radiotracer for characterization of its binding via autoradiography and/or internalisation into various organs, tissues and cells [104–120] (Table 4).

The radioligand [^{3}H]H-SP was examined in order to determine accumulation in feline urinary bladder interstitial cystitis (IC) [121]. The results showed low uptake of [^{3}H]H-SP in normal and inflamed tissues, while high accumulation was discovered in inflamed bladder tissue and small blood

vessels. In this case [^{3}H]H-SP appeared to be specific only for inflamed bladder of cats diagnosed with IC, possibly due to upregulation of NK1R as a part of the IC pathophysiology.

Further, the endogenous peptide SP has been used for syntheses of numerous radioligands. Radiobioconjugate [^{111}In]In-DTPA-[Arg^{1}]SP was used for the in vivo detection of SP receptor-positive (SPR+) immunologic disorders and certain tumours [122]. The in vitro binding and autoradiographic experiments performed on parotid gland, brain cortex membranes and the submandibular gland of rat, demonstrated high affinity of [^{111}In]In-DTPA-[Arg^{1}]SP to NK1Rs. Tissue distribution of radioligand in male Wistar rats 24 h after treatment with 3 MBq of [^{111}In]In-DTPA-[Arg^{1}]SP, revealed high concentration of radioactivity in the kidneys indicating renal excretion as the central route of radiobioconjugate elimination. The experimental results showed also rapid enzymatic degradation of the tested radiocompound resulting in an approximately 3 min half-life in blood. Interestingly, no significant uptake of [^{111}In]In-DTPA-[Arg^{1}]-SP in the brain cortex and striatum was observed. These data suggested that the radiobioconjugate was unable to cross the intact blood–brain barrier (BBB) and further visualize SP receptors (SPRs) in the central nervous system. Additionally, [^{111}In]In-DTPA-[Arg^{1}]-SP injected into rats bearing the autograft pancreatic tumour, CA20948, or rats with adjuvant mycobacteria tuberculosis-induced arthritic joints, exhibited significant uptake in the tumour, salivary glands, kidneys and arthritic hind leg joints. The authors further demonstrated the potential of this radiolabelled SP analogues for visualisation of pathological SPR+ processes in vivo by gamma camera scintigraphy.

The same [^{111}In]In-DTPA-[Arg^{1}]SP radiobioconjugate was involved in the first clinical trials on twelve patients with immune-mediated diseases in 1996 [123]. After intravenous administration of 150-250 MBq of [^{111}In]In-DTPA-[Arg^{1}]SP, rapid radiopharmaceutical degradation, within four minutes of treatment, was observed. Twenty-four hours postinjection, more than 95% of radioactivity was excreted in the urine. The uptake in areolae mammae (in women), liver, spleen, kidneys and urinary bladder was observed in all patients and in the thymus in eight patients. This radiobioconjugate can be used for scintigraphy of inflammatory sites in various diseases as well as for visualisation the thymus.

Studies of the diagnostic properties of ^{99m}Tc radiolabelled IMB-SP bioconjugate [124] have revealed uptake in the salivary glands, while the accumulation was decreased by factor of 2 in mice pretreated with excess of non-radiolabelled SP. The authors did not observe any cardiovascular side effects due to the slow rate of SP infusion.

SP ligand conjugated with Hynic chelator or monodentate bifunctional chelator isocyanobutyric succinimidyl ester and labelled with technetium-99m, [^{99m}Tc]Tc-Hynic-SP, [^{99m}Tc](NS$_3$)-Tc-CN-SP and [^{99m}Tc]((NS$_3$)-Tc-CN)$_2$-SP have been synthesised and studied to determine potential application in targeted radionuclide tumour diagnosis [125]. The radiobioconjugates were characterized by high stability in the presence of competitive cysteine/histidine solutions and various lipophilicity (logP) values, of −3.7, −0.24 and −0.89, respectively. SP ligands conjugated with two cysteine amino acids (Cys-Cys-SP) were used in the studies to apply ^{99m}Tc and ^{188}Re as theragnostic matching pairs based on the combined reaction of tridentate π-donor and monodentate π-acceptor chelators with the [Tc/Re≡N]$^{2+}$ metallic functional group [126]. [^{99m}Tc][Tc(N)(Cys-Cys-SP)(PCN)] and [^{188}Re][Re(N)(Cys-Cys-SP)(PCN)] radiobioconjugates incubated with U87MG cells expressing NK1R displayed predominant cell surface binding, whereas incubation with negative control cell line, L-929, resulted in no detectable interaction. Whole-body biodistribution studies using hybrid SPECT/CT YAP(S)PET small-animal tomography showed significant kidney and thymus uptake, in accordance with previous studies [123]. High radioactivity accumulation in salivary glands was also detected. The presented results ruled out myocardial uptake but did not confirm if the uptake of synthesised bioconjugates was specific.

The SP analogue [Tyr^{8},Met(O$_2$)^{11}]SP conjugated with DOTA chelator and labelled with diagnostic radionuclides ^{111}In or ^{68}Ga was used in glioma patient studies. The [^{111}In]In-DOTA-[Thi^{8},Met(O$_2$)^{11}]SP [55] and [^{68}Ga]Ga-DOTA-[Thi^{8},Met(O$_2$)^{11}]SP [127] receptor radiopharmaceuticals were injected simultaneously with therapeutic preparation [^{213}Bi]Bi-DOTA-[Thi^{8},Met(O$_2$)^{11}]SP to visualise distribution of radiopharmaceuticals in the whole body.

Similar to previous studies, SP analogue [Tyr^8,Met(O)^{11}]SP was applied for the synthesis of bioconjugate Hynic-[Tyr^8,Met(O)^{11}]SP. The obtained bioconjugate, labelled with ^{99m}Tc, was used for detection of NK1R positive tumours [128]. The obtained radiobioconjugate was characterized with high specific activity (84–112 GBq/μmol) and stability in human serum. Internalisation studies on U373 MG cells, an astrocytoma cell line, showed rapid (after 0.5 h) binding of the tested compound to the cell membrane and specific internalisation. Saturation binding assays indicated a mean K_d value in the nanomolar range, confirming the radioligand specificity to NK1R. Biodistribution studies in healthy mice and in tumour bearing nude mice demonstrated specific uptake in the tumour and the noticeable uptake in the stomachs, intestines and lungs, as well high accumulation in the kidneys, indicating excretion via the renal pathway. There was not significant accumulation in the salivary glands although this accumulation was moderately higher than in the other organs, including muscles and bones.

SP analogues [Pro^9]SP and [Met(O$_2$)^{11}]SP(7–11) labelled with ^{3}H radionuclide were applied in studies of different NK1R binding sites [11]. The researchers examined internalisation of two radioligands, [^{3}H]H-[Pro^9]SP and [^{3}H]H-propionyl[Met(O$_2$)^{11}]SP(7–11), using CHO cells transfected with human NK1Rs. The results showed existence of two nonstoichiometric binding sites NK-1M (majority) and NK-1m (minority). Both radiobioconjugates were internalized rapidly to achieve a maximum of 75% for specifically bound [^{3}H]H-[Pro^9]SP and of 35% for [^{3}H]H-propionyl[Met(O$_2$)^{11}]SP(7–11). [^{3}H]H-[Pro^9]SP interacted with the most abundant NK-1M binding site inducing adenylyl cyclase activation (temperature dependent internalisation), whereas [^{3}H]H-propionyl[Met(O$_2$)^{11}]SP(7–11) bound to the less abundant NK-1m binding site connected with the phospholipase C (PLC) pathway (temperature independent internalisation).

The binding properties of the [^{125}I]I-BH-[Sar^9,Met(O$_2$)^{11}]SP radiocompound based on the ligand [Sar^9,Met(O$_2$)^{11}]SP were tested using autoradiography and compared with properties of [^{125}I]I-BH-SP [129]. The results showed high uptake of both radiobiomolecules in the submandibular gland and in several regions of rat brain. Parallel in vitro binding experiments on rat brain membranes exhibited two to four fold higher affinity of [^{125}I]I-BH-[Sar^9,Met(O$_2$)^{11}]SP than that of [^{125}I]I-BH-SP. Despite higher affinity, [^{125}I]I-BH-[Sar^9,Met(O$_2$)^{11}]SP did not demonstrate significantly higher specificity than [^{125}I]I-BH-SP in NK1R binding sites, in agreement with previous studies of these two radiobiomolecules [130]. However, autoradiographic data of [^{3}H]H-[Sar^9,Met(O$_2$)^{11}]SP reported in [131] showed slightly different localization of NK1Rs in the rat brain compared to previously presented data for [^{125}I]I-BH-SP [130].

3.2. Radiolabelled NK1R Agonists for Targeted Radionuclide Tumour Therapy

Therapeutic radiopharmaceuticals used in cancer treatment or palliative therapy are often ligands labelled with radionuclides which emit corpuscular radiation of short range in the tissue (e.g., β^-, α or Auger electrons). Targeted radiopharmaceuticals characterized by high receptor affinity are selectively absorbed in the pathological tissues and their radiation energy is selectively and quantitatively deposited in the tumour mass. As a result, applications of these preparations are relatively safe for healthy tissues.

Nuclear characteristics of applied therapeutic radionuclides [102,103]: ^{90}Y: emitter β^-, $t_{1/2}$ = 64.00 h, E_{max} = 2.28 MeV, mean tissue range: 2.76 mm; ^{177}Lu: emitter β^-, $t_{1/2}$ = 6.65 days, E_{max} = 0.50 MeV, max. tissue range: 0.28 mm; ^{213}Bi: emitter α, $t_{1/2}$ = 45.59 min, E_{max} = 5.88 and 5.56 MeV, tissue range: 40–100 μm; ^{225}Ac: emitter α, $t_{1/2}$ = 9.92 d, E_{max} = 5.83 and 5.80 MeV, tissue range: 40–100 μm.

In addition to the high incidence of NK1Rs in GBM, NK1Rs are overexpressed in approximately 27% of human pancreatic tumours [132]. Bortoleti de Araújo et al. applied endogenous SP for the synthesis of [^{177}Lu]Lu-DOTA-SP radiobioconjugate (Table 5) and evaluated in vivo targeting of AR42J pancreatic tumour cells in Nude mice [133]. This study, along with others, reported that the radiobioconjugate was stable for more than 24 h at 37 °C in human plasma. Biodistribution studies on AR42J pancreatic tumour bearing mice showed high uptake in kidneys, suggesting excretion mainly by

renal pathway. Significant uptake of [^{177}Lu]Lu-DOTA-SP was also observed in intestine and stomach due to the presence of NK1Rs in the gastrointestinal tract. These results demonstrated the potential of [^{177}Lu]Lu-DOTA-SP as a treatment for pancreatic tumours.

Considering the high expression of NK1R on malignant glial brain tumours [132], studies of SP ligands have been initiated. The first in vivo studies concerned application of a SP with macrocyclic DOTAGA chelator, labelled with therapeutic radionuclides (mostly ^{90}Y and to reduce the "cross-fire effect", ^{177}Lu and ^{213}Bi), were performed by Kneifel et al. [134]. In clinical experiments with twenty patients, the radiopharmaceutical was administered via an implanted catheter directly into the tumour mass or via intracavitary implant after surgical resection (the local injection minimizes side effects and reduces the tubular reabsorption of the radiopharmaceutical in the kidneys). Malignant glioma therapy of WHO grade 2 to 4 tumours, by applying β^- and α emitters, was well tolerated with low toxicity and resulted in the radiation induced necrosis of cancer cells. However, due to infiltrative characteristics of GBM, its complete surgical resection cannot be achieved. Therefore, the novel approach of neoadjuvant therapy, with the use of ^{90}Y radionuclide as the primary therapeutic modality, was proposed by Cordier et al. [135]. Seventeen patients with newly diagnosed and histopathologically confirmed GBM were treated with [^{90}Y]Y-DOTAGA-SP before tumour surgical resection. The catheter systems were stereotactically implemented within the cancer margins and [^{90}Y]Y-DOTAGA-SP radiopharmaceutical (radioactivity ranged from 120 mCi to 345 mCi) was injected intratumorally. During the treatment, no increase or decompensation of intracranial pressure was observed. The pretreated tumours were demarcated by a capsule structure, leading to better separation from the cerebral tissue than in conventional glioma resection. Moreover, pseudo-encapsulation allowed for a marked reduction of intraoperative bleeding. The highest dose administered in ten patients caused the completed encapsulation of the tumour. This neoadjuvant local therapy was feasible without significant side effects, 15 of 16 patients treated so far exhibit stabilisation of neurological status. However, in critically located gliomas the use of ^{90}Y radionuclide with the resulting "cross-fire effect" may cause unacceptable damage of adjacent brain areas.

To minimize the neurological damage, the alpha radiation-emitting radionuclide ^{213}Bi, which has a shorter range in tissue and higher radiation energy in comparison with ^{90}Y and ^{177}Lu, was the first-line treatment [55]. Moreover, for the synthesis of novel radiopharmaceuticals, the [Thi^8,Met(O$_2$)^{11}]SP ligand, characterized by a longer half-life in vivo, was applied [53]. This SP analogue has been selected from various SP analogues tested (Table 2) in terms of the feasibility of vector application usage in targeted radionuclide tumour diagnosis or therapy. Pilot studies with [^{213}Bi]Bi-DOTA-[Thi^8,Met(O$_2$)^{11}]SP and [^{111}In]In-DOTA-[Thi^8,Met(O$_2$)^{11}]SP were conducted in five patients diagnosed with critically located gliomas (WHO, grade 2-4) [55]. Similarly to previous clinical trials, the radioactive compound [^{213}Bi]Bi-DOTA-[Thi^8,Met(O$_2$)^{11}]SP was administered intratumorally via implanted catheters. Simultaneously, the [^{111}In]In-DOTA-[Thi^8,Met(O$_2$)^{11}]SP [55] or [^{68}Ga]Ga-DOTA-[Thi^8,Met(O$_2$)^{11}]SP [127] radiocompounds were used for the visualisation of ^{213}Bi-radiopharmaceutical distribution. Sixty to ninety minutes postinjection of [^{213}Bi]Bi-DOTA-[Thi^8,Met(O$_2$)^{11}]SP, less than 4% of the activity was present in the blood, confirming high retention of this radiopharmaceutical in target site. The preliminary studies showed that this method is well tolerated and safe for patients; however, the short half-life of ^{213}Bi reduced the effectiveness of the treatment of larger tumours. Based on statistical data presented in the literature [127,136–138], the local treatment of brain tumours (intracavitary administration of radiopharmaceuticals) with the use of NK1R ligands in patients suffering from secondary GBM compares favourably with standard treatment options.

[Thi^8,Met(O$_2$)^{11}]SP ligand was also used for in vitro studies of potential ^{225}Ac-radiopharmaceuticals for targeted therapy of NK1R expressing gliomas performed by Majkowska et al. [139]. The efficacy of [^{225}Ac]Ac-DOTA-[Thi^8,Met(O$_2$)^{11}]SP was tested on three human glioblastoma cell lines (T98G, U87MG, U138MG), as well as GSCs. The binding experiments performed on T98G cells demonstrated high affinity (K_d = 19.2 ± 1.9 nM) of the radiobioconjugate

for NK1R, which agrees with previous studies [140]. [^{225}Ac]Ac-DOTA-[Thi^{8},Met(O$_2$)^{11}]SP caused significant reduction in glioblastoma cell viability compared to the conventional treatment with chemotherapeutic temozolomide. This radiobioconjugate has been shown to induce apoptosis and cell cycle arrest in G2/M phase. Importantly, [^{225}Ac]Ac-DOTA-[Thi^{8},Met(O$_2$)^{11}]SP was found to be highly cytotoxic, not only towards established GBM cell lines, but also to GSCs cells which are particularly resistant to radio- and chemotherapy. According to the literature [141–143], these stem cells (variable from 1% or less in the case of low-grade tumours and to 30% in highly aggressive glioblastomas) are responsible for initiation of tumour formation in vivo, sustaining tumour growth, and contributing to the creation of metastatic lesions. Therefore, therapy which can target GSCs and GBM cells, such as [^{225}Ac]Ac-DOTA-[Thi^{8},Met(O$_2$)^{11}]SP therapy, may decrease the recurrence of gliomas and improve survival rate. Clinical trials using this radiobioconjugate have been initiated [144].

Table 5. Structure and potential application of NK1R therapeutic radioligands based on SP and its analogues or derivatives.

NK1R Radioligand Molecules	Biological Properties and Potential Applications	Reference
[^{177}Lu]Lu-DOTA-SP	• Animal tests: biodistribution studies on mice bearing AR42J pancreatic tumour, high uptake in kidneys, satisfactory uptake in tumour, significant uptake in intestine and stomach; • In vitro study: high specific uptake and internalisation using LN319 cells isolated directly from the tumours;	[133]
[^{177}Lu]Lu-DOTAGA-SP [^{90}Y]Y-DOTAGA-SP [^{213}Bi]Bi-DOTAGA-SP	Medical experiments: well tolerated therapy of critically located gliomas, low toxicity;	[134]
[^{90}Y]Y-DOTAGA-SP	Medical experiments: recorded completed encapsulation of the tumour in patients administered with the highest dose;	[135]
[^{213}Bi]Bi-DOTA-[Thi^{8},Met(O$_2$)^{11}]SP [^{111}In]In-DOTA-[Thi^{8},Met(O$_2$)^{11}]SP	Medical experiments: treatment of critically located gliomas; well tolerated and safe for patients; complete necrosis of small tumours and necrosis only in the nearness of the implanted catheters in the case of large tumours;	[55]
[^{213}Bi]Bi-DOTA-[Thi^{8},Met(O$_2$)^{11}]SP [^{68}Ga]Ga-DOTA-[Thi^{8},Met(O$_2$)^{11}]SP	Medical experiments: treatment of patients with secondary GBM (after surgery, chemo- and radiotherapy); very low accumulation in kidneys, urine, bladder and blood; no side effects, necrosis and demarcation of the tumours;	[127]
[^{213}Bi]Bi-DOTA-[Thi^{8},Met(O$_2$)^{11}]SP	Medical experiments: higher efficiency of radiolabelled NK1R ligands application and local brain tumours treatment in patients suffering from secondary GBM compared to standard treatment options;	[136]
[^{225}Ac]Ac-DOTA-[Thi^{8},Met(O$_2$)^{11}]SP	• In vitro study: high affinity to glioblastoma cancer cells: T98G, U87MG, U138MG and glioblastoma stem cells (GSC); significant reduction in glioblastoma cell viability in comparison to the conventional treatment with temozolomide; high cytotoxicity towards GBM stem cells; [139] • Medical experiments: safe and well-tolerated therapy without side effects; [144]	[139] [144]
[^{177}Lu]Lu-DOTA-SP(4–11) [^{177}Lu]Lu-DOTA-SP(5–11) [^{177}Lu]Lu-DOTA-[Thi^{8},Met(O$_2$)^{11}]SP(5–11)	In vitro study: radiobioconjugates characterized with higher lipophilicity and lower molecular weight than those based on analogue [Thi^{8},Met(O$_2$)^{11}]SP—changes in physicochemical properties of radiobioconjugates leading to their deeper diffusion into the cavity walls after surgical resection of the tumour.	[145]

However, the main disadvantage of using [Thi^{8},Met(O$_2$)^{11}]SP ligand as a vector in ^{213}Bi/^{225}Ac-radiopharmaceuticals is poor radiopharmaceutical diffusion into the walls of the postsurgical cavity. Following these results, fragments of SP ligand and its derivatives (SP(5–11), SP(4–11), [Thi^{8},Met(O$_2$)^{11}]SP(5–11)) were tested as potential vectors to guide the radiobioconjugate to the NK1Rs expressed on cancer cells [145]. These studies were focused on the synthesis of new radiobioconjugates with higher lipophilicity and lower molecular weight than those of [Thi^{8},Met(O$_2$)^{11}]SP. The new radiobioconjugates were projected to be more effective at diffusing into solid tumours or postsurgical cavity walls. The results of these studies showed that shorter fragments of SP were characterized by a lower molecular weight and higher lipophilicity, whereas the exchange of Phe for Thi in position 8 and Met for MetO$_2$ in position 11 caused a decrease of lipophilicity. The newly prepared radiobioconjugates, such as [^{177}Lu]Lu-DOTA-SP(4–11) and [^{177}Lu]Lu-DOTA-[Thi^{8},Met(O$_2$)^{11}]SP(5–11) exhibited satisfactory affinity to NK1Rs presented on U373 MG glioblastoma cells with K_d values in the nanomolar range. Unfortunately, radiolabelled shorter

fragments of SP in HS were less stable than in CSF due to fast enzymatic ligand biodegradation. Considering the lipophilicity, molecular weight, affinity and stability of SP, its fragments and analogues, a balance should be feasible. The relatively low ligand stability in HS does not completely disqualify the local treatment of radiolabelled short SP fragments, because the content of serum peptidases in the cavity after tumour resection is rather low. Nevertheless, the application of receptor radiopharmaceuticals requires individual consideration (personalised medicine) for each patient.

The above paragraphs of this review cover rich aspects of the biological properties and potential applications of NK1R agonist radioligands in targeted radionuclide diagnosis and therapy. The cited literature are quite consistent besides stability evidence of radiobioconjugates ^{99m}Tc-Hynic-[Tyr^{8}-Met(O)^{11}]SP [128] and [^{177}Lu]Lu-DOTA-SP [133]. In contrast to plenteous literature, only these two papers provide data about radioligand stability in human serum. In our opinion this is questionable, due to endopeptidases present in HS leading to inevitable process of SP biodegradation.

Based on the data described in Sections 3.1 and 3.2, it is possible to conclude that NK1R ligands, labelled with diagnostic/therapeutic radionuclides, can be applied for imaging or therapy of cancers overexpressing the NK1Rs and for that these receptor radiopharmaceuticals are efficacious. This therapy seems to be prospective for the future in comparison to standard applied therapeutic options like temozolomide chemotherapy. Due to the relatively low stability of SP, its fragments and analogues, new NK1R ligands are constantly being investigated, starting innovative studies with the application of SP antagonists.

3.3. Antagonist Radioligands of NK1R for Targeted Radionuclide Imaging

A number of radiolabelled antagonists for NK1R are known to date. All radioligands exhibit high affinity to NK1R, but only some have potential future applications in targeted radionuclide tumour diagnosis or therapy. The features of those with potential are presented below (Table 6).

In contrast to SP and its peptide analogues, nonpeptide antagonists are stable and do not follow rapid enzymatic decomposition in vivo. First generation radiotracers were selected from many lead structures, based upon autoradiographic studies of NK1Rs. These compounds were initially investigated in vivo for their ability to be taken up by the brain and other organs in animal models [146–149] (Figure 4). Early evaluation of [^{11}C]CP-96,345 [146] concluded that despite radioligand high lipophilicity, the cationic form excluded radiotracer passage through the blood–brain barrier and allowed for peripheral tissue imaging only. PET detection of central and peripheral NK1R occupancy was performed later on hamsters using [^{11}C]CP-99,994 [147] and pigs using [^{11}C]CP-643,051 [148]. Both studies confirmed the known autoradiographic mappings. The first primate PET imaging was reported in 2000 at the Uppsala University PET Centre [149], and revealed the uptake kinetics of [^{11}C]GR205171 ([^{11}C]vofopitant) (Figure 5). Research includes regular imaging (baseline study) and imaging with receptor blocked active sites (using unlabelled compound) to demonstrate high specific binding in the striatum, thalamus and neocortex. Tracer analysis showed rapid uptake during 50 min of examination and fast cerebellar nonspecific washout, which introduced the possibility of in vivo assessment of receptor distribution. At the same time, the slow dissociation rate of this tracer from NK1Rs excludes dynamic PET imaging using [^{11}C]GR205171 for physiological receptor regulations. Thereby, the tracer evaluations in human were focused on brain NK1R mapping for further potential clinical application.

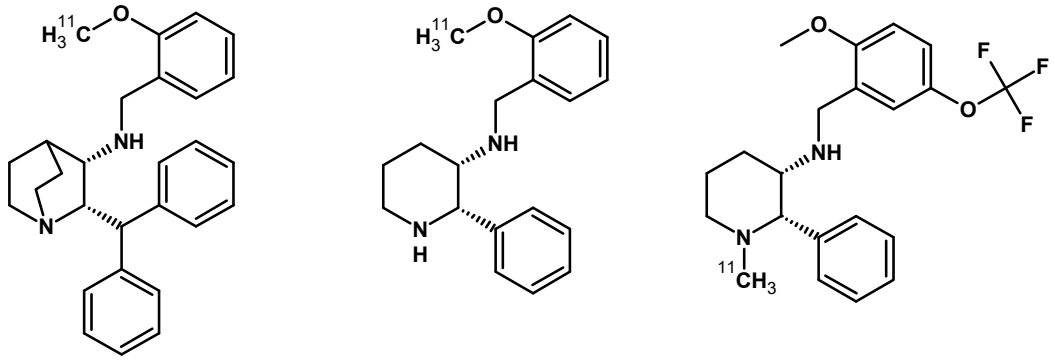

Figure 4. Structures of the first radioligands of neurokinin 1 receptor.

Alternative research were performed using similar highly specific radiotracer [^{18}F]SPA-RQ, a ^{18}F-labelled derivative of vofopitant (Figure 5), US patented by Merck & Co. in 2001 and investigated mainly in Merck Research Laboratories (West Point, Pennsylvania) and Turku Positron Emission Tomography Centre. The influence of gender and age on NK1R availability was investigated using [^{18}F]SPA-RQ 3D PET imaging [150], including 35 male and 10 female volunteers, aged 19 to 55 years. Results revealed a significant relationship of general 7% decrease rate of cerebral NK1Rs per decade of life, caused by physiological aging. This phenomenon was observed in frontal, temporal, parietal cortex and hippocampus structures. Moreover, NK1R availability, especially in the striatum, was found to be relatively lower in women than in men, what was later confirmed using [^{11}C]GR205171. Indeed, further investigations [151] provided data of similar interaction effects of age and sex on cerebral receptor availability using this radiotracer. These results indicated similar declines in the rate of NK1 receptor density in the frontal, temporal, and occipital cortices, but also in the brainstem, thalamus and caudate nucleus per each decade of life. Surprisingly, receptor availability loss in the amygdala and temporal cortex with an age increase was noted only in men. Additionally, in this study women showed lower general NK1R density in the thalamus compared to male volunteers.

[^{18}F]SPA-RQ and [^{11}C]GR205171 are based on the same pharmacophore. Both demonstrate fast brain uptake and very high affinity for NK1R with low nonspecific binding. Both radioligands enable efficient parametric PET imaging via a simple method based on reference ratio of region of interest (ROI) signal to cerebellar signal. This is a capability of the radioligands referenced due to fast washout of nonspecific bond tracer in the cerebellum bereft of NK1Rs. All of these features favour application of both radiotracers in localization and quantification of receptor studies in course of targeted radionuclide therapy.

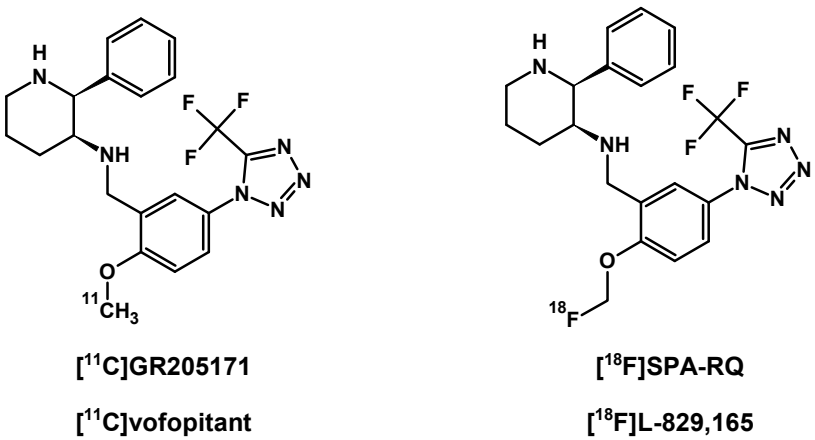

Figure 5. Twin structures of radiotracers [^{11}C]GR205171 and [^{18}F]SPA-RQ.

Preclinical evaluation of PET NK1R imaging in human brains, using [^{18}F]SPA-RQ, was performed in terms of further investigations of NK1R antagonists, accurate receptor neurodistribution and influence of receptor regulation on CNS pathologies. PET 3D studies [152] detailed multiple observations including the highest uptake of the radiotracer at the putamen and caudate, followed by uptake rates in adjacent substantia nigra and globus pallidus structures. Uniform and moderate uptake of radiotracer was widespread in limbic cortex and neocortex regions, while inconsiderable specific uptake was observed in the cerebellum. Autoradiographic post-mortem studies on the human brain confirmed similar affinity. However, examination via kinetic modelling revealed a few drawbacks among visualisation procedure. First, the low rate of radiotracer kinetics required a six hour time period for the binding equilibrium to occur (Figure 6). This time impacted imaging quality and reliability, but also favoured the radioactive agent metabolic decomposition; 90 min after injection, only 40% of the radioactivity in plasma still represented the initial [^{18}F]SPA-RQ concentration. Moreover, free fluoride was observed, likely resulting in the skull bone radioactivity that was observed during late scans In the end, a simplified reference tissue kinetic model of the radiotracer uptake was optimized. After 240 min, data acquisition was optimal, corresponding to set binding potential (BP, a combined measure of the density of "available" neuroreceptors and the affinity of a drug to this neuroreceptor). BP values were assigned from 4 to 5 in the basal ganglia structures and between 1.5 and 2.5 in the cortical regions, in reference to the cerebellum. Researchers also suggested that for clinical imaging utility, a commonly applied ratio method considering cerebellar reference is reliable and preferable, as it does not require arterial blood sampling and long acquisition time.

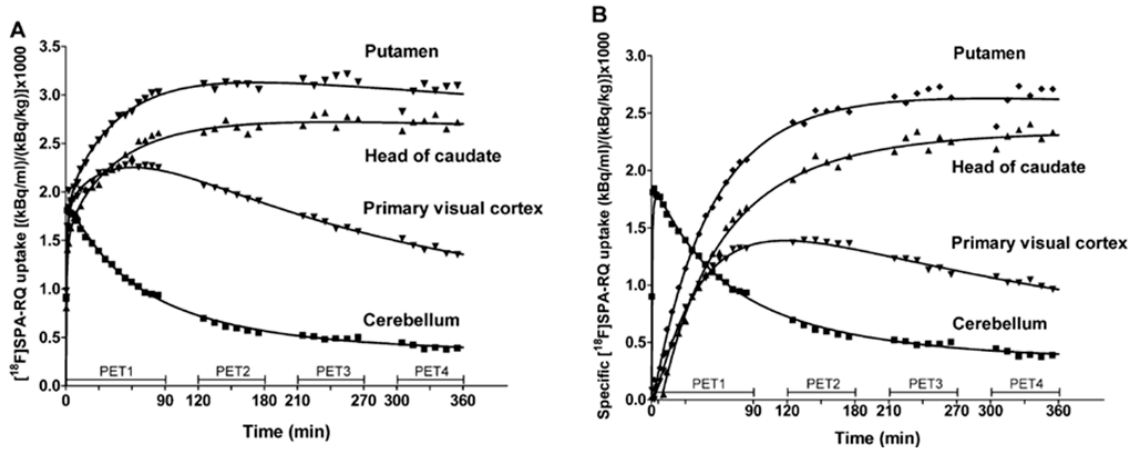

Figure 6. [^{18}F]SPA-RQ radiotracer total (**A**) and specific (**B**) uptake values in function of time in striatal structures and occipital cortex. As reference, both charts present cerebellar total binding curves [152].

In support of these measurements, a similar radioligand [^{18}F]fluoroethyl-SPA-RQ ([^{18}F]FE-SPA-RQ), with high affinity and selectivity to NK1R was developed and examined [153,154]. [^{18}F]FE-SPA-RQ featured lower in vivo defluorination relative to the previous analogue, [^{18}F]SPA-RQ, seen via reduced radioactivity in bone accumulation. A group from the Japanese Molecular Imaging Centre (National Institute of Radiological Sciences, Chiba, Japan) examined [^{18}F]FE-SPA-RQ characteristics on primates and rodents. These studies were followed by PET imaging with kinetic modelling to validate visualisation and quantification of NK1R distribution in healthy men. Although similar [^{18}F]SPA-RQ and [^{18}F]FE-SPA-RQ imaging of distribution on human brain receptors was observed; BP values obtained for [^{18}F]FE-SPA-RQ were lower, in fact, [^{18}F]FE-SPA-RQ showed little higher affinity for NK1R than [^{18}F]SPA-RQ.

All of these explorations enable further investigations of NK1R system contribution in targeted radionuclide therapy of CNS pathologies. So far, several early phase clinical trials using the discussed radiotracers have been conducted. Temporal lobe epilepsy [155] and social anxiety disorder [156] PET studies using [^{11}C]GR205171 were performed in small studies comparing NK1R availability in specific

cerebral structures of patients and healthy control subjects. In both studies, applied radiotracer imaging provided positive correlations between increased receptor availability and patient neuropathology. More precisely, significant enhanced in NK1R availability was determined in the ipsilateral and contralateral hemispheres of the temporal lobe in epileptic patients and in the right amygdala in patients with social anxiety disorder (Figure 7). Moreover, increased receptor availability correlated with epileptic seizure frequency in ipsilateral medial temporal structures. Another [^{11}C]GR205171 imaging study was performed on healthy volunteers with snake or spider phobias to investigate the effect of fear stimuli on NK1R availability [157]. During PET acquisitions, subjects were provoked by normal and fear stimulating animal pictures to distinguish baseline and fear stimulated scans of NK1R occupancy imaging. As a result, provocation of specific phobia had influence on signals in the right amygdala, which suggested that fear stimulated the release of endogenous SP in that region of the brain. Taken together, these findings demonstrate that [^{11}C]GR205171 voxel-based statistical analysis can substantially support NK1R mapping in specific anxiety, stress and epileptic disorders.

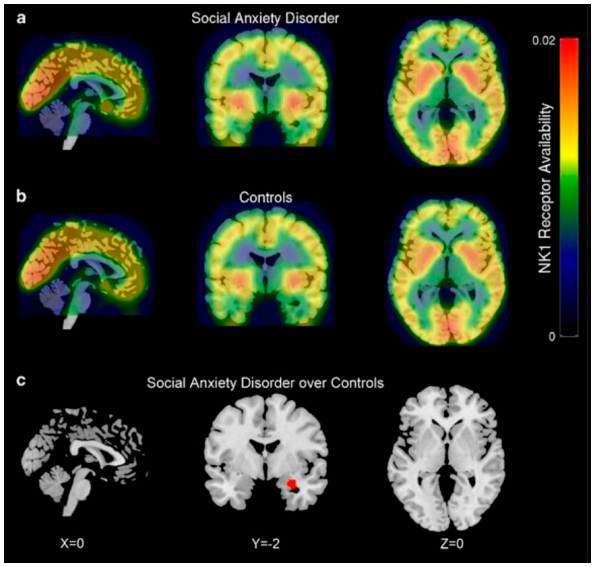

Figure 7. [^{11}C]GR205171 PET/MRI imaging of NK1R occupancy in social anxiety disorder patients (**a**) and healthy controls (**b**). Mean PET parametric scans (in colour) of radiotracer were overlaid on MRI images and compared between both groups. Patients with social anxiety disorder showed increased NK1 receptor availability in the right amygdala (**c**) [156].

[^{18}F]SPA-RQ was also employed in the quantification of NK1Rs in the brains of patients with panic disorder [158,159]. Baseline PET imaging and imaging after pharmacological induction of panic attacks were performed in patients and healthy volunteer cohorts. The result revealed a significant reduction of NK1Rs at baseline in patients compared with healthy subjects in all brain ROIs (12% to 21% reduction). Although this is in contrast to the above study focused on patient with social anxiety disorder, a similar outcome was demonstrated when two groups of female subjects were compared, with and without Irritable Bowel Syndrome [160]. Based on PET imaging supported with MRI scans, comparison of cerebral NK1R density revealed lower [^{18}F]SPA-RQ binding levels in patients in the globus pallidus. This radiotracer was also used in trials focused on post-traumatic stress disorder [161] and effective PET quantification of pancreatic cancer lesions for targeted radionuclide tumour therapy [162].

Meanwhile, it should also be noted that radiotracer molecular imaging is increasingly being used to determine receptor pharmacodynamics and optimize applicable effective doses of novel NK1R antagonists. One of the first clinical trials focused on this inspected a highly selective antagonist, aprepitant, while it was undergoing market authorisation. Determination of relationship between brain NK1R occupancy levels and aprepitant oral dose or plasma concentration was explored using [^{18}F]SPA-RQ in single-blind, randomised, placebo-controlled studies in healthy participants [163].

Indeed, reliable cerebral NK1R occupancy prediction, according to aprepitant plasma concentration was determined. More than 90% of striatal receptor occupancy was reached in subjects with aprepitant plasma concentration around 100 ng/mL, after >100 mg/day of aprepitant for 2 weeks. Even though the study was conducted with a limited number of subjects and small variety of doses, it provided valuable indications for dosage regimens by which to achieve effective receptor blockage in the CNS (Figure 8).

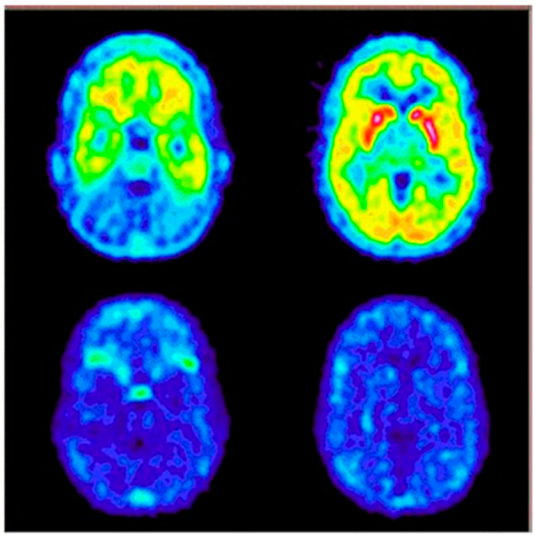

Figure 8. Predose (upper) and 100 mg aprepitant postdose (bottom) PET scans in the transverse section at the level of cerebellum (left) and striatum (right) in a human subject. Warmer colours symbolise higher uptake of radiotracer [^{18}F]SPA-RQ. Based on ratio method with cerebellum reference, estimated receptor occupancy by aprepitant for this subject was 94% at 1053 ng/mL of aprepitant in plasma [163].

NK1R occupancy PET mapping by the [^{18}F]SPA-RQ radiotracer was also applied in later clinical trials as verification of adequate target drug dose engagement. NK1R antagonists, aprepitant and its analogue L-759,274, were investigated in trials treating participants with major depressive disorder and anxiety disorder, respectively [76,78]. Unfortunately, both double-blind, randomised, placebo- and active-controlled, multicentre phase III clinical trials indicated not effective activity of aprepitant and L-759,274 for the treatment of depression or anxiety disorders, respectively. However, these researches demonstrated that radiotracer imaging can be used as a supportive tool in the proper context to validate negatively terminated trials.

[^{11}C]GR205171 tracer application in clinical trials was explored intensively by GlaxoSmithKlein. It is perfectly illustrated in determination of casopitant plasma concentration correlation with receptor occupancy [164]. Baseline and post-casopitant oral dose PET-[^{11}C]GR205171 brain imaging was performed in addition to collection of subject plasma for pharmacokinetic characterizations. The main goal of this study was to develop an estimation of suitable casopitant dose for subsequent patient clinical trials. Only the 15–30 mg drug dose was shown to achieve NK1R occupancy above 95%, which is a higher concentration than previously reported casopitant doses applied in depression trials [165,166]. This quantitative result was based on radiotracer pharmacokinetic model of NK1R binding initially established in the study [165]. Similar PET studies using [^{11}C]GR205171 were performed under phase 1 of interventional clinical trials to investigate receptor occupancy, safety, tolerability and pharmacokinetic features of rolapitant [167] and two other promising antagonists GSK1144814 [168] and GSK206136 [169]. Rolapitant PET evaluation indicated that a single oral treatment at 200 mg was a sufficient dose to occupy more than 90% of cerebral NK1Rs. Moreover, this receptor occupancy level was maintained for 120 h post-drug administration. These results suggest that treatment can provide properly long antiemetic action in case of highly emetogenic chemotherapy.

In 2005 at Amsterdam VU University Medical Centre a novel selective radiotracer [^{11}C]R116301 was developed (Figure 9) [170]. This radiotracer was evaluated in potential PET visualisation of NK1R in the human brain [171,172]. Similarly, as in above demonstrated cases, the highest uptake was recorded at striatum and lower in thalamus and other cortex regions. The cerebellar uptake level was negligible and nonspecific, as is presented in previous NK1R distribution reports. Receptor blocking with 125 mg oral dose of aprepitant reduced significantly in the striatum and cortex imaging signals relative to the cerebellar level. Further investigation of [^{11}C]R116301 specific binding was performed in 11 healthy volunteers using a test-retest method where baseline imaging and imaging after treatment with known doses of aprepitant were obtained in the same subjects. Researchers recommended to examine the ROI of the cerebellum as a semiquantitative ratio method for clinical applications, mainly due to [^{11}C]R116301 fast specific binding kinetics enabling realization of PET scans in 60–90 min after injection. In comparison, [^{18}F]SPA-RQ has slower kinetics, reaching cerebral receptor binding equilibrium only 6 h after treatment. Such slow kinetics present a considerable limitation to routine application, even if the given radiotracer provides relatively high specific imaging signal. This stands in accordance with NK1R-ligand affinity order [149], where the highest affinity ligands are GR205171 and SPA-RQ, followed by aprepitant, R116301 and SP. However, the use of [^{11}C]R116301 in dynamic brain receptor imaging seems to be promising in various concentrations of endogenous SP, for instance, in pharmacological test investigations.

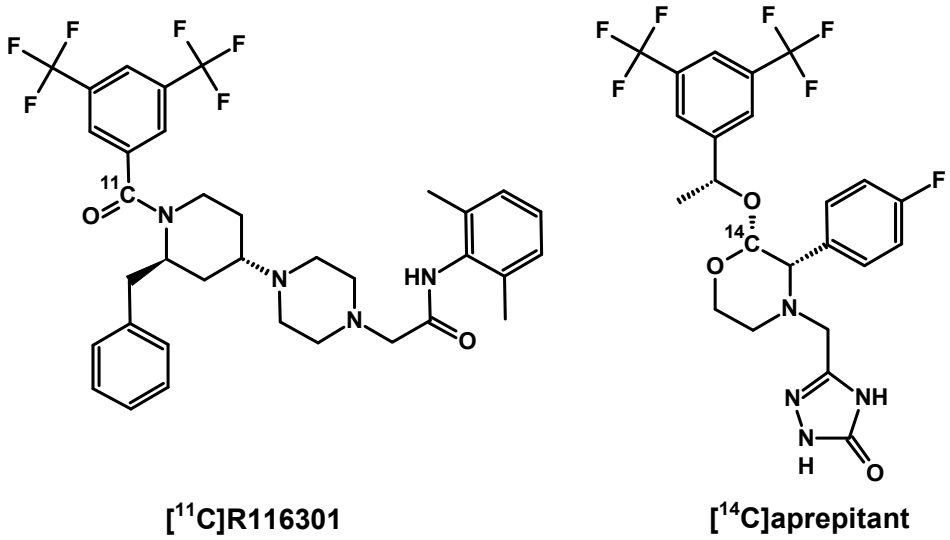

Figure 9. [^{11}C]R116301 (left) and exemplary [^{14}C]aprepitant (right) structures.

In the course of drug development and final market approval, radiolabelled aprepitant, casopitant and netupitant need to be studied in terms of bioavailability [173–176]. Determination of absorption, distribution, metabolism and excretion features were performed on ^{14}C-labelled derivatives of listed antagonists, synthesised for a biotransformation evaluation in rats, dogs and humans. The use of long-lived radionuclide traces for that purpose enabled investigation a range of metabolites (excreted or blood circuiting) after intravenous or oral administration.

Table 6. List of selected radiolabelled NK1R antagonists.

Radiotracer	Structure	Application	Reference
[^{11}C]CP-96,345 [1] [^{11}C]CP-99,994 [1] [^{11}C]CP-643,051 [1]	Investigational "lead structure" compounds	Preclinical tests in animal models	[146] [147] [148]
[^{11}C]GR205171([^{11}C]vofopitant) [2] [^{18}F]SPA-RQ ([^{18}F]L-829,165) [2] [^{18}F]FE-SPA-RQ [^{11}C]R116301 [3]	Optimized radiotracers	Pharmacodynamics and pharmacokinetics studies, receptor occupancy imaging in clinical trials	[149,151,155–157,164–169] [76,78,150,152,158–163] [153,154] [170–172]
[^{14}C]aprepitant [3,4] [^{14}C]casopitant [4] [^{14}C]netupitnat [4]	Well known high-selective antagonists indicated in CINV	ADME investigations in animals and men	[173] [174,175] [176]

[1] Structure illustrated in Figure 4; [2] Structure illustrated in Figure 5; [3] Structure illustrated in Figure 9; [4] Structure of nonlabelled compound illustrated in Figure 3.

4. Conclusions

This review discusses precisely literature data concerning the chemical and biological aspects of natural and synthetic NK1R ligands in classical (targeted therapy) and nuclear (targeted radionuclide therapy) medicine. Despite that standard nonspecific cancer treatments (e.g. chemotherapy, radiation therapy) are still the dominant form of therapy, the specific cancer treatments - targeted radionuclide tumour therapy is increasingly used in clinical trials. Due to expression of NK1Rs in a wide variety of cancers, the NK1R/SP system can be used as a modulator of biological functions related to tumour cell proliferation (favouring tumour growth), angiogenesis and migration. However, because of relatively low stability of SP, its fragments and analogues, new NK1R ligands are constantly being investigated. It initiated innovative studies with the application of SP antagonists.

To summarize, use of PET radiotracers supports progress in NK1R antagonist development and facilitates clinical investigations in terms of NK1R system correlation with CNS pathologies. Moreover, molecular imaging has the potential to improve therapeutic monitoring and to explore the duration of pharmacological effects in course of targeted radionuclide therapy. Although several clinical trials using radiotracers based on NK1R antagonists have been conducted to date, no serious attempts have been made in the oncological space yet.

Author Contributions: Conceptualisation, A.M.-P and E.G.; writing, A.M.-P.; P.K.H. and E.G.; visualisation, P.K.H.; supervision, A.M.-P. and E.G.

Funding: This research was carried out within grants HOMING PLUS/2013-8/9, supported by the Foundation for Polish Science, and 2017/25/B/NZ7/01896, supported by the National Science Centre (Poland).

Conflicts of Interest: The authors declare no conflicts of interest.

Abbreviations

5-HT$_3$R: 5-hydroxytryptamine receptor 3, serotonin receptor 3; AC: adenylyl cyclase; ACE: angiotensin-converting enzyme; AVP: vasopressin peptide; Bapa: biotinyl sulfone-5-aminopentanoic acid; BBB: blood–brain barrier; BH: Bolton–Hunter agent, 3-(3-iodo-4-hydroxyphenyl)propionic acid *N*-hydroxysuccinimide ester; Bmax: maximal concentration of binding sites; BP: binding potential; Bq: bequerel, Bzl: benzyl group; cAMP: cyclic adenosine monophosphate; Ci: curie; CINV: chemotherapy-induced nausea and vomiting; CN: isocyanide group; CNS: central nervous system; CSF: cerebrospinal fluid; CT: computed tomography; DOTA: 1,4,7,10-tetraazacyclododecane 1,4,7,10-tetracetic acid chelator; DTPA: pentetic acid, diethylenetriaminepentaacetic acid; DOTAGA: 1,4,7,10-tetraazacyclododecane-1-glutaric acid-4,7,10-triacetic acid chelator; EC: electron capture; EDDA: ethylenediamine-*N*,*N*-diacetic acid; EMA: European Medicines Agency; Emax: maximal emission energy; Emean: mean emission energy; GBM: glioblastoma multiforme; GPCR: G protein-coupled receptor; GSC: glioblastoma multiforme stem cell; Hcy: homocysteine; HcyO$_2$: homocysteine sulfone; HS: human serum; Hynic: hydrazinonicotinamide chelator; IC: interstitial cystitis; IC$_{50}$: half maximal inhibitory concentration; ID: injected dose; %ID/g; percent of injected dose per gram of tissue mass; IGF-1: insulin-like growth factor 1; IMB: bifunctional chelator 1-imino-4-mercaptobutyl; K$_d$: dissociation constant; keV: kiloelectronvolt; logP: logarithm of partition coefficient; MeV: megaelectronvolt; MRI: magnetic resonance imaging tomography; NEP: neutral endopeptidase; NK1R: neurokinin 1 receptor; NK-1m: minority binding site of neurokinin 1 receptor; NK-1M: majority binding site of neurokinin 1 receptor; NK1R-Tr: truncated form of neurokinin 1 receptor; NK2R: neurokinin 2 receptor; NK3R: neurokinin 3 receptor; NKA: neurokinin A; NKB: neurokinin B; NS$_3$: 2,2′,2′′-nitrilotriethanethiol; OS:

overall survival; PCN: tris(2-cyanoethyl)phosphine; PET: positron emission tomography; PFS: progression free survival; PLC: phospholipase C; PNS: peripheral nervous system; PONV: postoperative nausea and vomiting; ROI: region of interest; SAR: structure activity relationship; SP: Substance P; SPECT: single photon emission computed tomography; SPR: Substance P receptor; SPR+: Substance P receptor-positive; $t_{1/2}$: half-life; TACR1: tachykinin receptor 1; TACR2: tachykinin receptor 2; TACR3: tachykinin receptor 3; US FDA: United States Food and Drug Administration.

References

1. Muñoz, M.; Coveñas, R. Neurokinin-1 receptor: A new promising target in the treatment of cancer. *Discov. Med.* **2010**, *10*, 305–313. [PubMed]
2. Muñoz, M.; Rosso, M.; Coveñas, R. The NK-1 receptor: A new target in cancer therapy. *Curr. Drug Targets* **2011**, *12*, 909–921. [CrossRef] [PubMed]
3. Garcia-Recio, S.; Gascón, P. Biological and Pharmacological Aspects of the NK1-Receptor. *BioMed Res. Int.* **2015**. [CrossRef] [PubMed]
4. Yin, J.; Chapman, K.; Clark, L.D.; Shao, Z.; Borek, D.; Xu, Q.; Wang, J.; Rosenbaum, D.M. Crystal structure of the human NK_1 tachykinin receptor. *Proc. Natl. Acad. Sci. USA* **2018**, *115*, 13264–13269. [CrossRef] [PubMed]
5. Harrison, S.; Geppetti, P. Substance P. *Int. J. Biochem. Cell B* **2001**, *33*, 555–576. [CrossRef]
6. Palma, C. Tachykinins and their receptors in human malignancies. *Curr. Drug Targets* **2006**, *7*, 1043–1052. [CrossRef]
7. Chandrashekar, I.R.; Cowsik, S.M. Three-Dimensional Structure of the Mammalian Tachykinin Peptide Neurokinin A Bound to Lipid Micelles. *Biophys. J.* **2003**, *85*, 4002–4011. [CrossRef]
8. Steinhoff, M.S.; Mentzer, B.; Geppetti, P.; Pothoulakis, C.H.; Bunnett, N.W. Tachykinins and Their Receptors: Contributions to Physiological Control and the Mechanisms of Disease. *Physiol. Rev.* **2014**, *94*, 265–301. [CrossRef] [PubMed]
9. Valentin-Hansen, L.; Park, M.; Huber, T.; Grunbeck, A.; Naganathan, S.; Schwartz, T.W.; Sakmar, T.P. Mapping Substance P Binding Sites on the Neurokinin-1 Receptor Using Genetic Incorporation of a Photoreactive Amino Acid. *J. Biol Chem.* **2014**, *289*, 18045–18054. [CrossRef]
10. Sachon, E.; Girault-Lagrange, S.; Chassaing, G.; Lavielle, S.; Sagan, S. Analogs of Substance P modified at the C-terminus which are both agonist and antagonist of the NK-1 receptor depending on the second messenger pathway. *J. Pept. Res.* **2002**, *59*, 232–240. [CrossRef]
11. Sagan, S.; Lavielle, S. Internalization of [3H]substance P analogues in NK-1 receptor transfected CHO cells. *Biochem. Biophys. Res. Commun.* **2001**, *282*, 958–964. [CrossRef]
12. Sagan, S.; Quancard, J.; Lequin, O.; Karoyan, P.; Chassaing, G.; Lavielle, S. Conformational Analysis of the C-Terminal Gly-Leu-Met-NH_2 Tripeptide of Substance P Bound to the NK-1 Receptor. *Chem. Biol.* **2005**, *12*, 555–565. [CrossRef]
13. Quancard, J.; Karoyan, P.; Sagan, S.; Convert, O.; Lavielle, S.; Chassaing, G.; Lequin, O. Characterization of the bioactive conformation of the C-terminal tripeptide Gly-Leu-Met-NH_2 of substance P using [3-prolinoleucine10]SP analogues. *Eur. J. Biochem.* **2003**, *270*, 2869–2878. [CrossRef]
14. Alves, I.D.; Delaroche, D.; Mouillac, B.; Salamon, Z.; Tollin, G.; Hruby, V.J.; Lavielle, S.; Sagan, S. The Two NK-1 Binding Sites Correspond to Distinct, Independent, and Non-Interconvertible Receptor Conformational States as Confirmed by Plasmon-Waveguide Resonance Spectroscopy. *Biochemistry* **2006**, *45*, 5309–5318. [CrossRef]
15. Cordier, D.; Gerber, A.; Kluba, C.H.; Bauman, A.; Hutter, G.; Mindt, T.L.; Mariani, L. Expression of Different Neurokinin-1 Receptor (NK1R) Isoforms in Glioblastoma Multiforme: Potential Implications for Targeted Therapy. *Cancer Biother. Radiopharm.* **2014**, *29*, 221–226. [CrossRef]
16. Berger, M.; Neth, O.; Ilmer, M.; Garnier, A.; Salinas-Martín, M.V.; de Agustín Asencio, J.C.; von Schweinitz, D.; Kappler, R. Hepatoblastoma cells express truncated neurokinin-1 receptor and can be inhibited by aprepitant in vitro and in vivo. *J. Hepatol.* **2014**, *60*, 985–994. [CrossRef]
17. Rosso, M.; Robles-Frías, M.J.; Coveñas, R.; Salinas-Martín, M.V.; Muñoz, M. The NK-1 Receptor Is Expressed in Human Primary Gastric and Colon Adenocarcinomas and Is Involved in the Antitumor Action of L-733,060 and the Mitogenic Action of Substance P on Human Gastrointestinal Cancer Cell Lines. *Tumour. Biol.* **2008**, *29*, 245–254. [CrossRef]

18. Feng, F.; Yang, J.; Tong, L.; Yuan, S.; Tian, Y.; Hong, L.; Wang, W.; Zhang, H. Substance P immunoreactive nerve fibres are related to gastric cancer differentiation status and could promote proliferation and migration of gastric cancer cells. *Cell Biol. Int.* **2011**, *35*, 623–629. [CrossRef]
19. Severini, C.; Improta, G.; Falconieri-Erspamer, G.; Salvadori, S.; Erspamer, V. The Tachykinin Peptide Family. *Pharmacol. Rev.* **2002**, *54*, 285–322. [CrossRef]
20. Łazarczyk, M.; Matyja, E.; Lipkowski, A. Substance P and its receptors—A potential target for novel medicines in malignant brain tumour therapies (mini review). *Folia Neuropathol.* **2007**, *45*, 99–107.
21. Graham, G.J.; Stevens, J.M.; Page, N.M.; Grant, A.D.; Brain, S.D.; Lowry, P.J.; Gibbins, J.M. Tachykinins regulate the function of platelets. *Blood* **2004**, *104*, 1058–1065. [CrossRef]
22. Datar, P.; Srivastava, S.; Coutinho, E.; Govil, G. Substance P: Structure, Function, and Therapeutics. *Curr. Top. Med. Chem.* **2004**, *4*, 75–103. [CrossRef]
23. Page, N.M. New challenges in the study of the mammalian Tachykinins. *Peptides* **2005**, *26*, 1356–1368. [CrossRef]
24. Ho, W.Z.; Douglas, S.D. Substance P and neurokinin-1 receptor modulation of HIV. *J. Neuroimmunol.* **2004**, *157*, 48–55. [CrossRef]
25. Mashaghi, A.; Marmalidou, A.; Tehrani, M.; Grace, P.M.; Pothoulakis, C.H.; Dana, R. Neuropeptide Substance P and the Immune Response. *Cell Mol. Life Sci.* **2016**, *73*, 4249–4264. [CrossRef]
26. Grady, E.F.; Garland, A.M.; Gamp, P.D.; Lovett, M.; Payan, D.G.; Bunnett, N.W. Delineation of the Endocytic Pathway of Substance P and Its Seven-Transmembrane Domain NK1 Receptor. *Mol. Biol. Cell* **1995**, *6*, 509–524. [CrossRef]
27. Muñoz, M.; Martinez-Armesto, J.; Coveñas, R. NK-1 receptor antagonists as antitumor drugs: A survey of the literature from 2000 to 2011. *Expert Opin. Ther.* **2012**, *22*, 735–746. [CrossRef]
28. Joos, G.F.; Germonpre, P.R.; Pauwels, R.A. Role of tachykinins in asthma. *Allergy* **2000**, *55*, 321–337. [CrossRef]
29. Yip, J.; Chahl, L.A. Localization of NK1 and NK3 receptors in guinea-pig brain. *Regul. Pept.* **2001**, *98*, 55–62. [CrossRef]
30. Skidgel, R.A.; Engelbrecht, S.; Johnson, A.R.; Erdös, E.G. Hydrolysis of substance P and neurotensin by converting enzyme and neutral endopeptidase. *Peptides* **1984**, *5*, 769–776. [CrossRef]
31. Skidgel, R.A.; Erdos, E.G. Angiotensin converting enzyme (ACE) and neprilysin hydrolyze neuropeptides: A brief history, the beginning and follow-ups to early studies. *Peptides* **2004**, *25*, 521–525. [CrossRef]
32. Lockridge, O. Substance P hydrolysis by human serum cholinesterase. *J. Neurochem.* **1982**, *39*, 106–110. [CrossRef]
33. Sakurada, C.H.; Watanabe, C.H.; Sakurada, S.; Tan-No, K.; Sakurada, T. Major metabolites of substance P degraded by spinal synaptic membranes antagonize the behavioral response to substance P in rats. *J. Pharm. Sci.* **1999**, *88*, 1127–1132. [CrossRef]
34. Sandberg, B.E.; Lee, C.M.; Hanley, M.R.; Iversen, L.L. Synthesis and biological properties of enzyme-resistant analogues of substance P. *Eur. J. Biochem.* **1981**, *114*, 329–337. [CrossRef]
35. Wagner, E.; Partsch, G.; Dunky, A. Substance P and its cleavage products: Effects on interleukin-1 secretion of rheumatoid arthritis monocytes/macrophages. *Arthritis Res.* **2001**, *3*, P019. [CrossRef]
36. Skidgel, R.A.; Jackman, H.L.; Erdos, E.G. Metabolism of substance P and bradykinin by human neutrophils. *Biochem. Pharmacol.* **1991**, *41*, 1335–1344. [CrossRef]
37. Chubb, I.W.; Hodgson, A.J.; White, G.H. Acetylocholinoesterase hydrolyzes substance P. *Neuroscience* **1980**, *5*, 2065–2072. [CrossRef]
38. Mantyh, P.W. Neurobiology of substance P and the NK1 receptor. *J. Clin. Psychiatry* **2002**, *63*, 6–10.
39. Gesztesi, Z.; Scuderi, P.E.; White, P.F.; Wright, W.; Wender, R.H.; D'Angelo, R.; Black, L.S.; Dalby, P.L.; MacLean, D. Substance P (Neurokinin-1) antagonist prevents postoperative vomiting after abdominal hysterectomy procedures. *Anesthesiology* **2000**, *93*, 931–937. [CrossRef]
40. Aapro, M.S.; Walko, C.M. Aprepitant: Drug–drug interactions in perspective. *Ann. Oncol.* **2010**, *21*, 2316–2323. [CrossRef]
41. Schmidt, P.T.; Lordal, M.; Gazelius, B.; Hellstrom, P.M. Tachykinins potently stimulate human small bowel blood flow: A laser Doppler flowmetry study in humans. *Gut* **2003**, *52*, 53–56. [CrossRef]
42. Bernstein, C.N.; Robert, M.E.; Eysselein, V.E. Rectal substance P concentrations are increased in ulcerative colitis but not in Crohn's disease. *Am. J. Gastroenterol.* **1993**, *88*, 908–913.

43. Goode, T.; O'Connell, J.; Anton, P.; Wong, H.; Reeve, J.; O'Sullivan, G.C.; Collins, J.K.; Shanahan, F. Neurokinin-1 receptor expression in inflammatory bowel disease: Molecular quantitation and localisation. *Gut* **2000**, *47*, 387–396. [CrossRef]
44. Evangelista, S. Involvement of tachykinins in intestinal inflammation. *Curr. Pharm Des.* **2001**, *7*, 19–30. [CrossRef]
45. McMahona, S.B.; Cafferty, W.B.J.; Marchand, F. Review, Immune and glial cell factors as pain mediators and modulators. *Exp. Neurol.* **2005**, *192*, 444–462. [CrossRef]
46. El-Raziky, M.S.; Gohar, N.; El-Raziky, M. Study of substance P, renine and aldosterone in chronic liver disease in Egyptian children. *J. Top. Pediatr.* **2005**, *51*, 320–323. [CrossRef]
47. Goto, T.; Tanaka, T. Tachykinins and tachykinin receptors in bone. *Microsc. Res. Tech.* **2002**, *58*, 91–97. [CrossRef]
48. Lorente, L. New prognostic biomarkers of mortality in patients undergoing liver transplantation for hepatocellular carcinoma. *J. Neurochem.* **2018**, *24*, 4230–4242. [CrossRef]
49. Goto, T.; Nakao, K.; Gunjigake, K.K.; Kido, M.A.; Kobayashi, S.; Tanaka, T. Substance P stimulates late-stage rat osteoblastic bone formation through neurokinin-1 receptors. *Neuropeptides* **2007**, *41*, 25–31. [CrossRef]
50. Nowicki, M.; Ostalska-Nowicka, D.; Konwerska, A.; Miskowiak, B. The predicting role of substance P in the neoplastic transformation of the hypoplastic bone marrow. *J. Clin. Pathol.* **2006**, *59*, 935–941. [CrossRef]
51. Nakamura, M.; Chikama, T.; Nishida, T. Synergistic effect with Phe-Gly-Leu-Met-NH_2 of the C-terminal of substance P and insulin-like growth factor-1 on epithelial wound healing of rabbit cornea. *Br. J. Pharmacol.* **1999**, *127*, 489–497. [CrossRef]
52. Fan, T.P.; Hu, D.E.; Guard, S.; Gresham, G.A.; Watling, K.J. Stimulation of angiogenesis by substance P and interleukin-1 in the rat and its inhibition by NK1 or interleukin-1 receptor antagonists. *Br. J. Pharmacol.* **1993**, *110*, 43–49. [CrossRef]
53. Merlo, A.; Mäcke, H.; Reubi, J.C.; Good, S. Radiolabeled Conjugates Based on Substance P and the Uses. Thereof. Patent No. WO 2004/082722, 30 September 2004.
54. Hoover, D.B.; Chang, Y.; Hancock, J.C.; Zhang, L. Action of Tachykinins Within the Heart and Their Relevance to Cardiovascular Disease. *Jpn. J. Pharmacol.* **2000**, *84*, 367–373. [CrossRef]
55. Cordier, D.; Forrer, F.; Bruchertseifer, F.; Morgenstern, A.; Apostolidis, C.; Good, S.; Müller-Brand, J.; Mäcke, H.; Reubi, J.C.; Merlo, A. Targeted alpha-radionuclide therapy of functionally critically located gliomas with ^{213}Bi-DOTA-[Thi^{8},Met$(O_2)^{11}$]-substance P: A pilot trial. *Eur. J. Nucl. Med. Mol. Imaging* **2010**, *37*, 1335–1344. [CrossRef]
56. Juszczak, M.; Stempniak, B. Melatonin inhibits the substance P-induced secretion of vasopressin and oxytocin from the rat hypothalamo-neurohypophysial system: In vitro studies. *Brain Res. Bull.* **2003**, *59*, 393–397. [CrossRef]
57. Juszczak, M.; Boczek-Leszczyk, E.; Stempniak, B. Effect of melatonin on the vasopressin secretion as influenced by tachykinin NK-1 receptor agonist and antagonist: In vivo and in vitro studies. *J. Physiol. Pharmacol.* **2007**, *58*, 829–843.
58. Feng, Z.; Xu, B. Inspiration from the mirror: D-amino acid containing peptides in biomedical approaches. *Biomol. Concepts* **2016**, *7*, 179–187. [CrossRef]
59. Kasheverov, I.E.; Utkin, Y.N.; Franke, P.; Tsetlin, V.I. Substance P derivatives with photoactivatable labels in the N-terminal part of the molecule. *J. Pept. Res.* **1997**, *50*, 408–414. [CrossRef]
60. Pradier, L.; Menager, J.; Le Guern, J.; Bock, M.D.; Heuillet, F.; Fardin, V.; Garret, C.; Doble, A.; Mayaux, J.F. Septide: An agonist for the NK1 receptor acting at a site distinct from substance P. *Mol. Pharmmacol.* **1994**, *45*, 287–293.
61. Sakurada, C.; Watanabe, C.; Inoue, M.; Tan-No, K.; Ando, R.; Kisara, K.; Sakurada, T. Spinal actions of GR73632, a novel tachykinin NK1 receptor agonist. *Peptides* **1999**, *20*, 301–304. [CrossRef]
62. Lazarus, L.H.; Diaugustine, R.P.; Soldato, C.M. A Substance with Immunoreactivity to the Peptide Physalaemin in Mammalian Respiratory Tissue. *J. Exp. Lung Res.* **1982**, *3*, 329–341. [CrossRef]
63. Champagne, D.; Ribeiro, E.J.M. Sialokinin I and II: Vasodilatory tachykinins from the yellow fever mosquito Aedes aegypti. *Proc. Natl. Acad. Sci. USA* **1994**, *91*, 138–142. [CrossRef]
64. Schwyzer, R. Membrane-assisted molecular mechanism of neurokinin receptor subtype selection. *EMBO J.* **1987**, *6*, 2255–2259. [CrossRef]

65. Iwabuchi, Y.; Aoki, C.H.; Masuhara, T. Effects of Tachykinins on the Secretion of Fluid and Glycoproteins from the Submandibular Glands of Rat, Mouse, Hamster and Guinea Pig. *Jpn. J. Pharmacol.* **1989**, *51*, 428–431. [CrossRef]
66. Majumdar, A.K.; Howard, L.; Goldberg, M.R.; Hickey, L.; Constanzer, M.; Rothenberg, P.L.; Crumley, T.M.; Panebianco, D.; Bradstreet, T.E.; Bergman, A.J.; et al. Pharmacokinetics of Aprepitant After Single and Multiple Oral Doses in Healthy Volunteers. *J. Clin. Pharmacol.* **2006**, *46*, 291–300. [CrossRef]
67. Jin, Y.; Wu, X.; Guan, Y.; Gu, D.; Shen, Y.; Xu, Z.; Wei, X.; Chen, J. Efficacy and safety of aprepitant in the prevention of chemotherapy-induced nausea and vomiting: A pooled analysis. Support. *Care Cancer* **2012**, *20*, 1815–1822. [CrossRef]
68. Aapro, M.S.; Schmoll, H.J.; Jahn, F.; Carides, A.D.; Webb, R.T. Review of the efficacy of aprepitant for the prevention of chemotherapy-induced nausea and vomiting in a range of tumor types. *Cancer Treat. Rev.* **2013**, *39*, 113–117. [CrossRef]
69. Aoki, S.; Iihara, H.; Nishigaki, M.; Imanishi, Y.; Yamauchi, K.; Ishihara, M.; Kitaichi, K.; Itoh, Y. Difference in the emetic control among highly emetogenic chemotherapy regimens: Implementation for appropriate use of aprepitant. *Mol. Clin. Oncol.* **2013**, *1*, 41–46. [CrossRef]
70. Muñoz, M.; Coveñas, R. Safety of neurokinin-1 receptor antagonists. *Expert Opin. Drug Saf.* **2013**, *12*, 673–685. [CrossRef]
71. Varuby Product Characteristics-EMEA/H/C/004196-T/0015. Available online: Ema.europa.eu/en/documents/product-information/varuby-epar-product-information_en.pdf (accessed on 15 May 2019).
72. Cerenia Product Characteristics-EMEA/V/C/000106-IB/0035/G. Available online: Ema.europa.eu/en/documents/product-information/cerenia-epar-product-information_en.pdf (accessed on 15 May 2019).
73. Akynzeo Product Characteristics-EMEA/H/C/003728-N/0022. Available online: Ema.europa.eu/en/documents/product-information/akynzeo-epar-product-information_en.pdf (accessed on 15 May 2019).
74. Zunrisa Withdrawal Report EMEA/H/C/1040. Available online: Ema.europa.eu/en/documents/withdrawal-report/withdrawal-assessment-report-zunrisa_en.pdf (accessed on 15 May 2019).
75. Quartara, L.; Altamura, M.; Evangelista, S.; Maggi, C.A. Tachykinin receptor antagonists in clinical trials. *Expert Opin. Investig. Drugs* **2009**, *18*, 1843–1864. [CrossRef]
76. Keller, M.; Montgomery, S.; Ball, W.; Morrison, M.; Snavely, D.; Liu, G.; Hargreaves, R.; Hietala, J.; Lines, C.; Beebe, K.; et al. Lack of Efficacy of the Substance P (Neurokinin1 Receptor) Antagonist Aprepitant in the Treatment of Major Depressive Disorder. *Biol. Psychiatry* **2006**, *59*, 216–223. [CrossRef]
77. Huang, S.C.; Korlipara, V.L. Neurokinin-1 receptor antagonists: A comprehensive patent survey. *Expert Opin. Ther. Pat.* **2010**, *20*, 1019–1045. [CrossRef]
78. Michelson, D.; Hargreaves, R.; Alexander, R.; Ceesay, P.; Hietala, J.; Lines, C.; Reines, S. Lack of efficacy of L-759274, a novel neurokinin 1 (substance P) receptor antagonist, for the treatment of generalized anxiety disorder. *Int. J. Neuropsychopharmacol.* **2013**, *16*, 1–11. [CrossRef]
79. Muñoz, M.; Coveñas, R. Involvement of substance P and the NK-1 receptor in human pathology. *Amino Acids* **2014**, *46*, 1727–1750. [CrossRef]
80. George, D.T.; Gilman, J.; Hersh, J.; Thorsell, A.; Herion, D.; Geyer, C.; Peng, X.; Kielbasa, W.; Rawlings, R.; Brandt, J.E.; et al. Neurokinin 1 receptor antagonism as a possible therapy for alcoholism. *Science* **2008**, *319*, 1536–1539. [CrossRef]
81. Torres, T.; Fernandes, I.; Selores, M.; Alves, R.; Lima, M. Aprepitant: Evidence of its effectiveness in patients with refractory pruritus continues. *J. Am. Acad. Dermatol.* **2012**, *68*, e14–e15. [CrossRef]
82. Yosipovitch, G.; Ständer, S.; Kerby, M.B.; Larrick, J.W.; Perlman, A.J.; Schnipper, E.F.; Zhang, X.; Tang, J.Y.; Luger, T.; Steinhoff, M. Serlopitant for the treatment of chronic pruritus: Results of a randomized, multicenter, placebo-controlled phase 2 clinical trial. *J. Am. Acad. Dermatol.* **2018**, *78*, 882–891. [CrossRef]
83. Muñoz, M.; Rosso, M.; Pérez, A.; Coveñas, R.; Rosso, R.; Zamarriego, C.; Piruat, J.I. The NK1 receptor is involved in the antitumoural action of L-733,060 and the mitogenic action of substance P on neuroblastoma and glioma cell lines. *Neuropeptides* **2005**, *39*, 427–432. [CrossRef]
84. Muñoz, M.; Rosso, M.; Pérez, A.; Coveñas, R.; Rosso, R.; Zamarriego, C.; Soult, J.A.; Montero, I. Antitumoral action of the neurokinin-1-receptor antagonist L-733,060 and mitogenic action of substance P on human retinoblastoma cell lines. *Investig. Ophthalmol. Vis. Sci.* **2005**, *46*, 2567–2570. [CrossRef]

85. Muñoz, M.; Rosso, M.; Coveñas, R. The NK-1 receptor is involved in the antitumoural action of L-733,060 and in the mitogenic action of substance P on human pancreatic cancer cell lines. *Lett. Drug Des. Discov.* **2006**, *3*, 323–329. [CrossRef]
86. Muñoz, M.; Rosso, M.; Aguilar, F.J.; González-Moles, M.A.; Redondo, M.; Esteban, F. NK-1 receptor antagonists induce apoptosis and counteract substance P-related mitogenesis in human laryngeal cancer cell line HEp-2. *Investig. New Drugs* **2008**, *26*, 111–118. [CrossRef]
87. Muñoz, M.; Rosso, M.; Coveñas, R. A new frontier in the treatment of cancer: NK-1 receptor antagonists. *Curr. Med. Chem.* **2010**, *17*, 504–516. [CrossRef]
88. Muñoz, M.; Rosso, M.; Robles-Frías, M.J.; Salinas-Martín, M.V.; Coveñas, R. The NK-1 receptor is expressed in human melanoma and is involved in the antitumor action of the NK-1 receptor antagonist aprepitant on melanoma cell lines. *Lab. Investig.* **2010**, *90*, 1259–1269. [CrossRef]
89. Muñoz, M.; Rosso, M. The NK-1 receptor antagonist aprepitant as a broad-spectrum antitumor drug. *Investig. New Drugs* **2010**, *28*, 187–193. [CrossRef]
90. Muñoz, M.; Bernabeu-Wittel, J.; Coveñas, R. NK-1 as a melanoma target. *Expert Opin. Ther. Targets* **2011**, *15*, 889–897. [CrossRef]
91. Muñoz, M.; González-Ortega, A.; Coveñas, R. The NK-1 receptor is expressed in human leukemia and is involved in the antitumor action of aprepitant and other NK-1 receptor antagonists on acute lymphoblastic leukemia cell lines. *Investig. New Drugs* **2012**, *30*, 529–540. [CrossRef]
92. Muñoz, M.; González-Ortega, A.; Rosso, M.; Robles-Frías, M.J.; Carranza, A.; Salinas-Martín, M.V.; Coveñas, R. The substance P/neurokinin-1 receptor system in lung cancer: Focus on the antitumor action of neurokinin-1 receptor antagonists. *Peptides* **2012**, *38*, 318–325. [CrossRef]
93. Muñoz, M.; Rosso, M.; Coveñas, R. The NK-1 receptor antagonist L-732,138 induces apoptosis in human gastrointestinal cancer cell lines. *Pharm. Rep.* **2017**, *69*, 696–701. [CrossRef]
94. Muñoz, M.; Coveñas, R.; Esteban, F.; Redondo, M. The substance P/NK-1 receptor system: NK-1 receptor antagonists as anti-cancer drugs. *J. Biosci.* **2015**, *40*, 441–463. [CrossRef]
95. Muñoz, M.; Berger, M.; Rosso, M.; Gonzalez-Ortega, A.; Carranza, A.; Coveñas, R. Antitumor activity of neurokinin-1 receptor antagonists in MG-63 human osteosarcoma xenografts. *Int. J. Oncol.* **2014**, *44*, 137–146. [CrossRef]
96. Muñoz, M.; Coveñas, R. Involvement of substance P and the NK-1 receptor in cancer progression. *Peptides* **2013**, *48*, 1–9. [CrossRef]
97. Coveñas, R.; Muñoz, M. Cancer progression and substance P. *Histol. Histopathol.* **2014**, *29*, 881–890. [CrossRef]
98. Muñoz, M.; González-Ortega, A.; Salinas-Martín, M.V.; Carranza, A.; Garcia-Recio, S.; Almendro, V.; Coveñas, R. The neurokinin-1 receptor antagonist aprepitant is a promising candidate for the treatment of breast cancer. *Int. J. Oncol.* **2014**, *45*, 1658–1672. [CrossRef]
99. Kast, R.E.; Boockvar, J.A.; Brüning, A.; Cappello, F.; Chang, W.W.; Cvek, B.; Dou, Q.P.; Duenas-Gonzalez, A.; Efferth, T.; Focosi, D.; et al. A conceptually new treatment approach for relapsed glioblastoma: Coordinated undermining of survival paths with nine repurposed drugs (CUSP9) by the International Initiative for Accelerated Improvement of Glioblastoma Care. *Oncotarget* **2013**, *4*, 502–530. [CrossRef]
100. Muñoz, M.; Rosso, M.; González, A.; Saenz, J.; Coveñas, R. The broad-spectrum antitumor action of cyclosporin A is due to its tachykinin receptor antagonist pharmacological profile. *Peptides* **2010**, *31*, 1643–1648. [CrossRef]
101. González-Ortega, A.; Sánchez-Valderrábanos, E.; Ramiro-Fuentes, S.; Salinas-Martín, M.V.; Carranza, A.; Coveñas, R.; Muñoz, M. Uveal melanoma expresses NK-1 receptors and cyclosporin A induces apoptosis in human melanoma cell lines overexpressing the NK-1 receptor. *Peptides* **2014**, *55*, 1–12. [CrossRef]
102. Baum, R.P. *Therapeutic Nuclear Medicine*; Springer Publisher: Heidelberg, Germany, 2014.
103. International Atomic Energy Agency, Nuclear Data Services, Live Chart of Nuclides, Nuclear Structure and Decay Data. Available online: https://www-nds.iaea.org/relnsd/vcharthtml/VChartHTML.html (accessed on 28 July 2019).
104. Sjödin, L. Binding and internalization of ^{125}I-Bolton-Hunter-substance-P by pancreatic acinar cells. *Biochem. Biophys. Res. Commun.* **1984**, *124*, 578–584. [CrossRef]
105. Larsen, P.J.; Mikkelsen, J.D.; Saermark, T. Binding of a iodinated substance P analog to a NK-1 receptor on isolated cell membranes from rat anterior pituitary. *Endocrinology* **1989**, *124*, 2548–2557. [CrossRef]

106. Larsen, P.J.; Mikkelsen, J.D.; Mau, S.; Saermark, T. Binding and internalization of a iodinated substance P analog by cultured anterior pituitary cells. *Mol. Cell Endocrinol.* **1989**, *65*, 91–101. [CrossRef]
107. Larsen, P.J.; Saermark, T.; Mau, S.E. Binding of an iodinated substance P analogue to cultured anterior pituitary prolactin- and luteinizing hormone-containing cells. *J. Histochem. Cytochem.* **1992**, *40*, 487–493. [CrossRef]
108. Shigematsu, K.; Saavedra, J.M.; Kurihara, M. Specific substance P binding sites in rat thymus and spleen: In vitro autoradiographic study. *Regul. Pept.* **1986**, *16*, 147–156. [CrossRef]
109. Beaujouan, J.C.; Torrens, Y.; Saffroy, M.; Glowinski, J. Quantitative autoradiographic analysis of the distribution of binding sites for [^{125}I]Bolton Hunter derivatives of eledoisin and substance P in the rat brain. *Neuroscience* **1986**, *18*, 857–875. [CrossRef]
110. Geraghty, D.P.; Maguire, C.M. Reduced [^{125}I]-Bolton Hunter substance P binding (NK1 receptors) in the basal forebrain nuclei of aged rats. *Clin. Exp. Pharmacol. Physiol.* **2002**, *29*, 1112–1115. [CrossRef]
111. Charlton, C.G.; Helke, C.J. Characterization and segmental distribution of 125I-Bolton-Hunter-labeled substance P binding sites in rat spinal cord. *J. Neurosci.* **1985**, *5*, 1293–1299. [CrossRef]
112. Cridland, R.A.; Yashpal, K.; Romita, V.V.; Gauthier, S.; Henry, J.L. Distribution of label after intrathecal administration of 125I-substance P in the rat. *Peptides* **1987**, *8*, 213–221. [CrossRef]
113. Aanonsen, L.M.; Kajander, K.C.; Bennett, G.J.; Seybold, V.S. Autoradiographic analysis of ^{125}I-substance P binding in rat spinal cord following chronic constriction injury of the sciatic nerve. *Brain Res.* **1992**, *596*, 259–268. [CrossRef]
114. Stucky, C.L.; Galeazza, M.T.; Seybold, V.S. Time-dependent changes in Bolton-Hunter-labelled ^{125}I-substance P binding in rat spinal cord following unilateral adjuvant-induced peripheral inflammation. *Neuroscience* **1993**, *57*, 397–409. [CrossRef]
115. Maguire, C.M.; Geraghty, D.P. Comparison of [^{125}I]-bolton-hunter substance P binding in young and aged rat spinal cord. *Brain Res.* **1998**, *786*, 263–266. [CrossRef]
116. Liu, L.; Burcher, E. Radioligand binding and functional characterisation of tachykinin receptors in chicken small intestine. *Naunyn Schmiedebergs Arch. Pharmacol.* **2001**, *364*, 305–313. [CrossRef]
117. Garland, A.M.; Grady, E.F.; Payan, D.G.; Vigna, S.R.; Bunnett, N.W. Agonist-induced internalization of the substance P (NK1) receptor expressed in epithelial cells. *Biochem. J.* **1994**, *303*, 177–186. [CrossRef]
118. Beaujouan, J.C.; Torrens, Y.; Herbet, A.; Daguet, M.C.; Glowinski, J.; Prochiantz, A. Specific binding of an immunoreactive and biologically active 125I-labeled substance P derivative to mouse mesencephalic cells in primary culture. *Mol. Pharmacol.* **1982**, *22*, 48–55.
119. Liang, T.; Cascieri, M.A. Substance P receptor on parotid cell membranes. *J. Neurosci.* **1981**, *1*, 1133–1141. [CrossRef]
120. Kieselbach, G.F.; Ragaut, R.; Knaus, H.G.; König, P.; Wiedermann, C.J. Autoradiographic analysis of binding sites for ^{125}I-Bolton-Hunter-substance P in the human eye. *Peptides* **1990**, *11*, 655–659. [CrossRef]
121. Buffington, C.A.; Wolfe, S.A. High affinity binding sites for [^{3}H]substance P in urinary bladders of cats with interstitial cystitis. *J. Urol.* **1998**, *160*, 605–611. [CrossRef]
122. Breeman, W.A.P.; Van Hagen, M.P.; Visser-Wisselaar, H.A.; van der Pluijm, M.E.; Koper, J.W.; Setyono-Han, B.; Bakker, W.H.; Kwekkeboom, D.J.; Hazenberg, M.P.; Lamberts, S.W.J.; et al. In Vitro and In Vivo Studies of Substance Receptor Expression in Rats with the New Analog [Indium-111-DTPA-Arg^{1}]Substance P. *J. Nucl. Med.* **1996**, *37*, 108–117.
123. van Hagen, P.M.; Breeman, W.A.; Reubi, J.C.; Postema, P.T.; van den Anker-Lugtenburg, P.J.; Kwekkeboom, D.J.; Laissue, J.; Waser, B.; Lamberts, S.W.; Visser, T.J.; et al. Visualization of the thymus by substance P receptor scintigraphy in man. *Eur. J. Nucl. Med.* **1996**, *23*, 1508–1513. [CrossRef]
124. Ozker, S.K.; Hellman, R.S.; Krasnow, A.Z. Preparation of ^{99m}Tc labeled substance P (SP). *Appl. Radiat. Isot.* **2002**, *57*, 729–732. [CrossRef]
125. Gniazdowska, E.; Koźmiński, P.; Fuks, L. Synthesis, radiochemistry and stability of the conjugates of technetium-99m complexes with Substance P. *J. Radioanal. Nucl. Chem.* **2013**, *298*, 1171–1177. [CrossRef]
126. Smilkov, K.; Janevik, E.; Guerrini, R.; Pasquali, M.; Boschi, A.; Uccelli, L.; Duatti, G.D.A. Preparation and first biological evaluation of novel Re-188/Tc-99m peptide conjugates with substance-P. *Appl. Radiat. Isot.* **2014**, *92*, 25–31. [CrossRef]

127. Królicki, L.; Bruchertseifer, F.; Kunikowska, J.; Koziara, H.; Królicki, B.; Jakuciński, M.; Pawlak, D.; Apostolidis, C.; Mirzadeh, S.; Rola, R.; et al. Prolonged survival in secondary glioblastoma following local injection of targeted alpha therapy with 213Bi-substance P analogue. *Eur. J. Nucl. Med. Mol. Imaging* **2018**, *45*, 1636–1644. [CrossRef]
128. Mozaffari, S.; Erfani, M.; Beiki, D.; Johari Daha, F.; Kobarfard, F.; Balalaie, S.; Fallahi, B. Synthesis and preliminary evaluation of a new ^{99m}Tc labeled Substance P analogue as a potential tumor imaging agent. *Iranian J. Pharm. Res.* **2015**, *14*, 97–110.
129. Lew, R.; Geraghty, D.P.; Drapeau, G.; Regoli, D.; Burcher, E. Binding characteristics of [^{125}I]Bolton-Hunter [Sar^{9},Met(O$_2$)^{11}]substance P, a new selective radioligand for the NK1 receptor. *Eur. J. Pharmacol.* **1990**, *184*, 97–108. [CrossRef]
130. Tousignant, C.; Guillemette, G.; Drapeau, G.; Télémaque, S.; Dion, S.; Regoli, D. ^{125}I-BH[Sar^{9}, Met(O$_2$)^{11}]-SP, a new selective ligand for the NK-1 receptor in the central nervous system. *Brain Res.* **1990**, *524*, 263–270. [CrossRef]
131. Dam, T.V.; Martinelli, B.; Quirion, R. Autoradiographic distribution of brain neurokinin-1/substance P receptors using a highly selective ligand [^{3}H]-[Sar^{9}, Met(O$_2$)^{11}]-substance P. *Brain Res.* **1990**, *531*, 333–337. [CrossRef]
132. Oyen, W.J.G.; Bodei, L.; Giammarile, F.; Maecke, H.R.; Tenvall, J.; Luster, M.; Brans, B. Targeted therapy in nuclear medicine–current status and future prospects. *Ann. Oncol.* **2007**, *18*, 1782–1792. [CrossRef]
133. De Araújo, E.B.; Pujatti, P.B.; Barrio, O.; Caldeira, J.S.; Suzuki, M.F.; Mengatti, J. Radiolabeling of Substance P with Lutetium-177 and biodistribution study in AR42J pancreatic tumor xenografted Nude mice. *J. Nucl. Med.* **2008**, *49*, 6.
134. Kneifel, S.; Cordier, D.; Good, S.; Ionescu, M.C.S.; Ghaffari, A.; Hofer, S.; Kretzschmar, M.; Tolnay, M.; Apostolidis, C.; Waser, B.; et al. Local Targeting of Malignant Gliomas by the Diffusible Peptidic Vector 1,4,7,10-Tetraazacyclododecane-1-Glutaric Acid-4,7,10-Triacetic Acid-Substance P. *Clin. Cancer Res.* **2006**, *12*, 3843–3850. [CrossRef]
135. Cordier, D.; Forrer, F.; Kneifel, S.; Sailer, M.; Mariani, L.; Maecke, H.; Muller-Brand, J.; Merlo, A. Neoadjuvant targeting of glioblastoma multiforme with radiolabeled DOTAGA–substance P—Results from a phase I study. *J. Neurooncol.* **2010**, *100*, 129–136. [CrossRef]
136. Królicki, L.; Bruchertseifer, F.; Kunikowska, J.; Koziara, H.; Królicki, B.; Jakuciński, M.; Pawlak, D.; Apostolidis, C.; Mirzadeh, S.; Rola, R.; et al. Safety and efficacy of targeted alpha therapy with ^{213}Bi-DOTA-substance P in recurrent glioblastoma. *Eur. J. Nucl. Med. Mol. Imaging* **2019**, *46*, 614–622. [CrossRef]
137. Ohgaki, H.; Dessen, P.; Jourde, B.; Horstmann, S.; Nishikawa, T.; Di Patre, P.L.; Burkhard, C.; Schüler, D.; Probst-Hensch, N.M.; Maiorka, P.C.; et al. Genetic pathways to glioblastoma: A population-based study. *Cancer Res.* **2004**, *64*, 6892–6899. [CrossRef]
138. Park, J.K.; Hodges, T.; Arko, L.; Shen, M.; Dello Iacono, D.; McNabb, A.; Olsen Bailey, N.; Kreisl, T.N.; Iwamoto, F.M.; Sul, J.; et al. Scale to predict survival after surgery for recurrent glioblastoma multiforme. *J. Clin. Oncol.* **2010**, *28*, 3838–3843. [CrossRef]
139. Majkowska-Pilip, A.; Rius, M.; Bruchertseifer, F.; Apostolidis, C.; Weis, M.; Bonelli, M.; Laurenza, M.; Królicki, L.; Morgenstern, A. In vitro evaluation of ^{225}Ac-DOTA-substanceP for targeted alpha therapy of glioblastoma multiforme. *Chem. Biol. Drug Des.* **2018**, *92*, 1344–1356. [CrossRef]
140. Song, H.; Guerrero-Cazares, H.; Horti, A.; Wahl, R.L.; Quinones-Hinojosa, A.; Sgouros, G. Synthesis and Biodistribution of ^{225}Ac-substance P for Intracavitary Radiopharmaceutical Therapy of High-grade Recurrent Glioma. In *Cancer Research, Proceedings of the AACR 104th Annual Meeting, Washington, DC/Philadelphia, PA, USA, 6–10 April 2013*; AACR: Washington, DC, USA; Philadelphia, PA, USA, 2013; Volume 73, p. 4533.
141. Jordan, C.T.; Guzman, M.L.; Noble, M. Cancer stem cells. *N. Eng. J. Med.* **2006**, *355*, 1253–1261. [CrossRef]
142. Bao, S.; Wu, Q.; McLendon, R.E.; Hao, Y.; Shi, Q.; Hjelmeland, A.B.; Dewhirst, M.W.; Bigner, D.D.; Rich, J.N. Glioma stem cells promote radioresistance by preferential activation of the DNA damage response. *Nature* **2006**, *444*, 756–760. [CrossRef]
143. Liu, G.; Yuan, X.; Zeng, Z.; Tunici, P.; Ng, H.; Abdulkadir, I.R.; Lu, L.; Irvin, D.; Black, K.L.; Yu, J.S. Analysis of gene expression and chemoresistance of CD133^{+} cancer stem cells in glioblastoma. *Mol. Cancer* **2006**, *5*, 67–79. [CrossRef]

144. Krolicki, L.; Bruchertseifer, F.; Morgenstern, A.; Kunikowska, J.; Koziara, H.; Krolicki, B.; Jakucinski, M.; Pawlak, D.; Apostolidis, C.; Rola, R.; et al. Safety and Therapeutic Efficacy of ^{225}Ac-DOTA-SubstanceP for Therapy of Brain Tumors. *J. Med. Imaging Radiat. Sci.* **2019**, *50*, S22. [CrossRef]
145. Majkowska-Pilip, A.; Koźmiński, P.; Wawrzynowska, A.; Budlewski, T.; Kostkiewicz, B.; Gniazdowska, E. Application of Neurokinin-1 Receptor in Targeted Strategies for Glioma Treatment. Part I: Synthesis and Evaluation of Substance P Fragments Labeled with ^{99m}Tc and ^{177}Lu as Potential Receptor Radiopharmaceuticals. *Molecules* **2018**, *23*, 2542. [CrossRef]
146. Del Rosario, R.B.; Managner, T.J.; Gildersleeve, D.L.; Shreve, P.D.; Wieland, D.M.; Lowe III, J.A.; Drozda, S.E.; Snider, R.M. Synthesis of a Nonpeptide Carbon-11 Labeled Substance P Antagonist for PET Studies. *Nucl. Med. Biol.* **1993**, *20*, 545–547. [CrossRef]
147. Livni, E.; Babich, J.W.; Desa, M.C.; Godek, D.M.; Wilkinson, R.A.; Rubin, R.H.; Fischman, A.J. Synthesis of a 11 C-labeled NK1 Receptor Ligand for PET Studies. *Nucl. Med. Biol.* **1995**, *22*, 31–36. [CrossRef]
148. Bender, D.; Olsen, A.K.; Marthi, M.K.; Smith, D.F.; Cumming, P. PET evaluation of the uptake of N-[11C]methyl CP-643,051, an NK1 receptor antagonist, in the living porcine brain. *Nucl. Med. Biol.* **2004**, *31*, 699–704. [CrossRef]
149. Bergström, M.; Fasth, K.J.; Kilpatrick, G.; Ward, P.; Cable, K.M.; Wipperman, M.D.; Sutherland, D.R.; Langström, B. Brain uptake and receptor binding of two [11C]labelled selective high affinity NK1-antagonists, GR203040 and GR205171-PET studies in rhesus monkey. *Neuropharmacology* **2000**, *39*, 664–670. [CrossRef]
150. Nyman, M.J.; Eskola, O.; Kajander, J.; Vahlberg, T.; Sanabria, S.; Burns, D.; Hargreaves, R.; Solin, O.; Hietala, J. Gender and age affect NK1 receptors in the human brain—A positron emission tomography study with [18F]SPA-RQ. *Int. J. Neuropsychopharmacol.* **2007**, *10*, 219–229. [CrossRef]
151. Engman, J.; Åhs, F.; Furmark, T.; Linnman, C.; Pissiota, A.; Appel, L.; Frans, Ö.; Långström, B.; Fredrikson, M. Age, sex and NK1 receptors in the human brain—A positron emission tomography study with [11C]GR205171. *Eur. Neuropsychopharmacol.* **2012**, *22*, 562–568. [CrossRef]
152. Hietala, J.; Nyman, M.J.; Eskola, O.; Laakso, A.; Grönroos, T.; Oikonen, V.; Bergman, J.; Haaparanta, M.; Forsback, S.; Marjamäki, P.; et al. Visualization and Quantification of Neurokinin-1 (NK1) Receptors in the Human Brain. *Mol. Imaging Biol.* **2005**, *7*, 262–272. [CrossRef]
153. Haneda, E.; Higuchi, M.; Maeda, J.; Inaji, M.; Okauchi, T.; Ando, K.; Obayashi, S.; Nagai, Y.; Narazaki, M.; Ikehira, H.; et al. In Vivo Mapping of Substance P Receptors in Brains of Laboratory Animals by High-Resolution Imaging Systems. *Synapse* **2007**, *61*, 205–215. [CrossRef]
154. Okumura, M.; Arakawa, R.; Ito, H.; Seki, C.; Takahashi, H.; Takano, H.; Haneda, E.; Nakao, R.; Suzuki, H.; Suzuki, K.; et al. Quantitative Analysis of NK1 Receptor in the Human Brain Using PET with 18F-FE-SPA-RQ. *J. Nucl. Med.* **2008**, *49*, 1749–1755. [CrossRef]
155. Danfors, T.; Åhs, F.; Appel, L.; Linnman, C.; Fredrikson, M.; Furmark, T.; Kumlien, E. Increased neurokinin-1 receptor availability in temporal lobe epilepsy: A positron emission tomography study using [11C]GR205171. *Epilepsy Res.* **2011**, *97*, 183–189. [CrossRef]
156. Frick, A.; Åhs, F.; Linnman, C.; Jonasson, M.; Appel, L.; Lubberink, M.; Långström, B.; Fredrikson, M.; Furmark, T. Increased neurokinin-1 receptor availability in the amygdala in social anxiety disorder: A positron emission tomography study with [11C]GR205171. *Transl. Psychiatry* **2015**, *5*, e597. [CrossRef]
157. Michelgård, Å.; Appel, L.; Pissiota, A.; Frans, Ö.; Långström, B.; Bergström, M.; Fredrikson, M. Symptom Provocation in Specific Phobia Affects the Substance P Neurokinin-1 Receptor System. *Biol. Psychiatry* **2007**, *61*, 1002–1006. [CrossRef]
158. Fujimura, Y.; Yasuno, F.; Farris, A.; Liow, J.S.; Geraci, M.; Drevets, W.; Pine, D.S.; Ghose, S.; Lerner, A.; Hargreaves, R.; et al. Decreased Neurokinin-1 (Substance P) Receptor Binding in Patients with Panic Disorder: Positron Emission Tomographic Study with [18F]SPA-RQ. *Biol. Psychiatry* **2009**, *66*, 94–97. [CrossRef]
159. ClinicalTrials.gov Identifier: NCT00088738. Available online: https://clinicaltrials.gov/ct2/show/NCT00088738 (accessed on 15 May 2019).
160. Jarcho, J.M.; Mandelkern, M.; Ebrat, B.; Smith, S.R.; Naliboff, B.D.; Labus, J.S.; Tillisch, K.; Mayer, E.A. Reduced Neurokinin-1 (Substance P) Receptor Binding in Patients With Irritable Bowel Syndrome: A Positron Emission Tomography Study With [18f]SPA-RQ. *Gastroenterology* **2010**, *138*, S372. [CrossRef]
161. ClinicalTrials.gov Identifier: NCT00102102. Available online: https://clinicaltrials.gov/ct2/show/NCT00102102 (accessed on 15 May 2019).

162. ClinicalTrials.gov Identifier: NCT00547612. Available online: https://clinicaltrials.gov/ct2/show/NCT00547612 (accessed on 15 May 2019).
163. Bergström, M.; Hargreaves, R.J.; Burns, H.D.; Goldberg, M.R.; Sciberras, D.; Reines, S.A.; Petty, K.J.; Ögren, M.; Antoni, G.; Långström, B.; et al. Human Positron Emission Tomography Studies of Brain Neurokinin 1 Receptor Occupancy by Aprepitant. *Biol. Psychiatry* **2004**, *55*, 1007–1012. [CrossRef]
164. Zamuner, S.; Rabiner, E.A.; Fernandes, S.A.; Bani, M.; Gunn, R.N.; Gomeni, R.; Ratti, E.; Cunningham, V.J. A pharmacokinetic PET study of NK1 receptor occupancy. *Eur. J. Nucl. Med. Mol. Imaging* **2012**, *39*, 226–235. [CrossRef]
165. Ranga, K.; Krishnan, R. Clinical experience with substance P receptor (NK1) antagonists in depression. *J. Clin. Psychiatry* **2002**, *63*, 25–29.
166. Ratti, E.; Bellew, K.; Bettica, P.; Bryson, H.; Zamuner, S.; Archer, G.; Squassante, L.; Bye, A.; Trist, D.; Krishnan, R.; et al. Results From 2 Randomized, Double-Blind, Placebo-Controlled Studies of the Novel NK1 Receptor Antagonist Casopitant in Patients with Major Depressive Disorder. *J. Clin. Psychopharmacol.* **2011**, *31*, 727–733. [CrossRef]
167. Poma, A.; Christensen, J.; Davis, J.; Kansra, V.; Martell, R.E.; Hedley, M.L. Phase 1 positron emission tomography (PET) study of the receptor occupancy of rolapitant, a novel NK-1 receptor antagonist. *J. Clin. Oncol.* **2017**, *32*. [CrossRef]
168. ClinicalTrials.gov Identifier: NCT01381419. Available online: https://clinicaltrials.gov/ct2/show/NCT01381419 (accessed on 15 May 2019).
169. ClinicalTrials.gov Identifier: NCT01059578. Available online: https://clinicaltrials.gov/ct2/show/NCT01059578 (accessed on 15 May 2019).
170. Van der Mey, M.; Janssen, C.G.M.; Janssens, F.E.; Jurzak, M.; Langlois, X.; Sommen, F.M.; Verreet, B.; Windhorst, A.D.; Leysen, J.E.; Herscheid, J.D.M. Synthesis and biodistribution of [11C]R116301, a promising PET ligand for central NK1 receptors. *Bioorg. Med. Chem.* **2005**, *13*, 1579–1586. [CrossRef]
171. Wolfensberger, S.P.A.; van Berckel, B.N.M.; Airaksinen, A.J.; Maruyama, K.; Lubberink, M.; Boellaard, R.; Carey, W.D.H.; Reddingius, W.; Veltman, D.J.; Windhorst, A.D.; et al. First Evaluation of [11C]R116301 as an In Vivo Tracer of NK1 Receptors in Man. *Mol. Imaging Biol.* **2009**, *11*, 241–245. [CrossRef]
172. Wolfensberger, S.P.; Maruyama, K.; van Berckel, B.N.; Lubberink, M.; Airaksinen, A.J.; Boellaard, R.; Luurtsema, G.; Reddingius, W.; Janssens, F.E.; Veltman, D.J.; et al. Quantification of the NK1 Receptor ligand [11C]R116301. *Nucl. Med. Commun.* **2011**, *32*, 896–902. [CrossRef]
173. Huskey, S.E.W.; Dean, B.J.; Doss, G.A.; Wang, Z.; Hop, C.E.C.A.; Anari, R.; Finke, P.E.; Robichaud, A.J.; Zhang, M.; Wang, B.; et al. The metabolic disposition of aprepitant, a Substance P receptor antagonist, in rats and dogs. *Drug Metab. Dispos.* **2004**, *32*, 246–258. [CrossRef]
174. Miraglia, L.; Pagliarusco, S.; Bordini, E.; Martinucci, S.; Pellegatti, M. Metabolic disposition of casopitant, a potent NK1 receptor antagonist, in mice, rats and dogs. *Drug Metab. Dispos.* **2010**, *38*, 1876–1891. [CrossRef]
175. Pellegatti, M.; Bordini, E.; Fizzotti, P.; Roberts, A.; Johnson, B.M. Disposition and Metabolism of Radiolabeled Casopitant in Humans. *Drug Metab. Dispos.* **2009**, *37*, 1635–1645. [CrossRef]
176. Spinelli, T.; Calcagnile, S.; Giuliano, C.; Rossi, G.; Lanzarotti, C.; Mair, S.; Stevens, L.; Nisbet, I. Netupitant PET Imaging and ADME Studies in Humans. *J. Clin. Pharmacol.* **2014**, *54*, 97–108. [CrossRef]

3.3. Radiochemical Synthesis and Evaluation of Novel Radioconjugates of Neurokinin 1 Receptor Antagonist Aprepitant Dedicated for NK1R-Positive Tumors

Halik, P.K.; Lipiński, P.F.J.; Matalińska, J.; Koźmiński, P.; Misicka, A.; Gniazdowska, E. Radiochemical Synthesis and Evaluation of Novel Radioconjugates of Neurokinin 1 Receptor Antagonist Aprepitant Dedicated for NK1R-Positive Tumors. *Molecules* **2020**, *25*, 3756. DOI: 10.3390/molecules25163756

IF (2020) = 4,412; pkt. MNiSW (2022) = 140

Autorzy	Udział
Halik, P.K.	- opracowanie koncepcji funkcjonalizacji aprepitantu; - wykonanie preparatyki syntetycznej; - wykonanie preparatyki radiosyntetycznej; - wykonanie analiz radiochemicznych; - przygotowanie manuskryptu; - wizualizacja danych;
Lipiński, P.F.J.	- wykonanie badania modelowania molekularnego; - przygotowanie manuskryptu; - wizualizacja danych;
Matalińska, J.	- hodowla komórkowa; - wykonanie oznaczeń powinowactwa receptorowego metodą kompetycyjną; - praca nad manuskryptem (1. czytanie);
Koźmiński, P.	- wykonanie analiz spektrometrycznych; - praca nad manuskryptem (1. czytanie);
Misicka, A.	- koncepcja badań; - kierowanie grantem; - praca nad manuskryptem (2. czytanie);
Gniazdowska, E.	- koncepcja badań; - kierowanie grantem; - praca nad manuskryptem (2. czytanie);

molecules

MDPI

Article

Radiochemical Synthesis and Evaluation of Novel Radioconjugates of Neurokinin 1 Receptor Antagonist Aprepitant Dedicated for NK1R-Positive Tumors

Paweł K. Halik [1,*], Piotr F. J. Lipiński [2], Joanna Matalińska [2], Przemysław Koźmiński [1], Aleksandra Misicka [2] and Ewa Gniazdowska [1]

1 Centre of Radiochemistry and Nuclear Chemistry, Institute of Nuclear Chemistry and Technology, 03-195 Warsaw, Poland; p.kozminski@ichtj.waw.pl (P.K.); e.gniazdowska@ichtj.waw.pl (E.G.)
2 Department of Neuropeptides, Mossakowski Medical Research Centre, Polish Academy of Sciences, 02-106 Warsaw, Poland; plipinski@imdik.pan.pl (P.F.J.L.); jmatalinska@imdik.pan.pl (J.M.); misicka@chem.uw.edu.pl (A.M.)
* Correspondence: p.halik@ichtj.waw.pl; Tel.: +48-22-504-1316

Academic Editor: Krishan Kumar
Received: 31 July 2020; Accepted: 15 August 2020; Published: 18 August 2020

Abstract: Aprepitant, a lipophilic and small molecular representative of neurokinin 1 receptor antagonists, is known for its anti-proliferative activity on numerous cancer cell lines that are sensitive to Substance P mitogen action. In the presented research, we developed two novel structural modifications of aprepitant to create aprepitant conjugates with different radionuclide chelators. All of them were radiolabeled with ^{68}Ga and ^{177}Lu radionuclides and evaluated in terms of their lipophilicity and stability in human serum. Furthermore, fully stable conjugates were examined in molecular modelling with a human neurokinin 1 receptor structure and in a competitive radioligand binding assay using rat brain homogenates in comparison to the aprepitant molecule. This initial research is in the conceptual stage to give potential theranostic-like radiopharmaceutical pairs for the imaging and therapy of neurokinin 1 receptor-overexpressing cancers.

Keywords: aprepitant; radiopharmaceuticals; neurokinin 1 receptor antagonist; radionuclide chelators

1. Introduction

The knowledge of a suitable molecular target and its specificity for a given pathology is a necessary condition in a targeted radionuclide therapy approach. Many malignant tumors possess an infiltrating character with no defined margins or spread out metastases around the whole body. Only the selective binding of a radiopharmaceutical to a molecular target allows for the reliable imaging or safe ablation of cancer lesions with minimal side effects.

Neurokinin 1 receptor (NK1R; tachykinin 1 receptor) is a well-known G protein-coupled receptor for neuropeptide Substance P (SP) and a promising system for an anticancer therapeutic molecular target [1,2]. The activation of the NK1R by its endogenous ligand creates significant proliferative impulses for tumor cells promoting growth and development, including angiogenesis and metastasis. At the same time, the frequent formation of SP-NK1R complexes stimulate the cellular up-regulation of NK1R on tumor cell surfaces [3], thus providing an even greater cell sensitivity for the mitogen action of SP. On the other hand, the blockage of SP action by using antagonists of NK1R on SP-sensitive tumor cells can selectively induce an anti-tumor effect through the mechanism of cell apoptosis [4,5].

Antagonists of NK1R are a very diverse and numerous group of compounds, though clinical applications have only been found for four compounds. They are applied to the prevention of nausea and vomiting induced by chemotherapy or surgical complications [2,6]. One of the best known and

widely studied compounds in this group is aprepitant (APT; Figure 1)—a lipophilic and low molecular weight morpholine derivative with a high and selective affinity for NK1R. APT possesses anti-tumor activity, as has been determined in many cancer cell lines [5,7–12]. Moreover, the phenomenon of the synergism of the anti-tumor activity of NK1R antagonists with an inhibitory effect on the cancer cell growth of other agents has been confirmed [4]. It has been shown in vitro that the application of microtubule destabilizing agents in combination with antagonists of NK1R possess synergism in apoptotic effect in human glioblastoma, bladder, cervical and breast cancer cells [13]. More remarkable cytotoxic synergism has been proven in a combination of aprepitant and ritonavir (an antiretroviral agent) in the human glioblastoma GAMG cell line [14]. The application of these two drugs with temozolomide, an alkylating chemotherapeutic used clinically to treat glioblastoma, gives an even stronger synergistic effect.

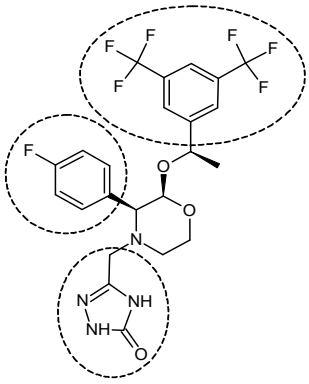

Figure 1. Structure of aprepitant with its key elements marked.

What is most relevant is that APT is a fairly safe drug with a known pharmacological profile, with tolerability similar to placebo- and dose- related action. This could be shown by the fact that aprepitant's half-maximal inhibitory concentration (IC_{50}) value determined for the human embryonic kidney (HEK) 293 cell line (a low expression NK1R control) is higher than the aprepitant IC_{100} values determined for numerous tumor cell lines overexpressing NK1R [15]. For the reasons described above, APT's structure is an interesting scaffold for creating conjugates for carrying radionuclides to NK1R-positive tumors.

By looking at aprepitant in terms of molecular structure, it can be seen that the compound (Figure 1) consists of a morpholine core decorated by three 'arms,' which are:

(i) *p*-fluorophenyl,
(ii) 3,5-bis-trifluoromethylphenyl suspended at an ether linker, and
(iii) a triazolinone moiety suspended at a methylene linker.

In the course of extensive structure-activity studies on NK1R antagonists [16–18], it has been established that the first two features (in particular: the distance and mutual positioning of two aromatic rings) are critical for high affinity and, therefore, for NK1R antagonism. On the other hand, the third element, triazolinone ring, can be, at least in some cases, safely modified without a significant loss of affinity [18]. This was exploited in attempts to improve the solubility of aprepitant derivatives, resulting in the derivative L-760,735.

That this site tolerates some modifications is now well-understood in terms of protein-ligand interactions. A recently reported X-ray structure of an NK1R-aprepitant complex [19] revealed that the triazolinone ring is located relatively close to the extracellular end of the receptor binding pocket, where it participates in hydrogen bonding to E193 and W184. However, E193A mutation has virtually no effect on aprepitant's affinity, thus suggesting that the interactions in this area are of less importance

to high affinity binding. Therefore, it seemed the most rational that a convenient site for functionalizing the APT structure is at this very ring. Nevertheless, the performed functionalization of the APT molecule required confirmation that the obtained conjugate still had a sufficiently high affinity for the receptor.

Based on that knowledge, we focused our efforts on the syntheses and in vitro evaluation of newly designed radioconjugates of aprepitant with gallium-68 or lutetium-177 radionuclides. For this purpose, we have proposed two functionalization routes of the APT molecule, followed by conjugation of different macrocyclic chelators DOTA, Bn-DOTA, and Bn-DOTAGA, as well as acrylic chelator DTPA dedicated to ^{68}Ga and ^{177}Lu. For conjugates showing full stability in human serum, molecular modelling studies for human NK1R and preliminary in vitro examination were performed. These reported findings indicate new perspectives of aprepitant applications in the form of selective theranostic-like concept radiopharmaceuticals for NK1R-positive tumors.

2. Results and Discussion

2.1. Syntheses of Aprepitant-Based Radioconjugates

2.1.1. Syntheses of Aprepitant Derivatives

The first stage of synthesis concerned the modification of the APT structure in order to introduce a primary amine group. This was realized according to synthetic pathways presented below by using one of selected alkyl linkers (Scheme 1) or acetamide linkers (Scheme 2) so as to receive APT-alkylamine (**2A**–**C**) or APT-acetamide derivatives (**4D**,**E**).

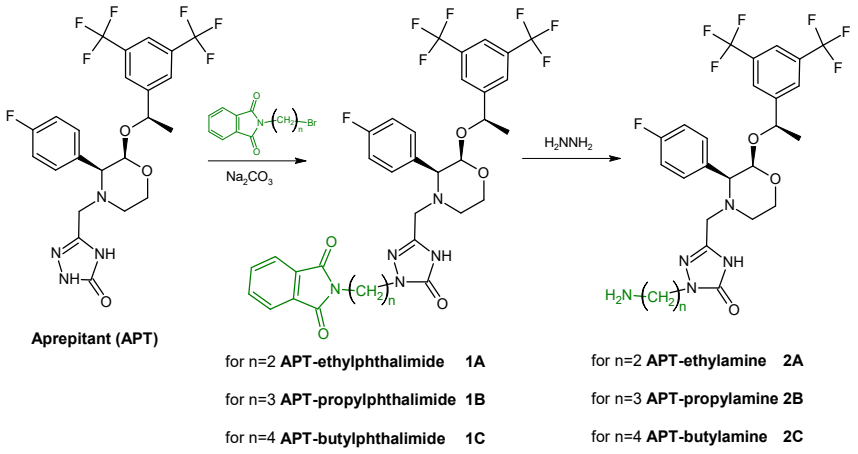

Scheme 1. Synthetic route of aprepitant derivatives with aminoalkyl linkers; where n = {2; 3; 4}.

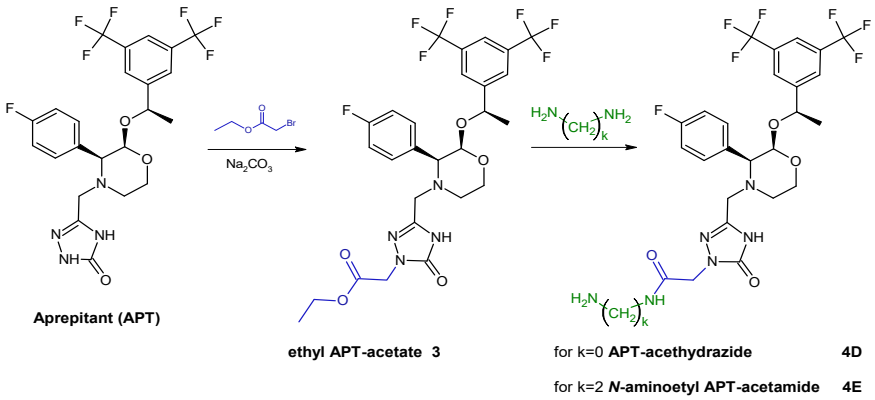

Scheme 2. Synthetic route of aprepitant derivatives with acetamide linkers; where k = {0; 2}.

2.1.2. Syntheses of Aprepitant Conjugates

The coupling reactions of APT-ethylamine, **2A**, with different bifunctional chelating agents, were as follows: DOTA-NHS ester, *p*-SCN-Bn-DOTA, *p*-SCN-Bn-DOTAGA, or DTPA dianhydride, as presented in Scheme 3. The use of different chelators allowed for the evaluation of the effect of the chelating moiety on the physicochemical properties of later radioconjugates. Based on the stability results obtained for these radioconjugates (presented in a section below), all other obtained APT derivatives (**2B**, **2C**, **4D**, and **4E**) were only conjugated with selected macrocyclic chelator DOTA. The application of different linkers allowed for the evaluation of their influence on the physicochemical properties of later radioconjugates.

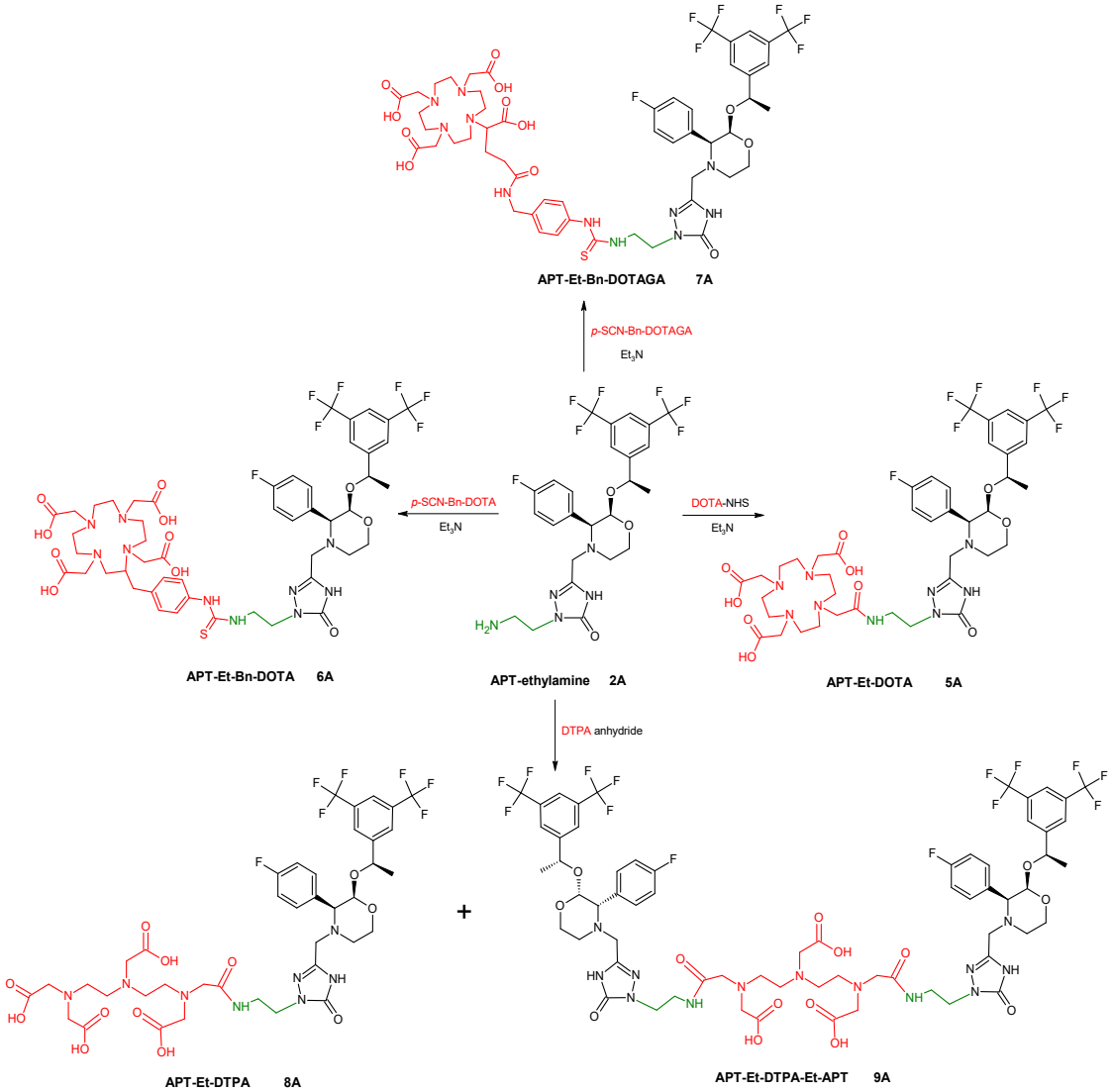

Scheme 3. Synthetic routes of conjugations of selected chelators to aprepitant-ethylamine **2A**.

2.1.3. Preparation of Radioconjugates

All APT conjugates with DOTA, Bn-DOTA, and Bn-DOTAGA were radiolabeled with ^{68}Ga and ^{177}Lu, while APT conjugates with DTPA were only radiolabeled with ^{68}Ga. Synthesized radioconjugates were purified using the solid phase extraction (SPE) method before HPLC identification (Figures 2 and 3) and further analyses.

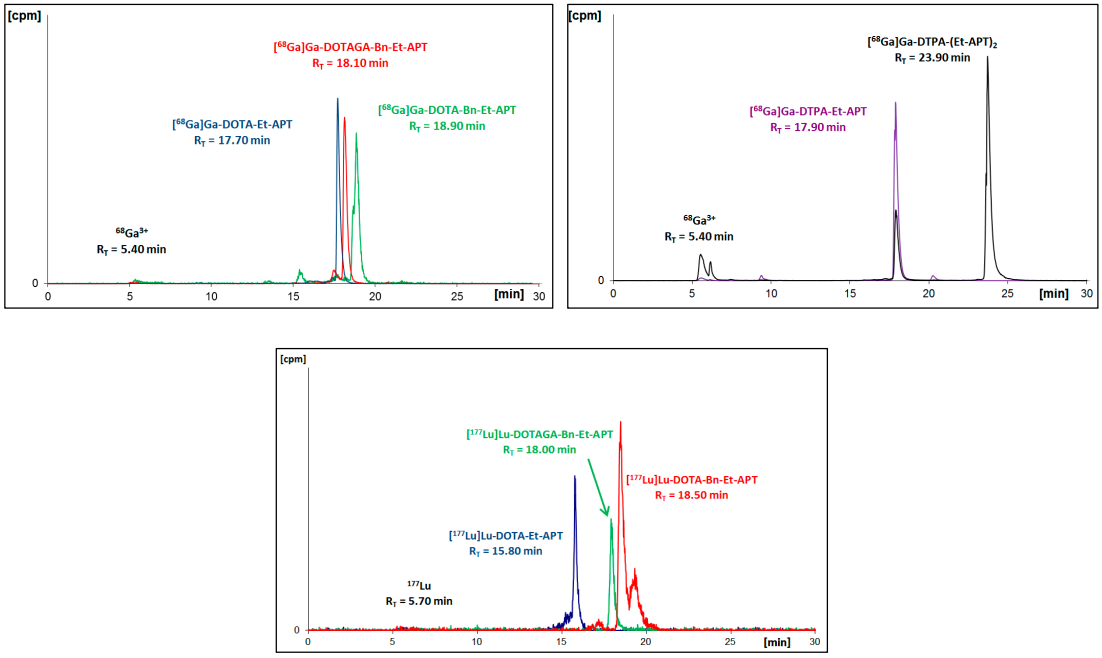

Figure 2. Radiochromatograms of aprepitant (APT)-ethylamine **2A** conjugates with DOTA, Bn-DOTA, Bn-DOTAGA or DTPA radiolabeled with gallium-68 (**upper** two) or with lutetium-177 (**bottom**).

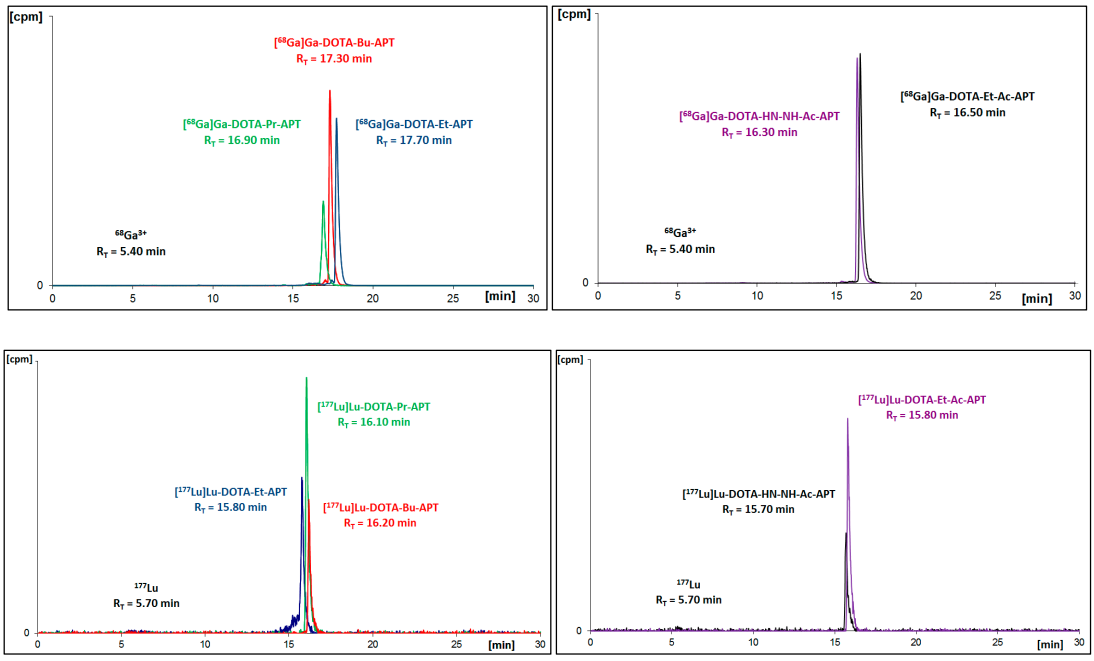

Figure 3. Radiochromatograms of DOTA conjugates with all APT derivatives radiolabeled with gallium-68 (**upper** two) or with lutetium-177 (**bottom** two).

As a result of the performed radiosyntheses, all radioconjugates were successfully obtained, except for [^{68}Ga]Ga-DTPA-(Et-APT)$_2$ ([**^{68}Ga]Ga-9A**), which proved to be immediately unstable. Moreover, in the radiochromatogram of [^{177}Lu]Lu-DOTA-Bn-Et-APT ([**^{177}Lu]Lu-6A**) one can see a small additional signal (about 19.3 min) that is recognized as an early by-product of an interaction with solvent (EtOH) from the purification process. To verify the identity of all synthesized [^{68}Ga]Ga-radioconjugates in a non-carrier added scale, the non-radioactive stable gallium reference compounds (**Ga-5A**–**Ga-9A** and **Ga-5A**–**Ga-5E**) were synthesized and characterized by mass spectrometry. The retention time values of the [^{68}Ga]Ga-radioconjugates and stable references presented below (Tables 1 and 2)

overlapped, and the differences between them resulted from the serial connection of UV-Vis and gamma detectors only.

Table 1. Retention times (R_T) of stable gallium conjugates and [^{68}Ga]Ga-radioconjugates of aprepitant-ethylamine **2A**.

Stable Ga-Conjugate	R_T	[^{68}Ga]Ga-Radioconjugate	R_T
Ga-DOTA-Et-APT, Ga-5A	17.4 min	**[^{68}Ga]Ga-DOTA-Et-APT, [^{68}Ga]Ga-5A**	17.7 min
Ga-DOTA-Bn-Et-APT, Ga-6A	18.5 min	**[^{68}Ga]Ga-DOTA-Bn-Et-APT, [^{68}Ga]Ga-6A**	18.9 min
Ga-DOTAGA-Bn-Et-APT, Ga-7A	17.7 min	**[^{68}Ga]Ga-DOTAGA-Bn-Et-APT, [^{68}Ga]Ga-7A**	18.1 min
Ga-DTPA-Et-APT, Ga-8A	17.6 min	**[^{68}Ga]Ga-DTPA-Et-APT, [^{68}Ga]Ga-8A**	17.9 min
Ga-DTPA-(Et-APT)$_2$, Ga-9A	23.6 min	**[^{68}Ga]Ga-DTPA-(Et-APT)$_2$, [^{68}Ga]Ga-9A**	23.9 min

Table 2. R_T of stable gallium conjugates and [^{68}Ga]Ga-radioconjugates of all aprepitant derivatives.

Stable Ga-Conjugate	R_T	[^{68}Ga]Ga-Radioconjugate	R_T
Ga-DOTA-Et-APT, Ga-5A	17.4 min	**[^{68}Ga]Ga-DOTA-Et-APT, [^{68}Ga]Ga-5A**	17.7 min
Ga-DOTA-Pr-APT, Ga-5B	16.8 min	**[^{68}Ga]Ga-DOTA-Pr-APT, [^{68}Ga]Ga-5B**	17.0 min
Ga-DOTA-Bu-APT, Ga-5C	16.9 min	**[^{68}Ga]Ga-DOTA-Bu-APT, [^{68}Ga]Ga-5C**	17.3 min
Ga-DOTA-HN-NH-Ac-APT, Ga-5D	15.8 min	**[^{68}Ga]Ga-DOTA-HN-NH-Ac-APT, [^{68}Ga]Ga-5D**	16.3 min
Ga-DOTA-Et-Ac-APT, Ga-5E	16.1 min	**[^{68}Ga]Ga-DOTA-Et-Ac-APT, [^{68}Ga]Ga-5E**	16.5 min

2.2. Physiochemical Evaluation of Radioconjugates

2.2.1. Stability Study

The sine qua non condition of a radionuclide's application in vivo is its radiopharmaceutical stability in biological fluids like serum or cerebrospinal fluid. For this purpose, each isolated and solvent-free radioconjugate was incubated at 37 °C in human serum (HS). At specific time points, small samples of radioconjugate mixture were analyzed by the HPLC method for the assessment of the radioconjugate condition. The collected data presented on the charts below (Figure 4) point out that only the DOTA radioconjugates remained stable in the biological fluid; thus, these radioconjugates were selected for further analyses.

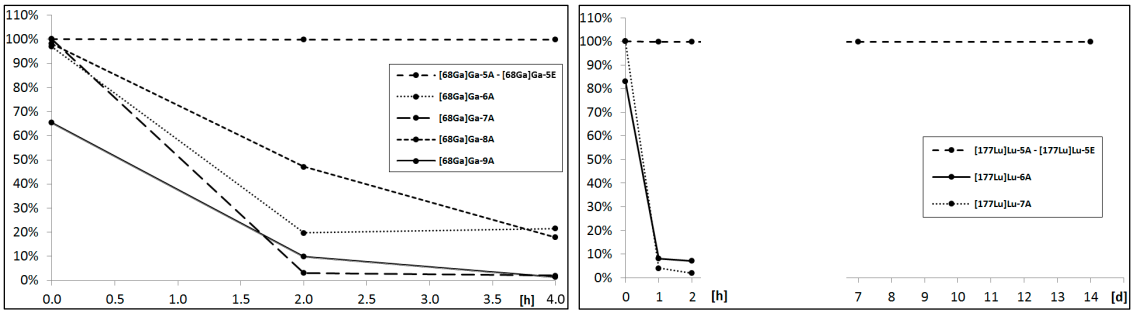

Figure 4. Percentage of intact [^{68}Ga]Ga-radioconjugates (**left**) and [^{177}Lu]Lu-radioconjugates (**right**) determined at specific time points during incubation in 37 °C human serum.

We concluded that for the demand of designed aprepitant radioconjugates, the acyclic chelator DTPA showed a poor radionuclide chelating ability during incubation in human serum. DOTA and its analogues presented a satisfactory radionuclide complex stability, however, for the overall stability of the radioconjugate results from the type of the formed chemical bond with the amine terminated aprepitant derivative and the presence of a negative charge on the chelator-metal complex moiety. The amide bond created by the DOTA-NHS ester and uncharged complex in the conjugates remained stable throughout the whole stability study, while the thiourea bonds and negatively charged complexes created by both *p*-SCN-Bn-DOTA and *p*-SCN-Bn-DOTAGA were found to gradually decompose in time. This phenomenon of instability in HS has been observed previously in various radiopharmaceuticals [20].

2.2.2. Lipophilicity Study

Drug distribution in vivo is highly related to both the lipophilicity and charge of a drug. The optimal radiotracer lipophilicity value for blood-brain barrier crossing lies within the range from 2.0 to 3.5 [21]. Non-peptide NK1R antagonists, like aprepitant, are characterized by a high lipophilicity (logD 4.8) [22], while the DOTA chelator is a highly hydrophilic moiety. In seeking to keep in lipophilicity of radioconjugates in a desired range, the choice of a proper linker (primary aprepitant modification) seems essential for distribution and pharmacokinetic aspects.

In the course of the lipophilicity study, each isolated DOTA radioconjugate (determined as fully stable in HS) was examined for distribution in the system of *n*-octanol and a phosphate-buffered saline (PBS) buffer (pH = 7.4) to estimate the lipophilicity of the radiocomplex. The lipophilicity of each radioconjugate (logD), defined as the logarithm of the distribution coefficient (D) is based on the ratio of the radioactivity of the organic phase to the radioactivity of the aqueous phase. The stability of the studied radioconjugate was verified simultaneously during the experiment through the HPLC analysis of the aqueous phase. LogD values of **[^{68}Ga]Ga-5A–[^{68}Ga]Ga-5E** and **[^{177}Lu]Lu-5A–[^{177}Lu]Lu-5E** are listed below in Table 3.

Table 3. LogD values of human serum stable radioconjugates determined in *n*-octanol/PBS buffer system.

Radioconjugate	logD	
	^{68}Ga-	^{177}Lu-
APT-Et-DOTA, 5A	0.141 ± 0.019	0.708 ± 0.021
APT-Pr-DOTA, 5B	0.058 ± 0.016	0.654 ± 0.022
APT-Bu-DOTA, 5C	0.290 ± 0.018	0.777 ± 0.021
APT-Ac-HN-NH-DOTA, 5D	−1.012 ± 0.017	−0.401 ± 0.015
APT-Ac-Et-DOTA, 5E	−0.231 ± 0.015	0.500 ± 0.017

The APT-alkylamine derivative-based radioconjugates showed similar lipophilicity values that were higher than those of the APT-acetamide derivative-based radioconjugates. The complexes with lutetium were more lipophilic by (on average) 0.6 logD units. However, the logD values for all radioconjugates significantly decreased in comparison to aprepitant, indicating possible divergences in the pharmacokinetic fate of the radioconjugates and the parent drug.

2.3. Binding Affinity

An important consideration in the search of conjugate vectors for radionuclides is whether the functionalization of a high affinity ligand would not reduce the binding strength for a desired receptor. For the preliminary addressing of this issue in the case of our conjugates, we measured the affinity of compounds **5A–E** (uncomplexed precursors) for the rat neurokinin-1 receptor. The human (hNK1R) and the rat (rNK1R) neurokinin 1 receptors differ in their sequences and pharmacology. It has been established that many (but not all) high affinity NK1R antagonists have a significantly lower affinity for the rat receptor than for that of human origin [23,24]. Still, the results presented below give some tentative insight into the affinity changes caused by the functionalization of the aprepitant structure at the triazolinone ring.

The results of the binding affinity determinations are given in Table 4. The parent compound, aprepitant, was found to exhibit IC_{50} = 128.4 nM. This value was roughly consistent with the reported potency of aprepitant in a functional assay. The compound was found to inhibit Substance P-evoked increases in intracellular Ca^{2+} mobilization in the cells expressing rNK1R with a pK_B reading 7.3 [25]. Note that in the assays with cells expressing hNK1R, aprepitant was significantly more potent (pK_B = 8.7), and the reported binding affinities for the human receptor were of the subnanomolar order (e.g., IC_{50} = 0.09 nM [17]).

Table 4. Binding affinity of aprepitant and compounds **5A**–**E** for the rat neurokinin 1 receptor.

Compound	IC_{50} ± SEM [a] [μM]	Ratio to APT
Aprepitant	0.13 ± 0.06	1.0
APT-Et-DOTA, 5A	6.2 ± 2.6	48.2
APT-Pr-DOTA, 5B	0.69 ± 0.07	5.3
APT-Bu-DOTA, 5C	1.8 ± 0.7	14.3
APT-Ac-HN-NH-DOTA, 5D	2.5 ± 0.7	19.1
APT-Ac-Et-DOTA, 5E	2.5 ± 0.5	19.7

[a] IC_{50} ± SEM: the half-maximal inhibitory concentration with the standard error of the mean of three independent experiments done in duplicate.

The aprepitant-based conjugates exhibited a diversified range of affinities. The strongest ligand in the set was the compound bearing a propylamine linker, **5B**. It was found to have an IC_{50} of 0.69 μM. This value was about five times worse than that of the parent compound. Interestingly, decreasing (**5A**) or increasing (**5C**) the linker length by one methylene unit was associated with much lower affinity of the micromolar order. The shorter **5A** exhibited the lowest binding in the set, with an IC_{50} of 6.2 μM. The analogue with the butylamine linker (**5C**) had an IC_{50} of 1.8 μM. Similar affinities (IC_{50}~2.5 μM) were found for the conjugates with the acylhydrazine (**5D**) or *N*-aminoethylacetamide (**5E**) linkers.

2.4. Molecular Modelling Study

In order to get insight into possible interactions between the aprepitant-DOTA conjugates reported herein and the NK1R, the complexes thereof were modelled by molecular docking. The applied procedure consisted in building the appropriate linker-DOTA fragments into the aprepitant structure crystallized with the receptor (Protein Data Bank (PDB) accession code: 6HLO [19]), followed by local search docking executed in AutoDock 4.2.6 [26].

According to this procedure, the presence of a linker-DOTA moiety in the aprepitant-based conjugates did not have a major impact on the interactions between the core of the molecule and the receptor. Only a slight repositioning of the morpholine core, 3,5-bis-trifluoromethylphenyl, or *p*-fluorophenyl moieties was observed compared to the 6HLO crystal structure (Figure 5A). Thus, the conjugates were predicted to bind with the 3,5-bis-trifluoromethylphenyl fragment located at the bottom of the ligand-binding pocket and the DOTA moiety closer to the extracellular side of the receptor (Figure 5A).

In the part that was common to all studied derivatives (and the parent aprepitant), the complexes were stabilized by (Figure 5B):

(i) hydrogen bonding between Q165 and the ether oxygen,
(ii) hydrophobic contacts of the morpholine ring and F268 and I182,
(iii) hydrophobic contacts with side chains of N109, P112, and I113,
(iv) hydrophobic contacts of the 3,5-bis-trifluoromethylphenyl with W261 and F264,
(v) hydrophobic contacts of the *p*-fluorophenyl ring and H197, V200, T201, I204, and H265.

These interactions were identical to those found for the parent aprepitant in 6HLO structure.

On the other hand, the presence of the linker-DOTA fragment was predicted to weaken the contacts that the triazolinone ring of the parent aprepitant had with the receptor in the crystal structure 6HLO [19]. In the optimized complexes for all the conjugates, this ring was displaced compared to the parent structure (Figure 6A,B), so hydrogen bonding to W184 was not possible. On the other hand, a better positioning of this ring for π–π stacking with H197 was predicted for the conjugates.

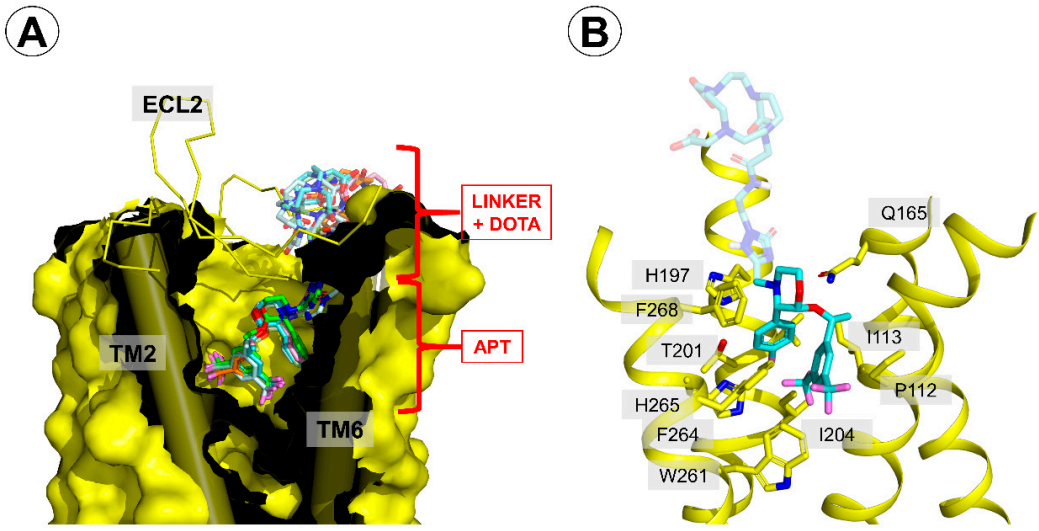

Figure 5. Binding mode of the reported conjugates in the neurokinin 1 receptor (NK1R) binding site. (**A**) A generalized view on the binding mode. The receptor is displayed as a yellow surface, with transmembrane helices (TMs) 2 and 6 shown as cylinders. The extracellular loop 2 (ECL2) is shown as a yellow ribbon. The conjugates are represented as colored sticks. (**B**) A view focused on the interactions of the part common to aprepitant and the conjugates. The conjugate shown is compound **5A** (pale blue sticks). Only several residues of the receptor are shown (yellow sticks).

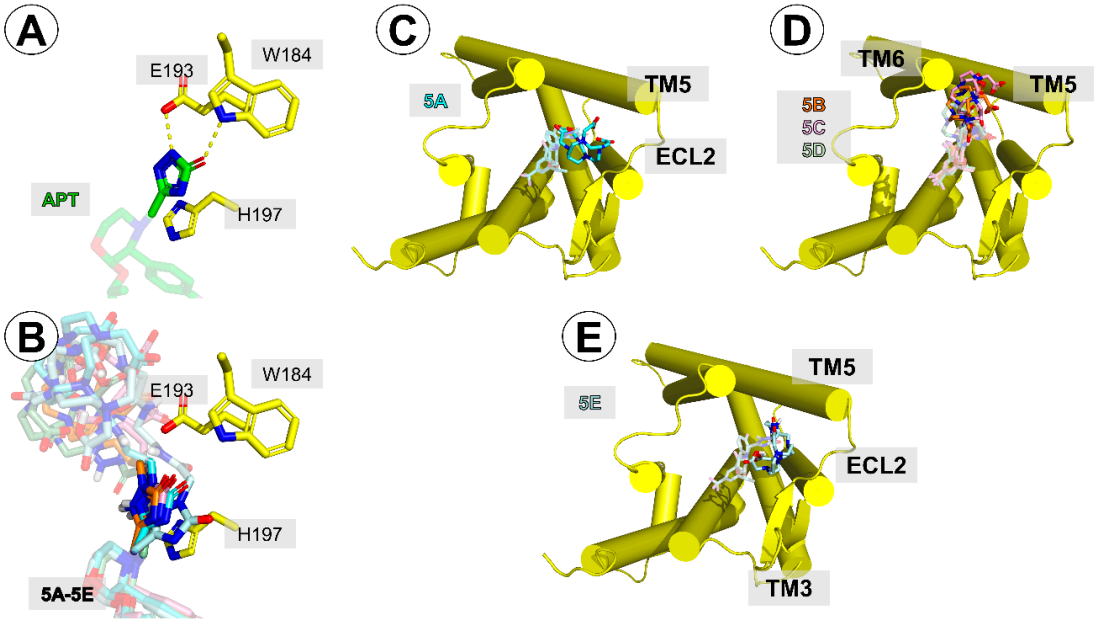

Figure 6. (**A**) Interactions of aprepitant's triazolinone ring with W184, E193, and H197 side-chains. (**B**) positioning of the triazolinone ring of the conjugates in the same projection as in (**A**). (**C**–**E**) Relative position of the DOTA moiety in conjugates **5A** (**C**), **5B**–**D** (**D**), and **5E** (**E**). The receptor helices are shown as yellow cylinders.

Regarding the positioning of the linker-DOTA part, in the case of **5A,** this fragment docked closely (Figure 6C) to the extracellular loop 2 (ECL2) and the extracellular terminus of the transmembrane helix 5 (TM5). One of the DOTA's carboxylate oxygens interacted with the side-chain of K190. For the analogues **5B**–**D**, the DOTA moiety was predicted to be located between the extracellular tips of TM5 and TM6 (Figure 6D). Its contacts included residues K194, K190, and P271. In the case of the longest

derivative, **5E**, the docking placed the DOTA moiety close to TM5 and ECL2 (Figure 6E). Here, it could interact with K190 and M181.

Since in the crystal structures 6HLO, 6HLL, and 6HLP [19], several residues by the extracellular end of the receptor were found to adopt different rotamers upon the binding of different ligands, we wanted to see if the flexibility of these residues could affect the docking results. Therefore, the local docking procedure with the enabled flexibility of E193 and H197 was performed. It yielded similar results with only minor adjustments of the side chain rotamers. Its results (in terms of interactions and binding poses) are not discussed herein since they are almost perfectly accounted for by the description of the docking procedure with the rigid receptor.

Regarding the quantitative evaluation (Table 5), AutoDock scoring function predicted that aprepitant would bind with the free energy of −10.43 kcal/mol. For the conjugates, the estimated energy varied between −9.64 kcal/mol (**5D**) and −13.74 kcal/mol (**5E**). The predicted energies did not correlate with the experimental data. This was perhaps due to the problems with estimating the entropic contribution because the conjugates differed with respect to the number of the rotatable bonds.

Table 5. Scoring results from molecular docking. The values are the estimated free energy of binding (kcal/mol).

	Rigid Receptor		Enabled Flexibility of E193 and H197	
Compound	**Lowest [a]**	**Mean [b]**	**Lowest [a]**	**Mean [b]**
APT-Et-DOTA, 5A	−11.26	−11.26	−12.37	−10.24
APT-Pr-DOTA, 5B	−10.84	−9.86	−10.74	−9.27
APT-Bu-DOTA, 5C	−12.26	−11.90	−12.21	−11.83
APT-Ac-HN-NH-DOTA, 5D	−9.64	−9.07	−9.19	−8.68
APT-Ac-Et-DOTA, 5E	−13.74	−13.16	−14.31	−13.60
Aprepitant (APT)	−10.43	−10.31	−10.57	−10.40

[a] lowest energy in the best scored cluster; [b] mean energy in the best scored cluster.

Other sources of significant error may have been the way the DOTA moiety was modelled (aimed at mimicking the presence of the cation in a simplified manner) and the fact that the experimentally evaluated conjugates were uncomplexed.

3. Materials and Methods

Aprepitant (Santa Cruz Biotechnology Inc., Dallas, TX, USA), the DOTA-NHS ester (1,4,7,10-tetraazacyclododecane-1,4,7,10-tetraacetic acid mono-*N*-hydroxysuccinimide ester), *p*-SCN-Bn-DOTAGA (2,2′,2′′-(10-(1-carboxy-4-((4-isothiocyanatobenzyl)amino)-4-oxobutyl)-1,4,7,10-tetraaza-cyclododecane-1,4,7-triyl)triacetic acid) (CheMatech, Dijon, France), *p*-SCN-Bn-DOTA (*S*-2-(4-isothiocyanatobenzyl)-1,4,7,10-tetraazacyclododecane tetraacetic acid) (Macrocyclics, Plano, TX, USA), DTPA dianhydride (diethylenetriaminepentaacetic dianhydride), and other substances and solvents (Sigma Aldrich/Merck, Darmstadt, Germany) were commercially available, defined as reagent grade, and applied without further purification. $^{68}GaCl_3$ was eluted from the commercially available $^{68}Ge/^{68}Ga$ generator (Eckert & Ziegler, Berlin, Germany). The $^{177}LuCl_3$ solution in 0.04 M HCl was purchased at Radioisotope Centre POLATOM, National Centre for Nuclear Research, Otwock-Świerk, Poland. Sep-Pack® Classic Short C18 Cartridges were purchased from WATERS, Milford, MA, USA. Human serum was isolated and purified at the Centre of Radiobiology and Biological Dosimetry, INCT Warsaw, Poland.

The HPLC conditions and gradient were as follows: a semi-preparative Phenomenex Jupiter Proteo column, 4 μm, 90 Å, 250 × 10 mm, with UV/Vis (220 nm) or/and radio γ-detection at gradient elution: 0–20 min 20 to 80% solvent B; 20–30 min 80% solvent B; 2 mL/min; solvent A: 0.1% (*v*/*v*) trifluoroacetic acid (TFA) in water; and solvent B: 0.1% (*v*/*v*) TFA in acetonitrile.

Mass spectra were measured on a Bruker 3000 Esquire mass spectrometer equipped with electrospray ionization (ESI) (Bruker, Billerica, MA, USA).

3.1. Syntheses of Aprepitant Derivatives and Aprepitant-Based Conjugates

3.1.1. General Procedure of Syntheses of Aprepitant Derivatives with Alkyl Linker, **2A–C**

The slight molar excess of the selected *n*-(terminal-bromoalkyl) phthalimide was added into an equimolar mixture of APT and sodium carbonate in dimethylformamide (DMF). The reaction mixture was vigorously stirred in about 50 °C for 12–18 h. Then, the triple molar excess of hydrazine was added into the reaction mixture for an additional 3 h. The progress of the reaction was monitored by HPLC. The crude reaction mixture was evaporated, dissolved in the HPLC mobile phase, purified by the HPLC method, and lyophilized. The isolated main product was identified as a mono-substituted APT-alkylamine derivative (**2A–C**, ~75% reaction yield) by MS analysis confirmation.

MS: Calculated monoisotopic mass for **APT-Et-NH$_2$, 2A**, $C_{25}H_{26}F_7N_5O_3$: 577.19; found: 578.27 *m*/*z* [M + H$^+$]
MS: Calculated monoisotopic mass for **APT-Pr-NH$_2$, 2B**, $C_{26}H_{28}F_7N_5O_3$: 591.21; found: 592.12 *m*/*z* [M + H$^+$]
MS: Calculated monoisotopic mass for **APT-Bu-NH$_2$, 2C**, $C_{27}H_{30}F_7N_5O_3$: 605.22; found: 606.38 *m*/*z* [M + H$^+$]

3.1.2. General Procedure of Syntheses of Aprepitant Derivatives with Acetamide Linker, **4D** and **4E**

The slight molar excess of ethyl 2-bromoacetate was added into an equimolar mixture of APT and sodium carbonate in DMF. The reaction mixture was vigorously stirred in about 50 °C for 24 h. Then, the triple molar excess of hydrazine or ethylenediamine was added into the reaction mixture for an additional 3 h. The progress of the reaction was monitored by HPLC. The crude reaction mixture was evaporated, dissolved in the HPLC mobile phase, purified by the HPLC method, and lyophilized. The isolated main product was identified as a mono-substituted amino-terminated APT-acetamide derivative (**4D** and **4E**, 65–70% reaction yield) by MS analysis confirmation.

MS: Calculated monoisotopic mass for **APT-Ac-HN-NH$_2$, 4D**, $C_{25}H_{25}F_7N_6O_4$: 606.19; found: 608.07 *m*/*z* [M + H$^+$]
MS: Calculated monoisotopic mass for **APT-Ac-Et-NH$_2$, 4E**, $C_{27}H_{29}F_7N_6O_4$: 634.21; found: 635.31 *m*/*z* [M + H$^+$]

3.1.3. General Procedure of Syntheses of Aprepitant Conjugates with DOTA, **5A–E**

The obtained APT derivative (**2A–C**, **4D**, and **4E**) and the DOTA-NHS ester in similar molar ratios were dissolved in DMF purged from oxygen with technical nitrogen and supplemented with a triple molar excess of triethylamine. The reaction mixture was vigorously stirred in about 50 °C for 24 h. The progress of the reaction was monitored by HPLC. The crude reaction mixture was evaporated, dissolved in the HPLC mobile phase, purified by the HPLC method, and lyophilized. The isolated main product was identified as a DOTA conjugate with an APT derivative (**5A–E**, >90% reaction yield) by MS analysis confirmation.

MS: Calculated monoisotopic mass for **APT-Et-DOTA**, **5A**, $C_{41}H_{52}F_7N_9O_{10}$: 963.37; found: 964.27 *m*/*z* [M + H$^+$]
MS: Calculated monoisotopic mass for **APT-Pr-DOTA**, **5B**, $C_{42}H_{54}F_7N_9O_{10}$: 977.39; found: 978.42 *m*/*z* [M + H$^+$]
MS: Calculated monoisotopic mass for **APT-Bu-DOTA**, **5C**, $C_{43}H_{56}F_7N_9O_{10}$: 991.40; found: 992.41 *m*/*z* [M + H$^+$]
MS: Calculated monoisotopic mass for **APT-Ac-HN-NH-DOTA**, **5D**, $C_{41}H_{51}F_7N_{10}O_{11}$: 992.36; found: 993.17 *m*/*z* [M + H$^+$]
MS: Calculated monoisotopic mass for **APT-Ac-Et-DOTA**, **5E**, $C_{43}H_{55}F_7N_{10}O_{11}$: 1020.39; found: 1021.43 *m*/*z* [M + H$^+$]

3.1.4. Procedure of Syntheses of Aprepitant-Ethylamine Conjugates with *p*-SCN-Bn-DOTA and *p*-SCN-Bn-DOTAGA, **6A** and **7A**

The APT-ethylamine (**2A**) and bifunctional chelating agent in similar molar ratios were dissolved in DMF and supplemented with a 5-fold molar excess of triethylamine. The reaction mixture was vigorously stirred in about 50 °C for 24 h. The progress of the reaction was monitored by HPLC. The crude reaction mixture was evaporated, dissolved in the HPLC mobile phase, purified by the HPLC method, and lyophilized. The isolated main product was identified as a DOTA-Bn or DOTAGA-Bn conjugate with an APT derivative (**6A** and **7A**, > 90% reaction yield) by MS analysis confirmation.

MS: Calculated monoisotopic mass for **APT-Et-Bn-DOTA**, **6A**, $C_{49}H_{59}F_7N_{10}O_{11}S$: 1128.40; found: 1129.55 *m*/*z* [M + H^+]
MS: Calculated monoisotopic mass for **APT-Et-Bn-DOTAGA**, **7A**, $C_{52}H_{64}F_7N_{11}O_{12}S$: 1199.43; found: 1200.66 *m*/*z* [M + H^+]

3.1.5. Procedure of Syntheses of Aprepitant-Ethylamine Conjugates with DTPA Anhydride, **8A**, **9A**

The APT-ethylamine (**2A**) and DTPA anhydride in a 3:2 molar ratio were dissolved in DMF purged from oxygen with technical nitrogen. The reaction mixture was vigorously stirred in room temperature for 2 h. The progress of the reaction was monitored by HPLC. The crude reaction mixture was evaporated, dissolved in the HPLC mobile phase, purified by the HPLC method, and lyophilized. Two isolated main products were identified as DTPA conjugated with one or two molecules of the APT derivative (**8A** and **9A** with ~45% and ~40% reaction yields, respectively) by MS analysis confirmation.

MS: Calculated for monoisotopic mass **APT-Et-DTPA**, **8A**, $C_{39}H_{47}F_7N_8O_{12}$: 952.32; found: 953.40 *m*/*z* [M + H^+]
MS: Calculated for monoisotopic mass **APT-Et-DTPA-Et-APT**, **9A**, $C_{64}H_{71}F_{14}N_{13}O_{14}$: 1511.50; found: 1512.64 *m*/*z* [M + H^+]

3.2. Preparation of Radioconjugates

3.2.1. ^{68}Ga Radiolabeling

The ^{68}Ga radiolabeling of the DOTA, Bn-DOTA, and Bn-DOTAGA conjugates of APT was performed according to the following procedure: 145 µL of a concentrated solution of [^{68}Ga]$GaCl_3$ in 0.1 M HCl from the ^{68}Ge/^{68}Ga generator (4.9 ÷ 7.2 MBq) was added into the solution of 25 nmol of the selected conjugate in 200 µL of a 0.2 M acetate buffer (pH = 4.5) and heated for 5–10 min at 95 °C. After this time, each radioconjugate was purified using Sep-Pack® Classic Short C18 Cartridges according to producer recommendations, thereby obtaining an easily vaporized ethanolic solution of each radioconjugate. The effectiveness of the purification was monitored by HPLC. DTPA radioconjugates were obtained via an analogical procedure in room temperature.

3.2.2. ^{177}Lu Radiolabeling

The ^{177}Lu radiolabeling of the DOTA, Bn-DOTA, and Bn-DOTAGA conjugates of APT was performed according to the following procedure: 2.7 ÷ 5.3 µL of a [^{177}Lu]$LuCl_3$ n.c.a. solution in 0.04 M HCl (4.6 ÷ 5.2 MBq) was added into the solution of 2.5 nmol of the selected conjugate in 200 µL of a 0.02 M acetate buffer (pH 4.5) and heated for 10 min at 95 °C. After this time, each radioconjugate was purified using Sep-Pack® C18 Cartridges according to the producer recommendations, thereby obtaining an easily vaporized ethanolic solution of each radioconjugate. The effectiveness of the purification was monitored by HPLC.

3.2.3. Preparation of Non-Radioactive References

The non-radioactive Ga labelling of the DOTA, Bn-DOTA, and Bn-DOTAGA conjugates of APT was performed according to the following procedure: 145 µL of a concentrated solution of 20 mM

$GaCl_3$ in 0.1 M HCl was added into the solution of 50 nmol of the selected conjugate in 200 µL of a 0.2 M acetate buffer (pH = 4.5) and heated for 5–10 min at 95 °C. After this time, each reaction mixture was purified by the HPLC method, lyophilized, and characterized by mass spectrometry. DTPA conjugates were obtained via an analogical procedure in room temperature.

MS: Calculated for monoisotopic mass **APT-Et-DOTA-Ga**, **5A-Ga**, $C_{41}H_{50}F_7N_9O_{10}Ga$: 1030.80 and 1032.28; found: 1030.40 and 1032.40 *m*/*z* [M^+]
MS: Calculated for monoisotopic mass **APT-Pr-DOTA-Ga**, **5B-Ga**, $C_{42}H_{52}F_7N_9O_{10}Ga$: 1044.30 and 1046.30; found: 1044.38 and 1046.39 *m*/*z* [M^+]
MS: Calculated for monoisotopic mass **APT-Bu-DOTA-Ga**, **5C-Ga**, $C_{43}H_{54}F_7N_9O_{10}Ga$: 1058.31 and 1060.31; found: 1058.37 and 1060.40 *m*/*z* [M^+]
MS: Calculated for monoisotopic mass **APT-Ac-HN-NH-DOTA-Ga**, **5D-Ga**, $C_{41}H_{49}F_7N_{10}O_{11}Ga$: 1059.27 and 1061.27; found: 1059.31 and 1061.40 *m*/*z* [M^+]
MS: Calculated for monoisotopic mass **APT-Ac-Et-DOTA-Ga**, **5E-Ga**, $C_{43}H_{53}F_7N_{10}O_{11}Ga$: 1087.30 and 1089.30; found: 1087.37 and 1089.44 *m*/*z* [M^+]
MS: Calculated for monoisotopic mass **APT-Et-Bn-DOTA-Ga**, **6A-Ga**, $C_{49}H_{57}F_7N_{10}O_{11}SGa$: 1095.31 and 1097.31; found: 1195.54 and 1197.51 *m*/*z* [M^+]
MS: Calculated for monoisotopic mass **APT-Et-Bn-DOTAGA-Ga**, **7A-Ga**, $C_{52}H_{62}F_7N_{11}O_{12}Sga$: 1266.34 and 1268.34; found: 1266.47 and 1268.47 *m*/*z* [M^+]
MS: Calculated for monoisotopic mass **APT-Et-DTPA-Ga**, **8A-Ga**, $C_{39}H_{44}F_7N_8O_{12}Ga$: 1018.22 and 1020.22; found: 1019.35 and 1021.37 *m*/*z* [M + H^+]
MS: Calculated for monoisotopic mass **APT-Et-DTPA-(Ga)-Et-APT**, **9A-Ga**, $C_{64}H_{68}F_{14}N_{13}O_{14}Ga$: 1577.40 and 1579.40; found: 1578.64 and 1580.66 *m*/*z* [M + H^+]

3.3. Physiochemical Evaluation of Radioconjugates

3.3.1. Stability Study

All obtained radioconjugates (isolated from the reaction mixtures using the SPE method and being solvent-free) were examined in terms of stability in human serum using HPLC analyses. A solution of each isolated selected radioconjugate in 100 µL of a 0.1M PBS buffer pH 7.40 was added to 900 µL of human serum and incubated at 37 °C for 4 h (^{68}Ga radioconjugates) or 14 days (^{177}Lu radioconjugates). At specific time points, 400 µL of the incubated mixture was added into 500 µL of ethanol, vigorously stirred to precipitate serum proteins, and centrifuged (13,500 rpm for 5 min) to separate the supernatant for HPLC analysis.

3.3.2. Lipophilicity Study

The lipophilicity values of the radioconjugates (logD), expressed as the logarithm of its D in the *n*-octanol/PBS (pH 7.40) system, mimicking the physiological conditions (Product Properties Test Guidelines of the Office of Prevention, Pesticides and Toxic Substances 830.7550, 1996), were determined right after the SPE method purification and ethanol evaporation processes. A solution of isolated selected radioconjugate in 500 µL of a 0.1 M PBS buffer at pH 7.40 and 500 µL of *n*-octanol was vigorously stirred and centrifuged (13,500 rpm for 5 min) to separate the immiscible phases. The radioactivities of the aqueous and organic layers were determined using a well-type NaI(Tl) detector. The distribution coefficient was calculated as the ratio of the radioactivity of the radioconjugate in the organic phase to that in the aqueous phase. Each measurement was performed in triplicate and averaged. Simultaneously, the aqueous phases were analyzed by HPLC to check whether the studied radioconjugate remained intact during the experiment.

3.4. Binding Affinity Determination

The binding affinity of aprepitant and compounds **5A**–**E** for rNK1R was determined in a competitive radioligand binding assay using rat brain homogenates, following a previously described method [27]. In brief, the membrane preparations obtained from rat brains were incubated at 25 °C for 60 min in the presence of a selective radioligand [^{3}H]-[Sar^9,Met(O$_2$)^{11}]-Substance P obtained from PerkinElmer, (Waltham, MA, USA) and the increasing concentrations of the tested compounds (each concentration in duplicate). Non-specific binding was measured in the presence of 10 µM cold Substance P. The assay buffer was composed of 50 mM Tris-HCl (pH 7.4), 5 mM $MnCl_2$, bovine serum albumin (BSA) (0.1 mg/mL), bacitracin (100 µg/mL), bestatin (30 µM), phenylmethylsulfonyl fluoride (30 µg/mL), and captopril (10 µM). The reaction total volume was 1 mL. With the incubation having been terminated, a rapid filtration through GF/B Whatman glass fiber strips was done with a M-24 Cell Harvester (Brandel, Gaithersburg, MD, USA). The filters were pre-soaked overnight with 0.5% polyethyleneimine so that the extent of non-specific binding could be minimized. After the filtration, the strips were dried, the filter discs were placed separately in 24-well plates, and a Betaplate Scint scintillation solution (PerkinElmer, Waltham, MA, USA) was added to each well. Radioactivity was measured with a MicroBeta LS scintillation counter, Trilux (PerkinElmer, Waltham, MA, USA). The data came from three independent experiments done in duplicate. The results are presented as IC_{50} with SEM.

3.5. Docking

In order to obtain the probable structures of the complexes of the neurokinin 1 receptor with the conjugates **5A**–**E**, the following modelling procedure was performed. The aprepitant structure (with neutral charge) in the complex with the receptor (PDB accession code: 6HLO [19]) was expanded by attaching to the triazolinone ring the appropriate linkers and the DOTA moiety. Such initial complexes were subjected to local search docking in AutoDock 4.2.6 [26].

The DOTA geometry was set based on the NOJYIU entry [28] of The Cambridge Structural Database [29]. This structure is a DOTA complex with Lu^{3+} (diaqua-lutetium(III)-sodium trihydrate). For the purposes of our modelling, DOTA carboxylate arms were protonated and frozen in the conformation found in the crystal structure of lutetium (III) chelate of DOTA (after removing the Lu^{3+} cation, Na^+ cations and waters). The rationale behind this gambit was the fact that the carboxylates would be primarily engaged in the interactions with a cation; therefore, they might have been expected to retain the conformation they had in the solid state structure. This approach could also give a rough approximation of the DOTA's steric influence on the binding of the conjugates despite a lack of properly scaled and validated parameters for modelling and scoring the complexes with the cations of interest.

The used receptor structure was a refined one (as provided by the GPCRdb service [30]) in order to have the mutated residues replaced with the native ones and to supply the side chains missing in the original PDB structure. The structure was pre-processed in AutoDock Tools [26]. The box was set around the experimental position of aprepitant in 6HLO and extended towards the extracellular part of the receptor so as to cover the expected length of the expanded conjugate. The grids were calculated with AutoGrid 4 [26]. We considered two variants of docking with respect to the flexibility of the receptor structure. In the first variant, all receptor residues were rigid. In the second variant, E193 and H197 side-chains were set to be flexible.

The docking procedure was the local search with the following parameters: 500 individuals in population, 500 iterations of the Solis-Wets local search, the *sw_rho* parameter of the local search space set to 20.0, and 1000 local search runs. The structures resulting from the local search were clustered, and the representative models of the lowest scored (on average) cluster were taken for further analysis. For the qualitative assessment of the binding energy, both the lowest and the mean energy of the clusters were collected. The molecular graphics were prepared in PyMol [31].

For comparative and validation purposes, the very same procedure of local docking (with and without the flexibility of the mentioned two residues) was performed for the parent aprepitant.

4. Conclusions

The presented paper describes the evaluation of aprepitant functionalization in order to provide an application of this NK1R antagonist in nuclear medicine.

Out of the corresponding ^{68}Ga/^{177}Lu radioconjugates of APT-ethylamine **2A** with DOTA, Bn-DOTA, Bn-DOTAGA, and DTPA, only the DOTA amide conjugates showed satisfactory stability in human serum throughout the whole incubation time. The evaluation of the linker effect on radioconjugate lipophilicity indicated APT-alkylamine derivatives as more promising biovectors with features closer to parent aprepitant. The physicochemical properties of obtained APT-alkylamine-DOTA derivatives labelled with ^{68}Ga (**[^{68}Ga]Ga-5A–[^{68}Ga]Ga-5C**) can be compared with those of [^{67}Ga]Ga-NOTA-NK1R radioligands based on another NK1R antagonist—L-733,060 [32]. The $^{67/68}$Ga-radioligands based on these two high affinity NK1R antagonists turned out to be very similar, as evidenced by the following parameters:

(i) they were labelled using macrocyclic chelators (DOTA and NOTA) incorporated in the same 'arm' of the antagonist molecule core,
(ii) the radioconjugates had similar molecular weights (about 1000),
(iii) they had comparable logD values (about 0.15 and 0.6 for the APT-radioligands and the L-733,060-radioligands, respectively),
(iv) all were fully stable in human serum examinations.

Regarding the affinity studies of the **5A**–**E** conjugates, on the assumption that the human NK1R affinities for aprepitant derivatives were generally much higher than the rat NK1R affinities and that structure-affinity trends were parallel in both species, all the synthesized compounds might be considered to retain reasonable NK1R affinity compared to their parent. In particular, the analogue **5B** (which only suffered a few-times decrease in affinity compared to APT) seems to be especially interesting for further development. Obtained results suggest that the functionalizing of the aprepitant structure via the triazolinone ring is the right strategy.

It is also worth mentioning that, in general, radiopharmaceuticals based on small non-peptide molecules (e.g., aprepitant and L-733,060) have many advantages over peptide-based radiopharmaceuticals [2]. They usually have lower molecular weights, higher lipophilicity values, and, hence, different pharmacokinetics; they are stable in vivo, but, more importantly, their radiosyntheses can be carried out at higher temperatures and in a wider pH range. Moreover, according to the literature, radiopharmaceuticals based on non-peptide antagonists interact with a receptor through more binding sites and accumulate better and for a longer time period in cancer cells [33,34]. Even though the further evaluation of aprepitant-based radiopharmaceuticals is still needed, the findings reported herein provide insight on the perspectives of their application in the theranostics paradigm.

5. Patent

In course of this study, the following national patent application was submitted: No. P430136 "The modified drug substance molecule, method of its production, diagnostic or therapeutic receptor radiopharmaceutical based on this molecule, method of its production and its application".

Author Contributions: Conceptualization, P.K.H. and P.F.J.L.; methodology, P.K.H., P.F.J.L., J.M., and P.K.; investigation, P.K.H. and J.M.; writing—original draft preparation, P.K.H. and P.F.J.L.; writing—review and editing, P.K. and E.G.; visualization, P.F.J.L.; supervision, A.M. and E.G.; project administration, A.M. and E.G.; funding acquisition, A.M. and E.G. All authors have read and agreed to the published version of the manuscript.

Funding: This research was funded by National Science Centre (Poland), grant number 2017/25/B/NZ7/01896.

Acknowledgments: The contribution of Paweł Krzysztof Halik has been done in the frame of the National Centre for Research and Development Project No POWR.03.02.00-00-I009/17 (Radiopharmaceuticals for molecularly targeted diagnosis and therapy, RadFarm. Operational Project Knowledge Education Development 2014–2020 co-financed by European Social Fund).

Conflicts of Interest: The authors declare no conflict of interest.

Abbreviations

6HLO, 6HLL, 6HLP	accession codes of co-ordinates and structure factors in PDB
APT	aprepitant
BBB	Blood-brain barrier
Bn	benzyl moiety
BSA	bovine serum albumin
DMF	dimethylformamide
DOTA	1,4,7,10-tetraazacyclododecane-1,4,7,10-tetraacetic acid
DOTAGA	1,4,7,10-tetraazacyclododecane, 1 glutaric acid - 4,7,10-acetic acid
DTPA	diethylenetriaminepentaacetic acid
ECL	extracellular loop
ESI	electrospray ionization
GAMG	human glioblastoma cell line
HEK 293	human embryonic kidney 293 cell line
hNK1R	human neurokinin 1 receptor
HS	human serum
IC_{100}	maximal inhibitory concentration
IC_{50}	half-maximal inhibitory concentration
logD	logarithm of distribution coefficient
MS	mass spectrometry
n.c.a.	non-carrier added
NHS	*N*-hydroxysuccinimide moiety
NK1R	neurokinin 1 receptor, tachykinin 1 receptor
PBS	phosphate-buffered saline
PDB	Protein Data Bank
pK_B	negative logarithm of Boltzmann constant
p-SCN	*para*-isocyanate group
rNK1R	rat neurokinin 1 receptor
R_T	retention time
SEM	standard error of the means
SP	Substance P
SPE	solid phase extraction
TFA	trifluoroacetic acid
TM	transmembrane helix

References

1. Muñoz, M.; Rosso, M.; Coveñas, R. The NK-1 receptor: A new target in cancer therapy. *Curr. Drug Targets* **2011**, *12*, 909–921. [CrossRef] [PubMed]
2. Majkowska-Pilip, A.; Halik, P.K.; Gniazdowska, E. The Significance of NK1 receptor ligands and their application in targeted radionuclide tumour therapy. *Pharmaceutics* **2019**, *11*, 443. [CrossRef] [PubMed]
3. Coveñas, R.; Muñoz, M. Cancer progression and substance P. *Histol. Histopathol.* **2014**, *29*, 881–890. [CrossRef] [PubMed]
4. Akazawa, T.; Kwatra, S.G.; Goldsmith, L.E.; Richardson, M.D.; Cox, E.A.; Sampson, J.H.; Kwatra, M.M. A constitutively active form of neurokinin 1 receptor and neurokinin 1 receptor-mediated apoptosis in glioblastomas. *J. Neurochem.* **2009**, *109*, 1079–1086. [CrossRef] [PubMed]
5. Berger, M.; Neth, O.; Ilmer, M.; Garnier, A.; Salinas-Martín, M.V.; de Agustín Asencio, J.C.; von Schweinitz, D.; Kappler, R. Hepatoblastoma cells express truncated neurokinin-1 receptor and can be inhibited by aprepitant in vitro and in vivo. *J. Hepatol.* **2014**, *60*, 985–994. [CrossRef] [PubMed]
6. Quartara, L.; Altamura, M.; Evangelista, S.; Maggi, C.A. Tachykinin receptor antagonists in clinical trials. *Expert Opin. Investig. Drugs* **2009**, *18*, 1843–1864. [CrossRef]
7. Muñoz, M.; Rosso, M.; Aguilar, F.J.; González-Moles, M.A.; Redondo, M.; Esteban, F. NK-1 receptor antagonists induce apoptosis and counteract substance P-related mitogenesis in human laryngeal cancer cell line HEp-2. *Investig. New Drugs* **2008**, *26*, 111–118. [CrossRef]

8. Muñoz, M.; Rosso, M.; Robles-Frías, M.J.; Salinas-Martín, M.V.; Coveñas, R. The NK-1 receptor is expressed in human melanoma and is involved in the antitumor action of the NK-1 receptor antagonist aprepitant on melanoma cell lines. *Lab Investig.* **2010**, *90*, 1259–1269. [CrossRef]
9. Muñoz, M.; González-Ortega, A.; Coveñas, R. The NK-1 receptor is expressed in human leukemia and is involved in the antitumor action of aprepitant and other NK-1 receptor antagonists on acute lymphoblastic leukemia cell lines. *Investig. New Drugs* **2012**, *30*, 529–540. [CrossRef]
10. Muñoz, M.; González-Ortega, A.; Salinas-Martín, M.V.; Carranza, A.; Garcia-Recio, S.; Almendro, V.; Coveñas, R. The neurokinin-1 receptor antagonist aprepitant is a promising candidate for the treatment of breast cancer. *Int. J. Oncol.* **2014**, *45*, 1658–1672. [CrossRef]
11. Muñoz, M.; Berger, M.; Rosso, M.; Gonzalez-Ortega, A.; Carranza, A.; Coveñas, R. Antitumor activity of neurokinin-1 receptor antagonists in MG-63 human osteosarcoma xenografts. *Int. J. Oncol.* **2014**, *44*, 137–146. [CrossRef] [PubMed]
12. Dikmen, M. Antiproliferative and apoptotic effects of aprepitant on human glioblastoma U87MG cells. *Marmara Pharm. J.* **2017**, *21*, 156–164. [CrossRef]
13. Kitchens, C.A.; McDonald, P.R.; Pollack, I.F.; Wipf, P.; Lazo, J.S. Synergy between microtubule destabilizing agents and neurokinin 1 receptor antagonists identified by an siRNA synthetic lethal screen. *FASEB J.* **2009**, *23*, 756–813.
14. Kast, R.E.; Ramiro, S.; Llado, S.; Toro, S.; Coveñas, R.; Muñoz, M. Antitumour action of temozolomide, ritonavir and aprepitant against human glioma cells. *J. Neurooncol.* **2016**, *126*, 425–431. [CrossRef] [PubMed]
15. Muñoz, M.; Rosso, M. The NK-1 receptor antagonist aprepitant as a broad-spectrum antitumor drug. *Investig. New Drugs* **2010**, *28*, 187–193. [CrossRef]
16. Hale, J.J.; Mills, S.G.; MacCoss, M.; Shah, S.K.; Qi, H.; Mathre, D.J.; Cascieri, M.A.; Sadowski, S.; Strader, C.D.; MacIntyre, D.E.; et al. 2(S)-((3,5-Bis(trifluoromethyl)benzyl)oxy)-3(S)-phenyl-4-((3-oxo-1,2,4-triazol-5-yl)methyl)morpholine (1): A potent, orally active, morpholine-based human neurokinin-1 receptor antagonist. *J. Med. Chem.* **1996**, *39*, 1760–1762. [CrossRef]
17. Hale, J.J.; Mills, S.G.; MacCoss, M.; Finke, P.E.; Cascieri, M.A.; Sadowski, S.; Ber, E.; Chicchi, G.G.; Kurtz, M.; Metzger, J.; et al. Structural optimization affording 2-(R)-(1-(R)-3,5-Bis(trifluoromethyl) phenylethoxy)-3-(S)-(4-fluoro)phenyl-4-(3-oxo-1,2,4-triazol-5-yl)methylmorpholine, a potent, orally active, long-acting Morpholine Acetal human NK-1 receptor antagonist. *J. Med. Chem.* **1998**, *41*, 4607–4614. [CrossRef]
18. Harrison, T.; Owens, A.P.; Williams, B.J.; Swain, C.J.; Williams, A.; Carlson, A.; Rycroft, W.; Tattersall, F.D.; Cascieri, M.A.; Chicchi, G.G.; et al. An orally active, water-soluble Neurokinin-1 receptor antagonist suitable for both intravenous and oral clinical administration. *J. Med. Chem.* **2001**, *44*, 4296–4299. [CrossRef]
19. Schöppe, J.; Ehrenmann, J.; Klenk, C.; Rucktooa, P.; Schütz, M.; Doré, A.S.; Plückthun, A. Crystal structures of the human neurokinin 1 receptor in complex with clinically used antagonists. *Nat. Commun.* **2019**, *10*, 17–27. [CrossRef]
20. Giannini, G.; Milazzo, F.M.; Battistuzzi, G.; Rosi, A.; Anastasi, A.M.; Petronzelli, F.; Albertoni, C.; Tei, L.; Leone, L.; Salvini, L.; et al. Synthesis and preliminary in vitro evaluation of DOTA-Tenatumomabconjugates for theranostic applications in tenascin expressing tumors. *Bioorg. Med. Chem.* **2019**, *27*, 3248–3253. [CrossRef]
21. Waterhouse, R.N. Determination of Lipophilicity and its use as a predictor of blood–brain barrier penetration of molecular imaging agents. *Mol. Imaging Biol.* **2003**, *5*, 376–389. [CrossRef] [PubMed]
22. Wu, Y.; Loper, A.; Landis, E.; Hettrick, L.; Novak, L.; Lynn, K.; Chen, C.; Thompson, K.; Higgins, R.; Batra, U.; et al. The role of biopharmaceutics in the development of a clinical nanoparticle formulation of MK-0869: A Beagle dog model predicts improved bioavailability and diminished food effect on absorption in human. *Int. J. Pharm.* **2004**, *285*, 135–146. [CrossRef] [PubMed]
23. Appell, K.C.; Fragale, B.J.; Loscig, J.; Singh, S.; Tomczuk, B.E. Antagonists that demonstrate species differences in neurokinin-1 receptors. *Mol. Pharmacol.* **1992**, *41*, 772–778. [PubMed]
24. Pradier, L.; Habert-Ortoli, E.; Emile, L.; Le Guern, J.; Loquet, I.; Bock, M.D.; Clot, J.; Mercken, L.; Fardin, V.; Garret, C. Molecular determinants of the species selectivity of neurokinin type 1 receptor antagonists. *Mol. Pharmacol.* **1995**, *47*, 314–321.
25. Leffer, A.; Ahlstedt, I.; Engberg, S.; Svensson, A.; Billger, M.; Oberg, L.; Bjursell, M.K.; Lindström, E.; von Mentzer, B. Characterization of species-related differences in the pharmacology of tachykinin NK receptors 1, 2 and 3. *Biochem. Pharmacol.* **2009**, *77*, 1522–1530. [CrossRef]

26. Morris, G.M.; Huey, R.; Lindstrom, W.; Sanner, M.F.; Belew, R.K.; Goodsell, D.S.; Olson, A.J. AutoDock4 and AutoDockTools4: Automated docking with selective receptor flexibility. *J. Comput. Chem.* **2009**, *30*, 2785–2791. [CrossRef]
27. Matalińska, J.; Lipiński, P.F.J.; Kotlarz, A.; Kosson, P.; Muchowska, A.; Dyniewicz, J. Evaluation of receptor affnity, analgesic activity and cytotoxicity of a hybrid peptide, AWL3020. *Int. J. Pept. Res. Ther.* **2020**. [CrossRef]
28. Aime, S.; Barge, A.; Botta, M.; Fasano, M.; Ayala, J.D.; Bombieri, G. Crystal structure and solution dynamics of the lutetium(III) chelate of DOTA. *Inorg. Chmica Acta* **1996**, *246*, 423–429. [CrossRef]
29. Allen, F.H. The cambridge structural database: A quarter of a million crystal structures and rising. *Acta Crystallogr. B* **2002**, *58*, 380–388. [CrossRef]
30. Pándy-Szekeres, G.; Munk, C.; Tsonkov, T.M.; Mordalski, S.; Harpsøe, K.; Hauser, A.S.; Bojarski, A.J.; Gloriam, D.E. GPCRdb in 2018: Adding GPCR structure models and ligands. *Nucleic Acids Res.* **2018**, *4*, D440–D446. [CrossRef]
31. Schrödinger LLC. The PyMOL Molecular Graphics System 2018. Available online: https://github.com/schrodinger/pymol-open-source (accessed on 31 July 2020).
32. Zhang, H.; Kanduluru, A.K.; Desai, P.; Ahad, A.; Carlin, S.; Tandon, N.; Weber, W.A.; Low, P.S. Synthesis and evaluation of a Novel ^{64}Cu- and ^{67}Ga-Labeled Neurokinin 1 receptor antagonist for in Vivo targeting of NK1R-Positive tumor Xenografts. *Bioconjug. Chem.* **2018**, *29*, 1319–1326. [CrossRef] [PubMed]
33. Ginj, M.; Zhang, H.; Waser, B.; Cescato, R.; Wild, D.; Wang, X.; Erchegyi, J.; Rivier, J.; Mäcke, H.R.; Reubi, J.C. Radiolabeled somatostatin receptor antagonists are preferable to agonists for in vivo peptide receptor targeting of tumors. *Proc. Natl. Acad. Sci. USA* **2006**, *103*, 16436–16441. [CrossRef] [PubMed]
34. Cescato, R.; Maina, T.; Nock, B.; Nikolopoulou, A.; Charalambidis, D.; Piccand, V.; Reubi, J.C. Bombesin receptor antagonists may be preferable to agonists for tumor targeting. *J. Nucl. Med.* **2008**, *49*, 318–326. [CrossRef] [PubMed]

Sample Availability: Samples of the compounds **2A**–**C**, **4D**, **E** are available from the authors.

3.4. Novel NK1R-Targeted ^{68}Ga-/^{177}Lu-Radioconjugates with Potential Application against Glioblastoma Multiforme: Preliminary Exploration of Structure-Activity Relationships

Matalińska, J.; Kosińska, K.; **Halik, P.K.;** Koźmiński, P.; Lipiński, P.F.J.; Gniazdowska, E.; Misicka, A. Novel NK1R-Targeted ^{68}Ga-/^{177}Lu-Radioconjugates with Potential Application against Glioblastoma Multiforme: Preliminary Exploration of Structure–Activity Relationships. *Int. J. Mol. Sci.* **2022**, *23*, 1214. DOI: 10.3390/ijms23031214

IF (2020) = 5,924; pkt. MNiSW (2022) = 140

Autorzy	Udział
Matalińska, J.	- hodowla komórkowa; - wykonanie oznaczeń powinowactwa receptorowego metodą kompetycyjną; - przygotowanie manuskryptu;
Kosińska, K.	- wykonanie preparatyki syntetycznej pochodnych L732,138; - opracowanie analiz spektroskopowych i spektrometrycznych; - praca nad manuskryptem (2. czytanie);
Halik, P.K.	- wykonanie preparatyki syntetycznej koniugatów L732,138; - wykonanie preparatyki radiosyntetycznej; - wykonanie analiz radiochemicznych; - hodowla komórkowa; - wykonanie oznaczeń powinowactwa receptorowego metodą saturacyjną; - przygotowanie manuskryptu; - wizualizacja danych;
Koźmiński, P.	- wykonanie analiz spektrometrycznych; - praca nad manuskryptem (1. czytanie);
Lipiński, P.F.J.	- wykonanie badania modelowania molekularnego; - przygotowanie manuskryptu; - przygotowanie suplementu; - wizualizacja danych;
Gniazdowska, E.	- koncepcja badań; - kierowanie grantem; - praca nad manuskryptem (2. czytanie);
Misicka, A.	- koncepcja badań; - kierowanie grantem; - praca nad manuskryptem (2. czytanie);

International Journal of
Molecular Sciences

MDPI

Article

Novel NK1R-Targeted ^{68}Ga-/^{177}Lu-Radioconjugates with Potential Application against Glioblastoma Multiforme: Preliminary Exploration of Structure–Activity Relationships

Joanna Matalińska [1,†], Katarzyna Kosińska [1,†], Paweł K. Halik [2], Przemysław Koźmiński [2], Piotr F. J. Lipiński [1,*], Ewa Gniazdowska [2] and Aleksandra Misicka [1,3,*]

1 Department of Neuropeptides, Mossakowski Medical Research Institute Polish Academy of Sciences, 5 Pawińskiego Street, 02-106 Warsaw, Poland; jmatalinska@imdik.pan.pl (J.M.); kkosinska@imdik.pan.pl (K.K.)
2 Centre of Radiochemistry and Nuclear Chemistry, Institute of Nuclear Chemistry and Technology, 16 Dorodna Street, 03-195 Warsaw, Poland; p.halik@ichtj.waw.pl (P.K.H.); p.kozminski@ichtj.waw.pl (P.K.); e.gniazdowska@ichtj.waw.pl (E.G.)
3 Faculty of Chemistry, University of Warsaw, 1 Pasteura Street, 02-093 Warsaw, Poland
* Correspondence: plipinski@imdik.pan.pl (P.F.J.L.); misicka@chem.uw.edu.pl (A.M.)
† These authors contributed equally to this work.

Abstract: Locoregionally administered, NK1 receptor (NK1R) targeted radionuclide therapy is a promising strategy for the treatment of glioblastoma multiforme. So far, the radiopharmaceuticals used in this approach have been based on the endogenous agonist of NK1R, Substance P or on its close analogues. Herein, we used a well-known, small molecular NK1R antagonist, L732,138, as the basis for the radiopharmaceutical vector. First, 14 analogues of this compound were evaluated to check whether extending the parent structure with linkers of different lengths would not deteriorate the NK1R binding. The tested analogues had affinity similar to or better than the parent compound, and none of the linkers had a negative impact on the binding. Next, five DOTA conjugates were synthesized and used for labelling with ^{68}Ga and ^{177}Lu. The obtained radioconjugates turned out to be fairly lipophilic but showed rather limited stability in human plasma. Evaluation of the receptor affinity of the (radio)conjugates showed that neither the chelator nor the metal negatively impacts the NK1R binding. The ^{177}Lu-radioconjugates exhibited the binding characteristics towards NK1R similar or better than that of the ^{177}Lu-labelled derivative of Substance P, which is in current clinical use. The experimental results presented herein, along with their structural rationalization provided by modelling, give insight for the further molecular design of small molecular NK1R-targeting vectors.

Keywords: L732,138; radiopharmaceuticals; neurokinin-1 receptor antagonist; radioconjugates; targeted radionuclide therapy; glioblastoma multiforme; molecular dynamics

Citation: Matalińska, J.; Kosińska, K.; Halik, P.K.; Koźmiński, P.; Lipiński, P.F.J.; Gniazdowska, E.; Misicka, A. Novel NK1R-Targeted ^{68}Ga-/^{177}Lu-Radioconjugates with Potential Application against Glioblastoma Multiforme: Preliminary Exploration of Structure–Activity Relationships. *Int. J. Mol. Sci.* **2022**, *23*, 1214. https://doi.org/10.3390/ijms23031214

Academic Editors: Giuseppe Lombardi and Ahmed Idbaih

Received: 30 November 2021
Accepted: 18 January 2022
Published: 21 January 2022

1. Introduction

Glioblastoma multiforme (GBM, IV WHO grade glioma) is among the most common primary malignant brain tumours [1]. It is also the most aggressive one of all gliomas, with very poor prognosis. The majority of patients do not survive beyond a year, and the median survival time is less than 16 months [2]. The current standard treatments (surgical resection followed by radio- and chemotherapy) are disappointingly ineffective. In almost all patients, a quick GBM recurrence is observed. The problem with treating GBM is in part associated with the heterogenous character of this tumour, its very high proliferation and its infiltrative nature [1]. Another problem is the limited distribution of the systemic drugs (due to the blood–brain barrier) as well as the tumour cells' resistance to them.

An experimental therapeutic option that holds promise for enhancing the effectiveness of GBM treatment is the locoregionally administered targeted radionuclide therapy (TRT) [3]. The principle of TRT is to deliver α- or β-emitting radionuclides into (or in the

close vicinity of) the cancer cells. This is accomplished by the means of radioconjugates of general structure: vector-linker-chelator-radionuclide. The vector fragment (small molecule, peptide or antibody) must have high affinity for a certain molecular target (a receptor) over-expressed at the surface of cancer cells. The linker enables attaching the chelating moiety onto the vector structure without compromising the affinity. A well-tuned radioconjugate diffuses within the tumour and penetrates the infiltrative zone, selectively concentrating the radioactivity around the neoplastic cells and destroying them. At the same time, the locoregional administration (that is into the tumour or into the post-operative resection cavity) allows for bypassing the blood–brain barrier and for sparing the radiation-sensitive organs.

A molecular target particularly suitable for TRT of GBM is the neurokinin-1 receptor (NK1R) [4], since it was shown to be widely overexpressed in GBM as well as in many grade II and grade III gliomas [5]. Moreover, in the normal CNS tissue, NK1R is not highly expressed, except for in a few specific areas (e.g., in the spinal cord) [5]. This should ensure that the critical brain regions are not damaged by the radioactivity.

Targeting NK1R with locally administered radioconjugates was evaluated clinically, showing indeed very promising therapeutic outcomes with little toxicity [5–9]. The attempts that have advanced to clinic so far utilized peptide vectors based on the endogenous NK1R ligand, Substance P (SP) or its close analogues modified to improve in vivo stability [10]. These peptides, conjugated with the macrocyclic chelators (DOTA or DOTAGA), were labelled with ^{90}Y, ^{177}Lu or ^{213}Bi. SP-based radioconjugates labelled with ^{225}Ac have also been subject to in vitro [11] and in vivo [8,12] investigations.

Despite the first success of the NK1R-directed TRT concept, the field is open for further developments. For example, it was postulated [8,13] that vectors of lower molecular mass and higher lipophilicity could be more advantageous than SP. Such carriers should distribute more rapidly and more thoroughly, in particular into the walls of the post-surgical cavity. This is especially important in the case of short-lived radionuclides, such as ^{213}Bi. In the desire to address this proposition, a search for vectors smaller than SP was initiated. Majkowska-Pilip et al. investigated short Substance P fragments labelled with ^{99m}Tc and ^{177}Lu [13]. An SP substructure was also used for labelling with ^{211}At by Lyczko et al. [14] Recently, we have synthesized radioconjugates based on the FDA-approved small molecular NK1R antagonist, aprepitant [15].

In another branch of our research, we have turned our attention to yet other small molecular NK1R antagonist, L732,138 (**1c**, Figure 1C), which had been reported for the first time by MacLeod et al. [16]. Using this compound as a basis for the radiopharmaceutical vector has several advantages from the perspective of structure–activity relationship (SAR) studies. L732,138 exhibits high affinity for NK1R [16]. At the same time, its structure is fairly simple. This makes the generation of analogues required for SAR exploration facile and quick. Moreover, the synthesis of novel vectors from scratch in quantities needed for exhaustive evaluation becomes inexpensive and easy. A potential liability is the presence of the ester linkage, which may be prone to hydrolysis by serum esterases. However, this is not necessarily disqualifying for a compound to be delivered locoregionally, since the activity of the serum enzymes in the cavity or in the cerebrospinal fluid is absent or very low [17]. Note that some of the excellent clinical results obtained so far were obtained with peptide vectors that are susceptible to very quick degradation in plasma [5,7]. Besides, planning the novel conjugates to be used for systemic administration, the issue of stability could be addressed at the later stage by, e.g., isosteric replacements.

Having considered the above-stated points, we designed and prepared several novel analogues of L732,138 to see whether expanding this structure by potential linking elements would not result in a loss of NK1R affinity. In the further step, the novel analogues served for the synthesis of conjugates and radioconjugates, which were subsequently evaluated for physicochemical and biological properties. The results were also analysed in the light of molecular modelling, including docking and molecular dynamics. These efforts are reported in the current contribution.

A

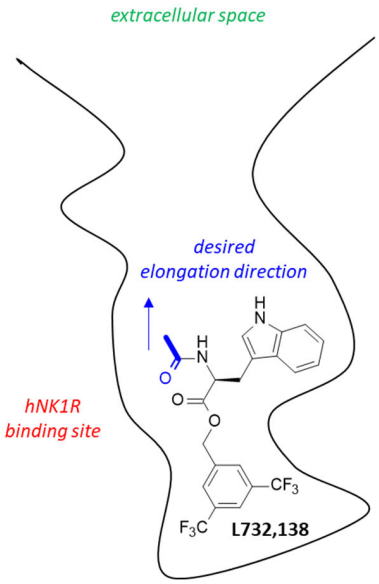

B

Compound	Linker	Linker length [n of atoms]	ΔALogP
1	-	0	0.000
2	-DAla-	3	-0.349
3	-DAla-DAla-	6	-0.698
4	-Ahx-	7	+0.542
5	-Ahx-Ahx-	14	+1.084

C

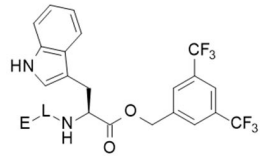

Compound	E *End cap*	L *Linker*
1a	Boc-	-
1b	H-	-
1c *L732,138* (parent)	Ac-	-
2a	Boc-	-DAla-
2b	H-	-DAla-
2c	Ac-	-DAla-
3a	Boc-	-DAla-DAla-
3b	H-	-DAla-DAla-
3c	Ac-	-DAla-DAla-
4a	Boc-	-Ahx-
4b	H-	-Ahx-
4c	Ac-	-Ahx-
5a	Boc-	-Ahx-Ahx-
5b	H-	-Ahx-Ahx-
5c	Ac-	-Ahx-Ahx-

Figure 1. (**A**) Schematic representation of the L732,138 binding model that guided the design. (**B**) The linkers chosen along with their lengths and their predicted effect on lipophilicity expressed as the change of theoretical lipophilicity parameter (ΔALogP). (**C**) The analogues to be synthesized. Abbreviations: Ac—acetyl, Ahx—ε-aminohexanoic acid, Boc—*tert*-butoxycarbonyl, DAla—D-alanine.

2. Results and Discussion

2.1. Structure–Activity Relationships of the Extended L732,138 Analogues

2.1.1. Design Rationale

In building bifunctional conjugates, an essential consideration is how and where to attach the (usually) bulky chelating moiety to the vector fragment so that the receptor affinity is not compromised. Molecular modelling based on homology models of human NK1R (executed before the crystal structures were available) had suggested that L732,138 binds by placing the 3,5-bis(trifluoromethyl)phenyl ring at the very bottom of the binding site (Figure 1A). The *N*-acetyl fragment would be oriented in the direction approximately towards the outlet of the binding site, with the terminal CH_3-group exposed to the solvent. It had seemed then that expanding the parent molecule by exchanging *N*-acetyl for other *N*-acylating elements should be optimal. Based on the model, we had expected that the direct introduction of a chelator moiety (e.g., DOTA) instead of the *N*-acetyl fragment would not be tolerated due to the bulkiness of the chelator. However, given the uncertainty associated with the homology model of the receptor and the modelling itself, we wanted to probe several depths of chelator placement in the binding site by using linkers of various lengths but not excluding the direct attachment of chelator. We also contemplated the impact of the spacers on the lipophilicity of the compounds (modelled by the change of the theoretical lipophilicity parameter, ALogP). From the point of view of pharmacology, lipophilicity is one of the most important physicochemical parameters for drugs and other medical preparations, because it characterizes their ability to distribute and to accumulate in organisms [18,19].

As a result of these considerations, it was decided to prepare five series of compounds (**1**–**5**) with linkers, as given in Figure 1B. At the 'end' of the *N*-terminus, the compounds were to have an unprotected amino group (**b**), *N*-*tert*-butyloxycarbonyl group (**a**) or *N*-acetyl group (**c**) (Figure 1C). Overall, this part of our work was meant to see if introduction of the potential linking fragments would not give loss of NK1R affinity.

2.1.2. Synthesis

The synthesis of the designed analogues was accomplished by the divergent approach outlined in Scheme 1. Starting from Boc-L-Trp-OH, the ester **1a** was obtained by *O*-alkylation by the appropriate bromide under standard conditions. Upon deprotection of the Boc group with trifluoroacetic acid (TFA), **1b** was obtained. This compound served either for *N*-acetylation (to give L732,138, **1c**) or for attaching the linking moieties. The latter was carried out by coupling **1b** with the *N*-hydroxysuccinimide (NHS) active esters of the N^{ε}- or N^{α}-protected aminohexanoic acid (Ahx; the ester preformed) or D-alanine (DAla; the ester formed in situ). All further analogues were furnished by this sequence of reactions (deprotection followed by acetylation or coupling and so on). In total, 15 compounds were synthesized and isolated, 13 of which are reported for the first time.

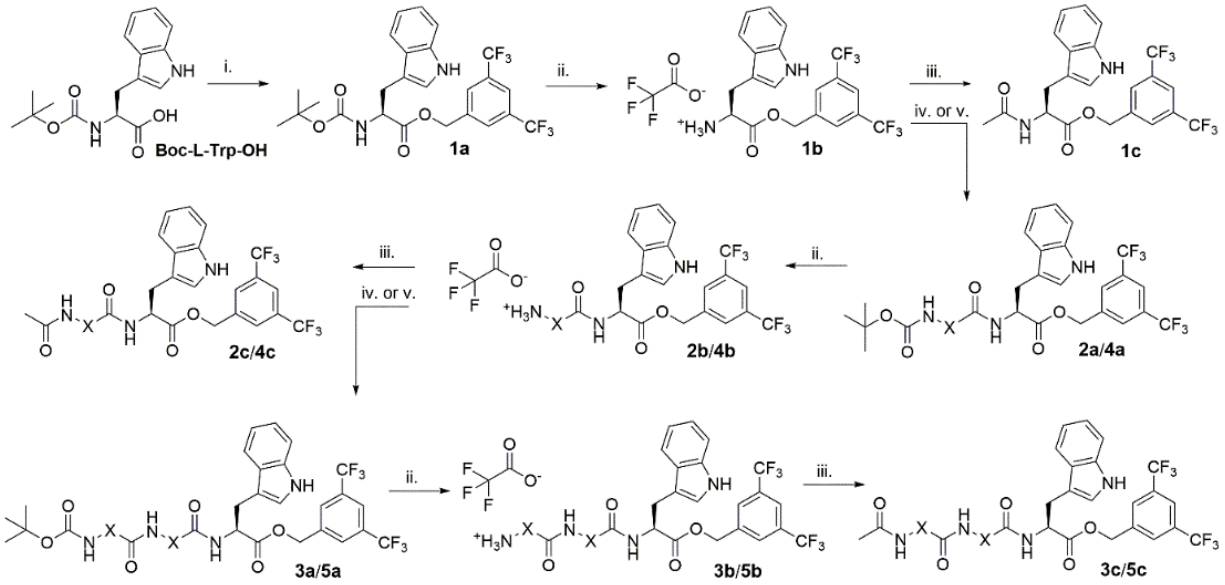

X	
(R) CH3	
2a	4a
2b	4b
2c	4c
3a	5a
3b	5b
3c	5c

Scheme 1. Synthesis of the designed analogues. Reagents and conditions: (i) caesium carbonate (Cs_2CO_3), 3,5-bis(trifluoromethyl)benzyl bromide, RT, 18 h, acetonitrile (ACN); (ii) trifluoroacetic acid (TFA): dichloromethane (DCM) (1:1), RT, 1h; (iii) acetic anhydride (Ac_2O), *N*,*N*,*N*′,*N*′-tetramethylguanidine (TMG), 0 °C–RT, 1,5 h, dimethylformamide (DMF); (iv) 6-(*N*-(*tert*-butyloxycarbonyl)-amino)hexanoic acid *N*-succinimidyl ester (Boc-6-Ahx-OSu), TMG, RT, 6 h, DMF; (v) *N*-hydroxysuccinimide (HOSu), DCC, *N*-(*tert*-butyloxycarbonyl)-D-alanine (Boc-D-Ala-OH), TMG, 0 C- RT, 2 days, DMF.

2.1.3. Binding Affinity Determination

The prepared analogues were tested as to their affinity for the rat and human NK1 receptors (rNK1R and hNK1R, respectively). This parameter is responsible for the weak or strong binding of tested compounds to the receptor, which results in the quality of the diagnostic imaging and/or the effectiveness of the therapy. Radiopharmaceuticals with high affinity to receptors cause selective destruction of pathological cells and do not affect healthy cells. Testing the compounds at receptors coming from different species is justified by the fact that some NK1R ligands show markedly different affinities for the human variant and the rat variant [20]. While the pursued radioconjugates are intended for potential use in human medicine, much of the in vivo testing is usually carried out in rats; hence, the information on the possible interspecies differences in affinity may be of value. The results of the binding assays are given in Table 1.

Table 1. NK1R binding affinity of the synthesized analogues.

Compound	Linker Length	Linker	*N*-Terminus	IC_{50} (Mean ± SD) [1]	
				rNK1R	hNK1R
	(n Atoms)			(nM)	(nM)
1a	0	none	Boc	2928 ± 1518	180.4 ± 112.4
1b	0	none	H	>10000	358.9 ± 132.0
1c L732,138 [2] (parent)	0	none	Ac	2879 ± 999	25.6 ± 15.9
2a	3	-DAla-	Boc	1532 ± 279	135.0 ± 108.3
2b	3	-DAla-	H	4681 ± 1322	25.4 ± 12.5
2c	3	-DAla-	Ac	2280 ± 703	25.3 ± 0.4
3a	6	-DAla-DAla-	Boc	745 ± 311	13.9 ± 11.2
3b	6	-DAla-DAla-	H	4007 ± 1373	80.8 ± 59.7
3c	6	-DAla-DAla-	Ac	1141 ± 289	13.5 ± 12.1
4a	7	-Ahx-	Boc	1658 ± 1051	60.7 ± 31.9
4b	7	-Ahx-	H	1399 ± 319	35.4 ± 23.6
4c	7	-Ahx-	Ac	1951 ± 641	83.1 ± 69.3
5a	14	-Ahx-Ahx-	Boc	762 ± 295	4.5 ± 2.8
5b	14	-Ahx-Ahx-	H	572 ± 41	20.4 ± 10.2
5c	14	-Ahx-Ahx-	Ac	655 ± 120	14.3 ± 5.2
Reference compounds					
Substance P	-	-	-	3.6 (n = 1)	30.7 ± 4.2 (n = 2)
Aprepitant	-	-	-	130 ± 60 [15]	27.7 (n = 1)

[1] IC_{50}, half maximal inhibitory concentration, mean of three independent experiments carried out in duplicate with the standard deviation, unless stated otherwise. [2] hNK1R binding affinity in the original report, IC_{50} = 1.6 nM [16].

The affinities for the human receptor will be discussed first and in detail. The parent L732,138 (**1c**) in our hands exhibits nanomolar affinity for hNK1R with IC_{50} = 25.6 nM. The deacetylated analogue (**1b**) binds 14× weaker (IC_{50} = 358.9 nM), while the Boc-protected derivative (**1a**) is a 7× weaker NK1R ligand (IC_{50} = 180.4 nM) than the parent compound. Similar hNK1R affinity order (*N*-acetyl > *N*-Boc > amino analogue) was reported previously for derivatives with 3,5-dimethyl substitution at the phenyl ring [21]. Vardanyan et al. previously reported the analogue with free amino group **1b** but in the form of ionic pairs with a few fentanyl carboxylate derivatives as the anions for which they found hNK1R binding with Ki in the order of 20–40 nM [22].

Expanding the parent compound by a single DAla unit (**2c**) yields an almost identical hNK1R affinity (IC_{50} = 25.4 nM), which is not affected by *N*-deacetylation (**2b**, IC_{50} = 25.4 nM). On the contrary, the Boc protected derivative **2a** is a clearly weaker ligand (IC_{50} = 135.0 nM).

An additional DAla residue is associated with some modest improvement of the affinity (**3c**, IC_{50} = 13.5 nM) compared to the parent. The Boc protected derivative **3a** has similar binding strength, but the *N*-deacetylated derivative **3b** binds slightly worse (IC_{50} = 80.8 nM) compared both to the parent **1c** or to **3c**.

Insertion of a single Ahx fragment leads to minor worsening of the affinity (**4c**, IC_{50} = 83.1 nM) in comparison to L732,138. Slightly better affinity is found for the Boc protected derivative **4a** (IC_{50} = 60.7 nM), and further improvement is observed with the *N*-deacetylated analogue **4b** (IC_{50} = 35.4 nM).

Among the longest analogues (with double Ahx fragment) is the most potent of the novel compounds, the *N*-Boc analogue **5a**, whose IC_{50} equals 4.5 nM and is about five times better than that of L732,138. The *N*-acetylated analogue (**5c**) is also slightly better than the parent with IC_{50} = 14.3 nM. The amino derivative **5b** exhibits binding similar to that of L732,138 (IC_{50} = 20.4 nM).

Overall, in the case of the human receptor, the affinity variations associated with the presence of linkers and/or of the capping groups are rather small. Most of the analogues show decent hNK1R affinity and some of them are better than the parent L732,138 (**1c**) or another reference hNK1R ligand, aprepitant (in our hands, IC_{50} = 27.7 nM).

Regarding the rat receptor, the parent L732,138 (**1c**) in our hands exhibits micromolar affinity for rNK1R with IC_{50} = 2879 nM. The difference in L732,138 binding to rNK1R and hNK1r had been already reported [23].

Four novel analogues exhibit submicromolar IC_{50} values (**3a**, **5a**, **5b** and **5c**), and the majority of the remaining ones are slightly better rNK1R ligands than the parent. The trends in structure/affinity changes are not parallel when comparing hNK1R and rNK1R binding. There is only a weak correlation (R^2 = 0.33) between the human and rat receptor affinities (Figure 2). Importantly, all novel compounds are weaker binders of the rat receptor than Substance P (IC_{50} = 3.6 nM) or aprepitant (IC_{50} = 130 nM [15]).

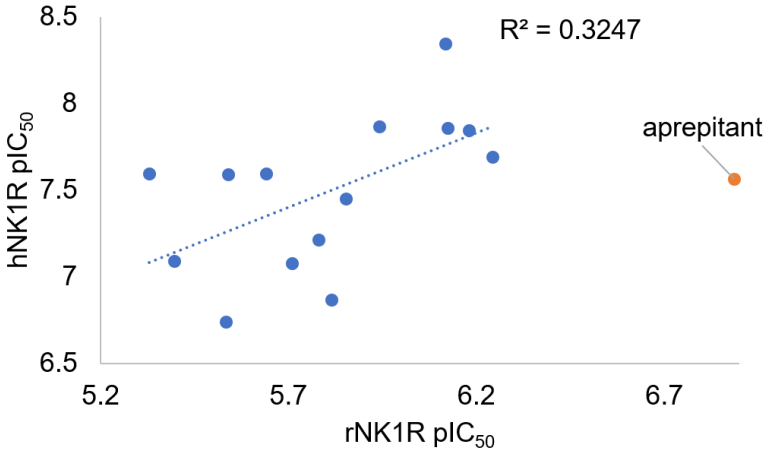

Figure 2. Plot of the hNK1R versus rNK1R binding affinity for compounds **1a**–**5c**. The affinities are shown as the negative logarithm of the IC_{50} value (pIC_{50}). Compound **1b** is excluded for having indeterminate rNK1R affinity (IC_{50} > 10 μM). The data for aprepitant are given for reference.

2.2. Radioconjugates

2.2.1. Synthesis of Radioconjugates

Since none of the linkers had a profoundly negative or positive effect on hNK1R affinity, it was rational to evaluate radioconjugates based upon each of them. To this aim, the derivatives with the primary amino group (**1b**–**5b**) were reacted with the NHS ester of the cyclic chelator DOTA to obtain the corresponding DOTA conjugates **1d**–**5d**

(Scheme 2, Figure 3). The choice of only one radionuclide chelator was dictated by stability issues evaluated previously [15].

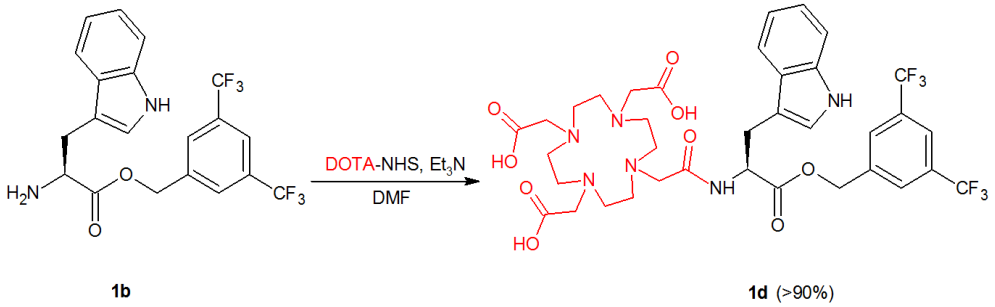

Scheme 2. An exemplary synthetic route of conjugation reaction of DOTA-NHS with **1b**. Other *N*-deacetylated derivatives of L-732,138, **2b**–**5b**, follow conjugation reaction in a similar manner.

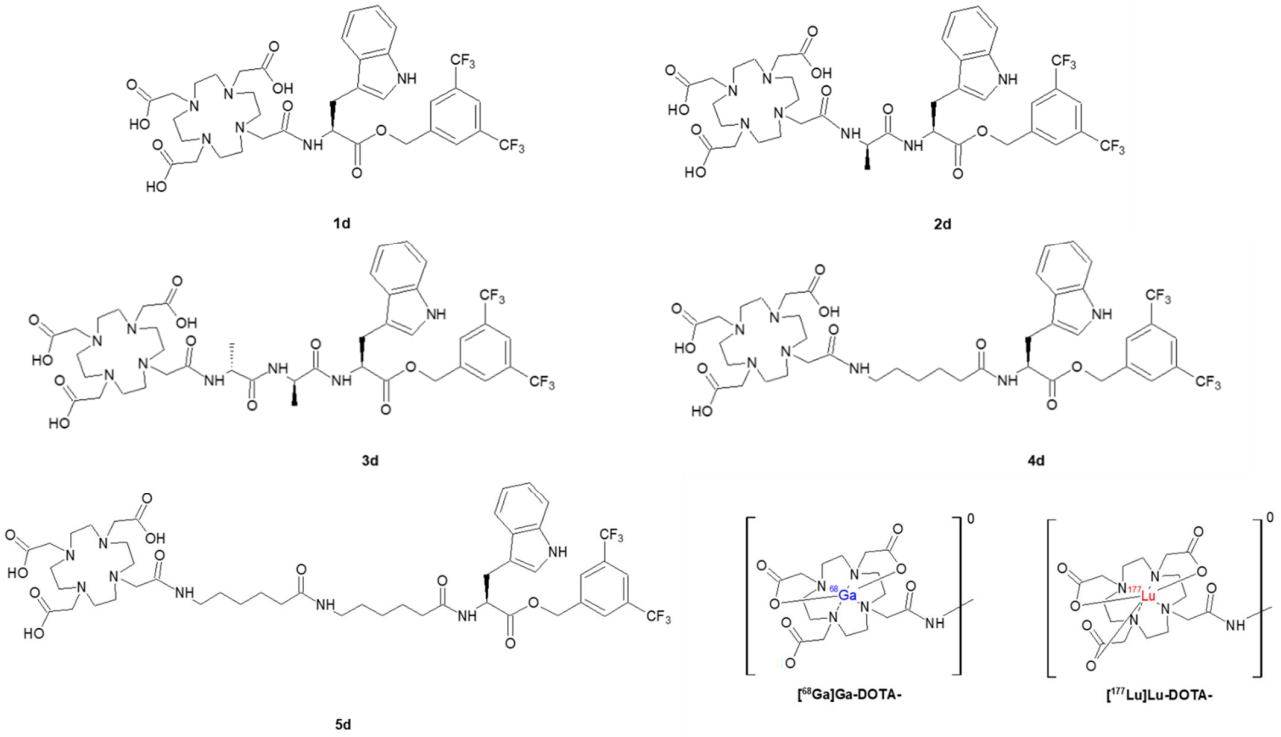

Figure 3. Structures of all DOTA conjugates, **1d**–**5d**, along with [^{68}Ga]Ga-DOTA- and [^{177}Lu]Lu-DOTA-radiocomplexes present in **[^{68}Ga]Ga-1d**–**[^{68}Ga]Ga-5d** and **[^{177}Lu]Lu-1d**–**[^{177}Lu]Lu-5d** radioconjugates.

Each of the DOTA conjugates was labelled with ^{68}Ga or ^{177}Lu, providing two series of radioconjugates. Radiolabelling was successfully performed at 95 °C for 10 min at specific activity of around 2 GBq/μmol and in high radiochemical yield above 95%. The obtained radioconjugates were purified using the solid phase extraction (SPE) method before HPLC identification (Figure 4) and further analyses.

In parallel, the verification of the obtained ^{68}Ga-radioconjugates was performed by synthesis of the non-radioactive stable gallium reference compounds (**Ga-1d**–**Ga-5d**). These were prepared in an analogous manner, as in the case of ^{68}Ga-radioconjugates, followed by the characterization using mass spectrometry. The comparison of HPLC retention times (t_R) of radioactive and non-radioactive products is presented in Table 2. The values are consistent, corroborating the identity of the conjugates (the differences between them result from the serial connection of UV-Vis and gamma detectors).

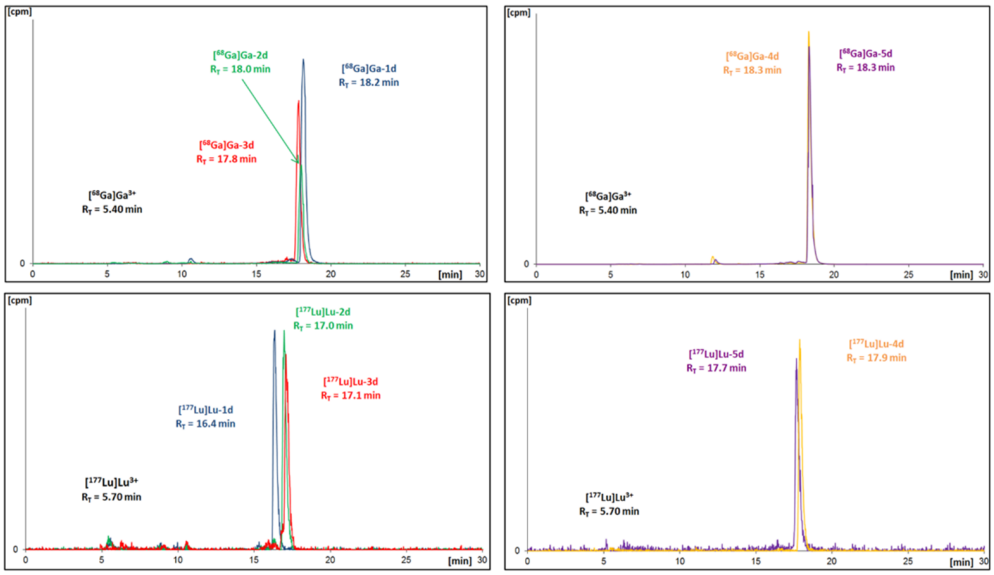

Figure 4. Radiochromatograms of obtained DOTA conjugates radiolabelled with gallium-68 (**upper**) or with lutetium-177 (**bottom**).

Table 2. Retention times (t_R) of stable gallium conjugates and ^{68}Ga-radioconjugates.

Stable Ga-Conjugate	t_R [1]	^{68}Ga-Radioconjugate	t_R
Ga-1d	17.9 min	**[^{68}Ga]Ga-1d**	18.2 min
Ga-2d	17.7 min	**[^{68}Ga]Ga-2d**	18.0 min
Ga-3d	17.6 min	**[^{68}Ga]Ga-3d**	17.8 min
Ga-4d	18.1 min	**[^{68}Ga]Ga-4d**	18.3 min
Ga-5d	18.2 min	**[^{68}Ga]Ga-5d**	18.3 min

[1] Gradient elution: 0–20 min 20 to 80% solvent B; 20–30 min 80% solvent B; 2 mL/min.; solvent A: 0.1% (*v*/*v*) TFA in H_2O; and solvent B: 0.1% (*v*/*v*) TFA in ACN.

2.2.2. Plasma Stability

All obtained radioconjugates, previously isolated from the reaction mixture using the SPE method and being solvent-free, were examined as to their stability in human serum (HS). For this purpose, each radioconjugate was mixed with HS and incubated at 37 °C. At specific time points, small samples of radioconjugate mixture were analysed using the HPLC method for the assessment of the radioconjugate stability.

The results of the plasma stability determinations are shown in Figure 5. Exemplary chromatograms are given in the Supplementary Materials in Figures SM-STAB-1 and SM-STAB-2. All the ^{68}Ga-radioconjugates begin to decompose as early as at the 1 h time point (79–98% radioactivity remaining). At the 4.5 h time point, 73% of the initial **[^{68}Ga]Ga-2d** activity is present in the sample, while only about 50% of the initial **[^{68}Ga]Ga-1d** and **[^{68}Ga]Ga-4d** is detected.

As to the Lu-labelled radioconjugates, at the 1-day time point, around 30% of **[^{177}Lu]Lu-2d** and **[^{177}Lu]Lu-3d** remains in the samples. On the other hand, **[^{177}Lu]Lu-1d**, **[^{177}Lu]Lu-4d**, **[^{177}Lu]Lu-5d** are almost undetectable.

We assume that the cause of the gradual decomposition over time may be the presence of an ester moiety in the compound structure. Additionally, in the case of Ahx-containing analogues, which are less stable than the analogues with the DAla moiety, a source of instability may also be the amide bond. Overall, the novel radioconjugates are significantly less stable than the aprepitant-based radioconjugates with DOTA chelator that we reported recently [15].

In parallel, we have corroborated full stability of ^{177}Lu-radioconjugates in PBS and cellular medium for 7 days for the purpose of further research.

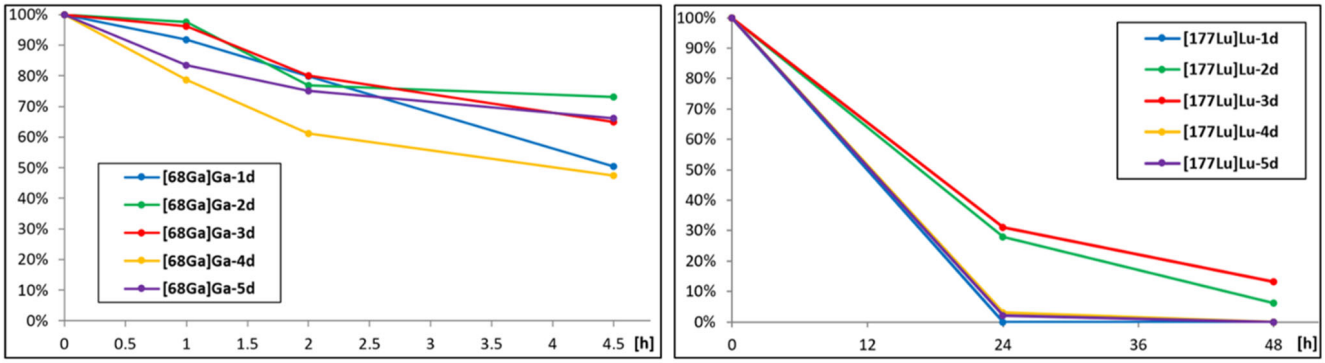

Figure 5. Percentage of intact ^{68}Ga-radioconjugates (**left**) and ^{177}Lu-radioconjugates (**right**) determined at specific time points during incubation in human serum.

2.2.3. Lipophilicity Study

A lipophilicity study was also performed right after the SPE method purification and ethanol evaporation. For each DOTA radioconjugate, the lipophilicity value was estimated as the logarithm of the distribution coefficient (D) based on the ratio of the radioactivity of the organic phase to the radioactivity of the aqueous phase in the *n*-octanol/PBS (pH 7.40) system. Simultaneously, the stability of the studied radioconjugate during the experiment was verified through the HPLC analysis of the aqueous phase. $LogD_{7.4}$ values of ^{68}Ga- and ^{177}Lu-radioconjugates of L-732,138 derivatives are listed in Table 3.

Table 3. $LogD_{7.4}$ values of all radioconjugates determined in *n*-octanol/PBS buffer system.

Radioconjugate	$logD_{7.4}$ (Mean ± SD) [1]	
	^{68}Ga-	^{177}Lu-
1d-	−0.085 ± 0.015	0.400 ± 0.004
2d-	−0.06 ± 0.02	0.704 ± 0.005
3d-	−0.259 ± 0.017	0.619 ± 0.007
4d-	0.071 ± 0.023	0.866 ± 0.019
5d-	−0.466 ± 0.016	0.294 ± 0.013

[1] logD values are presented as means of three independent experiments carried out in duplicate with the standard deviation.

At first glance, it is easily noticed that the ^{177}Lu-radioconjugates are more lipophilic by 0.5–0.8 unit than corresponding ^{68}Ga-radioconjugates (due to the different complex coordination and presence of the free carboxylate group in the gallium complex). This observation coincides with results for radioconjugates of aprepitant derivatives previously obtained [15]. Moreover, the overall lipophilicity results for radioconjugates of aprepitant and L-732,138 derivatives are fairly similar, despite considerable structure differences between both radioconjugate series. It also shows the substantial hydrophilic impact of DOTA chelator on the resultant lipophilicity of radioconjugates based on small molecular NK1R antagonists.

There is an interesting trend in $logD_{7.4}$ values in relation to the type of the linker used. The most lipophilic radioconjugates are the ones with the Ahx linker (**[^{68}Ga]Ga-4d** and **[^{177}Lu]Lu-4d**), but surprisingly the least lipophilic are those with a double Ahx linker (**[^{68}Ga]Ga-5d** and **[^{177}Lu]Lu-5d**). Similarly, the application of only one DAla residue as a linker increased the lipophilicity of ^{177}Lu-radioconjugate (**[^{177}Lu]Lu-2d**) in comparison to ^{177}Lu-radioconjugates based on the L-732,138 derivative without any linker (**[^{177}Lu]Lu-1d**), whereas ^{68}Ga-radioconjugates with a double DAla linker (**[^{68}Ga]Ga-3d**) are characterized by lower lipophilicity to ^{68}Ga-radioconjugates without any linker (**[^{68}Ga]Ga-1d**). Hypothetically, in the derivatives with doubled linkers, some intramolecular interactions and/or folding occurs, impacting the resultant lipophilicity.

2.2.4. Binding Affinity (Competitive Assay)

The obtained conjugates (both uncomplexed **1d-5d** as well as complexed with cold Ga^{3+}, **Ga-1d–Ga-5d** series) were evaluated in the competitive binding assay as to their affinity for human and rat NK1R (Table 4).

Table 4. NK1R binding affinity of the synthesized conjugates (competitive binding assays).

Compound	Linker Length	Linker	*N*-Terminus	IC_{50} (Mean ± SD) [1]	
				rNK1R	hNK1R
				(nM)	(nM)
1d	0	none	DOTA	n/d [2]	7.2 ± 1.4
Ga-1d	0	none	Ga-DOTA	112 ± 3	5.1 ± 2.0
2d	3	-DAla-	DOTA	1536 ± 231	21.4 ± 5.7
Ga-2d	3	-DAla-	Ga-DOTA	747 ± 348	38.7 ± 22.9
3d	6	-DAla-DAla-	DOTA	1270 ± 415	27.1 ± 1.1
Ga-3d	6	-DAla-DAla-	Ga-DOTA	2393 ± 1114	14.6 ± 2.3
4d	7	-Ahx-	DOTA	n/d [2]	8.7 ± 3.2
Ga-4d	7	-Ahx-	Ga-DOTA	1000 ± 71	15.5 ± 2.0
5d	14	-Ahx-Ahx-	DOTA	830 ± 236	4.2 ± 0.8
Ga-5d	14	-Ahx-Ahx-	Ga-DOTA	411 ± 183	8.7 ± 2.4

[1] IC_{50}, half maximal inhibitory concentration, mean of three independent experiments carried out in duplicate with the standard deviation, [2] n/d—not determined.

All conjugates exhibit very good binding to hNK1R (IC_{50} values in the range 4–40 nM). With the exception of the **3c**/**3d** pair, the exchange of the acetyl moiety for DOTA is at least slightly favourable to affinity. The presence of Ga^{3+} cation has little impact on the binding strength. The best hNK1R affinity is found for the longest (**5d**, IC_{50} = 4.2 nM; **Ga-5d**, IC_{50} = 8.7 nM) and the shortest (**1d**, IC_{50} = 7.2 nM; **Ga-1d**, IC_{50} = 5.1 nM) analogues. The latter is surprising in the light of our initial design considerations in which we had predicted that bulky chelator could interfere with the NK1R binding.

2.2.5. Binding Affinity (Saturation Assay)

The analogues labelled with ^{177}Lu were assayed for the receptor affinity in saturation binding experiments. For comparative purposes, we have also evaluated a well-known ^{177}Lu-radioconjugate of Substance P derivative, i.e., [^{177}Lu]Lu-DOTA-[Thi^8,$Met(O_2)^{11}$]SP. This very SP derivative is a currently used vector for an α therapy of glioblastoma multiforme [11,24]. The binding parameters are summarized in Table 5, while the illustrative binding profiles are presented in Figure 6.

Table 5. The results of saturation binding assays towards the hNK1Rr for the novel ^{177}Lu-radioconjugates, compared to the reference derivative of Substance P.

Radioconjugate	K_d ± SD [1] (nM)	Ratio to SP	B_{MAX} ± SD [1] (nM)	Ratio to SP
[^{177}Lu]Lu-DOTA-[Thi^8,$Met(O_2)^{11}$]SP (reference)	6.15 ± 0.64	1.00	0.929 ± 0.027	1.00
[^{177}Lu]Lu-1d	6.98 ± 0.69	1.13	0.762 ± 0.046	0.82
[^{177}Lu]Lu-2d	10.52 ± 0.77	1.71	2.497 ± 0.046	2.69
[^{177}Lu]Lu-3d	2.002 ± 0.051	0.33	0.5939 ± 0.0063	0.64
[^{177}Lu]Lu-4d	5.40 ± 0.30	0.88	2.363 ± 0.060	2.54
[^{177}Lu]Lu-5d	8.70 ± 0.46	1.42	4.93 ± 0.26	5.31

[1] Values are presented as means of three independent experiments carried out in duplicate with the standard deviation.

It is noteworthy that all examined ^{177}Lu-radioconjugates exhibit high binding ability towards hNK1R in a quite similar nanomolar range. The highest affinity was obtained for **[^{177}Lu]Lu-3d** (K_d = 2.002 nM), which was about three times better than the affinity of the reference radioconjugate **[^{177}Lu]Lu-DOTA-[Thi^8,$Met(O_2)^{11}$]SP** (K_d = 6.15 nM). On the other hand, the binding capacity of **[^{177}Lu]Lu-3d** was found to be the smallest (B_{MAX} = 0.5939 nM).

Better affinity than **[^{177}Lu]Lu-DOTA-[Thi^{8},Met(O$_2$)^{11}]SP** is shown also by **[^{177}Lu]Lu-4d** (K_d = 5.40 nM), which presents a fairly high binding capacity (B_{MAX} = 2.363 nM), more than 2.5 higher than **[^{177}Lu]Lu-DOTA-[Thi^{8},Met(O$_2$)^{11}]SP** (B_{MAX} = 0.929 nM).

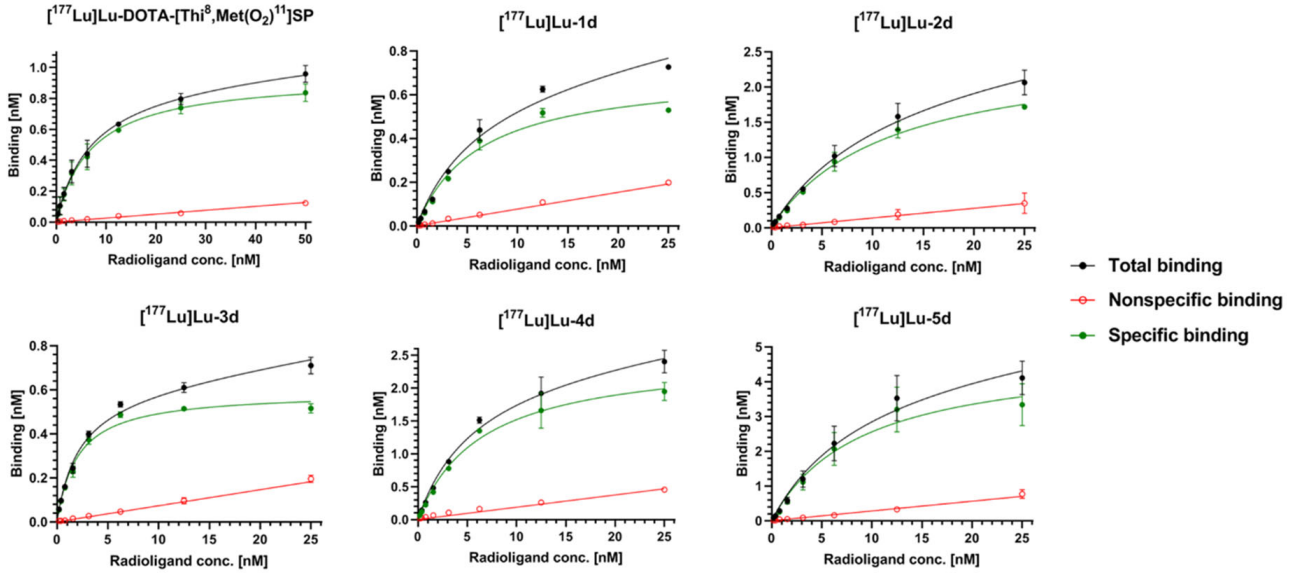

Figure 6. Illustrative binding profiles of ^{177}Lu-radioconjugates of Substance P or L-732,138 derivatives.

The ^{177}Lu-radioconjugate of the derivative without any linker (**[^{177}Lu]Lu-1d**) exhibits binding parameters that are a little worse (K_d = 6.98 nM, B_{MAX} = 0.762 nM) than the reference radioconjugate of the SP derivative. **[^{177}Lu]Lu-2d** and **[^{177}Lu]Lu-5d** presented around a 1.5-times worse binding affinity (K_d = 10.52 nM and K_d = 8.70 nM) than **[^{177}Lu]Lu-DOTA-[Thi^{8},Met(O$_2$)^{11}]SP**, while both radioconjugates show the highest binding capacities (B_{MAX} = 2.497 nM and B_{MAX} = 4.93 nM).

2.3. Retrospective Molecular Modelling

2.3.1. Binding Mode of L732,138

In order to rationalize the SAR data found, we performed molecular modelling for some of the reported compounds. The modelling included molecular docking and molecular dynamics (MD) simulations of the ligand–receptor complexes.

First, we wanted to understand the binding of the parent compound **1c** (L732,138). The compound was docked to 6HLO, 6HLL and 6HLP hNK1R structures [25], and the top scored binding pose was subject to three MD runs of 150 ns production length (RMSD plots Figures SM-MOD-1 to SM-MOD-3). As a result, the binding mode with the following features was obtained (Figure 7). The 3,5-bis(trifluoromethyl)phenyl fragment is located at the bottom of the binding pocket and involved in the hydrophobic interactions with Met81, Asn85, Pro112, Ile113, Val116, Ile204, Trp261, Phe264, His265 and Met291. The indole ring approaches transmembrane helices 6 (TM6) and 7 (TM7). It forms apolar interactions with Gln165, Tyr196, His197 (π-π stacking or π-H-bond donor interactions), Val200, Thr201, Phe268 and Tyr272. The *N*-acetyl fragment of the ligand molecule is exposed to the solvent (in some vicinity of Pro271 and Tyr278 side chains) and directed to the receptor binding site outlet.

Interestingly, the discussed binding pose of **1c** has no direct polar contact between the ligand and the receptor residues. All the interactions are of apolar type. In some of the top docking poses, there was an H-bond between the *N*-acetyl or the ester group and the side-chain of Gln165, but this interaction was not observed during MD runs. Indeed, data from mutagenesis experiments suggest that Gln165 is not important to affinity of L732,138 (**1c**) for hNK1R, as Gln165Ala mutation was associated with a marginal change in affinity (wild type IC_{50} = 3.3 nM; Q165A mutant, IC_{50} = 8.1 nM [26]). The interaction of

the indole with H197 is supported by the fact that the His197Ala mutation had been found to be associated with about a ten-fold decrease of L732,138 affinity, while the His197Phe mutation had no effect thereupon [23].

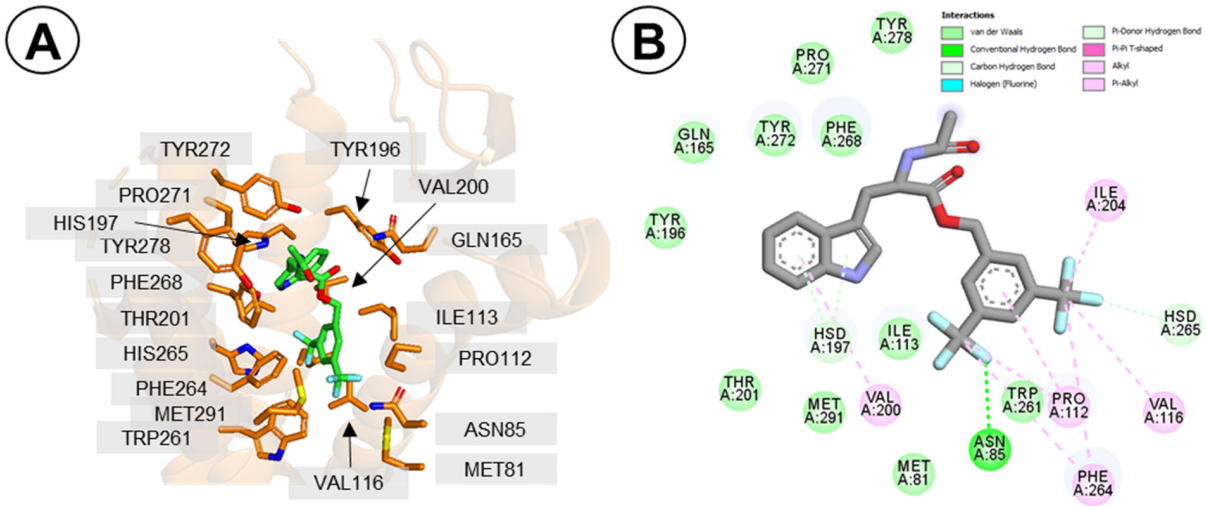

Figure 7. Binding mode of compound **1c** (L732,138) to hNK1R. (**A**) The molecule in the receptor binding site. Only selected residues of the receptor are displayed (orange). The ligand is shown in green. Hydrogen atoms' display is suppressed. (**B**) Interaction diagram. The interacting residues are coloured according to the legend in the Figure. The presented binding pose is the final snapshot of MD simulation (run nr **1c-1**).

Further support for the modelled binding mode comes from the fact that a partially rigidified analogue with an oxazolidinedione core that was reported to have the slightly lower affinity than the parent L732,138 [27] may be decently overlaid on our proposed binding mode (Figure SM-MOD-4).

In general terms, the premises upon which the design was based (see Section 2.1.1) are corroborated by the modelling with the receptor crystal structures.

2.3.2. Binding Mode of Compound **1d**

Of the experimental results that surprised us during the study were the very good affinities for the conjugates in which DOTA was attached directly to the vector structure, without the linker (**1d**, **Ga-1d** and [^{177}**Lu]Lu-1d**). As mentioned in 2.1.1., based on modelling with hNK1R homology models, we had expected **1d** to have worse affinity, for steric reasons. Even now, with the X-ray crystals available, when **1d** was docked to the receptor, the predicted binding poses were significantly displaced compared to ones found for **1c.** In these poses, the 3,5-bis(trifluoromethyl)benzyl fragment was not placed deep in the pocket (Figure SM-MOD-5) but closer to the extracellular space, which could be intuitively expected to give diminished binding strength. This displacement seemed to be driven by the steric requirements and by the bias of docking in favour of polar interactions that could not be found if the ligand's core remained deep in the pocket.

We suspected then that some receptor flexibility (not captured by docking to a rigid receptor) may enable the formation of favourable contacts with the DOTA moiety and simultaneous accommodation of the core deep in the pocket. To see if it is possible, we built a **1d–hNK1R** complex by manually installing the DOTA fragment into the **1c** structure in the conformation found in the **1c** binding pose from docking and subjected this structure to MD simulations (three runs of 150 ns production length).

Comparing simulations with **1c** and **1d**, one can observe some readjustments of the side chains close to the extracellular outlet (Figure 8A) and a change in positioning of the extracellular loop 3 (ECL3). With these, **1d** was able to stay bound deep in the site, with only a slight change of positioning compared to **1c** (with respect to the indole and

3,5-bis(trifluoromethyl)phenyl rings, Figure 8B and Figure SM-MOD-6). A few positively charged or polar side chains (e.g., Arg177, Lys190, Lys194, Gln274; Figures SM-MOD-9 to SM-MOD-11) adopt conformation such that their interactions with DOTA's carboxylate arms are enabled. These additional interactions formed by the DOTA are likely only slightly beneficial to binding strength due to conformational entropic penalty and/or their solvent exposed positioning. The net result is some minor improvement of affinity.

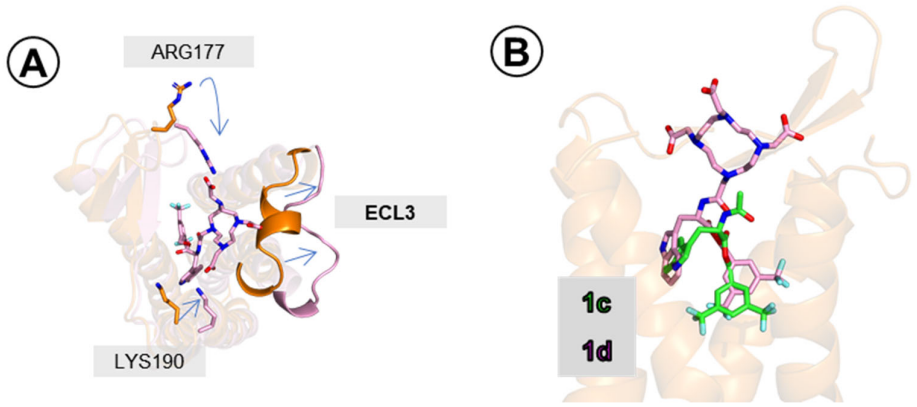

Figure 8. Compound **1d** (pink sticks) in the hNK1 binding site. (**A**) Readjustments of ECL3 and of side-chains of Arg177 and Lys190. In orange are the positions as found in simulation **1c-1**, in pink are the positions as found in simulation **1d-1** (final snapshots). (**B**) Binding pose of **1d** (pink) superposed on that of **1c** (green). Poses taken from final snapshot of **1c-1** and **1d-1** simulations. Only a few receptor (orange) helices are shown.

2.3.3. Binding Modes of Compounds **5a** and **5b**

Another point of interest (with implications for further SAR work) was also the binding mode of the potent long analogues. We studied this problem by the examples of compounds **5a** and **5b**. Docking of these compounds yielded binding poses in which the core fragment is located, as in the case of the parent **1c**, while the linkers are extended and interact with the residues of ECL2 or ECL1. For both compounds, docking finds a set of energetically close binding poses. This picture is somehow corroborated by the MD simulations. Each of the three production runs for **5a** (3 × 210 ns) and **5b** (3 × 250 ns) end with different binding poses (distinct from those found in docking).

In the case of the *N*-Boc analogue derivative **5a**, in all three simulations the core fragment remains bound in a manner similar to the parent **1c** (Figure 9A–C, Figures SM-MOD-19 to SM-MOD-21), although some differences can be observed (e.g., formation of a H-bond to Gln165 in two simulations, Figures SM-MOD-19 and SM-MOD-21). The position of the core is rather stable in the simulations (Figures SM-MOD-14 and SM-MOD-15). The long linker arm undergoes significant rearrangement compared to the starting pose (Figure SM-MOD-16), in particular the second Ahx residue changes its position a lot (Figure SM-MOD-17). The final snapshot binding poses (Figure 9A–C) are characterized by a half-coiled conformation of the linker arm, with the *N*-Boc fragment of the molecule locating close to the tips of TM2 or TM6 (possible interaction partners for the *N*-butyloxy group include but are not restricted to the side chains of Tyr92, Tyr278, Gln284; see Figures SM-MOD-19 to SM-MOD-21).

In the case of the amine derivative **5b**, the core fragment has different interactions than the parent compound **1c**. Still, however, the core is bound deep at the similar level as **1c** (in two of three simulations, Figure 9E,F) or retracted slightly higher (in one simulation, Figure 9D). Upon initial rearrangement, the positions of the core fragment (notice that in all three simulations, they are different) remain stable (Figures SM-MOD-23 and SM-MOD-24). On the contrary, the linker arm and especially the Ahx residue with the free terminal amino group retain some mobility (Figures SM-MOD-25 to SM-MOD-27). The linker elements form transient hydrogen bonds and ionic interactions with a few residues, including Tyr92,

Asn96, Ile182, Glu183, Glu186, Tyr278, Tyr287, etc. Exemplary snapshots with these contacts are shown in Figures SM-MOD-31 to SM-MOD-33.

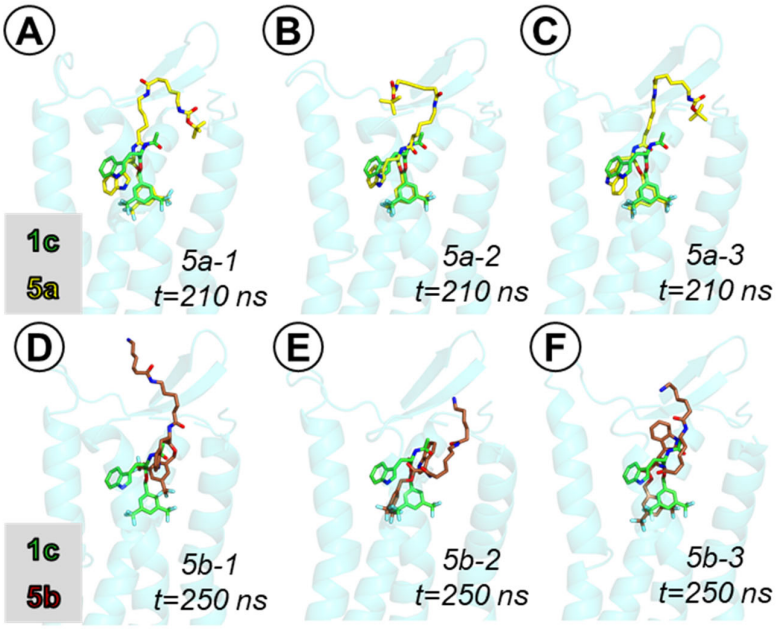

Figure 9. Binding poses of compounds **5a** (yellow sticks, (**A**–**C**)) and **5b** (brown sticks, (**D**–**F**)) in the hNK1 binding site, superposed on the binding pose of compound **1c** (green sticks). Poses taken from final snapshot of the MD simulations. Only a few receptor (light blue) helices are shown.

3. Materials and Methods

3.1. Synthesis of L732,138 Analogues

3.1.1. General

All solvents and reagents were obtained in analytical or reagent quality from commercial suppliers and were used without further purification. Thin-layer chromatography (TLC) was used to monitor the progress of the reaction (silica gel 60 F254, Merck, Warsaw, Poland) with UV detection (wavelength: 254 nm) with 1% ninhydrin solution in MeOH as the visualization reagent. Crude products were purified by preparative RP-HPLC on Shimadzu system (Shim-pol, Warsaw, Poland) with reverse phase column Jupiter® 10 µm, 250 × 21.2 mm, Proteo 90 Å, AXIA (Phenomenex, Shim-pol, Warsaw, Poland), using 0.1% TFA in water/acetonitrile (gradients chosen for particular separations) as the mobile phase. The purity of the products was estimated by analytical LC-MS Shimadzu system (Shim-pol, Warsaw, Poland). The conditions of the analytical HPLC method were: gradient of 3–97% phase B in 31 min (phase A: 0.05% aq. formic acid (FA), phase B: ACN + 0.05% FA), total flow 1.2 mL/min, column Jupiter® 4 µm, 250 × 4.6 mm, Proteo 90 Å, UV detection at λ = 210 nm, 254 nm and 280 nm. The identity of the products was confirmed using ESI-MS (Shimadzu LCMS-2020, Kyoto, Japan). The NMR measurements were carried out in DMSO-d6 on Varian-Agilent 500 MHz VNMRS spectrometer at ambient temperature, with trimethylsilane as the internal standard for chemical shifts. ^{13}C-NMR spectra of **4b** and **5b** were registered for the hydrochloride salts (given in Supplementary Materials). ^{13}C-NMR spectra for **2b**, **2c** and **3c** were not registered.

3.1.2. Synthesis of Compound **1a**

Compound **1a** was prepared according to the procedure described by MacLeod et al. [21] with a change of solvent from dimethylformamide to acetonitrile.

3,5-bis(trifluoromethyl)benzyl (tert-butoxycarbonyl)-L-tryptophanate, Boc-L-Trp-O-CH_2-3,5$(CF_3)_2$Ph, **1a**, white powder, yield 72%, purity > 98% (HPLC-UV), ESI-MS ion found m/z $[M+H]^+$: 531.10 calculated $[M+H]^+$: 531.17; t_R = 21.46 min; ^{1}H NMR (600 MHz, DMSO-

*d*6) δ (ppm) 10.89 and 10.82 (1H, s), 8.05 and 8.03 (1H, s), 7.97 and 7.95 (2H, s), 7.45 (1H, d, *J* = 7.8 Hz), 7.36 (1H, m), 7.30 (1H, m), 7.14 (1H, bs), 7.03 (1H, m), 6.94 (1H, m), 5.28 (1H, d, *J* = 13.5 Hz), 5.15 (1H, d, *J* = 13.5 Hz), 4.23 (1H, m), 3.12 (1H, m), 3.03 (1H, m), 1.28 and 1.10 (9H, 2s). Some of the signals exhibit doubling that can be ascribed to the presence of two conformers, likely associated with the restricted rotation in the carbamate C–N bond. Similar was found previously for Boc-protected amino acids, e.g., Boc-L-Phe [28]. ^{13}C NMR (125 MHz, DMSO-*d*6) δ (ppm), 172.35, 155.93, 140.02, 136.54, 130.72 (q, $^{2}J_{CF}$ = 32.5 Hz), 128.72 (broad, likely an unresolved quartet with $^{3}J_{CF}$ ~4Hz), 127.44, 124.27, 123.72 (q, $^{1}J_{CF}$ = 270.8 Hz), 122.03 (broad, likely an unresolved quartet with $^{3}J_{CF}$ ~4Hz), 121.40, 118.86, 118.32, 111.92, 110.03, 78.80, 64.75, 55.45, 28.44, 27.05.

3.1.3. Synthesis of Compounds **2a** and **3a**

HOSu (1.2 equiv) was added to a solution of Boc-D-Ala-OH (1 equiv) in DMF and the reaction mixture was cooled to 0 °C in an ice bath. Next, DCC (1 equiv) was added, and the mixture was stirred for one hour at 0–5 °C and for further two hours at room temperature. Then, compound **1b** or **2b** (1.2 equiv), respectively, with the addition TMG (1.2 equiv) was added to the reaction mixture. The reaction was allowed to stir at room temperature for 48 h. After this time, the precipitated *N*,*N*′-dicyclohexylurea (DCU) was filtered off and the filtrate was concentrated and extracted with ethyl acetate (AcOEt). The organic phase was dried with anhydrous magnesium sulfate (anh.MgSO4), the solvent was removed in vacuo and the resulting oil was dried.

3,5-bis(trifluoromethyl)benzyl (tert-butoxycarbonyl)-D-alanyl-L-tryptophanate, Boc-D-Ala-L-Trp-O-CH_2-3,5$(CF_3)_2$Ph, **2a**, white powder, yield 38%, purity > 98% (HPLC-UV), ESI-MS ion found m/z $[M+H]^+$: 602.15 calculated $[M+H]^+$: 602.21; t_R = 20.28 min; ^{1}H NMR (500 MHz, DMSO-*d*6) δ (ppm), 10.85 (1H, s), 8.22 (1H, d, *J* = 7.5 Hz), 8.05 (1H, s), 7.99 (2H, s), 7.46 (1H, m), 7.31 (1H, m), 7.13 (1H, d, *J* = 2.2 Hz), 7.05 (1H, m), 6.96 (1H, m), 6.72 (1H, d, *J* = 7.3 Hz), 5.29 (1H, d, *J* = 13.6 Hz), 5.20 (1H, d, *J* = 13.6 Hz), 4.56 (1H, m), 4.00 (1H, m), 3.21 (1H, m), 3.10 (1H, m), 1.34 (9H, s), 1.16 and 1.06 (3H, 2d, *J* = 6.9 Hz). ^{13}C NMR (125 MHz, DMSO-*d*6) δ (ppm), 173.37, 172.09, 155.33, 139.77, 136.53, 130.64 (q, $^{2}J_{CF}$ = 32.5 Hz), 128.89 (broad, likely an unresolved quartet with $^{3}J_{CF}$ ~4Hz), 127.41, 124.71, 123.67 (q, $^{1}J_{CF}$ = 271.6 Hz), 121.41, 122.13 (broad, likely an unresolved quartet with $^{3}J_{CF}$ ~4Hz), 118.83, 118.27, 111.89, 109.60, 78.45, 64.98, 53.60, 49.90, 28.55, 27.40, 16.68.

3,5-bis(trifluoromethyl)benzyl (tert-butoxycarbonyl)-D-alanyl-D-alanyl-L-tryptophanate, Boc-D-Ala-D-Ala-L-Trp-O-CH_2-3,5$(CF_3)_2$Ph, **3a**, white powder, yield 38%, purity > 98% (HPLC-UV), ESI-MS ion found m/z $[M+H]^+$: 673.15 calculated $[M+H]^+$: 673.25; t_R = 19.60 min. ^{1}H NMR (600 MHz, DMSO-*d*6) δ (ppm), 10.83 (1H, s), 8.32 (1H, d, *J* = 7.6 Hz), 8.03 (1H, s), 7.95 (2H, s), 7.70 (1H, d, *J* = 7.3 Hz), 7.43 (1H, m), 7.28 (1H, m), 7.12 (1H, d, *J* = 2.1 Hz), 7.02 (1H, m), 6.92 (1H, m), 6.47 (1H, bs), 5.25 (1H, d, *J* = 13.3 Hz), 5.15 (1H, d, *J* = 13.3 Hz), 4.50 (1H, m), 4.25 (1H, m), 3.90 (1H, m), 3.19 (1H, m), 3.05 (1H, m), 1.32 and 1.27 (9H, 2bs), 1.08 (3H, d, *J* =7.1 Hz), 1.03 (3H, d, *J* = 7.1 Hz). ^{13}C NMR (125 MHz, DMSO-*d*6) δ (ppm), 172.72, 172.64, 172.00, 155.60, 139.75, 136.51, 130.74 (q, $^{2}J_{CF}$ = 32.5 Hz), 128.92 (broad, likely an unresolved quartet with $^{3}J_{CF}$ ~4Hz), 127.39, 123.67 (q, $^{2}J_{CF}$ = 271.3 Hz), 122.17 (broad, likely an unresolved quartet with $^{3}J_{CF}$ ~4Hz), 121.40, 124.33, 118.83, 118.25, 111.89, 109.58, 78.59, 65.01, 53.63, 50.17, 48.27, 28.58, 27.34, 18.82, 18.30.

3.1.4. Synthesis of Compounds **4a** and **5a**

Boc-6-Ahx-OSu (1 equiv) was dissolved in the minimum amount of DMF and compound **1b** or **4b** (1.2 equiv) was added, respectively, with the addition of TMG (1.2 equiv). The reaction was carried out for 6 h at room temperature. The reaction mixture was concentrated and extracted with ethyl acetate. The organic phase was dried, the solvent was removed in vacuo and the resulting oil was dried.

3,5-bis(trifluoromethyl)benzyl (6-((tert-butoxycarbonyl)amino)hexanoyl)-L-tryptophanate, Boc-Ahx-L-Trp-O-CH_2-3,5$(CF_3)_2$Ph, **4a**, white powder, yield 57%, purity > 97% (HPLC-UV), ESI-MS ion found m/z $[M+H]^+$: 644.15 calculated $[M+H]^+$: 644.26; t_R = 20.57 min;

^{1}H NMR (500 MHz, DMSO-*d*6) δ (ppm), 10.83 (1H, s), 8.32 (1H, d, *J* = 7.4 Hz), 8.04 (1H, s), 7.95 (2H, s), 7.47 (1H, m), 7.32 (1H, m), 7.15 (1H, d, *J* = 2.2 Hz), 7.05 (1H, m), 6.96 (1H, m), 6.69 (1H, bs), 5.28 (1H, d, *J* = 13.5 Hz), 5.17 (1H, d, *J* = 13.5 Hz), 4.53 (1H, m), 3.18 (1H, m), 3.07 (1H, m), 2.82 (2H, m), 2.06 (2H, t, *J* = 7.4 Hz), 1.40 (2H, m), 1.36 (9H, s), 1.29 (2H, m), 1.13 (2H, m). ^{13}C NMR (125 MHz, DMSO-*d*6) δ (ppm), 172.89, 172.40, 156.82, 139.96, 136.53, 130.71 (q, $^{2}J_{CF}$ ~32.5 Hz), 128.66 (broad, likely an unresolved quartet with $^{3}J_{CF}$ ~4Hz), 127.45, 124.11, 123.69 (q, $^{1}J_{CF}$ ~272 Hz), 122.05 (broad, likely an unresolved quartet with $^{3}J_{CF}$ ~4Hz), 121.41, 118.83, 118.32, 111.91, 109.91, 77.74, 64.73, 53.85, 35.30, 29.68, 28.70, 27.27, 26.32, 25.26. C_{ε} signal of Ahx overlapped by the DMSO-d6 signal at around 40 ppm.

3,5-bis(trifluoromethyl)benzyl (6-(6-((tert-butoxycarbonyl)amino)hexanamido)hexanoyl)-L-tryptophanate, Boc-Ahx-Ahx-L-Trp-O-CH_2-3,5$(CF_3)_2$Ph, **5a**, white powder, yield 55%, purity > 98% (HPLC-UV), ESI-MS ion found m/z $[M+H]^+$: 757.30 calculated $[M+H]^+$: 757.34; t_R = 19.61 min. ^{1}H NMR (500 MHz, DMSO-*d*6) δ (ppm), 10.83 (1H, s), 8.32 (1H, d, *J* = 7.1 Hz), 8.04 (1H, s), 7.96 (2H, s), 7.66 (1H, t, *J* = 5.5 Hz), 7.48 (1H, m), 7.21 (1H, m), 7.15 (1H, d, *J* = 2.1 Hz), 7.05 (1H, m), 6.96 (1H, m), 6.71 (1H, t, *J* = 5.1 Hz), 5.28 (1H, d, *J* = 13.5 Hz), 5.17 (1H, d, *J* = 13.5 Hz), 4.53 (1H, m), 3.19 (1H, m), 3.08 (1H, m), 2.95 (2H, m), 2.87 (2H, m), 2.07 (2H, t, *J* = 7.6 Hz), 2.01 (2H, t, *J* = 7.5 Hz), 1.43 (4H, m), 1.36 (9H, s), 1.33 (4H, m), 1.16 (4H, m). ^{13}C NMR (125 MHz, DMSO-*d*6) δ (ppm), 172.88, 172.41, 172.27, 156.01, 139.97, 136.54, 130.72 (q, $^{1}J_{CF}$ ~32.5 Hz), 128.65 (likely an unresolved quartet with $^{3}J_{CF}$ ~4Hz), 127.45, 124.12, 123.68 (q, $^{1}J_{CF}$ ~272 Hz), 122.05 (likely an unresolved quartet with $^{3}J_{CF}$ ~4Hz), 121.41, 118.82, 118.31, 111.91, 109.90, 77.73, 64.73, 55.83, 38.71, 35.84, 35.29, 29.73, 29.38, 28.71, 27.28, 26.45, 25.51, 25.25. C_{ε} signals of both Ahx residues overlapped by the DMSO-d6 signal at around 40 ppm.

3.1.5. Deprotection Reaction (**1b**, **2b**, **3b**, **4b**, **5b**)

N^{α}-Boc protected derivatives (**1a** or **2a** or **3a** or **4a** or **5a**) were dissolved in a mixture of TFA and DCM) (1:1). The reaction was left to stir for one hour at room temperature. The reaction mixture was concentrated in vacuo, the product was precipitated using cold diethyl ether and the resulting oil was dried.

(*S*)-1-((3,5-bis(trifluoromethyl)benzyl)oxy)-3-(1H-indol-3-yl)-1-oxopropan-2-aminium 2,2,2-trifluoroacetate, TFA*NH_2-L-Trp-O-CH_2-3,5$(CF_3)_2$Ph, **1b**, white powder, yield 81%, purity > 98% (HPLC-UV), ESI-MS ion found m/z $[M_{base}+H]^+$: 431.05, $[M_{base}-H]^-$: 429.00, $[M_{sal}t-H]^-$: 542.95 calculated $[M_{base}+H]^+$: 431.12, $[M_{base}-H]^-$: 429.10, $[M_{sal}t-H]^-$: 543.10; t_R = 11.38 min; ^{1}H NMR (500 MHz, DMSO-*d*6) δ (ppm), 11.03 (1H, s), 8.52 (3H, s), 8.09 (1H, s), 7.99 (2H, s), 7.48 (1H, m), 7.35 (1H, m), 7.22 (1H, d, *J* = 2.2 Hz), 7.07 (1H, m), 6.97 (1H, m), 5.37 (1H, d, *J* = 13.2 Hz), 5.24 (1H, d, *J* = 13.2 Hz), 4.37 (1H, m), 3.30–3.26 (2H, m). ^{13}C NMR (125 MHz, DMSO-*d*6) δ (ppm), 169.70, 158.45 (weak, probably q with $^{2}J_{CF}$ ~ 30 Hz, consistent with TFA salt), 138.83, 136.66, 130.77 (q, $^{2}J_{CF}$ = 32.5 Hz), 129.35 (broad, likely an unresolved quartet with $^{3}J_{CF}$ ~4Hz), 127.27, 125.29, 123.65 (q, $^{1}J_{CF}$ = 271 Hz), 122.56 (broad, likely an unresolved quartet with $^{3}J_{CF}$ ~4Hz, overlapped with signal for CF_3 carbon), 121.64, 119.06, 118.26, 117.75 (weak, probably q with $^{1}J_{CF}$ ~300 Hz, consistent with TFA salt), 112.74, 106.84, 65.98, 53.27, 26.83.

(*R*)-1-(((S)-1-((3,5-bis(trifluoromethyl)benzyl)oxy)-3-(1H-indol-3-yl)-1-oxopropan-2-yl)amino)-1-oxopropan-2-aminium 2,2,2-trifluoroacetate, TFA*NH_2-D-Ala-L-Trp-O-CH_2-3,5$(CF_3)_2$Ph, 2b, white powder, yield 48%, purity > 95% (HPLC-UV), ESI-MS ion found m/z $[M_{base}+H]^+$: 502.10, $[M_{base}-H]^-$: 500.05, $[M_{sal}t-H]^-$: 614.00 calculated $[M_{base}+H]^+$: 502.16, $[M_{base}-H]^-$: 500.14, $[M_{sal}t-H]^-$: 614.14; t_R = 11.40 min; ^{1}H NMR (600 MHz, DMSO-*d*6) δ (ppm), 10.84 (1H, s), 8.84 (1H, d, *J* = 7.8 Hz), 8.07 (1H, s), 7.99 (2H, s), 7.88 (3H, bs), 7.46 (1H, d, *J* = 7.8 Hz), 7.29 (1H, d, *J* = 8.4 Hz), 7.11 (1H, d, *J* = 2.1 Hz), 7.02 (1H, m), 6.93 (1H, m), 5.29 (1H, d, *J* = 13.2 Hz), 5.22 (1H, d, *J* = 13.2 Hz), 4.70 (1H, m), 3.77 (1H, m), 3.25 (1H, m), 3.08 (1H, m), 1.12 (3H, d, *J* =7.0 Hz).

(*R*)-1-(((R)-1-(((S)-1-((3,5-bis(trifluoromethyl)benzyl)oxy)-3-(1H-indol-3-yl)-1-oxopropan-2-yl)amino)-1-oxopropan-2-yl)amino)-1-oxopropan-2-aminium 2,2,2-trifluoroacetate, TFA*NH_2-D-Ala-D-Ala-L-Trp-O-CH_2-3,5$(CF_3)_2$Ph, 3b, white powder, yield 32%, purity > 98%

(HPLC-UV), ESI-MS ion found m/z $[M_{base}+H]^+$: 573.15, $[M_{base}-H]^-$: 571.05, $[M_{sal}t-H]^-$: 685.00 calculated $[M_{base}+H]^+$: 573.20, $[M_{base}-H]^-$: 571.18, $[M_{sal}t-H]^-$: 685.18; t_R = 11.62 min; ^{1}H NMR (500 MHz, DMSO-*d*6) δ (ppm), 10.85 (1H, s), 8.51 (1H, d, *J* = 7.5 Hz), 8.44 (1H, d, *J* = 7.5 Hz), 8.07 (1H, s), 7.99 (2H, s), 7.89 (3H, bs), 7.48 (1H, m), 7.32 (1H, m), 7.15 (1H, d, *J* = 2.2 Hz), 7.05 (1H, m), 6.96 (1H, m), 5.30 (1H, d, *J* = 13.3 Hz), 5.21 (1H, d, *J* = 13.3 Hz), 4.58 (1H, m), 4.39 (1H, m), 3.81 (1H, m), 3.24 (1H, m), 3.09 (1H, m), 1.26 (3H, d, *J* =7.0 Hz), 1.09 (3H, d, *J* =7.1 Hz). ^{13}C NMR (125 MHz, DMSO-*d*6) δ (ppm), 172.21, 172.03, 169.45, 158.31 (weak, probably q with $^2J_{CF}$ ~ 30 Hz, consistent with TFA salt), 139.78, 136.54, 130.74 (q, $^2J_{CF}$ = 32.5 Hz), 128.87 (likely an unresolved quartet with $^3J_{CF}$ ~4Hz), 127.40, 124.30, 123.67 (q, $^2J_{CF}$ ~272 Hz), 122.20 (likely an unresolved quartet with $^3J_{CF}$ ~4Hz), 121.43, 118.84, 118.30, 111.90, 109.63, 65.02, 53.62, 48.48, 48.43, 27.45, 18.93, 17.58. A signal coming from the CF_3 group of the trifluoroacetate anion not observed (expected around 117.8 as a quartet with $^1J_{CF}$ ~300 Hz).

(*S*)-6-((1-((3,5-bis(trifluoromethyl)benzyl)oxy)-3-(1H-indol-3-yl)-1-oxopropan-2-yl) amino)-6-oxohexan-1-aminium 2,2,2-trifluoroacetate, TFA*NH_2-Ahx-L-Trp-O-CH_2-3,5$(CF_3)_2$Ph, 4b, off-white powder, yield 65%, purity > 98% (HPLC-UV), ESI-MS ion found m/z $[M_{base}+H]^+$: 544.15, $[M_{base}-H]^-$: 542.10, $[M_{sal}t-H]^-$: 656.05 calculated $[M_{base}+H]^+$: 544.21, $[M_{base}-H]^-$: 542.19, $[M_{sal}t-H]^-$: 656.19; t_R = 11.67 min; ^{1}H NMR (500 MHz, DMSO-*d*6) δ (ppm), 10.84 (1H, s), 8.35 (1H, d, *J* = 7.1 Hz), 8.05 (1H, s), 7.95 (2H, s), 7.59 (3H, bs), 7.48 (1H, m), 7.32 (1H, m), 7.15 (1H, d, *J* = 2.0 Hz), 7.06 (1H, m), 6.97 (1H, m), 5.28 (1H, d, *J* = 13.5 Hz), 5.17 (1H, d, *J* = 13.5 Hz), 4.54 (1H, m), 3.19 (1H, m), 3.07 (1H, m), 2.70 (2H, m), 2.09 (2H, t, *J* = 7.6 Hz), 1.50–1.38 (4H, m), 1.20 (2H, m). ^{13}C-NMR spectra of the corresponding hydrochloride salt are given in SM.

(*S*)-6-((6-((1-((3,5-bis(trifluoromethyl)benzyl)oxy)-3-(1H-indol-3-yl)-1-oxopropan-2-yl) amino)-6-oxohexyl)amino)-6-oxohexan-1-aminium 2,2,2-trifluoroacetate, TFA*NH_2-Ahx-Ahx-L-Trp-O-CH_2-3,5$(CF_3)_2$Ph, 5b, off-white powder, yield 57%, purity > 97% (HPLC-UV), ESI-MS ion found m/z $[M_{base}+H]^+$: 657.20, $[M_{base}-H]^-$: 655.10, $[M_{sal}t-H]^-$: 769.10 calculated $[M_{base}+H]^+$: 657.29, $[M_{base}-H]^-$: 655.27, $[M_{sal}t-H]^-$: 769.26; t_R = 11.73 min. ^{1}H NMR (500 MHz, DMSO-*d*6) δ (ppm), 10.84 (1H, s), 8.32 (1H, d, *J* = 7.2 Hz), 8.04 (1H, s), 7.96 (2H, s), 7.69 (1H, t, *J* = 5.5 Hz), 7.60 (3H, bs), 7.48 (1H, m), 7.32 (1H, m), 7.15 (1H, d, *J* = 2.0 Hz), 7.05 (1H, m), 6.96 (1H, m), 5.28 (1H, d, *J* = 13.7 Hz), 5.17 (1H, d, *J* = 13.7 Hz), 4.53 (1H, m), 3.19 (1H, m), 3.08 (1H, m), 2.95 (2H, m), 2.76 (2H, m), 2.10–2.00 (4H, m), 1.49 (4H, m), 1.42 (2H, m), 1.34–1.22 (4H, m), 1.15 (2H, s). ^{13}C-NMR spectra of the corresponding hydrochloride salt are given in SM.

3.1.6. Acetylation Reaction (**1c**, **2c**, **3c**, **4c**, **5c**)

To a cooled solution (0–5 °C) of N^{α}-deprotected derivatives (**1b** or **2b** or **3b** or **4b** or **5b**, 1 equiv) and TMG (2 equiv) in DMF/DCM (1:1), Ac_2O (2 equiv) was added and the reaction mixture was allowed to stir for half an hour at 5 °C and for the next hour at room temperature. After concentration, the reaction mixture was acidified with 10% aqueous citric acid and extracted with AcOEt. The organic phase was dried with anh. $MgSO_4$, the solvent was removed in vacuo and the resulting oil was dried.

3,5-bis(trifluoromethyl)benzyl acetyl-L-tryptophanate, Ac-NH-L-Trp-O-CH_2-3,5 $(CF_3)_2$Ph, **1c** (L732,138 [16]), white powder, yield 98%, purity > 98% (HPLC-UV), ESI-MS ion found m/z $[M+H]^+$: 473.10 calculated $[M+H]^+$: 473.13; t_R = 18.61 min; ^{1}H NMR (500 MHz, DMSO-*d*6) δ (ppm) 10.84 (1H, s), 8.41 (1H, d, *J* = 6.9 Hz), 8.05 (1H, s), 7.96 (2H, s), 7.47 (1H, m), 7.32 (1H, m), 7.16 (1H, d, *J* = 2.2 Hz), 7.06 (1H, m), 6.97 (1H, m), 5.28 (1H, d, *J* = 13.5 Hz), 5.18 (1H, d, *J* = 13.5 Hz), 4.53 (1H, m), 3.18 (1H, m), 3.07 (1H, m), 1.82 (3H, s). ^{13}C NMR (125 MHz, DMSO-*d*6) δ (ppm), 172.35, 169.99, 139.99, 136.55, 130.72 (q, $^2J_{CF}$ = 32.5 Hz), 128.59 (broad, likely an unresolved quartet with $^3J_{CF}$ ~4Hz), 127.44, 124.13, 123.68 (q, $^1J_{CF}$ = 270.8 Hz), 121.43, 122.02 (broad, likely an unresolved quartet with $^3J_{CF}$ ~4Hz), 118.86, 118.29, 111.93, 109.82, 64.69, 53.97, 27.31, 22.58.

3,5-bis(trifluoromethyl)benzyl acetyl-D-alanyl-L-tryptophanate, Ac-NH-D-Ala-L-Trp-O-CH_2-3,5$(CF_3)_2$Ph, **2c**, white powder, yield 61%, purity > 97% (HPLC-UV), ESI-

MS ion found m/z $[M+H]^+$: 544.15 calculated $[M+H]^+$: 544.17; t_R = 17.72 min; ^{1}H NMR (600 MHz, DMSO-*d*6) δ (ppm), 10.84 (1H, s), 8.29 (1H, d, *J* = 7.5 Hz), 8.03 (1H, s), 7.96 (2H, s), 7.9 (1H, d, *J* = 7.5 Hz), 7.44 (1H, d, *J* = 7.8 Hz), 7.28 (1H, m), 7.11 (1H, d, *J* = 2.1 Hz), 7.02 (1H, m), 6.92 (1H, m), 5.25 (1H, d, *J* = 13.2 Hz), 5.16 (1H, d, *J* = 13.2 Hz), 4.49 (1H, m), 4.26 (1H, m), 3.18 (1H, m), 3.06 (1H, m), 1.76 (3H, s), 1.01 (3H, d, *J* =7.1 Hz).

3,5-bis(trifluoromethyl)benzyl acetyl-D-alanyl-D-alanyl-L-tryptophanate, Ac-NH-D-Ala-D-Ala-L-Trp-O-CH_2-3,5$(CF_3)_2$Ph, **3c**, white powder, yield 62%, purity > 98% (HPLC-UV), ESI-MS ion found m/z $[M+H]^+$: 615.20 calculated $[M+H]^+$: 615.21; t_R = 17.07 min; ^{1}H NMR (600 MHz, DMSO-*d*6) δ (ppm), 10.83 (1H, s), 8.25 (1H, d, *J* = 7.4 Hz), 8.03 (1H, s), 7.98 (1H, d, *J* = 7.3 Hz), 7.96 (2H, s), 7.86 (1H, d, *J* = 7.75 Hz), 7.43 (1H, m), 7.28 (1H, m), 7.13 (1H, d, *J* = 2.1 Hz), 7.02 (1H, m), 6.92 (1H, m), 5.23 (1H, d, *J* = 13.3 Hz), 5.16 (1H, d, *J* = 13.3 Hz), 4.50 (1H, m), 4.24 (1H, m), 4.19 (1H, m), 3.18 (1H, m), 3.06 (1H, m), 1.79 (3H, s), 1.09 (3H, d, *J* =7.2 Hz), 1.05 (3H, d, *J* =7.2 Hz).

3,5-bis(trifluoromethyl)benzyl (6-acetamidohexanoyl)-L-tryptophanate, Ac-NH-Ahx-L-Trp-O-CH_2-3,5$(CF_3)_2$Ph, **4c**, white powder, yield 63%, purity > 98% (HPLC-UV), ESI-MS ion found m/z $[M+H]^+$: 586.15 calculated $[M+H]^+$: 586.22; t_R = 17.58 min; ^{1}H NMR (600 MHz, DMSO-*d*6) δ (ppm), 10.82 (1H, s), 8.31 (1H, d, *J* = 7.0 Hz), 8.02 (1H, s), 7.93 (2H, s), 7.71 (1H, bs), 7.44 (1H, m), 7.29 (1H, m), 7.12 (1H, d, *J* = 2.0 Hz), 7.05 (1H, m), 6.96 (1H, m), 5.25 (1H, d, *J* = 13.6 Hz), 5.14 (1H, d, *J* = 13.6 Hz), 4.50 (1H, m), 3.16 (1H, m), 3.04 (1H, m), 2.91 (2H, m), 2.04 (2H, t, *J* = 7.3 Hz), 1.74 (3H, s), 1.38 (2H, m), 1.27 (2H, m), 1.11 (2H, m). ^{13}C NMR (125 MHz, DMSO-*d*6) δ (ppm), 172.87, 172.41, 169.30, 139.98, 136.54, 130.71 (q, $^2J_{CF}$ ~ 32.5 Hz), 128.67 (likely an unresolved quartet with $^3J_{CF}$ ~4 Hz), 127.45, 124.13, 123.68 (q, $^1J_{CF}$ ~ 272 Hz), 122.07 (likely an unresolved quartet with $^3J_{CF}$ ~4 Hz), 121.41, 118.82, 118.32, 111.91, 109.91, 64.73, 53.83, 35.28, 29.36, 27.28, 26.45, 25.26, 23.04. C_ε signal of Ahx overlapped by the DMSO-d6 signal at around 40 ppm.

3,5-bis(trifluoromethyl)benzyl (6-(6-acetamidohexanamido)hexanoyl)-L-tryptophanate, Ac-NH-Ahx-Ahx-L-Trp-O-CH_2-3,5$(CF_3)_2$Ph, **5c**, white powder, yield 68%, purity > 98% (HPLC-UV), ESI-MS ion found m/z $[M+H]^+$: 699.25 calculated $[M+H]^+$: 699.30; t_R = 17.01 min; ^{1}H NMR (500 MHz, DMSO-*d*6) δ (ppm), 10.84 (1H, s), 8.32 (1H, d, *J* = 7.4 Hz), 8.04 (1H, s), 7.96 (2H, s), 7.75 (1H, bs), 7.66 (1H, t, *J* = 5.6 Hz), 7.47 (1H, m), 7.32 (1H, m), 7.15 (1H, d, *J* = 2.3 Hz), 7.05 (1H, m), 6.96 (1H, m), 5.28 (1H, d, *J* = 13.5 Hz), 5.17 (1H, d, *J* = 13.5 Hz), 4.53 (1H, m), 3.19 (1H, m), 3.07 (1H, m), 3.02–2.92 (4H, m), 2.07 (2H, t, *J* = 7.4 Hz), 2.01 (2H, t, *J* = 7.4 Hz), 1.77 (3H, s), 1.49–1.27 (8H, m), 1.23–1.10 (4H, m). ^{13}C NMR (125 MHz, DMSO-*d*6) δ (ppm), 172.87, 172.41, 172.23, 169.31, 139.98, 136.54, 130.71 (q, $^1J_{CF}$ ~32.5 Hz), 128.65 (likely an unresolved quartet with $^3J_{CF}$ ~4Hz), 127.45, 124.12, 123.97 (q, $^1J_{CF}$ ~272 Hz), 122.05 (likely an unresolved quartet with $^3J_{CF}$ ~4Hz), 121.41, 118.82, 118.32, 111.91, 109.91, 64.73, 53.83, 38.85, 38.69, 35.81, 35.29, 29.39, 27.28, 26.58, 26.45, 25.51, 25.26, 23.04. C_ε signal of one of the Ahx residues overlapped by the DMSO-d6 signal at around 40 ppm.

3.2. Synthesis of Conjugates and Radioconjugates

3.2.1. General

All applied chemicals and solvents were purchased as a reagent grade (Sigma-Aldrich/Merck, Darmstadt, Germany) and applied without further purification. DOTA-NHS ester (1,4,7,10-tetraazacyclododecane-1,4,7,10-tetraacetic acid mono-*N*-hydroxysuccinimide ester) was purchased from CheMatech, Dijon, France. [^{68}Ga]$GaCl_3$ was eluted from the commercially available ^{68}Ge/^{68}Ga generator (Eckert & Ziegler, Berlin, Germany), while the solution of [^{177}Lu]$LuCl_3$ in 0.04 M HCl was purchased from Radioisotope Centre POLATOM, National Centre for Nuclear Research, Otwock-Świerk, Poland. ^{68}Ge/^{68}Ga generator eluates were obtained by semi-automated syringe pump that enables convenient and safe fractioning, allowing the use of fractions with the highest radionuclide content in the labeling reaction; no other processing was applied.

The HPLC conditions and gradient were set as follows: a semi-preparative Phenomenex Jupiter Proteo column (C12, reversed phase) 4 μm, 90 Å, 250 × 10 mm, with

UV/Vis (220 nm) or/and radio γ-detection at gradient elution: 0–20 min 20 to 80% solvent B; 20–30 min 80% solvent B; 2 mL/min.; solvent A: 0.1% (*v*/*v*) trifluoroacetic acid (TFA) in water; and solvent B: 0.1% (*v*/*v*) TFA in acetonitrile. Sep-Pack® Classic Short C18 Cartridges were purchased from WATERS, Milford, MA, USA.

Mass spectra were measured on the Bruker 3000 Esquire mass spectrometer equipped with electrospray ionization (Bruker, Billerica, MA, USA).

3.2.2. General Procedure of Syntheses of Conjugates with DOTA

A derivative with the primary amino group (**1b**–**5b**) (1 equiv.) and the DOTA-NHS ester (1 equiv.) were dissolved in DMF purged from oxygen with technical nitrogen and supplemented with a 3 equiv. of triethylamine. The reaction mixture was vigorously stirred overnight at about 50 °C. The progress of the reaction was monitored by HPLC. The crude reaction mixture was evaporated, dissolved in the HPLC mobile phase, purified by the HPLC method and lyophilized. The isolated main product was identified as a DOTA conjugate (**1d**–**5d**, >90% reaction yield) by MS analysis confirmation.

MS: Calculated monoisotopic mass for **1d**, $C_{36}H_{42}F_6N_6O_9$: 816.74; found: 817.38 *m*/*z* $[M + H]^+$
MS: Calculated monoisotopic mass for **2d**, $C_{39}H_{47}F_6N_7O_{10}$: 887.82; found: 888.35 *m*/*z* $[M + H]^+$
MS: Calculated monoisotopic mass for **3d**, $C_{42}H_{52}F_8N_8O_{11}$: 958.90; found: 959.40 *m*/*z* $[M + H]^+$
MS: Calculated monoisotopic mass for **4d**, $C_{42}H_{53}F_6N_7O_{10}$: 929.90; found: 930.38 *m*/*z* $[M + H]^+$
MS: Calculated monoisotopic mass for **5d**, $C_{48}H_{64}F_6N_8O_{11}$: 1043.06; found: 1043.58 *m*/*z* $[M + H]^+$

3.2.3. ^{68}Ga Radiolabelling

The ^{68}Ga radiolabelling of DOTA conjugates for physiochemical evaluation was performed in accordance with the following procedure: 220 µL of $[^{68}Ga]GaCl_3$ in 0.1 M HCl from the $^{68}Ge/^{68}Ga$ generator (42.3–54.5 MBq) was added into the solution of 25 nmol of the selected conjugate in 300 µL of a 0.2 M acetate buffer (pH = 4.5) and heated for 10 min at 95 °C. Subsequently, radioconjugate was purified using Sep-Pack® Classic Short C18 cartridge in accordance with the producer recommendations, thereby obtaining an easily vaporized ethanolic solution of radioconjugate. The effectiveness of the purification was monitored by HPLC.

3.2.4. ^{177}Lu Radiolabelling

The ^{177} Lu radiolabelling of DOTA conjugates for physiochemical and in vitro evaluation was performed in accordance with the following procedure: 2.5–5 MBq of a $[^{177}Lu]LuCl_3$ solution in 0.04 M HCl (1.5–5.7 µL) was added into the solution of 2.5 nmol of the selected conjugate in 200 µL of a 0.02 M acetate buffer (pH 4.5) and heated for 10 min at 95 °C. Subsequently, radioconjugate was purified using Sep-Pack® C18 cartridge in accordance with the producer recommendations, thereby obtaining an easily vaporized ethanolic solution of radioconjugate. The effectiveness of the purification was monitored by HPLC.

3.2.5. Preparation of Non-Radioactive References

The non-radioactive Ga labelling of DOTA conjugates was performed in accordance with the following procedure: 220 µL of a solution of 20 mM $GaCl_3$ in 0.1 M HCl was added into the solution of 50 nmol of the selected conjugate in 300 µL of a 0.2 M acetate buffer (pH = 4.5) and heated for 10 min at 95 °C. Subsequently, reaction product was purified by the HPLC method, lyophilized and characterized by mass spectrometry.

MS: Calculated for monoisotopic mass **Ga-1d**, $C_{41}H_{50}F_7N_9O_{10}Ga$: 883.20 and 885.20; found: 883.31 and 885.28 *m*/*z* $[M]^+$
MS: Calculated for monoisotopic mass **Ga-2d**, $C_{41}H_{49}F_7N_{10}O_{11}Ga$: 954.24 and 956.24; found: 954.33 and 956.65 *m*/*z* $[M]^+$
MS: Calculated for monoisotopic mass **Ga-3d**, $C_{43}H_{53}F_7N_{10}O_{11}Ga$: 1025.28 and 1027.27; found: 1025.37 and 1027.38 *m*/*z* $[M^+]$

MS: Calculated for monoisotopic mass **Ga-4d**, $C_{42}H_{52}F_7N_9O_{10}Ga$: 996.29 and 998.28; found: 996.39 and 998.38 m/z $[M]^+$
MS: Calculated for monoisotopic mass **Ga-5d**, $C_{43}H_{54}F_7N_9O_{10}Ga$: 1109.37 and 1111.37; found: 1109.09 and 1111.20 m/z $[M]^+$

3.3. Plasma Stability Study

Human serum aliquots were isolated and purified at the Centre of Radiobiology and Biological Dosimetry, INCT Warsaw, Poland. A solution of isolated radioconjugate in 100 µL of 0.1M PBS buffer (pH 7.40) was added into 900 µL of human serum and incubated at 37 °C for 4.5 h (in case of ^{68}Ga-radioconjugates) or 2 days (^{177}Lu-radioconjugates). At specific time points, 400 µL of the incubated mixture was added into 500 µL of ethanol, vigorously stirred to precipitate serum proteins and centrifuged (13,500 rpm for 5 min) to separate the supernatant for HPLC analysis.

3.4. Lipophilicity Determination

A solution of isolated radioconjugate (approximately 0.5 MBq for ^{177}Lu-radioconjugates or 5 MBq for ^{68}Ga-radioconjugates) in 500 µL of 0.1 M PBS buffer (pH 7.40) and 500 µL of *n*-octanol was vigorously stirred and centrifuged (13,500 rpm for 5 min) to separate the immiscible phases. Then, the radioactivity of samples from both phases were measured using a well-type NaI(Tl) detector. The distribution coefficient, D, was calculated dividing the radioactivity of the radioconjugate in the organic phase to that in the aqueous phase. Each experiment was performed in triplicate and averaged. In parallel, the aqueous phases were analysed by HPLC to confirm the stability of studied radioconjugate during the experiment period. The lipophilicity value of each radioconjugates was expressed as the logarithm of its D value.

3.5. Cell Culture

The CHO-K1 cells with a stable overexpression of the human NK1 receptor, denoted further on as hNK1-CHO cells, were obtained as a gift from Dr. Attila Keresztes and Dr. John M. Streicher [29]. The cells were maintained in a humidified atmosphere with 5% CO_2 at 37 °C, in Ham's F12 medium (Corning, Corning, NY, USA) supplemented with 10% Foetal Bovine Serum (CytoGen, Wetzlar, Germany) and 400 µg/mL G418 (Corning, Corning, NY, USA).

3.6. hNK1-CHO Membrane Preparation

When the cells reached approximately 90% confluence, they were harvested by treatment with 0.05% trypsin/EDTA (Corning, Corning, NY, USA). After centrifugation at 1500 rpm for 5 min, the cells were homogenized in a glass tissue homogenizer in ice-cold 50 mM Tris-HCl buffer (pH 7.4) with 5 mM $MnCl_2$. The preparation was collected by centrifugation at 13,000 rpm for 25 min at 4 °C, and then the pellet was suspended in 50 mM Tris-HCl buffer. The homogenates were stored at −80 °C for later use. The BCA assay (Thermo Scientific, Waltham, MA, USA) was used to determine the protein concentration in the homogenates.

3.7. Competitive Binding Assays

The binding affinity of the tested compounds for human and rat NK1R was determined in competitive radioligand binding assays following the method previously described [15]. As a source of the receptor proteins, homogenates obtained from rat brains (obtained as described in Ref [30]) or homogenates made from hNK1-CHO cells were used. Different concentrations of the test compounds were incubated with the appropriate membrane preparation (in concentrations of 1.125 mg/mL or 3.8 mg/mL for human and rat preparations, respectively) and 1 nM [2-Prolyl-3,4-^{3}H]-(Sar^9,Met$(O_2)^{11}$)-Substance P (PerkinElmer, Waltham, MA, USA) in the assay buffer (50 mM Tris–HCl (pH 7.4), 5 mM $MnCl_2$, bovine serum albumin (BSA) (0.1 mg/mL), bacitracin (100 µg/mL), bestatin (30 µM), phenyl-

methylsulphonyl fluoride (30 µg/mL) and captopril (10 µM)). The final reaction volumes were 250 µL and 1 mL, for the human and rat NK1R determinations, respectively. Substance P (10 µM, Tocris, United Kingdom) was used to measure the non-specific binding. The binding reaction mixtures were incubated in a shaking water bath at 25 °C for 60 min. The reaction was terminated by rapid filtration through Whatman GF/B filter (Gaithersburg, MD) presoaked in 0.5% polyethyleneimine and washed three times with 2 mL of cold saline. The filters were placed in 24-well plates and immersed in a Betaplate Scint scintillation solution (Perkin Elmer, Waltham, MA, USA). The filter-bound radioactivity was determined by scintillation counter MicroBeta LS, Trilux (PerkinElmer, Waltham, MA, USA).

The displacement curves were drawn and the mean IC_{50} values were determined with standard deviations (GraphPad Prism version 8.0, San Diego, CA, USA). At least three independent experiments (carried out in duplicate) were performed.

3.8. Saturation Binding Assays

The saturation binding studies of ^{177}Lu-radioconjugates were performed using transfected CHO-NK1R cell line, and all radioconjugates were obtained according to the common labelling protocol given above with the same specific activity. In brief, 10^5 cells per well were seeded into 24-well plates and incubated 24 h before the experiment. Just before the assay, cells were washed with 37 °C Dulbecco's PBS and then incubated with different concentrations of radioconjugate (0.2–25 nM at a final volume) with or without 1000-fold molar excess of blocker (NK1R high affinity nonpeptide antagonist aprepitant) for 60 min at 37 °C. After that time, the assay medium was collected into plastic tubes and cells were washed twice with cold Dulbecco's PBS. Subsequently, cells were lysed using 1M NaOH and collected into plastic tubes for radioactivity measurement.

The radioactivity of collected medium and lysed cells was measured using a Wizard^2 2-Detector Gamma Counter (PerkinElmer, Waltham, MA, USA) with the energy window of 50–500 keV. The study data came from three independent experiments carried out in duplicate, while the results, presented as the Kd and BMAX with SD, were calculated using a total and nonspecific binding (one site) nonlinear regression curve fit (GraphPad Prism version 8.0, GraphPad, San Diego, CA, USA).

3.9. Molecular Docking

Molecular docking was executed using AutoDock 4.2.6. [31]. The structure of **1c** (separate for *cis* and *trans* conformers around the amide bond) was optimized at the B3LYP/6-31G(d,p) level by using Gaussian09 [32]. Both *cis* and *trans* conformers of 1c were used for docking. The structures of further analogues were built by manually expanding the structure of **1c** in the binding site of hNK1R, whereafter the optimization was performed by local search routine in AutoDock 4.2.6 [31].

The ligands and the protein structure were processed in AutoDock Tools 4 [31] with standard routines. Full ligand flexibility (except for amide bonds) was allowed. The receptor was treated as rigid. In order to take into account side-chain flexibility in the binding site, in the first stages of docking three separate hNK1R structures (6HLL, 6HLO and 6HLP [25]) were used. With the initial results in hand, it was decided to use only the 6HLO structure.

The receptor structures were the refined models provided by the GPCRdb service [33]. This was chosen in order to have the mutated residues replaced with native ones, as well as to have side chains missing in the original PDB structures supplemented. Before docking, the model coordinates were transformed to match the coordinates of corresponding models in OPM database [34]. This was carried out to facilitate embedding in lipid membrane for the purposes of molecular dynamics.

The docking boxes encompassed the orthosteric binding site of hNK1R and the extracellular outlet of the binding sites. The grids were calculated with AutoGrid 4 [31].

For global docking, default AutoDock parameters were used. For local searches, we used the following settings: 300 individuals in population, 500 iterations of the Solis-Wets

local search, the *sw_rho* parameter of the local search space set to 100.0 and 1000 local search runs. The calculations were repeated several times. The local docking results were clustered, and structures from the best scored clusters were taken for further analyses.

3.10. Molecular Dynamics

The receptor–ligand complexes as obtained by docking were embedded in POPC membrane (128 lipid molecules) and solvated with TIP3P water (about 13000 water molecules, TIP3P). Na^+ and Cl^- ions (0.154 M concentration) were added too. The systems were prepared by using the CHARMM-GUI service [35]. CHARMM 36 force field was used for the proteins, lipids, water and ions, while the ligands were modelled using CHARMM CGenFF [36].

Molecular dynamics simulations were run in GROMACS 5.1.2 [37]. The complexes were minimized and equilibrated. The production runs were obtained using the following parameters: NPT ensemble, temperature = 303.15 K, integration step = 2 fs, cut-off scheme Verlet, Nose–Hoover thermostat, Parrinello–Rahman barostat, LINCS H-bonds constraints. For each system, 3 runs of 150 ns production length were obtained.

For analysing conformational behaviour of the complexes, the trajectories for each complex were concatenated and superposed on a common reference snapshot. The superposition was based on backbone atoms of the helical part of the receptors. The root-mean-square deviations of the atomic positions of the protein (in helical part), the ligand or ligand's parts were monitored over simulation times (using built-in GROMACS tools).

The molecular graphics were prepared in open-source PyMol [38] and in Biovia Discovery Studio Visualizer v. 19 [39].

4. Conclusions

The work reported herein shows that a small molecular NK1R antagonist, L732,138, may be a good basis for creating radioconjugates. Such radioconjugates (containing therapeutic radionuclides) could be useful agents for the targeted radionuclide therapy of glioblastoma multiforme, for the locoregional administration. If labelled with diagnostic radionuclides, they might also be applied for diagnostic purposes.

In the first stage of our work, we showed that novel (expanded) L732,138 analogues are good hNK1R binders, practically regardless of the length of the linker used. None of the evaluated linkers exhibited unequivocally negative or unequivocally positive effects on the receptor affinity. The best analogues (e.g., **5a**) showed some improvement compared to the parent analogue.

The obtained radioconjugates, containing DOTA chelator coupled to L732,138 and its four analogues with different linker lengths, after labelling with ^{68}Ga and ^{177}Lu, turned out to be fairly lipophilic ($logD_{7.4}$). Unfortunately, they showed rather limited stability in human plasma, with degradation occurring within a few hours. However, it is not necessarily disqualifying, as their prospective application is for the locoregional administration into the post-operation cavity where the enzymatic activity might be expected to be negligible.

Evaluation of the receptor affinity for the DOTA-conjugates and their complexes with Ga^{3+} and Lu^{3+} showed that neither the chelator nor the metal negatively impact the hNK1R binding. For the ^{177}Lu-radioconjugates, we found K_d values in the range 2–10 nM, which is comparable to the K_d found for the reference SP-based radioconjugate. Very importantly, in the saturation assays for the novel radioconjugates, one observes a higher binding capacity (B_{MAX} values) than in the case of the reference radiopharmaceutical. This is probably due to the use of a small molecular, lipophilic structure as the vector.

By the means of molecular modelling, a binding mode (consistent with the previous experimental hints) for the parent L732,138 was established. Interestingly, this compound's binding is predicted to be stabilized by exclusively apolar contacts. On the contrary, in the cases of other analogues, polar interactions are of importance. Modelling also sheds light on the binding mode of the conjugate **1d** (no linker), whose accommodation in the binding

site is predicted to be associated with the flexibility of the receptor. The results of the modelling and of the experimental part are going to guide future SAR work.

The work reported herein is a further step towards the development of NK1R-targeted radioconjugates based on small molecular vectors. Of course, these results do not allow for the direct application of our radioconjugates in medicine. Further experimental work on these analogues or some novel ones is required (including in vivo experiments).

It is to be noted that NK1R-targeting conjugates and polyfunctional ligands are also contemplated outside of the radiopharmacy, e.g., in the research on multitarget analgesics [40–42] or in the efforts towards therapeutic gene delivery [43,44]. In these areas, the novel NK1R ligands that were reported herein and the SAR data may be of use too.

Supplementary Materials: The following are available online at https://www.mdpi.com/article/10.3390/ijms23031214/s1.

Author Contributions: Conceptualization, P.K.H., J.M. and K.K.; methodology, P.F.J.L., J.M., P.K.H., K.K. and P.K.; investigation, P.F.J.L., J.M., P.K.H. and K.K.; writing—original draft preparation, P.F.J.L., J.M. and P.K.H.; writing—review and editing, P.F.J.L., J.M., P.K.H., E.G., P.K. and K.K.; visualization, P.F.J.L.; supervision, A.M. and E.G.; project administration, A.M. and E.G.; funding acquisition, A.M. and E.G. All authors have read and agreed to the published version of the manuscript.

Funding: The research was funded by a grant from the National Science Centre in Poland (Grant No. 2017/25/B/NZ7/01896).

Institutional Review Board Statement: Not applicable.

Informed Consent Statement: Not applicable.

Data Availability Statement: The data presented in this study are available on request from the corresponding author.

Acknowledgments: The authors gratefully acknowledge Attila Keresztes and John M. Streicher from the University of Arizona for sharing the hNK1-CHO cells. Katarzyna Kosińska acknowledges her contribution having been carried out within the doctoral studies programme "POWEROch!DOK", and this project is supported by the European Social Fund (ESF), POWR.03.02.00-00-I028/17-00. The contribution of Paweł Krzysztof Halik was performed in the frame of the National Centre for Research and Development Project No POWR.03.02.00-00-I009/17 (Radiopharmaceuticals for molecularly targeted diagnosis and therapy, RadFarm. Operational Project Knowledge Education Development 2014–2020 co-financed by European Social Fund). The molecular modelling was performed using the resources of the Świerk Computing Centre, National Centre for Nuclear Research, Świerk, Poland.

Conflicts of Interest: The authors declare no conflict of interest. The funders had no role in the design of the study, in the collection, analyses or interpretation of data, in the writing of the manuscript or in the decision to publish the results.

References

1. Holland, E.C. Glioblastoma multiforme: The terminator. *Proc. Natl. Acad. Sci. USA* **2000**, *97*, 6242–6244. [CrossRef]
2. Lapointe, S.; Perry, A.; Butowski, N.A. Primary brain tumours in adults. *Lancet* **2018**, *392*, 432–446. [CrossRef]
3. Reulen, H.-J.; Suero Molina, E.; Zeidler, R.; Gildehaus, F.J.; Böning, G.; Gosewisch, A.; Stummer, W. Intracavitary radioimmunotherapy of high-grade gliomas: Present status and future developments. *Acta Neurochir.* **2019**, *161*, 1109–1124. [CrossRef]
4. Majkowska-Pilip, A.; Halik, P.K.; Gniazdowska, E. The Significance of NK1 Receptor Ligands and Their Application in Targeted Radionuclide Tumour Therapy. *Pharmaceutics* **2019**, *11*, 443. [CrossRef]
5. Kneifel, S.; Cordier, D.; Good, S.; Ionescu, M.C.S.; Ghaffari, A.; Hofer, S.; Kretzschmar, M.; Tolnay, M.; Apostolidis, C.; Waser, B.; et al. Local Targeting of Malignant Gliomas by the Diffusible Peptidic Vector 1,4,7,10-Tetraazacyclododecane-1-Glutaric Acid-4,7,10-Triacetic Acid-Substance P. *Clin. Cancer Res.* **2006**, *12*, 3843–3850. [CrossRef]
6. Cordier, D.; Forrer, F.; Bruchertseifer, F.; Morgenstern, A.; Apostolidis, C.; Good, S.; Müller-Brand, J.; Mäcke, H.; Reubi, J.C.; Merlo, A. Targeted alpha-radionuclide therapy of functionally critically located gliomas with 213Bi-DOTA-[Thi8,Met(O2)11]- substance P: A pilot trial. *Eur. J. Nucl. Med. Mol. Imaging* **2010**, *37*, 1335–1344. [CrossRef]
7. Cordier, D.; Forrer, F.; Kneifel, S.; Sailer, M.; Mariani, L.; Mäcke, H.; Müller-Brand, J.; Merlo, A. Neoadjuvant targeting of glioblastoma multiforme with radiolabeled DOTAGA–substance P—results from a phase I study. *J. Neurooncol.* **2010**, *100*, 129–136. [CrossRef]

8. Królicki, L.; Kunikowska, J.; Bruchertseifer, F.; Koziara, H.; Królicki, B.; Jakuciński, M.; Pawlak, D.; Rola, R.; Morgenstern, A.; Rosiak, E.; et al. 225Ac- and 213Bi-Substance P Analogues for Glioma Therapy. *Semin. Nucl. Med.* **2020**, *50*, 141–151. [CrossRef]
9. Królicki, L.; Bruchertseifer, F.; Kunikowska, J.; Koziara, H.; Królicki, B.; Jakuciński, M.; Pawlak, D.; Apostolidis, C.; Mirzadeh, S.; Rola, R.; et al. Safety and efficacy of targeted alpha therapy with 213Bi-DOTA-substance P in recurrent glioblastoma. *Eur. J. Nucl. Med. Mol. Imaging* **2019**, *46*, 614–622. [CrossRef]
10. Merlo, A.; Mäcke, H.; Reubi, J.C.; Good, S. Radiolabeled Conjugates Based on Substance P and the Uses. Thereof. Patent Application No. WO 2004/082722, 30 September 2004.
11. Majkowska-Pilip, A.; Rius, M.; Bruchertseifer, F.; Apostolidis, C.; Weis, M.; Bonelli, M.; Laurenza, M.; Królicki, L.; Morgenstern, A. In vitro evaluation of 225 Ac-DOTA-substance P for targeted alpha therapy of glioblastoma multiforme. *Chem. Biol. Drug Des.* **2018**, *92*, 1344–1356. [CrossRef]
12. Królicki, L.; Bruchertseifer, F.; Kunikowska, J.; Koziara, H.; Pawlak, D.; Kuliński, R.; Rola, R.; Merlo, A.; Morgenstern, A. Dose escalation study of targeted alpha therapy with [225Ac]Ac-DOTA-substance P in recurrence glioblastoma–safety and efficacy. *Eur. J. Nucl. Med. Mol. Imaging* **2021**, *48*, 3595–3605. [CrossRef] [PubMed]
13. Majkowska-Pilip, A.; Koźmiński, P.; Wawrzynowska, A.; Budlewski, T.; Kostkiewicz, B.; Gniazdowska, E. Application of Neurokinin-1 Receptor in Targeted Strategies for Glioma Treatment. Part I: Synthesis and Evaluation of Substance P Fragments Labeled with 99mTc and 177Lu as Potential Receptor Radiopharmaceuticals. *Molecules* **2018**, *23*, 2542. [CrossRef] [PubMed]
14. Lyczko, M.; Pruszynski, M.; Majkowska-Pilip, A.; Lyczko, K.; Was, B.; Meczynska-Wielgosz, S.; Kruszewski, M.; Szkliniarz, K.; Jastrzebski, J.; Stolarz, A.; et al. 211 At labeled substance P (5–11) as potential radiopharmaceutical for glioma treatment. *Nucl. Med. Biol.* **2017**, *53*, 1–8. [CrossRef]
15. Halik, P.K.; Lipiński, P.F.J.; Matalińska, J.; Koźmiński, P.; Misicka, A.; Gniazdowska, E. Radiochemical Synthesis and Evaluation of Novel Radioconjugates of Neurokinin 1 Receptor Antagonist Aprepitant Dedicated for NK1R-Positive Tumors. *Molecules* **2020**, *25*, 3756. [CrossRef] [PubMed]
16. MacLeod, A.M.; Merchant, K.J.; Cascieri, M.A.; Sadowski, S.; Ber, E.; Swain, C.J.; Baker, R. N-Acyl-L-tryptophan benzyl esters: Potent substance P receptor antagonists. *J. Med. Chem.* **1993**, *36*, 2044–2045. [CrossRef]
17. Spector, R.; Robert Snodgrass, S.; Johanson, C.E. A balanced view of the cerebrospinal fluid composition and functions: Focus on adult humans. *Exp. Neurol.* **2015**, *273*, 57–68. [CrossRef]
18. Arnott, J.A.; Planey, S.L. The influence of lipophilicity in drug discovery and design. *Expert Opin. Drug Discov.* **2012**, *7*, 863–875. [CrossRef]
19. Waring, M.J. Lipophilicity in drug discovery. *Expert Opin. Drug Discov.* **2010**, *5*, 235–248. [CrossRef]
20. Leffler, A.; Ahlstedt, I.; Engberg, S.; Svensson, A.; Billger, M.; Öberg, L.; Bjursell, M.K.; Lindström, E.; von Mentzer, B. Characterization of species-related differences in the pharmacology of tachykinin NK receptors 1, 2 and 3. *Biochem. Pharmacol.* **2009**, *77*, 1522–1530. [CrossRef]
21. MacLeod, A.M.; Merchant, K.J.; Brookfield, F.; Kelleher, F.; Stevenson, G.; Owens, A.P.; Swain, C.J.; Cascieri, M.A.; Sadowski, S. Identification of L-Tryptophan Derivatives with Potent and Selective Antagonist Activity at the NK1 Receptor. *J. Med. Chem.* **1994**, *37*, 1269–1274. [CrossRef]
22. Vardanyan, R.; Kumirov, V.K.; Nichol, G.S.; Davis, P.; Liktor-Busa, E.; Rankin, D.; Varga, E.; Vanderah, T.; Porreca, F.; Lai, J.; et al. Synthesis and biological evaluation of new opioid agonist and neurokinin-1 antagonist bivalent ligands. *Bioorg. Med. Chem.* **2011**, *19*, 6135–6142. [CrossRef]
23. Cascieri, M.A.; Macleod, A.M.; Underwood, D.; Shiao, L.L.; Ber, E.; Sadowski, S.; Yu, H.; Merchant, K.J.; Swain, C.J.; Strader, C.D. Characterization of the interaction of N-acyl-L-tryptophan benzyl ester neurokinin antagonists with the human neurokinin-1 receptor. *J. Biol. Chem.* **1994**, *269*, 6587–6591. [CrossRef]
24. Morgenstern, A.; Apostolidis, C.; Kratochwil, C.; Sathekge, M.; Krolicki, L.; Bruchertseifer, F. An Overview of Targeted Alpha Therapy with 225 Actinium and 213 Bismuth. *Curr. Radiopharm.* **2018**, *11*, 200–208. [CrossRef] [PubMed]
25. Schöppe, J.; Ehrenmann, J.; Klenk, C.; Rucktooa, P.; Schütz, M.; Doré, A.S.; Plückthun, A. Crystal structures of the human neurokinin 1 receptor in complex with clinically used antagonists. *Nat. Commun.* **2019**, *10*, 17. [CrossRef] [PubMed]
26. MacLeod, A.M.; Cascieri, M.A.; Merchant, K.J.; Sadowski, S.; Hardwicke, S.; Lewis, R.T.; MacIntyre, D.E.; Metzger, J.M.; Fong, T.M. Synthesis and Biological Evaluation of NK1 Antagonists Derived from L-Tryptophan. *J. Med. Chem.* **1995**, *38*, 934–941. [CrossRef]
27. Lewis, R.T.; Macleod, A.M.; Merchant, K.J.; Kelleher, F.; Sanderson, I.; Herbert, R.H.; Cascieri, M.A.; Sadowski, S.; Ball, R.G.; Hoogsteen, K. Tryptophan-Derived NK1 Antagonists: Conformationally Constrained Heterocyclic Bioisosteres of the Ester Linkage. *J. Med. Chem.* **1995**, *38*, 923–933. [CrossRef]
28. Branik, M.; Kessler, H. Zur Konformation geschützter Aminosäuren, III. NMR- und IR-Untersuchungen von Boc-L-α-Aminosäuren. *Chem. Ber.* **1975**, *108*, 2176–2188. [CrossRef]
29. Starnowska, J.; Costante, R.; Guillemyn, K.; Popiolek-Barczyk, K.; Chung, N.N.; Lemieux, C.; Keresztes, A.; Van Duppen, J.; Mollica, A.; Streicher, J.M.; et al. Analgesic properties of opioid/NK1 multitarget ligands with distinct in vitro profiles in naive and chronic constriction injury (CCI)-mice. *ACS Chem. Neurosci.* **2017**, *8*, 2315–2324. [CrossRef]
30. Matalińska, J.; Lipiński, P.F.J.; Kotlarz, A.; Kosson, P.; Muchowska, A.; Dyniewicz, J. Evaluation of Receptor Affinity, Analgesic Activity and Cytotoxicity of a Hybrid Peptide, AWL3020. *Int. J. Pept. Res. Ther.* **2020**, *26*, 2603–2617. [CrossRef]

31. Morris, G.M.; Huey, R.; Lindstrom, W.; Sanner, M.F.; Belew, R.K.; Goodsell, D.S.; Olson, A.J. AutoDock4 and AutoDockTools4: Automated docking with selective receptor flexibility. *J. Comput. Chem.* **2009**, *30*, 2785–2791. [CrossRef]
32. Frisch, M.J.; Trucks, G.W.; Schlegel, H.B.; Scuseria, G.E.; Robb, M.A.; Cheeseman, J.R.; Scalmani, G.; Barone, V.; Mennucci, B.; Petersson, G.A.; et al. *Gaussian 09, Revision D.01*; Gaussian Inc.: Wallingford, CT, USA, 2013.
33. Pándy-Szekeres, G.; Munk, C.; Tsonkov, T.M.; Mordalski, S.; Harpsøe, K.; Hauser, A.S.; Bojarski, A.J.; Gloriam, D.E. GPCRdb in 2018: Adding GPCR structure models and ligands. *Nucleic Acids Res.* **2018**, *46*, D440–D446. [CrossRef] [PubMed]
34. Lomize, M.A.; Lomize, A.L.; Pogozheva, I.D.; Mosberg, H.I. OPM: Orientations of proteins in membranes database. *Bioinformatics* **2006**, *22*, 623–625. [CrossRef] [PubMed]
35. Lee, J.; Cheng, X.; Swails, J.M.; Yeom, M.S.; Eastman, P.K.; Lemkul, J.A.; Wei, S.; Buckner, J.; Jeong, J.C.; Qi, Y.; et al. CHARMM-GUI Input Generator for NAMD, GROMACS, AMBER, OpenMM, and CHARMM/OpenMM Simulations Using the CHARMM36 Additive Force Field. *J. Chem. Theory Comput.* **2016**, *12*, 405–413. [CrossRef] [PubMed]
36. Vanommeslaeghe, K.; Hatcher, E.; Acharya, C.; Kundu, S.; Zhong, S.; Shim, J.; Darian, E.; Guvench, O.; Lopes, P.; Vorobyov, I.; et al. CHARMM general force field: A force field for drug-like molecules compatible with the CHARMM all-atom additive biological force fields. *J. Comput. Chem.* **2009**, *31*, 671–690. [CrossRef] [PubMed]
37. Abraham, M.J.; Murtola, T.; Schulz, R.; Páll, S.; Smith, J.C.; Hess, B.; Lindahl, E. GROMACS: High performance molecular simulations through multi-level parallelism from laptops to supercomputers. *SoftwareX* **2015**, *1*, 19–25. [CrossRef]
38. Schrödinger LLC. The PyMOL Molecular Graphics System. 2018. Available online: https://sourceforge.net/p/pymol/code/HEAD/tree/trunk/pymol/ (accessed on 1 November 2020).
39. *Biovia Discovery Studio Visualizer v.19*; Dassault Systèmes: San Diego, CA, USA, 2018.
40. Matalińska, J.; Lipiński, P.F.J.; Kosson, P.; Kosińska, K.; Misicka, A. In Vivo, In Vitro and In Silico Studies of the Hybrid Compound AA3266, an Opioid Agonist/NK1R Antagonist with Selective Cytotoxicity. *Int. J. Mol. Sci.* **2020**, *21*, 7738. [CrossRef]
41. Dyniewicz, J.; Lipiński, P.F.J.; Kosson, P.; Leśniak, A.; Bochyńska-Czyż, M.; Muchowska, A.; Tourwé, D.; Ballet, S.; Misicka, A.; Lipkowski, A.W. Hydrazone Linker as a Useful Tool for Preparing Chimeric Peptide/Nonpeptide Bifunctional Compounds. *ACS Med. Chem. Lett.* **2017**, *8*, 73–77. [CrossRef]
42. Kleczkowska, P.; Nowicka, K.; Bujalska-Zadrozny, M.; Hermans, E. Neurokinin-1 receptor-based bivalent drugs in pain management: The journey to nowhere? *Pharmacol. Ther.* **2019**, *196*, 44–58. [CrossRef]
43. Rizk, S.S.; Misiura, A.; Paduch, M.; Kossiakoff, A.A. Substance P Derivatives as Versatile Tools for Specific Delivery of Various Types of Biomolecular Cargo. *Bioconjug. Chem.* **2012**, *23*, 42–46. [CrossRef]
44. Ding, G.; Wang, T.; Han, Z.; Tian, L.; Cheng, Q.; Luo, L.; Zhao, B.; Wang, C.; Feng, S.; Wang, L.; et al. Substance P containing peptide gene delivery vectors for specifically transfecting glioma cells mediated by a neurokinin-1 receptor. *J. Mater. Chem. B* **2021**, *9*, 6347–6356. [CrossRef]

3.5. In Vitro Biological Evaluation of Aprepitant based ^{177}Lu-Radioconjugates

Halik, P.K.; Koźmiński, P.; Matalińska, J.; Lipiński, P.F.J.; Misicka, A.; Gniazdowska, E. In Vitro Biological Evaluation of Aprepitant Based ^{177}Lu-Radioconjugates. *Pharmaceutics* **2022**, *14*, 607. DOI: 10.3390/pharmaceutics14030607

IF (2020) = 6,321; pkt. MNiSW (2022) = 100

Autor	Udział
Halik, P.K	- wykonanie preparatyki syntetycznej; - wykonanie preparatyki radiosyntetycznej; - wykonanie analiz radiochemicznych; - opracowanie analiz spektroskopowych; - hodowla komórkowa; - wykonanie oznaczeń powinowactwa receptorowego metodą saturacyjną; - przygotowanie manuskryptu; - wizualizacja danych;
Koźmiński, P.	- wykonanie analiz spektrometrycznych; - praca nad manuskryptem (1. czytanie);
Matalińska, J.	- praca nad manuskryptem (1. czytanie);
Lipiński, P.F.J.	- wykonanie badania modelowania molekularnego; - przygotowanie manuskryptu; - przygotowanie suplementu; - wizualizacja danych;
Misicka, A.	- koncepcja badań; - kierowanie grantem; - praca nad manuskryptem (2. czytanie);
Gniazdowska, E.	- koncepcja badań; - kierowanie grantem; - praca nad manuskryptem (2. czytanie);

pharmaceutics

MDPI

Article

In Vitro Biological Evaluation of Aprepitant Based ^{177}Lu-Radioconjugates

Paweł K. Halik [1,*], Przemysław Koźmiński [1], Joanna Matalińska [2], Piotr F. J. Lipiński [2], Aleksandra Misicka [2,3] and Ewa Gniazdowska [1]

1 Centre of Radiochemistry and Nuclear Chemistry, Institute of Nuclear Chemistry and Technology, 03-195 Warsaw, Poland; p.kozminski@ichtj.waw.pl (P.K.); e.gniazdowska@ichtj.waw.pl (E.G.)
2 Department of Neuropeptides, Mossakowski Medical Research Institute, Polish Academy of Sciences, 02-106 Warsaw, Poland; jmatalinska@imdik.pan.pl (J.M.); plipinski@imdik.pan.pl (P.F.J.L.); misicka@chem.uw.edu.pl (A.M.)
3 Faculty of Chemistry, University of Warsaw, 02-093 Warsaw, Poland
* Correspondence: p.halik@ichtj.waw.pl; Tel.: +48-22-504-13-16

Abstract: Currently, the search for promising NK1R-positive tumor-targeting radiopharmaceuticals based on the structure of small molecular antagonists of neurokinin-1 receptor can be observed. Following this trend, we continued our evaluation of aprepitant-based ^{177}Lu-radioconjugates in terms of future oncological applications. For this purpose, three novel aprepitant homologues were synthesized to broaden the previously obtained derivative portfolio, functionalized with the DOTA chelator and labeled with ^{68}Ga and ^{177}Lu. The newly evaluated radioconjugates showed the intended significant increase in lipophilicity compared to the previous ones, while maintaining stability in the human serum. Then, in a receptor binding study to the human NK1 receptor, we compared the two series of ^{177}Lu-radioconjugates of aprepitant with each other and with the reference Substance P derivative currently used in glioblastoma therapy, clearly indicating the high affinity and better binding capacity of the novel radioconjugates. The in vitro experimental results included in the presented study, supported by labeling optimization, radioconjugate characterization and docking modeling of new aprepitant-derived radioagents, confirm our assumptions about the usefulness of aprepitant as a NK1R targeting vector and point out the perspectives for the forthcoming first in vivo trials.

Keywords: aprepitant; radiopharmaceuticals; neurokinin 1 receptor antagonist

Citation: Halik, P.K.; Koźmiński, P.; Matalińska, J.; Lipiński, P.F.J.; Misicka, A.; Gniazdowska, E. In Vitro Biological Evaluation of Aprepitant Based ^{177}Lu-Radioconjugates. *Pharmaceutics* **2022**, *14*, 607. https://doi.org/10.3390/pharmaceutics14030607

Academic Editors: Clément Morgat and David Kryza

Received: 14 February 2022
Accepted: 7 March 2022
Published: 10 March 2022

1. Introduction

Over the last few years, a significant increase of the interest in small molecular antagonists of neurokinin-1 receptor (NK1R) in terms of oncological applications can be observed. Some reports indicate new perspectives for the use of aprepitant [1] and of other NK1R antagonists [2–4] as vectors for selective radiopharmaceutical agents for NK1R-positive tumors.

At the same time, it results in a distraction from the radiopharmaceuticals based on derivatives of Substance P (SP) or other peptide ligands of this receptor, due to several inconveniences that characterize this group of compounds. These radiopharmaceuticals currently used in therapy of gliomas (e.g., [^{213}Bi]Bi-DOTA-[Thi^{8},Met(O_2)^{11}]Substance P [5–7]) are administered intracavitarily in a controlled manner through an appropriate preinstalled canal port into the postoperative cavity for radiopharmaceutical administration. Unfortunately, simple intravenous administration of SP derivatives is ineffective due to their low metabolic stability, unfavorable pharmacokinetic [8], and the fact that in micromolar amounts both Substance P and its analogues could produce a severe hypotension in peripheral circulatory system [9]. Nevertheless, targeted alpha therapy utilizing [^{213}Bi]Bi/[^{225}Ac]Ac-DOTA-[Thi^{8},Met(O_2)^{11}]SP in locoregional application is a promising

and favorable step towards the future treatment. Still, the clinicians point out that new treatment options are urgently needed [6].

Increased NK1R expression on various types of cancer correlates with tumor progression, migration and angiogenesis [10–13]. This applies to nervous system cancers as gliomas [14–16], but also to neoplasms of other organs. On the other hand, normal tissues show significantly lower (often negligible) levels of NK1R expression [13,16–18]. This fact gives the green light to the concept of selective imaging and targeting of tumor cells overexpressing NK1R.

Aprepitant may be the solution to the search for an appropriate vector to be used in targeted radionuclide tumor therapy. This representative of NK1R antagonists is of increasing attentiveness due to its broad anti-tumor activity of very promising therapeutic significance [12,13,19,20] and many years of experience in clinical application against chemotherapy-induced nausea and vomiting in oncological patients. Most significantly, it is a drug of known pharmacokinetics, metabolically stable, showing the ability to cross the blood–brain barrier after intravenous or oral administration [20–22]. In comparison to peptide antagonists, aprepitant is a smaller molecule with undoubtedly higher lipophilicity and a favorable biding mode towards the cognate receptor [23].

In the preceding report [1], we presented a drug design concept for convenient modification of the aprepitant structure including an extensive rationale for the selection of its triazolinone ring as a site of functionalization. We specified that this fragment of the molecule tolerates some modification, and as we indicated by several examples, it is possible to introduce modifications effectively without significant compromise to the receptor affinity. This particular knowledge of how to constructively modify the structure of the compound without adversely affecting the receptor binding affinity was implemented to report this consideration on aprepitant-based radiopharmaceuticals for NK1R-positive tumors. At the same time, we wanted to broaden previously obtained derivative portfolio with sufficiently high lipophilic derivatives and to explore the impact of much longer linkers on the chelator placement in (or nearby) the binding site, and thus on the receptor affinity of the aprepitant radioconjugate.

In this part of our research, we set ourselves the goal of obtaining three novel aprepitant-related homologues with higher lipophilicity using longer aliphatic linkers. Then, we obtained DOTA conjugates and optimized the conjugate labeling with ^{68}Ga and ^{177}Lu isotopes. Finally, we investigated a binding profile towards human NK1 receptor for all eight reported (synthesized now and previously) ^{177}Lu-radioconjugates at their highest specific activity in reference to binding characteristics of ^{177}Lu-labeled Substance P derivative currently used in clinical therapy. These results were also supplemented with the physicochemical evaluation of newly obtained radioconjugates and molecular modelling rationalization of the obtained affinity data.

2. Materials and Methods

Aprepitant (Santa Cruz Biotechnology Inc., Dallas, TX, USA), DOTA-NHS ester (1,4,7,10-tetraazacyclododecane-1,4,7,10-tetraacetic acid mono-*N*-hydroxysuccinimide ester) (CheMatech, France), and other substances and solvents (Sigma Aldrich/Merck, Darmstadt, Germany) were commercially available, defined as reagent grade, and applied without further purification. [^{68}Ga]$GaCl_3$ was eluted from the commercially available ^{68}Ge/^{68}Ga generator (Eckert & Ziegler, Berlin, Germany) by semi-automated syringe pump to fractionate the highest radionuclide content solution for the labeling reactions; no other processing was applied. [^{177}Lu]$LuCl_3$ solution in 0.04 M HCl was purchased from Radioisotope Centre POLATOM, National Centre for Nuclear Research, Otwock-Świerk, Poland. Human serum was a gift from the Regional Centre for Blood Donation and Blood Treatment in Warsaw, Poland. The HPLC analyses were performed using a semi-preparative Phenomenex Jupiter Proteo column, 4 µm, 90 Å, 250 × 10 mm, with UV/Vis (wavelength 220 nm) or/and radio γ-detection at gradient elution: 0–20 min 20 to 80% solvent B; 20–30 min 80% solvent B; total flow 2 mL/min.; solvent A: 0.1% (*v*/*v*) trifluoroacetic

acid (TFA) in water; and solvent B: 0.1% (*v*/*v*) TFA in acetonitrile. Mass spectra were measured on a Bruker 3000 Esquire mass spectrometer equipped with electrospray ionization (ESI) (Bruker, Billerica, MA, USA). The NMR measurements were done in CD_3OD or CD_3CN on Varian-Agilent 600 MHz VNMRS spectrometer at ambient temperature, with trimethylsilane as the internal standard for chemical shifts.

2.1. Syntheses and Characterization of Aprepitant-Based Conjugates

2.1.1. General Procedure of Syntheses of Aprepitant Derivatives with Alkyl Linker

The corresponding *N*-(terminal-bromoalkyl)phthalimide (2 equiv.) was added into the mixture of aprepitant (1 equiv.) and sodium carbonate (1 equiv.) in 100–200 µL of DMF. The reaction mixture was vigorously stirred at about 80 °C for 72 h. Then, the hydrazine monohydrate (3 equiv.) was added into the reaction mixture and left for additional 2–3 h. The progress of the reaction was monitored by HPLC. After this time, the reaction mixture was evaporated, dissolved in the HPLC mobile phase and purified by the HPLC method. Each main product was isolated and verified by MS analysis confirmation as a mono-substituted APT-alkylamine derivative. The purified products were collected, lyophilized and characterized by ^{1}H-NMR analysis.

2-(6-aminohexyl)-5-([(2*R*,3*S*)-2-((*R*)-1-[3,5-bis(trifluoromethyl)phenyl]ethoxy)-3-(4-fluorophenyl)morpholino]methyl)-1*H*-1,2,4-triazol-3-one, APT-Hex-NH_2, white powder, yield 24.0%, purity > 97% (HPLC-UV; t_R = 19.1 min), ESI-MS: calculated monoisotopic mass for $C_{29}H_{34}F_7N_5O_3$: 633.60; found: 634.22 *m*/*z* $[M+H]^+$; ^{1}H NMR (600 MHz, CD_3OD) (s—singlet, d—doublet, t—triplet, q—quartet, td—triplet of doublets, m—multiplet) δ (ppm), 7.73 (s, 1H), 7.56 (s, 2H), 7.39 (s, 2H), 7.12–7.09 (t, *J* = 8.8 Hz, 2H), 5.01–4.98 (q, *J* = 6.6 Hz, 1H), 4.37 (d, *J* = 2.9 Hz, 1H), 4.28–4.24 (td, *J* = 11.8, 2.5 Hz, 1H), 3.87–3.82 (m, 1H), 3.69–3.65 (m, 2H), 3.58–3.56 (d, *J* = 14.0 Hz, 2H), 3.49–3.48 (d, *J* = 2.9 Hz, 1H), 2.94–2.88 (m, 2H), 2.83–2.81 (d, *J* = 11.7 Hz, 1H), 2.52–2.47 (td, *J* = 12.0, 3.5 Hz, 1H), 1.75–1.65 (m, 4H), 1.50–1.48 (d, *J* = 6.6 Hz, 3H), 1.47–1.39 (m, 4H). In deuterated methanol, it was not possible to observe signals from the hydrogens of the amino group -NH_2 (around 6.9 ppm) and hydrogen of the nitrogen in the triazolinone ring (around 10.1 ppm).

2-(8-aminooctyl)-5-([(2*R*,3*S*)-2-((*R*)-1-[3,5-bis(trifluoromethyl)phenyl]ethoxy)-3-(4-fluorophenyl)morpholino]methyl)-1*H*-1,2,4-triazol-3-one, APT-Oct-NH_2, white powder, yield 19.1%, purity > 97% (HPLC-UV; t_R = 20.0 min), ESI-MS: calculated monoisotopic mass for $C_{31}H_{38}F_7N_5O_3$: 661.65; found: 662.21 *m*/*z* $[M+H]^+$; ^{1}H NMR (600 MHz, CD_3CN) (s—singlet, d—doublet, t—triplet, q—quartet, td—triplet of doublets, m—multiplet) δ (ppm), 10.07 (s, 1H), 7.78 (s, 1H), 7.54 (s, 2H), 7.40 (s, 2H), 7.12–7.09 (t, *J* = 8.9 Hz, 2H), 7.01 (s, 2H), 4.95–4.92 (q, *J* = 6.5 Hz, 1H), 4.38 (d, *J* = 2.8 Hz, 1H), 4.23–4.18 (td, *J* = 11.7, 2.5 Hz, 1H), 3.74–3.69 (m, 1H), 3.66–3.63 (m, 1H), 3.57–3.52 (m, 1H), 3.52–3.50 (d, *J* = 14.0 Hz, 2H), 3.47–3.46 (d, *J* = 2.8 Hz, 1H), 2.82 (s, 2H), 2.46–2.41 (td, *J* = 11.9, 3.5 Hz, 1H), 1.69–1.62 (m, 4H), 1.47–1.46 (d, *J* = 6.6 Hz, 3H), 1.34 (s, 8H).

2-(10-aminodecyl)-5-([(2*R*,3*S*)-2-((*R*)-1-[3,5-bis(trifluoromethyl)phenyl]ethoxy)-3-(4-fluorophenyl)morpholino]methyl)-1*H*-1,2,4-triazol-3-one, APT-Dec-NH_2, white powder, yield 18.9%, purity > 97% (HPLC-UV; t_R = 20.5 min), ESI-MS: calculated monoisotopic mass for $C_{33}H_{42}F_7N_5O_3$: 689.71; found: 690.32 *m*/*z* $[M+H]^+$; ^{1}H NMR (600 MHz, CD_3CN) (s—singlet, d—doublet, t—triplet, q—quartet, td—triplet of doublets, m—multiplet) δ (ppm), 10.11 (s, 1H), 7.78 (s, 1H), 7.55 (s, 2H), 7.41 (s, 2H), 7.12-7.09 (t, *J* = 8.9 Hz, 2H), 6.88 (s, 2H), 4.9–4.92 (q, *J* = 6.5 Hz, 1H), 4.39 (d, *J* = 2.8 Hz, 1H), 4.24–4.19 (td, *J* = 11.8, 2.5 Hz, 1H), 3.72–3.68 (m, 1H), 3.66–3.63 (m, 1H), 3.56–3.51 (d, *J* = 14.0 Hz, 2H), 3.55–3.48 (d, *J* = 2.8 Hz, 1H), 2.95–2.91 (m, 2H), 2.87–2.85 (d, *J* = 13.9 Hz, 2H), 2.49–2.44 (td, *J* = 11.9, 3.6 Hz, 1H), 1.64–1.60 (m, 4H), 1.47 (d, *J* = 6.6 Hz, 3H), 1.37–1.30 (m, 12H).

2.1.2. General Procedure of Syntheses of Aprepitant Conjugates with DOTA

Each obtained aprepitant-alkylamine derivative (1 equiv.) and the DOTA-NHS ester (1.2 equiv.) were dissolved in 100 µL of DMF, purged from oxygen with technical nitrogen and supplemented with triethylamine (3 equiv.). The reaction mixture was vigorously

stirred overnight at about 50 °C. The progress of the reaction was monitored by HPLC. Afterwards, the reaction mixture was evaporated, dissolved in the HPLC mobile phase and purified by the HPLC method. Each main product was isolated and verified by MS analysis as a desired DOTA conjugate. The purified products were collected and lyophilized. Due to low, sub-microgram scale of reactions, NMR analyses were not possible to be performed.

2-(6-(2-(1,4,7-tris(carboxymethyl)-1,4,7,10-tetraazacyclododecan-10-yl)acetamido) hexyl)-5-([(2*R*,3*S*)-2-((*R*)-1-[3,5-bis(trifluoromethyl)phenyl]ethoxy)-3-(4-fluorophenyl) morpholino]methyl)-1*H*-1,2,4-triazol-3-one, APT-Hex-DOTA, white powder, yield 90.6%, purity > 97% (HPLC-UV; t_R = 17.1 min), ESI-MS: calculated monoisotopic mass for $C_{45}H_{60}F_7N_9O_{10}$: 1019.44; found: 1020.39 *m*/*z* $[M+H]^+$;

2-(8-(2-(1,4,7-tris(carboxymethyl)-1,4,7,10-tetraazacyclododecan-10-yl)acetamido) octyl)-5-([(2*R*,3*S*)-2-((*R*)-1-[3,5-bis(trifluoromethyl)phenyl]ethoxy)-3-(4-fluorophenyl) morpholino]methyl)-1*H*-1,2,4-triazol-3-one, APT-Oct-DOTA, white powder, yield 89.1%, purity > 97% (HPLC-UV; t_R = 17.7 min), ESI-MS: calculated monoisotopic mass for $C_{47}H_{64}F_7N_9O_{10}$: 1047.47; found: 1048.43 *m*/*z* $[M+H]^+$;

2-(10-(2-(1,4,7-tris(carboxymethyl)-1,4,7,10-tetraazacyclododecan-10-yl)acetamido) decyl)-5-([(2*R*,3*S*)-2-((*R*)-1-[3,5-bis(trifluoromethyl)phenyl]ethoxy)-3-(4-fluorophenyl) morpholino]methyl)-1*H*-1,2,4-triazol-3-one, APT-Dec-DOTA, white powder, yield 94.5%, purity > 97% (HPLC-UV; t_R = 18.3 min), ESI-MS: calculated monoisotopic mass for $C_{49}H_{68}F_7N_9O_{10}$: 1075.50; found: 1076.41 *m*/*z* $[M+H]^+$.

2.2. Preparation of Radioconjugates

2.2.1. ^{68}Ga Radiolabeling

For the purpose of specific activity evaluation, different concentrations of APT-Oct-DOTA conjugate (10–25 nmol) dissolved in 410 µL of 0.2 M acetate buffer (pH 4.5) were incubated with a 50 MBq (300 µL) of $[^{68}Ga]GaCl_3$ in 0.1 M HCl from the $^{68}Ge/^{68}Ga$ generator at 95 °C for 10 or 30 min. After this time, each sample was instantly analyzed by HPLC for radiochemical yield (RCY) determination. For the purpose of physiochemical evaluation, each radioconjugate was obtained analogously with 3 MBq/nmol specific activity, purified by HPLC and evaporated.

2.2.2. ^{177}Lu Radiolabeling

For the purpose of specific activity evaluation, different amounts of APT-Oct-DOTA conjugate (0.5–5 nmol) dissolved in 200 µL of 0.2 M acetate buffer (pH 4.5) were incubated with a 5 MBq (5.2–6.7 µL) of $[^{177}Lu]LuCl_3$ in 0.04 M HCl at 95 °C for 10 or 60 min. After this time, each sample was instantly analyzed by HPLC for RCY determination. For the purpose of physiochemical evaluation, each radioconjugate was obtained analogously with 5 MBq/nmol specific activity, purified by HPLC and evaporated. However, for the purpose of biological evaluation all radioconjugates were obtained with 5 MBq/nmol specific activity in diluted 0.02 M acetate buffer (pH 4.5) and directly applied for cellular binding studies without any purification.

2.2.3. Preparation of Non-Radioactive References

The non-radioactive Ga/Lu references were obtained by reaction of 220 µL of a 20 mM $GaCl_3$ or 80 µL of a 20 mM $LuCl_3$ in 0.1 M HCl with 100 nmol of the selected DOTA-conjugate in 300 µL of a 0.2 M acetate buffer (pH = 4.5) for 10 min at 95 °C. Subsequently, reaction products were purified by the HPLC method, lyophilized, and verified by mass spectrometry. Complexation yields for all conjugates were above 97%.

ESI-MS: calculated monoisotopic mass for **Ga-DOTA-Hex-APT,** $C_{45}H_{57}F_7N_9O_{10}Ga$: 1085.34 and 1087.34; found: 1086.54 and 1088.53 *m*/*z* $[M+H]^+$;

ESI-MS: calculated monoisotopic mass for **Ga-DOTA-Oct-APT,** $C_{47}H_{61}F_7N_9O_{10}Ga$: 1113.37 and 1115.37; found: 1114.57 and 1116.57 *m*/*z* $[M+H]^+$;

ESI-MS: calculated monoisotopic mass for **Ga-DOTA-Dec-APT,** $C_{49}H_{65}F_7N_9O_{10}Ga$: 1141.40 and 1143.40; found: 1142.54 and 1144.59 *m*/*z* $[M+H]^+$;

ESI-MS: calculated monoisotopic mass for **Lu-DOTA-Hex-APT,** $C_{45}H_{57}F_7N_9O_{10}Lu$: 1191.35; found: 1192.54 m/z $[M+H]^+$;

ESI-MS: calculated monoisotopic mass for **Lu-DOTA-Oct-APT,** $C_{47}H_{61}F_7N_9O_{10}Lu$: 1219.38; found: 1220.53 m/z $[M+H]^+$;

ESI-MS: calculated monoisotopic mass for **Lu-DOTA-Dec-APT,** $C_{49}H_{65}F_7N_9O_{10}Lu$: 1247.42; found: 1248.59 m/z $[M+H]^+$.

2.3. Physiochemical Evaluation of Radioconjugates

2.3.1. Stability Study

A solution of purified ^{177}Lu-radioconjugate (around 2.5 MBq) in 50 µL of 0.1M DPBS buffer (pH 7.40) was added into 450 µL of human serum and incubated at 37 °C for 7 days. After 1 day and at the end of incubation, the 200 µL of the incubated mixture was added into 400 µL of ethanol, vigorously stirred to precipitate serum proteins, and centrifuged at 13,500 rpm for 5 min to separate the supernatant, which was utilized for HPLC analysis with gamma measurement.

2.3.2. Lipophilicity Study

A solution of purified ^{177}Lu-radioconjugate (around 1 MBq) or ^{68}Ga-radioconjugate (around 10 MBq) in 100 µL of 0.1M DPBS buffer was added into of 900 µL of 0.1 M DPBS buffer and 1000 µL of *N*-octanol (saturated with each other), vigorously stirred and centrifuged at 13,500 rpm for 5 min. Then, similar aliquots of both separated phases were taken for radioactivity measurement using a well-type NaI(Tl) detector. The lipophilicity values were expressed as the decimal logarithm of the distribution coefficient, D, which was calculated as a ratio of the radioconjugate radioactivity in the organic phase to that in the aqueous phase. Each experiment was performed in triplicate and the obtained values averaged. In parallel, the aqueous phases were analyzed by HPLC to confirm the stability of the studied radioconjugate during the experiment time.

2.4. Cell Culture

The Chinese hamster ovary CHO-K1 cell line with a stable overexpression of the human NK1 receptor (hNK1R-CHO cells) were obtained as a gift from Dr. Attila Keresztes and Dr. John M. Streicher [24]. Cells were grown in Ham's F12 medium (Biological Industries, Beit HaEmek, Israel) supplemented with 10% Foetal Bovine Serum (Biological Industries, Beit HaEmek, Israel) and 400 µg/mL G418 (Capricorn Scientific, Ebsdorfergrund, Germany), incubated in a humidified atmosphere with 5% CO_2 at 37 °C.

After reaching almost total confluence, the cells were washed with Dulbecco's PBS (Biological Industries, Beit HaEmek, Israel), detached from the flasks using 0.05% trypsin-EDTA (Biological Industries, Beit HaEmek, Israel) at 37 °C, then diluted with medium and centrifuged for 10 min at 200× *g*. Obtained pellets were resuspended in the medium for the manual calculation of the cell quantity using Trypan Blue Solution (Biological Industries, Beit HaEmek, Israel) contrast.

2.5. Binding Affinity Determination

The saturation binding studies were performed according to the procedure published previously [4] for all ^{177}Lu-radioconjugates obtained according to the common labeling protocol given above with the same specific activity of 5 MBq/nmol. In brief, 10^5 cells per well were seeded into 24-well plates and incubated 24 h before the experiment. Just before the assay, the cells were washed with 37 °C Dulbecco's PBS and then incubated with different concentrations of an analyzed radioconjugate (0.2–50 nM at a final volume) in the medium, with or without a 1000-fold molar excess of blocker (aprepitant or [Thi^8,Met(O_2)^{11}]SP) in relation to the highest radioconjugate concentration applied for 60 min at 37 °C. After incubation time, the assay medium was collected into plastic tubes for radioactivity measurement and the cells were washed twice with ice-cold Dulbecco's

PBS. Subsequently, the cells were lysed using 1 M NaOH and collected into plastic tubes also for radioactivity measurement.

The radioactivity of collected samples were measured using a Wizard2 2-Detector Gamma Counter (PerkinElmer, Waltham, MA, USA). The study data came from three independent experiments done in duplicate. The Kd and BMAX with standard deviations (SD), were calculated using the "One site-total and nonspecific binding" nonlinear regression curve fit (GraphPad Prism 8, GraphPad, San Diego, CA, USA).

2.6. Docking

The complexes of the studied conjugates with the neurokinin 1 receptor were prepared in the following manner. The aprepitant structure (in neutral form) as found in the complex with the NK1R (PDB accession code: 6HLO [23]) was manually expanded by attaching linkers and DOTA moiety to the triazolinone ring. The geometry of DOTA-fragment was adjusted to mimic the geometry of DOTA in the HODCEI entry [25] of The Cambridge Structural Database [26]. This structure is one of the DOTA-Phe-NH_2 complex with Y^{3+}. In our modelling, DOTA carboxylate arms were protonated and frozen in the starting conformation in order to emulate the interactions of DOTA with the cation. Such an approach is hoped to give a rough approximation of the DOTA steric influence on the binding of the conjugates even though properly scaled and validated parameters for modelling and scoring of the complexes with the cations of interest are lacking.

For each compound, several different starting orientations were considered. Such initial complexes were subjected to local search docking in AutoDock 4.2.6 (Scripps Research Institute, La Jolla, CA, USA) [27].

The receptor structure for docking was a refined one (as provided by the GPCRdb service [28]). In this model, the mutated residues have been replaced with the native ones and the side chains missing in the original PDB structure have been added. The structure was pre-processed in AutoDock Tools [27]. The grids were calculated with AutoGrid 4 [27]. The docking box size was 34.5 Å × 34.5 Å × 41.25 Å.

All receptor residues were rigid. The ligands' torsional freedom was allowed, except for the DOTA-fragment, that was frozen in the initial geometry. The docking procedure was the local search with the following parameters: 300 individuals in a population, 500 iterations of the Solis–Wets local search, local search space (*sw_rho* parameter) set to 100.0, and 1000 local search runs. The structures resulting from the local search were clustered and the representative models of the lowest scored (on average) cluster were taken for further analysis.

For qualitative assessment of the binding energy, both the lowest and the mean energy of the clusters were collected.

Molecular graphics were prepared in the Open-Source PyMOL [29] and in the Biovia Discovery Studio Visualizer [30].

3. Results and Discussion

3.1. Syntheses and Characterization of Aprepitant-Based Radioconjugates

3.1.1. Syntheses of Aprepitant Derivative Conjugates

First, we have modified the structure of aprepitant in order to introduce a primary amino group following strategy similar to the one reported previously [1] with the aim of obtaining three new aprepitant-alkylamine derivatives (Scheme 1). Guided by the fact that, the previously obtained alkylamine derivatives were the most promising, we synthesized further homologues in this series with longer aliphatic chains. Afterwards, we have performed the coupling reaction with DOTA-NHS ester to obtain desired aprepitant conjugates. The choice of only one radionuclide chelator was dictated by stability issues evaluated previously [1].

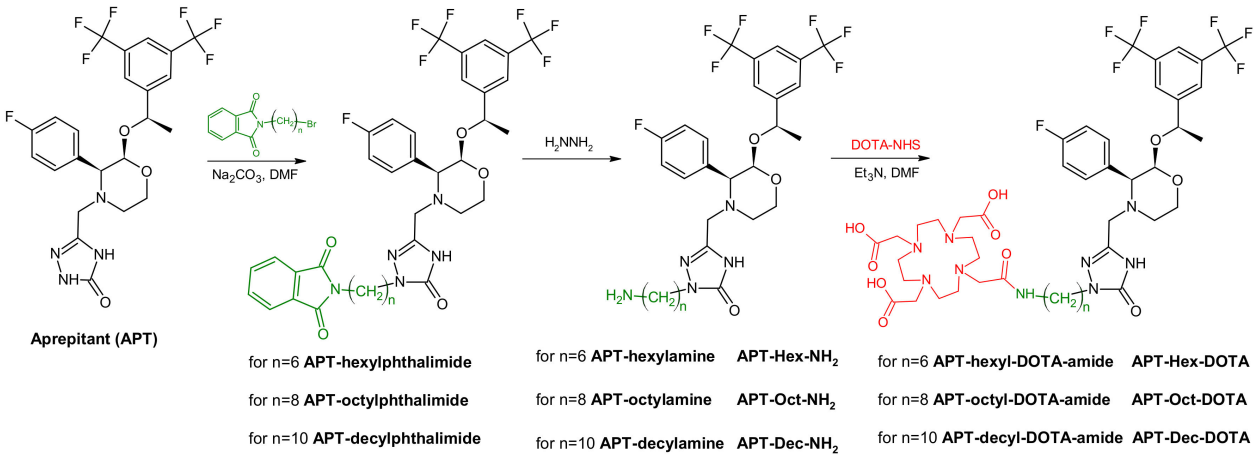

Scheme 1. Synthetic route towards aprepitant derivative conjugates with DOTA chelator via aminoalkyl linkers of various lengths.

3.1.2. Preparation of Radioconjugates and Labeling Optimization

To evaluate the labeling procedure of the obtained aprepitant-DOTA conjugates, 50 MBq of [^{68}Ga]GaCl$_3$ or 5 MBq of [^{177}Lu]LuCl$_3$ were incubated with different amounts (10–25 or 0.5–5 nmol, respectively) of APT-Oct-DOTA conjugate at 95 °C. The labeling RCYs determined at two time points using HPLC with gamma detection are presented in Table 1. The labeling of the APT-Hex-DOTA and APT-Dec-DOTA conjugates were performed under the conditions corresponding to the highest specific activity determined, i.e., 3 MBq/nmol for ^{68}Ga and 5 MBq/nmol for ^{177}Lu. Radiochromatograms of these labeling reactions of the newly obtained aprepitant radioconjugates are presented in Figure 1. All investigated aprepitant conjugates showed an excellent ability to complex metal radioisotopes with a satisfactorily high specific activity for further in vitro evaluation.

Table 1. Radiochemical yields of APT-Oct-DOTA labeling with [^{68}Ga]GaCl$_3$ or [^{177}Lu]LuCl$_3$.

$^{68}Ga^{3+}$	2 MBq/nmol	3 MBq/nmol	4 MBq/nmol	5 MBq/nmol
10 min	>98%	>98%	93.5%	61.2%
30 min	-	-	93.8%	67.6%
$^{177}Lu^{3+}$	**1 MBq/nmol**	**5 MBq/nmol**	**7.5 MBq/nmol**	**10 MBq/nmol**
10 min	>98%	>98%	87.8%	21.9%
60 min	-	-	92.2%	27.0%

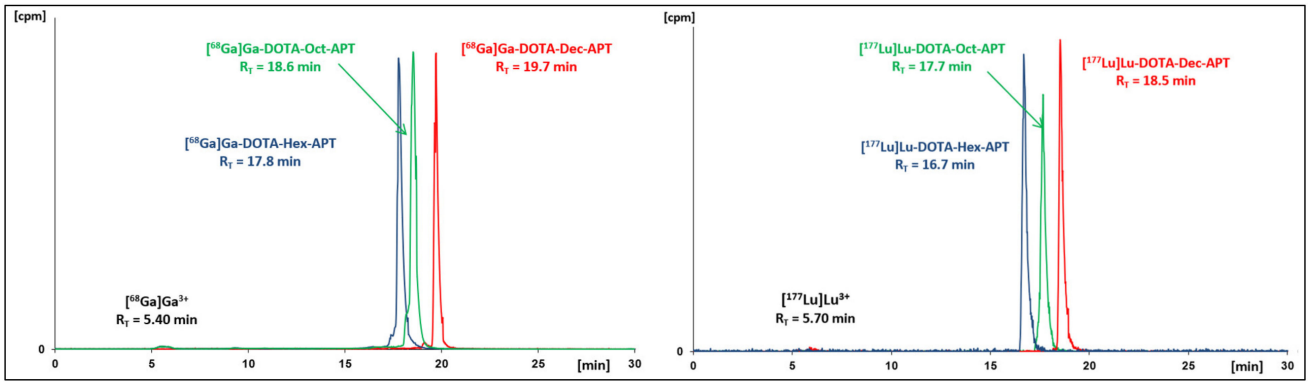

Figure 1. Radiochromatograms of DOTA conjugates with novel aprepitant derivatives radiolabeled with gallium-68 (**left**) or with lutetium-177 (**right**).

At the same time, syntheses of the non-radioactive reference compounds using stable gallium and lutetium were performed to verify the reliability of ^{68}Ga and ^{177}Lu-radioconjugate preparation. These syntheses were carried out in an analogous manner to those with radioactive metals, with the only difference being the use of an excess of metals in their concentrated solutions. The obtained non-radioactive references were purified using HPLC and followed by the characterization using mass spectrometry. The comparison of HPLC retention times (t_R) of corresponding radioactive and stable metal aprepitant conjugates is presented in Table 2. For all pairs of radioconjugate and its non-radioactive reference, the obtained values are compatible (within ±0.1 min), which corroborates the identity of the investigated radioconjugates.

Table 2. Retention times (t_R) of stable metal conjugates and ^{68}Ga/^{177}Lu-radioconjugates of aprepitant derivatives.

Stable Ga/Lu-Conjugate	t_R	^{68}Ga/^{177}Lu-Radioconjugate	t_R
Ga-DOTA-Hex-APT	17.8 min	**[^{68}Ga]Ga-DOTA-Hex-APT**	17.8 min
Ga-DOTA-Oct-APT	18.6 min	**[^{68}Ga]Ga-DOTA-Oct-APT**	18.6 min
Ga-DOTA-Dec-APT	19.7 min	**[^{68}Ga]Ga-DOTA-Dec-APT**	19.7 min
Lu-DOTA-Hex-APT	16.7 min	**[^{177}Lu]Lu-DOTA-Hex-APT**	16.7 min
Lu-DOTA-Oct-APT	17.7 min	**[^{177}Lu]Lu-DOTA-Oct-APT**	17.7 min
Lu-DOTA-Dec-APT	18.4 min	**[^{177}Lu]Lu-DOTA-Dec-APT**	18.5 min

3.2. Physiochemical Evaluation of Radioconjugates

3.2.1. Stability Study

The ^{177}Lu-radioconjugates, purified using the HPLC method and evaporated, were examined as to their stability in human serum (HS). For this purpose, each radioconjugate was mixed with HS and incubated at 37 °C for period of 7 days. At both 1-day and 7-day time points, samples of the radioconjugate mixture were analyzed using the HPLC method for the assessment of the radioconjugate stability. All three novel ^{177}Lu-radioconjugates corroborated their full stability in HS, the same as we reported previously [1].

3.2.2. Lipophilicity Study

All six ^{68}Ga/^{177}Lu-radioconjugates (also purified using the HPLC method and evaporated) were evaluated in terms of their lipophilicity. For each radioconjugate was determined the distribution coefficient (D) between the organic and aqueous phases in the *N*-octanol/DPBS (pH 7.40) system. Simultaneously, the stability of investigated radioconjugate during the experiment was verified through the HPLC analysis of the aqueous phase. The lipophilicity values were established as the logarithm of the distribution coefficient acquired in three independent experiments done in duplicates, and are listed in Table 3.

Table 3. LogD values of aprepitant radioconjugates determined in *n*-octanol/DPBS buffer system.

Radioconjugate	logD	
	^{68}Ga-	^{177}Lu-
APT-Et-DOTA	0.14 ± 0.02 [1]	0.71 ± 0.02 [1]
APT-Pr-DOTA	0.06 ± 0.02 [1]	0.65 ± 0.02 [1]
APT-Bu-DOTA	0.29 ± 0.02 [1]	0.78 ± 0.02 [1]
APT-Hex-DOTA	0.58 ± 0.03	1.23 ± 0.03
APT-Oct-DOTA	1.32 ± 0.04	1.64 ± 0.02
APT-Dec-DOTA	1.60 ± 0.04	1.97 ± 0.02
APT-Ac-HN-NH-DOTA	−1.01 ± 0.02 [1]	−0.40 ± 0.02 [1]
APT-Ac-Et-DOTA	−0.23 ± 0.02 [1]	0.50 ± 0.02 [1]

[1] data taken from ref. [1]

For the newly obtained radiolabeled aprepitant derivatives, an increase in radioconjugate lipophilicity is clearly visible in relation to the previously obtained radioconjugates of aprepitant derivatives with an aliphatic or an acetamide linkers. Thus, an upward trend in the value of lipophilicity for a series of homologues containing an aliphatic linker was revealed, as intuitively expected.

Moreover, exactly the same manner as in the previous studies, novel radioconjugates containing ^{177}Lu were more lipophilic than those with ^{68}Ga; the differences between the radioconjugates obtained from the same precursor being around 0.3–0.65 logD units. Speaking in more detail, it was the first four conjugates containing shorter aliphatic linkers that showed similar differences in lipophilicity between the corresponding ^{68}Ga and ^{177}Lu labeling products (0.5–0.65 logD unit), while for APT-Oct-DOTA and APT-Dec-DOTA derived radioconjugates these differences were twice as low (0.32–0.37 logD unit). For the two pairs of the most lipophilic radioconjugates, namely **[^{68}Ga]Ga/[^{177}Lu]Lu-DOTA-Oct-APT** (logD = 1.32 and 1.64) and **[^{68}Ga]Ga/[^{177}Lu]Lu-DOTA-Dec-APT** (logD = 1.60 and 1.97), the effect of a long aliphatic linker noticeably eliminated the differences resulting from the different structure of the metal-DOTA complexes (cation coordination and the number of carboxylate group employed in metal chelation) and the significant hydrophilic contribution of the macrocyclic chelator to the resultant lipophilicity value of the radioconjugates. This fact may impact on diverse pharmacokinetic profiles among individual aprepitant-based radioconjugates, and the most lipophilic ones may behave similar to the parent drug. Nevertheless, it is difficult to unequivocally assess the ability of the obtained aprepitant radioconjugates to cross the blood–brain barrier. On the one hand, the lipophilicity of compounds is often expected to be a predicting factor for brain penetration, and the most optimal lipophilicity value is in the range of 2.0 to 3.5 [31]. The most lipophilic radioconjugates of aprepitant have slightly lower values than those, however, it should be borne in mind that oncological pathologies of the brain are often accompanied by the disruption of the blood–brain barrier [32].

3.3. Binding Affinity

The saturation binding studies using transfected hNK1R-CHO cells were performed to evaluate the binding characteristics of the ^{177}Lu-radioconjugates of aprepitant derivatives in comparison to reference radioconjugate **[^{177}Lu]Lu-DOTA-[Thi^{8},Met(O$_2$)^{11}]SP**. Obtained results confirm the hypothesis that the functionalization of the aprepitant molecule proposed by us allowed to obtain radiotracers with high binding affinity to the receptor of interest and sensitive to unmodified aprepitant blocking, likewise as is in the case of the reference [Thi^{8},Met(O$_2$)^{11}]SP. All determined K_d and B_{MAX} values for the investigated ^{177}Lu-radioconjugates are presented in Table 4, supplemented with binding curves shown in Figure 2.

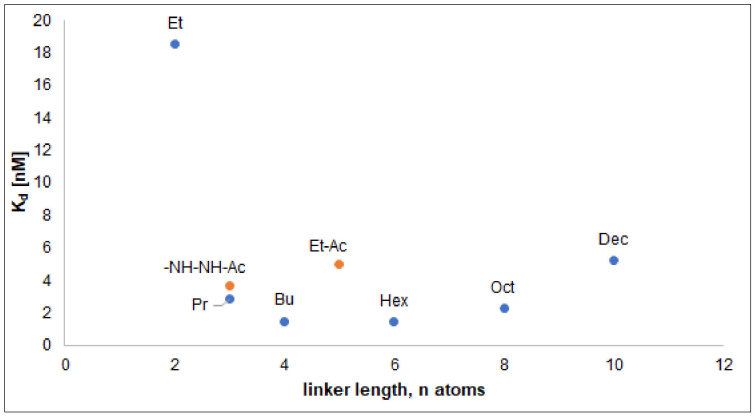

Figure 2. Plot of the K_d values versus the number of carbon atoms in linkers for evaluated ^{177}Lu-radioconjuagtes of all DOTA-aprepitant derivatives. Points are marked with the abbreviations of linkers of the corresponding radioconjugates.

Table 4. Binding characteristics of the ^{177}Lu-radioconjugates of aprepitant derivatives and reference radioconjugate **[^{177}Lu]Lu-DOTA-[Thi^{8},Met(O$_2$)^{11}]SP** to hNK1R-CHO cells.

^{177}Lu-Radioconjugate	$K_d \pm SD$ [1] [nM]	$B_{MAX} \pm SD$ [1] [nM]	Specific Binding [2] [%]
[^{177}Lu]Lu-DOTA-[Thi^{8},Met(O$_2$)^{11}]SP	2.74 ± 0.13	0.38 ± 0.02	85.77 ± 1.44
[^{177}Lu]Lu-DOTA-Et-APT	18.9 ± 1.4	9.16 ± 0.10	92.82 ± 0.20
[^{177}Lu]Lu-DOTA-Pr-APT	2.92 ± 0.31	1.89 ± 0.05	74.04 ± 0.85
[^{177}Lu]Lu-DOTA-Bu-APT	1.66 ± 0.19	1.84 ± 0.16	57.53 ± 1.68
[^{177}Lu]Lu-DOTA-Hex-APT	1.56 ± 0.13	1.88 ± 0.11	57.90 ± 3.07
[^{177}Lu]Lu-DOTA-Oct-APT	2.48 ± 0.09	2.63 ± 0.03	41.67 ± 4.42
[^{177}Lu]Lu-DOTA-Dec-APT	6.26 ± 0.72	3.45 ± 0.10	34.44 ± 5.99
[^{177}Lu]Lu-DOTA-NH-NH-Ac-APT	2.77 ± 0.24	1.24 ± 0.05	77.97 ± 1.37
[^{177}Lu]Lu-DOTA-Et-Ac-APT	5.17 ± 0.18	5.29 ± 0.25	88.52 ± 0.81

[1] The dissociation constant (Kd) and the maximal binding concentration (BMAX) are presented for three independent experiments done in duplicates as averaged values with the standard deviation (SD). Kd and BMAX were calculated using a "One site-total and nonspecific binding" nonlinear regression curve fit by the GraphPad Prism 8 software. [2] Specific binding is presented as a percentage of specific binding to total binding calculated at the 25 nM radioligand concentration.

Binding affinity of all examined ^{177}Lu-radioconjugates and reference radioconjugate **[^{177}Lu]Lu-DOTA-[Thi^{8},Met(O$_2$)^{11}]SP** was relatively similar in low nanomolar range. The only distinctive K_d value was found for the **[^{177}Lu]Lu-DOTA-Et-APT** radioconjugate (containing the shortest aliphatic linker, K_d = 18.9 nM), which was more than threefold worse than that of next in order, determined for **[^{177}Lu]Lu-DOTA-Dec-APT** (K_d = 6.26 nM). The reference **[^{177}Lu]Lu-DOTA-[Thi^{8},Met(O$_2$)^{11}]SP** showed values of K_d and B_{MAX} equal to 2.74 nM and 0.38 nM, respectively, with high specific binding at the level of about 85%.

The highest binding affinities were obtained for **[^{177}Lu]Lu-DOTA-Hex-APT** (K_d = 1.56 nM), **[^{177}Lu]Lu-DOTA-Bu-APT** (K_d = 1.66 nM), and **[^{177}Lu]Lu-DOTA-Oct-APT** (K_d = 2.48 nM). These values were better than the one found for the reference radioconjugate. Then, K_d values similar to K_d value of the reference were found for **[^{177}Lu]Lu-DOTA-NH-NH-Ac-APT** (K_d = 2.77 nM) and **[^{177}Lu]Lu-DOTA-Pr-APT** (K_d = 2.92 nM). Thus, an interesting trend can be observed for radioconjugates with aliphatic linkers (Figure 2), since initially the affinity for the receptor increases with linker lengthening for radioconjugates with butyl and hexyl linker the affinity is optimal, and then it decreases with further elongation of the aliphatic linker in the molecule.

A phenomenon of particular importance is the fact that all eight aprepitant-based radioconjugates showed more than threefold higher binding capacity (B_{MAX} in range from 1.24 to 9.16 nM) than that of the reference SP-based radioconjugate (B_{MAX} = 0.38 nM). Moreover, this is in line with the observation made for a similar comparison of non-peptide L732,138-based radioconjugates to the same reference compound [4].

For all radioconjugates, we also determined the ratio of specific binding to total binding (expressed as a percentage, last column in Table 4) using the values corresponding to the radioconjugate concentration of 25 nM (at this concentration, the plateau generally begins in the specific binding curves, Figure 3). This parameter presents the trend that as the aliphatic linker length increases, the share of specific binding drops in favor of nonspecific binding. Furthermore, for the two most lipophilic radioconjugates, **[^{177}Lu]Lu-DOTA-Oct-APT** and **[^{177}Lu]Lu-DOTA-Dec-APT**, at the concentration of 25 nM, nonspecific binding exceeded specific binding. In terms of the percentage of specific binding, radioconjugates with the lowest lipophilicity look best, **[^{177}Lu]Lu-DOTA-Et-APT** (above 90%), **[^{177}Lu]Lu-DOTA-Et-Ac-APT** (slightly below 90%) as well as **[^{177}Lu]Lu-DOTA-NH-NH-Ac-APT** and **[^{177}Lu]Lu-DOTA-Pr-APT** (both about 75%).

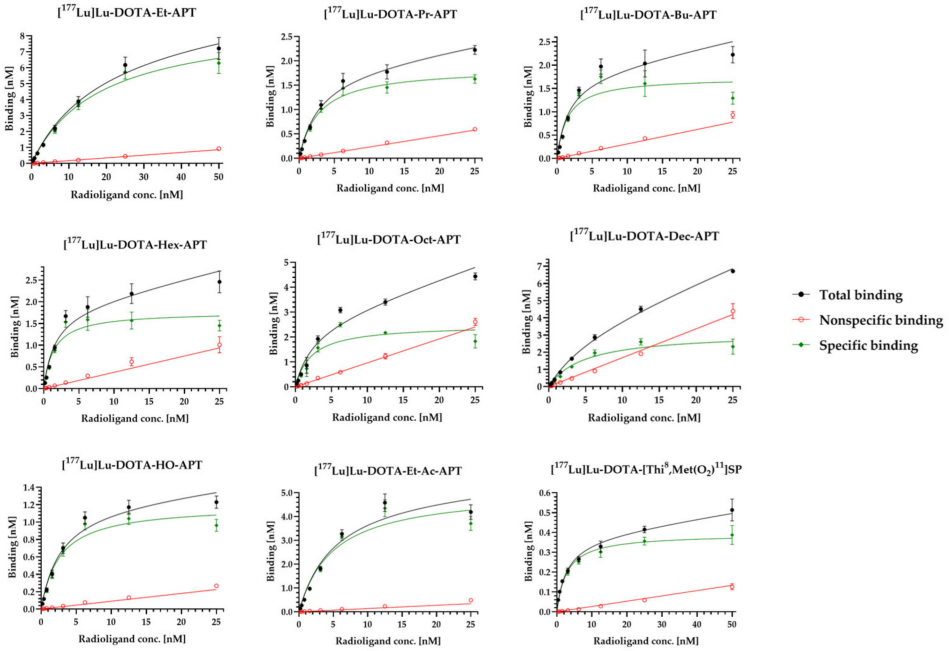

Figure 3. Saturation binding curves for ^{177}Lu-radioconjuagtes of all DOTA-aprepitant derivatives and of reference molecule **DOTA-[Thi^{8},Met(O$_2$)^{11}]SP**. Total binding was measured in the absence and nonspecific binding in the presence of 1000-molar excess of unmodified aprepitant (or [Thi^{8},Met(O$_2$)^{11}]SP peptide) in relation to the highest radioconjugate concentration used. Specific binding was calculated as the difference between total and nonspecific binding (data were acquired in three independent experiments done in duplicate).

3.4. Molecular Modelling Study

In order to rationalize the obtained experimental affinities in terms of ligand-receptor interactions, the conjugates containing aliphatic linkers were modelled in complex with the human NK1R. The aprepitant structure (as found in the crystal with the receptor, PDB accession code: 6HLO [23]) was manually expanded with linker-DOTA fragments and the local search docking was performed in AutoDock 4.2.6 (Scripps Research Institute, La Jolla, CA, USA) [27]. The studied model ligands did not include Lu^{3+} cation, therefore their names are marked with the asterisk, e.g., ***DOTA-Et-APT**, etc.

With all modelled conjugates, the overall architecture of the binding mode is similar (Figure 4). The aprepitant core resides deep in the binding pocket, in a position slightly displaced with regard to the position of aprepitant in the 6HLO crystal structures [23] (Figure 4A, Figures S1–S11 in the Supplementary Materials). A major difference, compared to the small molecular parent, is the rotation of the triazolinone ring (at which the linker fragment is attached) that prevents interactions of this element with E193 and W184. The linker-DOTA fragments of the studied ligands extend towards the binding site outlet (Figure 4B,C). In shorter analogues, the linkers are rather extended and DOTA-moiety is placed close to the extracellular tip of transmembrane helix 5 (TM5) and the extracellular loop 2 (ECL2). On the contrary, in octyl- and decyl-based analogues, the linkers are bent and DOTA-fragment approaches ECL1, TM3 and TM2 (Figure 4C).

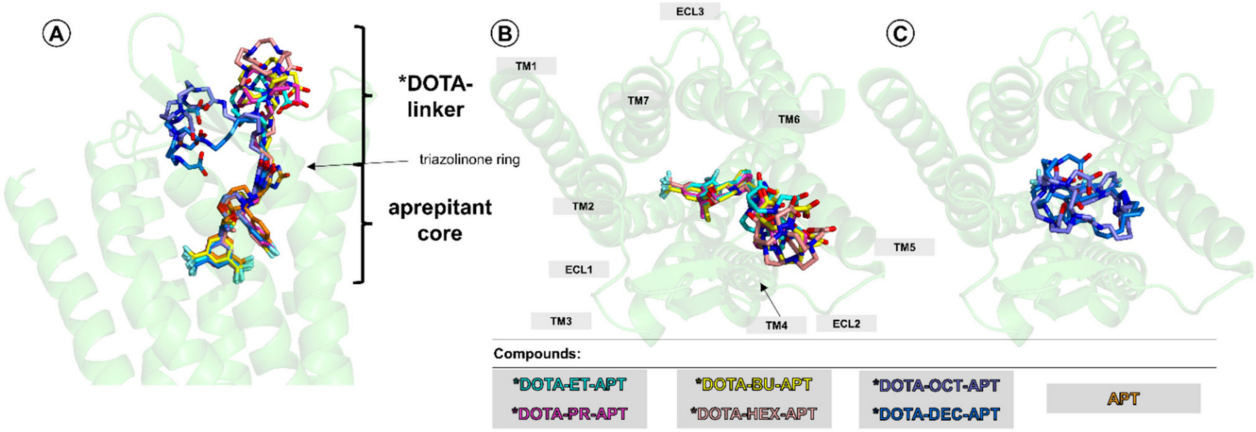

Figure 4. Overall architecture of binding modes of the studied compounds (**A**) side view, superposition of all docked compounds and aprepitant (**B**) top view, superposition of ***DOTA-Et-APT**, ***DOTA-Pr-APT**, ***DOTA-Bu-APT** and ***DOTA-Hex-APT** (**C**) top view, superposition of ***DOTA-Oct-APT** and ***DOTA-Dec-APT**. The receptor (green) is shown in cartoon display (in green; transmembrane helices, TM; extracellular loops, ECL). The ligands are shown as sticks, with colors according to the legend in Figure. Hydrogen display is suppressed.

The binding interactions are discussed below for the ***DOTA-Hex-APT** ligand, which corresponds to **[^{177}Lu]Lu-DOTA-Hex-APT** for which the lowest K_d value was found (Figures 5 and S7). 3,5-bis-trifluoromethylphenyl ring of the ligand forms numerous hydrophobic interactions with M81, N89, P112, V116, I204, W261, M291, A294 and M295. The morpholine ring is hanged between F268 and Q165 side chains. The latter provides further stabilization of the binding mode by hydrogen bonding with the ether oxygen of the ligand. The *p*-fluorophenyl ring stacks with the side chain of F264. Additional contacts of this fragment are to V200, T201 and H265. The triazolinone ring π-stacks with H197. The hexyl linker runs along TM5, contacting K190 and E193. The chelating moiety lays against ECL2, forming interactions with, i.e., M174, M181, E183 and E186.

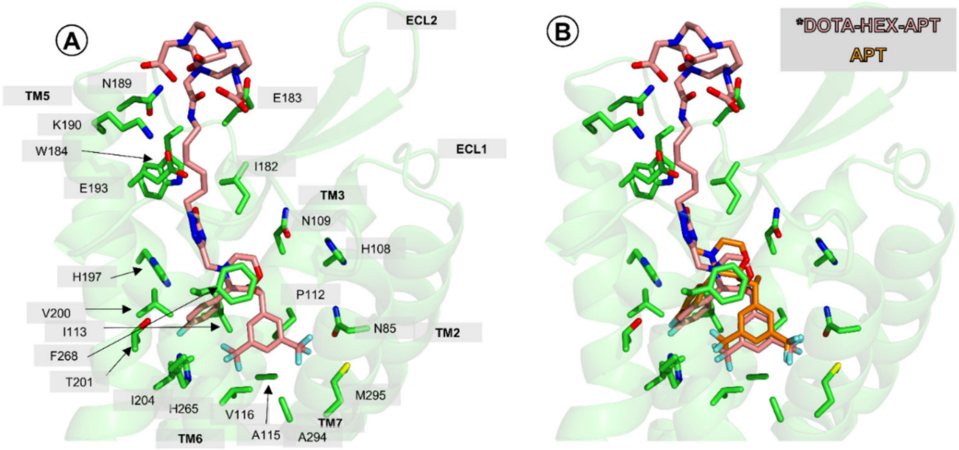

Figure 5. Binding mode of ***DOTA-HEX-APT** in the NK1R binding site. (**A**) The compound alone (salmon sticks) or (**B**) superposed on the crystallographic position of aprepitant (orange sticks). The receptor (green) is shown in cartoon display (in green; transmembrane helices, TM; extracellular loops, ECL). Selected receptor side-chains shown as green sticks. TM1 not shown. Hydrogen display is suppressed.

The interactions of the remaining analogues in the part common to all of them ('aprepitant core') are generally similar to these described for ***DOTA-Hex-APT**, although some details may differ for particular compounds (see Figures S1–S11 for detailed schemes of interactions). The presence of the linker and DOTA fragments has little impact on the

position of the 'aprepitant core', and it is from this very part of the considered molecules that most of the binding strength is likely to come. This finding fits in qualitative terms to the experimental affinities reported in this contribution.

Quantitative prediction of affinities from docking is given in Table 5. Unfortunately, neither the lowest nor the mean predicted binding energies of the best scored cluster correlate with the experimental affinities. This could be associated with artificial overpenalization of conformational freedom for the analogues with long flexible linkers.

Table 5. Predicted binding energies for lowest lying clusters for the docked ligands.

Compound	Predicted Binding Energies [kcal/mol]		Number of Poses in the Cluster
	Lowest	Mean	
***DOTA-Et-APT**	−12.31	−11.9 ± 0.1	1000
***DOTA-Pr-APT**	−13.53	−12.4 ± 0.5	786
***DOTA-Bu-APT**	−12.36	−11.1 ± 0.5	9
***DOTA-Hex-APT**	−10.82	−9.1 ± 0.5	205
***DOTA-Oct-APT**	−9.87	−9.1 ± 0.3	718
***DOTA-Dec-APT**	−10.15	−9.2 ± 0.4	16

The issue of conformational freedom is undoubtedly a limitation of the current modelling study. For the longest analogues, it is very likely that more than one binding mode is realized (with respect to the DOTA-linker fragment). Indeed, the performed docking shows that there are many different (but closely lying in energy) docked clusters (not reported) for the longest analogues. Moreover, in our recent contribution [4], molecular dynamics simulations of small molecular NK1R ligands with long (14 atoms) linkers found significant mobility of the pendant fragment despite relative stability of the deep-bound core. This problem is going to be addressed in the further modelling study. Nevertheless, the binding modes reported herein are going to guide further design work in the field of NK1R-targeted radiopharmaceuticals.

4. Conclusions

The contribution presented herein describes the evaluation of three novel aprepitant-based DOTA conjugates, effectively labeled with ^{68}Ga and ^{177}Lu with high RCY and specific activity. These developed radioconjugates were characterized by high lipophilicity and full stability in human serum. In vitro investigation on binding characteristics towards NK1R of novel ^{177}Lu-radioconjugates showed their high receptor affinity (K_d = 1.56–6.26 nM), but concomitantly revealed significant non-specificity (up to 60% of specific binding).

At the same time, most of previously reported radioconjugates based on less lipophilic aprepitant derivatives presented much the same high receptor affinity (K_d = 1.66–5.17 nM) like the reference **[^{177}Lu]Lu-DOTA-[Thi^{8},Met(O$_2$)^{11}]SP** (K_d = 2.74 nM), however, with the binding capacity more than three times higher (B_{MAX} = 1.24–5.29 nM) in relation to the SP-based reference radioconjugate (B_{MAX} = 0.38 nM). Furthermore, it was the radioconjugates with the lowest lipophilicity that had the highest specific binding rate (75% and above), at a level comparable to that of the reference radioconjugate.

Assessing the overall properties of all eight radiopharmaceuticals developed, in particular the lipophilicity parameter and the tendency to decrease the share of specific binding with an increase in the length of the aliphatic linker, the most promising radiopharmaceutical seem to be **[^{177}Lu]Lu-DOTA-Pr-APT** radioconjugate, containing three CH_2 groups in the aliphatic linker between the radionuclide complex and an aprepitant molecule.

In conclusion, our efforts confirmed the assumptions about the effectiveness of aprepitant in the role of a NK1R targeting vector, in particular referring to ^{177}Lu-labeled Substance P derivative currently used in clinical therapy. An application of this NK1R antagonist in nuclear medicine may initiate a potential alternative approach to NK1R-positive cancer imaging following intravenous administration. The reported results provide the encouraging perspectives for the future first in vivo trials.

Supplementary Materials: The following supporting information can be downloaded at: https://www.mdpi.com/article/10.3390/pharmaceutics14030607/s1. Figure S1. Scheme of the interactions of ***DOTA-Et-APT** with the NK1R. Figure S2. Binding mode of ***DOTA-Et-APT** in the NK1R (general view). Figure S3. Scheme of the interactions of ***DOTA-Pr-APT** with the NK1R. Figure S4. Binding mode of ***DOTA-Pr-APT** in the NK1R (general view). Figure S5. Scheme of the interactions of ***DOTA-Bu-APT** with the NK1R. Figure S6. Binding mode of ***DOTA-Bu-APT** in the NK1R (general view). Figure S7. Scheme of the interactions of ***DOTA-Hex-APT** with the NK1R. Figure S8. Scheme of the interactions of ***DOTA-Oct-APT** with the NK1R. Figure S9. Binding mode of ***DOTA-Oct-APT** in the NK1R (general view). Figure S10. Scheme of the interactions of ***DOTA-Dec-APT** with the NK1R. Figure S11. Binding mode of ***DOTA-Dec-APT** in the NK1R (general view).

Author Contributions: Conceptualization, P.K.H. and P.F.J.L.; methodology, P.K.H. and P.F.J.L.; software, P.K.H. and P.F.J.L.; formal analysis, P.K.H. and P.F.J.L.; investigation, P.K.H.; writing—original draft preparation, P.K.H. and P.F.J.L.; writing—review and editing, J.M., P.K. and E.G.; visualization, P.K.H. and P.F.J.L.; supervision, E.G.; project administration, A.M. and E.G.; funding acquisition, A.M. and E.G. All authors have read and agreed to the published version of the manuscript.

Funding: This research was funded by National Science Centre (Poland), grant number 2017/25/B/NZ7/01896.

Institutional Review Board Statement: Not applicable.

Informed Consent Statement: Not applicable.

Data Availability Statement: Not applicable.

Acknowledgments: The authors gratefully acknowledge Attila Keresztes and John M. Streicher from the University of Arizona for sharing the hNK1-CHO cells. The contribution of Paweł Krzysztof Halik has been done in the frame of the National Centre for Research and Development Project No POWR.03.02.00-00-I009/17 (Radiopharmaceuticals for molecularly targeted diagnosis and therapy, RadFarm. Operational Project Knowledge Education Development 2014–2020 co-financed by European Social Fund). The molecular modelling was performed using the resources of the Świerk Computing Centre, National Centre for Nuclear Research, Świerk, Poland.

Conflicts of Interest: The authors declare no conflict of interest.

Abbreviations

6HLO	accession code of coordinates and structure factors in PDB
APT	aprepitant
B_{MAX}	maximal binding parameter
CHO	Chinese hamster ovaries cell line
D	distribution coefficient
DMF	dimethylformamide
DOTA	1,4,7,10-tetraazacyclododecane-1,4,7,10-tetraacetic acid
DPBS	Dulbecco's phosphate-buffered saline buffer
ECL	extracellular loop
ESI	electrospray ionization
hNK1R	human neurokinin 1 receptor
HS	human serum
K_d	dissociation constant
logD	logarithm of the distribution coefficient
MS	mass spectrometry
NHS	*N*-hydroxysuccinimide moiety
NK1R	neurokinin 1 receptor, tachykinin 1 receptor
PDB	Protein Data Bank
RCY	radiochemical yield
SD	standard deviation
SP	Substance P
TFA	trifluoroacetic acid
TM	transmembrane helix
t_R	retention time

References

1. Halik, P.K.; Lipiński, P.F.J.; Matalińska, J.; Koźmiński, P.; Misicka, A.; Gniazdowska, E. Radiochemical synthesis and evaluation of novel radioconjugates of neurokinin 1 receptor antagonist aprepitant dedicated for NK1R-Positive tumors. *Molecules* **2020**, *25*, 3756. [CrossRef] [PubMed]
2. Zhang, H.; Kanduluru, A.K.; Desai, P.; Ahad, A.; Carlin, S.; Tandon, N.; Weber, W.A.; Low, P.S. Synthesis and evaluation of a novel ^{64}Cu- and ^{67}Ga-labeled neurokinin 1 receptor antagonist for in vivo targeting of NK1R-Positive tumor xenografts. *Bioconjug. Chem.* **2018**, *29*, 1319–1326. [CrossRef] [PubMed]
3. Kanduluru, A.K.; Srinivasarao, M.; Wayua, C.; Low, P.S. Evaluation of a neurokinin-1 receptor–targeted technetium-99m conjugate for neuroendocrine cancer imaging. *Mol. Imaging Biol.* **2019**, *22*, 377–383. [CrossRef] [PubMed]
4. Matalińska, J.; Kosińska, K.; Halik, P.K.; Koźmiński, P.; Lipiński, P.F.J.; Gniazdowska, E.; Misicka, A. Novel NK1R-targeted ^{68}Ga-/^{177}Lu-radioconjugates with potential application against glioblastoma multiforme: Preliminary exploration of structure–activity relationships. *Int. J. Mol. Sci.* **2022**, *23*, 1214. [CrossRef] [PubMed]
5. Kneifel, S.; Cordier, D.; Good, S.; Ionescu, M.C.S.; Ghaffari, A.; Hofer, S.; Kretzschmar, M.; Tolnay, M.; Apostolidis, C.; Waser, B.; et al. Local targeting of malignant gliomas by the diffusible peptidic vector 1,4,7,10-tetraazacyclododecane-1-glutaric acid-4,7,10-triacetic acid-substance P. *Clin. Cancer Res.* **2006**, *12*, 3843–3850. [CrossRef] [PubMed]
6. Królicki, L.; Bruchertseifer, F.; Kunikowska, J.; Koziara, H.; Królicki, B.; Jakuciński, M.; Pawlak, D.; Apostolidis, C.; Mirzadeh, S.; Rola, R.; et al. Safety and efficacy of targeted alpha therapy with 213Bi-DOTA-substance P in recurrent glioblastoma. *Eur. J. Nucl. Med. Mol. Imaging* **2018**, *46*, 614–622. [CrossRef] [PubMed]
7. Królicki, L.; Kunikowska, J.; Bruchertseifer, F.; Koziara, H.; Królicki, B.; Jakuciński, M.; Pawlak, D.; Rola, R.; Morgenstern, A.; Rosiak, E.; et al. ^{225}Ac- and ^{213}Bi-substance P analogues for glioma therapy. *Semin. Nucl. Med.* **2020**, *50*, 141–151. [CrossRef]
8. De Araújo, E.B.; Pujatti, P.B.; Mengatti, J. Radiolabeling of substance P with lutetium-177 and biodistribution study in AR42J pancreatic tumor xenografted nude mice. *Cell. Mol. Biol.* **2010**, *56*, 12–17.
9. Bossaller, C.; Reither, K.; Hehlert-Friedrich, C.; Auch-Schwelk, W.; Graf, K.; Gräfe, M.; Fleck, E. In vivo measurement of endothelium-dependent vasodilation with substance P in man. *Herz* **1992**, *17*, 284–290.
10. Muñoz, M.; Coveñas, R. Involvement of substance P and the NK-1 receptor in cancer progression. *Peptides* **2013**, *48*, 1–9. [CrossRef]
11. Garcia-Recio, S.; Fuster, G.; Fernandez-Nogueira, P.; Pastor-Arroyo, E.M.; Park, S.Y.; Mayordomo, C.; Ametller, E.; Mancino, M.; Farré, X.G.; Russnes, H.G.; et al. Substance P autocrine signaling contributes to persistent HER2 activation that drives malignant progression and drug resistance in breast cancer. *Cancer Res.* **2013**, *73*, 6424–6434. [CrossRef]
12. Muñoz, M.; Coveñas, R. The neurokinin-1 receptor antagonist aprepitant, a new drug for the treatment of hematological malignancies: Focus on acute myeloid leukemia. *J. Clin. Med.* **2020**, *9*, 1659. [CrossRef]
13. Muñoz, M.; Coveñas, R. The neurokinin-1 receptor antagonist aprepitant: An intelligent bullet against cancer? *Cancers* **2020**, *12*, 2682. [CrossRef]
14. Palma, C.; Nardelli, F.; Manzini, S.; Maggi, C.A. Substance P activates responses correlated with tumour growth in human glioma cell lines bearing tachykinin NK1 receptors. *Br. J. Cancer* **1998**, *79*, 236–243. [CrossRef]
15. Akazawa, T.; Kwatra, S.G.; Goldsmith, L.E.; Richardson, M.D.; Cox, E.A.; Sampson, J.H.; Kwatra, M.M. A constitutively active form of neurokinin 1 receptor and neurokinin 1 receptor-mediated apoptosis in glioblastomas. *J. Neurochem.* **2009**, *109*, 1079–1086. [CrossRef]
16. Cordier, D.; Gerber, A.; Kluba, C.; Bauman, A.; Hutter, G.; Mindt, T.L.; Mariani, L. Expression of different neurokinin-1 receptor (NK1R) isoforms in glioblastomamultiforme: Potential implications for targeted therapy. *Cancer Biother. Radiopharm.* **2014**, *29*, 221–226. [CrossRef]
17. Berger, M.; Neth, O.; Ilmer, M.; Garnier, A.; Salinas-Martín, M.V.; de Agustín Asencio, J.C.; von Schweinitz, D.; Kappler, R.; Muñoz, M. Hepatoblastoma cells express truncated neurokinin-1 receptor and can be growth inhibited by aprepitant in vitro and in vivo. *J. Hepatol.* **2014**, *60*, 985–994. [CrossRef]
18. Muñoz, M.; Rosso, M.; Coveñas, R. The NK-1 receptor: A new target in cancer therapy. *Curr. Drug Targets* **2011**, *12*, 909–921. [CrossRef]
19. Muñoz, M.; Coveñas, R.; Esteban, F.; Redondo, M. The substance P/NK-1 receptor system: NK-1 receptor antagonists as anti-cancer drugs. *J. Biosci.* **2015**, *40*, 441–463. [CrossRef]
20. Majkowska-Pilip, A.; Halik, P.K.; Gniazdowska, E. The significance of NK1 receptor ligands and their application in targeted radionuclide tumour therapy. *Pharmaceutics* **2019**, *11*, 443. [CrossRef]
21. Merck. Product Information. Emend (Aprepitant). 2003. Available online: https://www.merck.com/product/usa/pi_circulars/e/emend/emend_pi.pdf (accessed on 13 January 2022).
22. Majumdar, A.K.; Howard, L.; Goldberg, M.R.; Hickey, L.; Bs, M.C.; Rothenberg, P.L.; Crumley, T.M.; Panebianco, D.; Bradstreet, T.E.; Bergman, A.J.; et al. Pharmacokinetics of aprepitant after single and multiple oral doses in healthy volunteers. *J. Clin. Pharmacol.* **2006**, *46*, 291–300. [CrossRef]
23. Schöppe, J.; Ehrenmann, J.; Klenk, C.; Rucktooa, P.; Schütz, M.; Doré, A.S.; Plückthun, A. Crystal structures of the human neurokinin 1 receptor in complex with clinically used antagonists. *Nat. Commun.* **2019**, *10*, 1–11. [CrossRef]
24. Starnowska, J.; Costante, R.; Guillemyn, K.; Popiolek-Barczyk, K.; Chung, N.N.; Lemieux, C.; Keresztes, A.; Van Duppen, J.; Mollica, A.; Streicher, J.; et al. Analgesic properties of opioid/NK1 multitarget ligands with distinct in vitro profiles in naive and chronic constriction injury (CCI)-mice. *ACS Chem. Neurosci.* **2017**, *8*, 2315–2324. [CrossRef]

25. Heppeler, A.; Froidevaux, S.; Mäcke, H.R.; Jermann, E.; Béhé, M.; Powell, P.; Hennig, M. Radiometal-labelled macrocyclic chelator-derivatised somatostatin analogue with superb tumour-targeting properties and potential for receptor-mediated internal radiotherapy. *Chem. Eur. J.* **1999**, *5*, 1974–1981. [CrossRef]
26. Allen, F.H. The cambridge structural database: A quarter of a million crystal structures and rising. *Acta Crystallogr. Sect. B Struct. Sci.* **2002**, *58*, 380–388. [CrossRef]
27. Morris, G.M.; Huey, R.; Lindstrom, W.; Sanner, M.F.; Belew, R.K.; Goodsell, D.S.; Olson, A.J. AutoDock4 and AutoDockTools4: Automated docking with selective receptor flexibility. *J. Comput. Chem.* **2009**, *30*, 2785–2791. [CrossRef]
28. Kooistra, A.J.; Mordalski, S.; Pándy-Szekeres, G.; Esguerra, M.; Mamyrbekov, A.; Munk, C.; Keserű, G.M.; E Gloriam, D. GPCRdb in 2021: Integrating GPCR sequence, structure and function. *Nucleic Acids Res.* **2020**, *49*, D335–D343. [CrossRef]
29. Schrödinger LLC. The PyMOL Molecular Graphics System. 2018. Available online: https://sourceforge.net/p/pymol/code/HEAD/tree/trunk/pymol/ (accessed on 1 November 2020).
30. *Biovia Discovery Studio Visualizer*, Version 19; Dassault Systèmes: San Diego, CA, USA, 2018.
31. Waterhouse, R.N. Determination of lipophilicity and its use as a predictor of blood–brain barrier penetration of molecular imaging agents. *Mol. Imaging Biol.* **2003**, *5*, 376–389. [CrossRef]
32. Wolburg, H.; Noell, S.; Fallier-Becker, P.; Mack, A.F.; Wolburg-Buchholz, K. The disturbed blood–brain barrier in human glioblastoma. *Mol. Asp. Med.* **2012**, *33*, 579–589. [CrossRef]

Spis literatury

1. Majkowska-Pilip, A.; Halik, P.K.; Gniazdowska, E. The Significance of NK1 Receptor Ligands and Their Application in Targeted Radionuclide Tumour Therapy. *Pharmaceutics* **2019**, *11*, 443.
2. Halik, P.K.; Gniazdowska, E.; Koźmiński, P.; et al.. ^{68}Ga- and ^{177}Lu-radiopharmaceuticals based on neurokinin-1 receptor antagonist SPANTIDE I (5-11) peptide for glioblastoma multiforme treatment. *INCT Annual Report 2017* **2017**, 25.
3. Halik, P.K.; Lipiński, P.F.J.; Matalińska, J.; et al. Radiochemical Synthesis and Evaluation of Novel Radioconjugates of Neurokinin 1 Receptor Antagonist Aprepitant Dedicated for NK1R-Positive Tumors. *Molecules* **2020**, *25*, 3756.
4. Matalińska, J.; Kosińska, K.**;** Halik, P.K.; et al. Novel NK1R-Targeted ^{68}Ga-/^{177}Lu-Radioconjugates with Potential Application against Glioblastoma Multiforme: Preliminary Exploration of Structure–Activity Relationships. *Int. J. Mol. Sci.* **2022**, *23*, 1214.
5. Halik, P.K.; Koźmiński, P.; Matalińska, J.; et al. E. In Vitro Biological Evaluation of Aprepitant Based ^{177}Lu-Radioconjugates. *Pharmaceutics* **2022**, *14*, 607.
6. Vallabhajosula, S.; Owunwanne, A. Pathophysiology and Mechanisms of Radiopharmaceutical Localization. Rozdział w: The Pathophysiologic Basis of Nuclear Medicine. **2006**, *second edition*.
7. Stöcklin, G.; Qaim, S.M.; Rösch, F. The Impact of Radioactivity on Medicine. *Radiochim. Acta* **1995**, *70*, 249.
8. Vallabhajosula, S.; Killeen, R.P.; Osborne, J.R. Altered biodistribution of radiopharmaceuticals: role of radiochemical/pharmaceutical purity, physiological, and pharmacologic factors. *Semin. Nucl. Med.* **2010**, *40*, 220.
9. Alavi, A.; Lakhami, P.; Mavi, A.; et al. PET: a revolution in medical imaging. *Radiol. Clin. North Am.* **2004**, *42*, 983.
10. Volkert, W.A.; Hoffman, T.J. Therapeutic radiopharmaceuticals. *Chem. Rev.* **1999**, *99*, 2269.
11. Quality Control in the Production of Radiopharmaceuticals. IAEA-TECDOC1856, **2018**. Dostęp online (02-03-2022): www-pub.iaea.org/MTCD/Publications/PDF/TE-1856web.pdf
12. Doherty, J.; Graham, D. The Radiopharmacy. Rozdział w: Practical Nuclear Medicine. **2005**, *third edition.*
13. Radiopharmaceutical preparations. Monografia ogólna 0125 w Farmakopei Europejskiej 10.0.
14. Ramogida, C.F.; Orvig, C. Tumour targeting with radiometals for diagnosis and therapy. *Chem. Commun.* **2013**, *49*, 4720.
15. Zeglis, B.M.; Lewis, J.S. A practical guide to the construction of radiometallated bioconjugates for positron emission tomography. *Dalton Trans.* **2011**, *40*, 6168.
16. Kassis, A.I. Therapeutic radionuclides: biophysical and radiobiologic principles. *Semin. Nucl. Med.* **2008**, *38*, 358.
17. Qaim, S.M.; Scholten, B.; Neumaier, B. New developments in the production of theranostic pairs of radionuclides. *J. Radioanal. Nucl. Chem*. **2018**, *318*, 1493.
18. Tolmachev, V.; Stone-Elander, S. Radiolabelled proteins for positron emission tomography: Pros and cons of labelling methods. *Biochim. Biophys. Acta* **2010**, *1800*, 487.
19. Kluba, C.A.; Bauman, A.; Valverde, I.E.; et al. Dual-targeting conjugates designed to improve the efficacy of radiolabeled peptides. *Org. Biomol. Chem.* **2012**, 10, 7594.
20. Dong, C.; Zhao, H.; Yang, S.; et al. ^{99m}Tc-labeled dimeric octreotide peptide: a radiotracer with high tumor uptake for single-photon emission computed tomography imaging of somatostatin receptor subtype 2-positive tumors. *Mol. Pharm.* **2013**, 10, 2925.

21. Majkowska-Pilip, A.; Gawęda, W.; Żelechowska-Matysiak, K.; et al. Nanoparticles in Targeted Alpha Therapy. *Nanomaterials* **2020**, *10*, 1366.
22. Forstrom, L.A.; Mullan, B.P.; Hung, J.C.; et al. ^{18}F-FDG labelling of human leukocytes. *Nucl. Med. Commun.* **2000**, *21*, 691.
23. Srivastava, S.C.; Chervu, L.R. Radionuclide-labeled red blood cells: current status and future prospects. *Semin. Nucl. Med.* **1984**, *14*, 68.
24. Alviar, M.; Miranda, J.; Bedregal, P. A proposal of excipients mixture for the elaboration of Na^{131}I capsules. *J. Radioanal. Nucl. Chem.* **2020**, *325*, 857.
25. Donohoe, K.J.; Maurer, A.H.; Ziessman, H.A.; et al. Procedure guideline for adult solid-meal gastric-emptying study 3.0. *J. Nucl. Med. Technol.* **2009**, *37*, 196.
26. Garin, E.; Rolland, Y.; Boucher, E.; et al. First experience of hepatic radioembolization using microspheres labelled with yttrium-90 (TheraSphere): practical aspects concerning its implementation. *Eur. J. Nucl. Med. Mol. Imaging* **2010**, *37*, 453.
27. Evbuomwan, O.; Purbhoo, K.; Vangu, M.D.T. A prospective study comparing ^{99m}Tc-MIBI and ^{99m}Tc-MDP with ^{99m}Tc-DTPA for lung ventilation scintigraphy in pulmonary thromboembolism. *Nucl. Med. Commun.* **2018**, *39*, 1103.
28. Suga, K.; Kawakami, Y.; Yamashita, T.; et al. Characterization of ^{133}Xe gas washout in pulmonary emphysema with dynamic 133Xe SPECT functional images. *Nucl. Med. Commun*. **2006**, *27*, 71.
29. Kumar, L.; Harish, P.; Malik, P.S.; et al. Chemotherapy and targeted therapy in the management of cervical cancer. *Curr. Probl. Cancer* **2018**, *42*, 120.
30. Gudkov, S.V.; Shilyagina, N.Y.; Vodeneev, V.A.; et al. Targeted Radionuclide Therapy of Human Tumors. *Int. J. Mol. Sci.* **2016**, *17*, 33.
31. Goldsmith, S.J. Targeted Radionuclide Therapy: A Historical and Personal Review. *Semin. Nucl. Med.* **2020**, *50*, 87.
32. Artigas, C.; Mileva, M.; Flamen, P.; et al. Targeted radionuclide therapy: an emerging field in solid tumours. *Curr. Opin. Oncol.* **2021**, *33*, 493.
33. Kratochwil, C.; Flechsig, P.; Lindner, T.; et al. ^{68}Ga-FAPI PET/CT: tracer uptake in 28 different kinds of cancer. *J. Nucl. Med.* **2019**, *60*, 801.
34. Baskar, R.; Lee, K.A.; Yeo, R.; et al. Cancer and Radiation Therapy: Current Advances and Future Directions. *Int. J. Med. Sci.* **2012**, *9*, 193.
35. Pouget, J.P.; Lozza, C.; Deshayes, E.; et al. Introduction to radiobiology of targeted radionuclide therapy. *Front. Med.* **2015**, *2*, 12.
36. Bedard, P.L.; Hyman, D.M.; Davids, M.S.; et al. Small molecules, big impact: 20 years of targeted therapy in oncology. *Lancet* **2020**, *395*, 1078.
37. Koper, K.; Wileński, S.; Koper, A. Advancements in cancer chemotherapy. *Phys. Sci. Rev.* **2021.**
38. Williams, L.E.; DeNardo, G.L.; Meredith, R.F. Targeted radionuclide therapy. *Med. Phys.* **2008**, *35*, 3062.
39. Cardinal Health Review No. 22 on FDA approved radiopharmaceuticals Dostęp online (02-03-2022): www.cardinalhealth.com/content/dam/corp/web/documents/fact-sheet/cardinal-health-fda-approved-radiopharmaceuticals.pdf
40. Chandran, E.; Figg, W.D.; Madan, R. Lutetium-177-PSMA-617: A Vision of the Future. *Cancer Biol. Ther.* **2022**, *23*, 186.
41. Kratochwil, C.; Giesel, F.L.; Stefanova, M. et al. PSMA-Targeted Radionuclide Therapy of Metastatic Castration-Resistant Prostate Cancer with ^{177}Lu-Labeled PSMA-617. *J. Nucl. Med.* **2016**, *57*, 1170.

42. Kratochwil, C.; Bruchertseifer, F.; Giesel, F.L. et al. ^{225}Ac-PSMA-617 for PSMA-Targeted α-Radiation Therapy of Metastatic Castration-Resistant Prostate Cancer. *J. Nucl. Med.* **2016**, *57*, 1941.
43. Kratochwil, C.; Haberkorn, U.; Giesel, F.L. ^{225}Ac-PSMA-617 for Therapy of Prostate Cancer. *Semin. Nucl. Med.* **2020**, *50*, 133.
44. Scott, A. 2018 SNMMI Highlights Lecture: Oncology and Therapy, Part 2. *Nucl. Med.* **2019**, *60*, 7N.
45. Mirzadeh, S.; Mausner, L.F.; Garland, M.A. Reactor-Produced Medical Radionuclides. Rozdział w: Handbook of Nuclear Chemistry. **2011**, *second edition*.
46. Qaim, S.M. Nuclear data for production and medical application of radionuclides: Present status and future needs. *Nucl. Med. Biol.* **2017**, *44*, 31.
47. Haddad, F.; Ferrer, L.; Guertin, A.; et al. ARRONAX, a high-energy and high-intensity cyclotron for nuclear medicine *Eur. J. Nucl. Med. Mol. Imaging* **2008**, *35*, 1377.
48. Roesch, F.; Riss, P.J. The renaissance of the ^{68}Ge/^{68}Ga radionuclide generator initiates new developments in ^{68}Ga radiopharmaceutical chemistry. *Curr. Top. Med. Chem.* **2010**, *10*, 1633.
49. Live Chart of Nuclides, nuclear structure and decay data, IAEA Nuclear Data Section. Dostęp online (02-03-2022): www-nds.iaea.org/relnsd/vcharthtml/VChartHTML.html
50. Goodhead, D.T. Mechanisms for the biological effectiveness of high-LET radiations. *J. Radiat. Res.* **1999**, *40*, S1.
51. Nikjoo, H.; Munson, R.J.; Bridges, B.A. RBE-LET relationships in mutagenesis by ionizing radiation. *J. Radiat. Res.* **1999**, *40*, S85.
52. Aghevlian, S.; Boyle, A.J.; Reilly, R.M. Radioimmunotherapy of cancer with high linear energy transfer (LET) radiation delivered by radionuclides emitting α-particles or Auger electrons. *Adv. Drug Deliv. Rev*. **2017**, *109*, 102.
53. Tavitian, B. Oligonucleotides as radiopharmaceuticals. Rozdział w: Molecular Imaging. **2005**, *first edition*.
54. Gee, A.D.; Bongarzone, S.; Wilson, A.A. Small Molecules as Radiopharmaceutical Vectors. Rozdział w: Radiopharmaceutical Chemistry. **2019**, *first edition*.
55. Vermeulen, K.; Vandamme, M.; Bormans, G.; et al. Design and Challenges of Radiopharmaceuticals. *Semin. Nucl. Med.* **2019**, *49*, 339.
56. Knowles, S.M.; Zettlitz, K.A.; Tavare, R.; et al. Quantitative immunoPET of prostate cancer xenografts with ^{89}Zr- and ^{124}I-labeled anti-PSCA A11 minibody. *J. Nucl. Med.* **2014**, *55*, 452.
57. Kratochwil, C.; Giesel, F.L.; Bruchertseifer, F.; et al. ^{213}Bi-DOTATOC receptor-targeted alpha-radionuclide therapy induces remission in neuroendocrine tumours refractory to beta radiation: a first-in-human experience. *Eur. J. Nucl. Med. Mol. Imaging* **2014**, *41*, 2106.
58. Younes, C.K.; Boisgard, R.; Tavitian, B. Labelled oligonucleotides as radiopharmaceuticals: pitfalls, problems and perspectives. *Curr. Pharm. Des*. **2002**, *8*, 1451.
59. Viola-Villegas, N.T.; Sevak, K.K.; Carlin, S.D.; et al. Noninvasive imaging of PSMA in prostate tumors with ^{89}Zr-labeled huJ591 engineered antibody fragments: the faster alternatives. *Mol. Pharm.* **2014**, *11*, 3965.
60. Wong, D.F.; Pomper, M. P. Predicting the success of a radiopharmaceutical for in vivo imaging of central nervous system neuroreceptor systems. *Mol. Imaging Biol.* **2003**, *5*, 350.
61. Saha, G.B. Radiopharmaceuticals and Methods of Radiolabeling. Rozdział w: Fundamentals of Nuclear Pharmacy. **2010**, *Sixth Edition*.
62. Boll, R.A.; Malkemus, D.; Mirzadeh, S. Production of actinium-225 for alpha particle mediated radioimmunotherapy. *Appl. Radiat. Isot.* **2005**, 62, 667.

63. Peltek, O.O.; Muslimov, A.R.; Zyuzin, M.V.; et al. Current outlook on radionuclide delivery systems: from design consideration to translation into clinics. *J. Nanobiotechnology* **2019**, *17*, 90.
64. Phelps, M.E. Molecular imaging with positron emission tomography. *Annu. Rev. Nucl. Part. Sci.* **2002**, *52*, 303.
65. Wadas, T.J.; Wong, E.H.; Weisman, G.R.; et al. Coordinating radiometals of copper, gallium, indium, yttrium, and zirconium for PET and SPECT imaging of disease. *Chem. Rev.* **2010**, *110*, 2858.
66. Madsen, M.T. Recent advances in SPECT imaging. *J. Nucl. Med.* **2007**, *48*, 661.
67. Carter, L.M.; Poty, S.; Sharma, S.K.; et al. Preclinical optimization of antibody-based radiopharmaceuticals for cancer imaging and radionuclide therapy-Model, vector, and radionuclide selection. *J. Labelled Comp. Radiopharm*. **2018**, *61*, 611.
68. Blower, P.J. A nuclear chocolate box: the periodic table of nuclear medicine. *Dalton Trans.* **2015**, *44*, 4819.
69. Miller, P.W.; Long, N.J.; Vilar, R.; et al. Synthesis of ^{11}C, ^{18}F, ^{15}O, and ^{13}N radiolabels for positron emission tomography. *Angew. Chem. Int. Ed. Engl*. **2008**, *47*, 8998.
70. Chaple, I.F.; Lapi, S.E. Production and Use of the First-Row Transition Metal PET Radionuclides ^{43,44}Sc, ^{52}Mn, and ^{45}Ti. *J. Nucl. Med.* **2018**, *59*, 1655.
71. Papagiannopoulou, D. Technetium-99m radiochemistry for pharmaceutical applications. *J. Labelled Comp. Radiopharm.* **2017**, *60*, 502.
72. Alberto, R.; Braband, H.; Nadeem, Q. Bioorganometallic Technetium and Rhenium Chemistry: Fundamentals for Applications. *Chimia* **2020**, *74*, 953.
73. Liu, S.; Edwards, D.S. Bifunctional chelators for therapeutic lanthanide radiopharmaceuticals. *Bioconjug. Chem.* **2001**, *12*, 7.
74. Liu, Y.; Liu, G.; Hnatowich, D.J. A Brief Review of Chelators for Radiolabeling Oligomers. *Materials* **2010**, *3*, 3204.
75. Cai, Z.; Anderson, C.J. Chelators for copper radionuclides in positron emission tomography radiopharmaceuticals. *J. Labelled Comp. Radiopharm.* **2014**, *57*, 224.
76. Yu, M.D.; Huang, W.S.; Cherng, C.C.; et al. The effect of formulation on reduced radioiodide thyroid uptake. *J. Nucl. Med.* **2002**, *43*, 56.
77. Biological test for sterility. Rozdział ogólny 2.6.1. w Farmakopei Europejskiej 10.0.
78. Biological test for pyrogens. Rozdział ogólny 2.6.8. w Farmakopei Europejskiej 10.7.
79. Biological test for bacterial endotoxins. Rozdział ogólny 2.6.14 w Farmakopei Europejskiej 10.0.
80. Coenen, H.H.; Gee, A.D.; Adam, M.; et al. Consensus nomenclature rules for radiopharmaceutical chemistry - Setting the record straight. *Nucl. Med. Biol*. **2017**, *55*, v.
81. Breeman, W.A.P.; de Jong, M.; Visser, T.J.; et al. Optimising conditions for radiolabelling of DOTA-peptides with ^{90}Y, ^{111}In and ^{177}Lu at high specific activities. *Eur. J. Nucl. Med. Mol. Imaging* **2003**, *30*, 917.
82. Wadas, T.J.; Anderson, C.J. Radiolabeling of TETA- and CB-TE2A-conjugated peptides with copper-64. *Nat. Protoc.* **2006**, *1*, 3062.
83. Chakravarty, R.; Chakraborty, S.; Dash, A.; et al. Detailed evaluation on the effect of metal ion impurities on complexation of generator eluted ^{68}Ga with different bifunctional chelators. *Nucl. Med. Biol*. **2013**, *40*, 197.
84. Cole, W.C.; DeNardo, S.J.; Meares, C.F.; et al. Comparative serum stability of radiochelates for antibody radiopharmaceuticals. *J. Nucl. Med.* **1987**, *28*, 83.

85. Bass, L.A.; Wang, M.; Welch, M.J.; et al. In vivo transchelation of copper-64 from TETA-octreotide to superoxide dismutase in rat liver. *Bioconjug. Chem*. **2000**, *11*, 527.
86. Liu, S.; Ellars, C.E.; Edwards, D.S. Ascorbic acid: useful as a buffer agent and radiolytic stabilizer for metalloradiopharmaceuticals. *Bioconjug. Chem*. **2003**, *14*, 1052.
87. de Blois, E.; Chan, H.S.; Konijnenberg, M.; et al. Efectiveness of quenchers to reduce radiolysis of ^{111}In- or ^{177}Lu-labelled methionine-containing regulatory peptides. Maintaining radiochemical purity as measured by HPLC. *Curr. Top. Med. Chem.* **2012**, *12*, 2677.
88. de Zanger, R.M.S.; Chan, H.S.; Breeman, W.A.P.; et al. Maintaining radiochemical purity of [^{177}Lu]Lu-DOTA-PSMA-617 for PRRT by reducing radiolysis. *J. Radioanal. Nucl. Chem.* **2019**, *321*, 285.
89. Ponto, J. A review of radiopharmaceutical formulation problems and their clinical manifestations. Rozdział w: Correspondence continuing education courses for nuclear pharmacists and nuclear medicine professions. **1993**, *Volume II, Number 3*.
90. Breeman, W.A.; de Jong, M.; Kwekkeboom, D.J.; et al. Somatostatin receptor-mediated imaging and therapy: basic science, current knowledge, limitations and future perspectives. *Eur. J. Nucl. Med.* **2001**, *28*, 1421.
91. Rousseau, E.; Lau, J.; Kuo, H.T.; et al. Monosodium Glutamate Reduces ^{68}Ga-PSMA-11 Uptake in Salivary Glands and Kidneys in a Preclinical Prostate Cancer Model. *J. Nucl. Med.* **2018**, *59*, 1865.
92. Rolleman, E.J.; Valkema, R.; de Jong, M.; et al. Safe and effective inhibition of renal uptake of radiolabelled octreotide by a combination of lysine and arginine. *Eur. J. Nucl. Med. Mol. Imaging* **2003**, *30*, 9.
93. Xiong, C.; Yin, D.; Li, J.; et al. Metformin Reduces Renal Uptake of Radiotracers and Protects Kidneys from Radiation-Induced Damage. *Mol. Pharm.* **2019**, *16*, 808.
94. Tönnesmann, R.; Meyer, P.T.; Eder, M.; Baranski, A.C. [^{177}Lu]Lu-PSMA-617 Salivary Gland Uptake Characterized by Quantitative In Vitro Autoradiography. *Pharmaceuticals* **2019**, *12*, 18.
95. Harsini, S.; Saprunoff, H.; Alden, T.; et al. The Effects of Monosodium Glutamate on PSMA Radiotracer Uptake in Men with Recurrent Prostate Cancer: A Prospective, Randomized, Double-Blind, Placebo-Controlled Intraindividual Imaging Study. *J. Nucl. Med*. **2021**, *62*, 81.
96. Saleem, A.; Aboagye, E.O.; Price, P.M. In vivo monitoring of drugs using radiotracer techniques. *Adv. Drug Deliv. Rev.* **2000**, *41*, 21.
97. Jaffer, F.A.; Weissleder, R. Molecular imaging in the clinical arena. *JAMA* **2005**, *293*, 855.
98. Yuan, Z.; Lu, F.M. PET/SPECT molecular imaging in clinical neuroscience: recent advances in the investigation of CNS diseases. *Quant Imaging Med. Surg*. **2015**, *5*, 433.
99. Maggi, C.A. The mammalian tachykinin receptors. *Gen. Pharmacol*. **1995**, *26*, 911.
100. Roush, E.D.; Kwatra, M.M. Human substance P receptor expressed in Chinese hamster ovary cells directly activates G($\alpha_{q/11}$), G(α_s), G(α_o). *FEBS Lett*. **1998**, *428*, 291.
101. Fong, T.M.; Anderson, S.A.; Yu, H.; et al. Differential activation of intracellular effector by two isoforms of human neurokinin-1 receptor. *Mol. Pharmacol*. **1992**, *41*, 24.
102. Cordier, D.; Gerber, A.; Kluba, C.; et al. Expression of different neurokinin-1 receptor (NK1R) isoforms in glioblastoma multiforme: potential implications for targeted therapy. *Cancer Biother Radiopharm* **2014**, *29*, 221.
103. Tuluc, F.; Lai, J.P.; Kilpatrick, L.E.; Neurokinin 1 receptor isoforms and the control of innate immunity. *Trends Immunol*. **2009**, *30*, 271.
104. Yin, J.; Chapman, K.; Clark, L.D.; et al. Crystal structure of the human NK 1 tachykinin receptor. *Proc. Natl. Acad. Sci. USA* **2018**, *115*, 13264.

105. Mai, J.K.; Stephens, P.H.; Hopf, A.; et al. Substance P in the human brain. *Neuroscience* **1986**, *17*, 709.
106. Ribeiro-da Silva, A.; Hökfelt, T. Neuroanatomical localisation of Substance P in the CNS and sensory neurons. *Neuropeptides* **2000**, *34*, 256.
107. Bergström, M.; Hargreaves, R.J.; Burns, H.D.; et al. Human positron emission tomography studies of brain neurokinin 1 receptor occupancy by aprepitant. *Biol. Psychiatry* **2004**, *55*, 1007.
108. Mistrova, E.; Kruzliak, P.; Chottova-Dvorakova, M. Role of substance P in the cardiovascular system. *Neuropeptides*, **2016**, *58*, 41.
109. Garcia-Recio, S.; Gascon, P. Biological and Pharmacological Aspects of the NK1-Receptor. *Biomed. Res. Int*. **2015**, *2015*, 495704.
110. Lecci, A.; Capriati, A.; Altamura, M.; et al. Tachykinins and tachykinin receptors in the gut, with special reference to NK2 receptors in human. *Auton. Neurosci*. **2006**, *126*, 232.
111. Holzer, P. Neurogenic vasodilatation and plasma leakage in the skin. *Gen. Pharmacol*. **1998**, *30*, 5.
112. Kramer, M.S.; Cutler, N.; Feighner, J.; et al. Distinct mechanism for antidepressant activity by blockade of central substance P receptors. *Science* **1998**, *281*, 1640.
113. Muñoz, M.; Rosso, M.; Coveñas, R. The NK-1 Receptor: A New Target in Cancer Therapy. *Curr. Drug Targets* **2011**, *12*, 909-921.
114. Chang, M.M.; Leeman, S.E.; Niall, H.D. Amino-acid sequence of substance P. *Nat. New. Biol.* **1971**, *232*, 86.
115. Werge, T. The tachykinin tale: molecular recognition in a historical perspective. *J. Mol. Recognit.* **2007**, *20*, 145.
116. Mantyh, P.W.; Rogers, S.D.; Honore, P.; et al. Inhibition of hyperalgesia by ablation of lamina I spinal neurons expressing the substance P receptor. *Science* **1997**, *278*, 275.
117. De Felipe, C.; Herrero, J.F.; O'Brian, J.A.; et al. Altered nociception, analgesia and aggression in mice lacking the receptor for substance P. *Nature* **1998**, *392*, 394.
118. Nichols, M.L.; Allen, B.J.; Rogers, S.D.; et al. Transmission of chronic nociception by spinal neurons expressing the substance P receptor. *Science* **1999**, *286*, 1558.
119. Lewin, G.R.; Mendell, L.M. Nerve growth factor and nociception. *TINS* **1993**; *16*: 353.
120. Bozic, C.R.; Lu, B.; Höpken, U.E.; et al. Neurogenic amplification of immune complex inflammation. *Science* **1996**, *273*, 1722.
121. Bossaller, C.; Reither, K.; Hehlert-Friedrich, C.; et al. In vivo measurement of endothelium-dependent vasodilation with substance P in man. *Herz* **1992**, *17*, 284.
122. Watson, J.W.; Gonsalves, S.F.; Fossa, A.A.; et al. The anti-emetic effects of CP-99,994 in the ferret and the dog: role of the NK1 receptor. *Br. J. Pharmacol*. **1995**, *115*, 84.
123. Navari, R.M.; Reinhardt, R.R.; Gralla, R.J.; et al. Reduction of cisplatin-induced emesis by a selective neurokinin-1-receptor antagonist. L-754,030 Antiemetic Trials Group. *N. Engl. J. Med.* **1999**, *340*, 190.
124. Ebner, K.; Singewald, N. The role of substance P in stress and anxiety responses. *Amino Acids* **2006**, *31*, 251.
125. Benarroch, E.E.; Schmeichel, A.M.; Low, P.A.; et al. Depletion of ventromedullary NK-1 receptor-immunoreactive neurons in multiple system atrophy. *Brain* **2003**, *126*, 2183.
126. Chen, L.W.; Yung, K.K.L.; Chan, Y.S. Neurokinin peptides and neurokinin receptors as potential therapeutic intervention targets of basal ganglia in the prevention and treatment of Parkinson's disease. *Curr. Drug Targets* **2004**, *5*, 197.

127. Severini, C.; Petrella, C.; Calissano, P. Substance P and Alzheimer's Disease: Emerging Novel Roles. *Curr. Alzheimer Res*. **2016**, *13*, 964.
128. Palma, C.; Nardelli, F.; Manzini, S.; et al. Substance P activates responses correlated with tumour growth in human glioma cell lines bearing tachykinin NK1 receptors. *Br. J. Cancer* **1999**, *79*, 236.
129. Muñoz, M., and Coveñas, R. Involvement of substance P and the NK-1 receptor in cancer progression. *Peptides* **2013**, *48*, 1.
130. Steinhof, M.S.; von Mentzer, B.; Geppetti, P.; et al. Tachykinins and their receptors: contributions to physiological control and the mechanisms of disease. *Physiol. Rev*. **2014**, *94*, 265.
131. Fukuhara, S.; Shimizu, M.; Matsushima, H.; et al. Signaling pathways via NK1 receptors and their desensitization in an AR42J cell line. *Peptides* **1998**, *19*, 1349.
132. Nakajima, Y.; Tsuchida, K.; Negishi, M.; et al. Direct linkage of three tachykinin receptors to stimulation of both phosphatidylinositol hydrolysis and cyclic AMP cascades in transfected Chinese hamster ovary cells. *J. Biol. Chem*. **1992**, *267*, 2437.
133. Garcia, M.; Sakamoto, K.; Shigekawa, M.; et al. Multiple mechanisms of arachidonic acid release in Chinese hamster ovary cells transfected with cDNA of substance P receptor. *Biochem. Pharmacol*. **1994**, 48, 1735.
134. Meshki. J.; Douglas, S.D.; Lai, J.P.; et al. Neurokinin 1 receptor mediates membrane blebbing in HEK293 cells through a Rho/Rho-associated coiled-coil kinase-dependent mechanism. *J. Biol. Chem.* **2009**, *284*, 9280.
135. Lai, J.P.; Lai, S.; Tuluc, F.; et al. Differences in the length of the carboxyl terminus mediate functional properties of neurokinin-1 receptor. *Proc. Natl. Acad. Sci. USA* **2008**, *105*, 12605.
136. Spitsin, S.; Pappa, V.; Douglas, S.D. Truncation of neurokinin-1 receptor-Negative regulation of substance P signaling. *J. Leukoc. Biol.* **2018**, *103*, 1043.
137. DeFea, K.A.; Vaughn, Z.D.; O'Brian, E.M.; et al. The proliferative and antiapoptotic effects of substance P are facilitated by formation of a beta-arrestin-dependent scaffolding complex. *Proc. Natl. Acad. Sci. USA* **2000**, 97, 11086.
138. Zhou, Y.; Zhao, L.; Xiong, T.; et al. Roles of full-length and truncated neurokinin-1 receptors on tumor progression and distant metastasis in human breast cancer. *Breast Cancer Res. Treat*. **2013**, *140*, 61.
139. Pohl, A.; Kappler, R.; Muhling, J.; et al. Expression of truncated neurokinin-1 receptor in childhood neuroblastoma is independent of tumor biology and stage. *Anticancer Res.* **2017**, *37*, 6079.
140. Santos, R.; Ursu, O.; Gaulton, A.; et al. A comprehensive map of molecular drug targets. *Nat. Rev. Drug Discov*. **2017**, *16*, 19.
141. Muñoz, M.; Coveñas, R.; Esteban, F.; et al. The substance P/NK-1 receptor system: NK-1 receptor antagonists as anti-cancer drugs. *J. Biosci*. **2015**, *40*, 441.
142. Javid, H.; Mohammadi, F.; Zahiri, E.; et al. The emerging role of substance P/neurokinin-1 receptor signaling pathways in growth and development of tumor cells. *J. Physiol. Biochem*. **2019**, *75*, 415.
143. Muñoz, M.; Coveñas, R. The neurokinin-1 receptor antagonist aprepitant, a new drug for the treatment of hematological malignancies: Focus on acute myeloid leukemia. *J. Clin. Med.* **2020**, *9*, 1659.
144. Muñoz, M.; Coveñas, R. The Neurokinin-1 Receptor Antagonist Aprepitant: An Intelligent Bullet against Cancer? *Cancers* **2020**, *12*, 2682.

145. Medrano, S.; Gruenstein, E.; Dimlich, R.V. Substance P receptors on human astrocytoma cells are linked to glycogen breakdown. *Neurosci. Lett.* **1994**, *167*, 14.
146. Garcia-Recio, S.; Fuster, G.; Fernandez-Nogueira, P.; et al. Substance P autocrine signaling contributes to persistent HER2 activation that drives malignant progression and drug resistance in breast cancer. *Cancer Res*. **2013**, *73*, 6424.
147. Ziche, M.; Morbidelli, L.; Pacini, M.; et al. Substance P stimulates neovascularization in vivo and proliferation of cultured endothelial cells. *Microvasc. Res.* **1990**, *40*, 264.
148. Luo, W.; Sharif, T.R.; Sharif, M. Substance P-induced mitogenesis in human astrocytoma cells correlates with activation of the mitogen-activated protein kinase signaling pathway. *Cancer Res.* **1996**, *56*, 4983.
149. Esteban, F.; Gonzalez-Moles, M.A.; Castro, D.; et al. Expression of substance P and neurokinin-1-receptor in laryngeal cancer: linking chronic inflammation to cancer promotion and progression. *Histopathology* **2009**, *54*, 258.
150. Davoodian, M.; Boroumand, N.; Mehrabi, M.; et al. Evaluation of serum level of substance P and tissue distribution of NK-1 receptor in breast cancer. *Mol. Biol. Rep*. **2019**, *46*, 1285.
151. Lorestani, S.; Ghahremanloo, A.; Jangjoo, A.; et al. Evaluation of serum level of substance P and tissue distribution of NK-1 receptor in colorectal cancer. *Mol. Biol. Rep*. **2020**, *47*, 3469.
152. Gillespie, E.; Leeman, S.E.; Watts, L.A.; et al. Truncated neurokinin-1 receptor is increased in colonic epithelial cells from patients with colitis-associated cancer. *Proc. Natl. Acad. Sci. USA* **2011**, *108*, 17420.
153. Berger, M.; Neth, O.; Ilmer, M.; et al. Hepatoblastoma cells express truncated neurokinin-1 receptor and can be growth inhibited by aprepitant in vitro and in vivo. *J. Hepatol*. **2014**, *60*, 985.
154. Molinos-Quintana, A.; Trujillo-Hacha, P.; Piruat, J.I.; et al. Human acute myeloid leukemia cells express neurokinin-1 receptor, which is involved in the antileukemic effect of neurokinin-1 receptor antagonists. *Invest. New Drugs* **2019**, *37*, 17.
155. Zhang, L.; Wang, L.; Dong, D.; et al. miR-34b/c-5p and the neurokinin-1 receptor regulate breast cancer cell proliferation and apoptosis. *Cell Prolif*. **2019**, *52*, e12527.
156. Zhou, Y.; Wang, L.; Wang, N.; et al. TGFβ regulates NK1R-Tr to affect the proliferation and apoptosis of breast cancer cells. *Life Sci*. **2020**, *256*, 117674.
157. Hennig, I.M.; Laissue, J.A.; Horisberger, U.; et al. Substance-P receptors in human primary neoplasms: tumoral and vascular localization. *Int. J. Cancer* **1995**, *61*, 786.
158. González-Moles, M.A.; Brener, S.; Ruiz-Avila, I.; et al. Substance P and NK-1R expression in oral precancerous epithelium. *Oncol. Rep.* **2009**, *22*, 1325.
159. Feng, F.; Yang, J.; Tong, L.; et al. Substance P immunoreactive nerve fibres are related to gastric cancer differentiation status and could promote proliferation and migration of gastric cancer cells. *Cell Biol. Int*. **2011**, *35*, 623.
160. Misawa, K.; Kanazawa, T.; Misawa, Y.; et al. Frequent promoter hypermethylation of tachykinin-1 and tachykinin receptor type 1 is a potential biomarker for head and neck cancer. *J. Cancer Res. Clin. Oncol*. **2013**, *139*, 879.
161. Ma, J.; Yuan, S.; Cheng, J.; et al. Substance P promotes the progression of endometrial adenocarcinoma. *Int. J. Gynecol. Cancer* **2016**, *26*, 845.
162. Cordier, D.; Merlo, A. Long-Term Results of Targeted Low-Grade Glioma Treatment with ^{213}Bi-DOTA-[Thi^{8},Met(O$_2$)^{11}]-Substance P. *Cancer Biother. Radiopharm*. **2019**, *34*, 413.

163. Królicki, L.; Bruchertseifer, F.; Kunikowska, J.; et al. Safety and efficacy of targeted alpha therapy with ^{213}Bi-DOTA-substance P in recurrent glioblastoma. *Eur. J. Nucl. Med. Mol. Imaging* **2019**, *46*, 614.
164. Królicki, L.; Kunikowska, J.; Bruchertseifer, F.; et al. ^{225}Ac- and ^{213}Bi-Substance P Analogues for Glioma Therapy. *Semin. Nucl. Med.* **2020**, *50*, 141.
165. Weller, M.; Wick, W.; Aldape, K.; et al. Glioma. *Nat. Rev. Dis. Primers* **2015**, *1*, 15017.
166. Mawrin, C.; Schulz, S.; Pauli, S.U.; et al. Differential expression of sst1, sst2A, and sst3 somatostatin receptor proteins in low-grade and high-grade astrocytomas. *J. Neuropathol. Exp. Neurol*. **2004**, *63*, 13.
167. He, J.H.; Wnag, J.; Yang, Y.Z.; et al. SSTR2 is a prognostic factor and a promising therapeutic target in glioma. *Am. J. Transl. Res.* **2021**, *13*, 11223.
168. Merlo, A.; Hausmann, O.; Wasner, M.; et al. Locoregional regulatory peptide receptor targeting with the diffusible somatostatin analogue ^{90}Y-labeled DOTA^{0}-D-Phe^{1}-Tyr^{3}-octreotide (DOTATOC): a pilot study in human gliomas. *Clin. Cancer Res.* **1999**, *5*, 1025.
169. Schumacher, T.; Hofer, S.; Eichhorn, K.; et al. Local injection of the ^{90}Y-labelled peptidic vector DOTATOC to control gliomas of WHO grades II and III: an extended pilot study. *Eur. J. Nucl. Med. Mol. Imaging* **2002**, *29*, 486.
170. Hofer, S.; Eichhorn, K.; Freitag, P.; et al. Successful diffusible brachytherapy (dBT) of a progressive low-grade astrocytoma using the locally injected peptidic vector and somatostatin analogue [^{90}Y]-DOTA^{0}-D-Phe^{1}-Tyr^{3}-octreotide (DOTATOC). *Swiss Med. Wkly*. **2001**, *131*, 640.
171. Akazawa, T.; Kwatra, S.G.; Goldsmith, L.E.; et al. A constitutively active form of neurokinin 1 receptor and neurokinin 1 receptor-mediated apoptosis in glioblastomas. *J. Neurochem*. **2009**, *109*, 1079.
172. Kneifel, S.; Cordier, D.; Good, S.; et al. Local Targeting of Malignant Gliomas by the Diffusible Peptidic Vector 1,4,7,10-Tetraazacyclododecane-1-Glutaric Acid-4,7,10-triacetic acid-Substance P. *Clin. Cancer Res.* **2006**, *12*, 3843.
173. Cordier, D.; Forrer, F.; Kneifel, S.; et al. Neoadjuvant targeting of glioblastoma multiforme with radiolabeled DOTAGA-substance P--results from a phase I study. *J. Neurooncol*. **2010**, *100*, 129.
174. van Hagen, P.M.; Breeman, W.A.; Reubi, J.C.; et al. Visualization of the thymus by substance P receptor scintigraphy in man. *Eur. J. Nucl. Med*. **1996**, *23*, 1508.
175. Sandberg, B.E.; Lee, C.M.; Hanley, M.R.; et al. Synthesis and biological properties of enzyme-resistant analogues of substance P. *Eur. J. Biochem.* **1981**, *114*, 329.
176. Chorev, M.; Rubini, E.; Hart, Y.; et al. Metabolically stable analogues of substance P: persistent action of partially modified retro-inverso analogues of substance P on rat parotid and hypothalamic slices. *Eur. J. Pharmacol*. **1986**, *127*, 187.
177. Majkowska-Pilip, A.; Koźmiński, P.; Wawrzynowska, A.; et al. Application of Neurokinin-1 Receptor in Targeted Strategies for Glioma Treatment. Part I: Synthesis and Evaluation of Substance P Fragments Labeled with ^{99m}Tc and ^{177}Lu as Potential Receptor Radiopharmaceuticals. *Molecules* **2018**, *23*, 2542.
178. Cordier, D.; Forrer, F.; Bruchertseifer, F.; et al. Targeted alpha-radionuclide therapy of functionally critically located gliomas with ^{213}Bi-DOTA-[Thi^{8},Met(O$_2$)^{11}]-substance P: a pilot trial. *Eur. J. Nucl. Med. Mol. Imaging* **2010**, *37*, 1335.
179. Królicki, L.; Bruchertseifer, F.; Kunikowska, J.; et al. Prolonged survival in secondary glioblastoma following local injection of targeted alpha therapy with ^{213}Bi-substance P analogue. *Eur. J Nucl. Med. Mol. Imaging* **2018**, *45*, 1636.

180. Majkowska-Pilip, A.; Rius, M.; Bruchertseifer, F.; et al. In vitro evaluation of ^{225}Ac-DOTA-substance P for targeted alpha therapy of glioblastoma multiforme. *Chem. Biol. Drug Des*. **2018**, *92*, 1344.
181. Królicki, L.; Bruchertseifer, F.; Kunikowska, J.; et al. Dose escalation study of targeted alpha therapy with [^{225}Ac]Ac-DOTA-substance P in recurrence glioblastoma - safety and efficacy. *Eur. J. Nucl. Med. Mol. Imaging* **2021**, *48*, 3595.
182. Skidgel, R.A.; Erdös, E.G. Cleavage of peptide bonds by angiotensin I converting enzyme. *Agents Actions Suppl*. **1987**, *22*, 289.
183. Wang, L.H.; Ahmad, S.; Benter, I.F.; et al. Differential processing of substance P and neurokinin A by plasma dipeptidyl(amino)peptidase IV, aminopeptidase M and angiotensin converting enzyme. *Peptides* **1991**, *12*, 1357.
184. Waterhouse, R.N. Determination of Lipophilicity and its use as a predictor of blood–brain barrier penetration of molecular imaging agents. *Mol. Imaging Biol.* **2003**, *5*, 376.
185. Folkers, K.; Hakanson, R.; Hörig, J.; et al. Biological evaluation of substance P antagonists. *Br. J. Pharmacol*. **1984**, *83*, 449.
186. Beaujouan, J.C.; Heuillet, E.; Petitet, F.; et al. Higher potency of RP 67580, in the mouse and the rat compared with other nonpeptide and peptide tachykinin NK1 antagonists. *Br. J. Pharmacol*. **1993**, *108*, 793.
187. Janecka, A.; Poels, J.; Fichna, J.; et al. Comparison of antagonist activity of spantide family at human neurokinin receptors measured by aequorin luminescence-based functional calcium assay. *Regul. Pept*. **2005**, *131*, 23.
188. Hökfelt, T.; Vincent, S.; Hellsten, L.; et al. Immunohistochemical evidence for a "neurotoxic" action of (D-Pro^{2}, D-Trp^{7,9})-substance P, an analogue with substance P antagonistic activity. *Acta Physiol. Scand*. **1981**, *113*, 571.
189. Hale, J.J.; Mills, S.G.; MacCoss, M.; et al. 2(S)-((3,5-bis(trifluoromethyl)benzyl)-oxy)-3(S)-phenyl-4-((3-oxo-1,2,4-triazol-5-yl)methyl)morpholine (1): a potent, orally active, morpholine-based human neurokinin-1 receptor antagonist. *J. Med. Chem*. **1996**, *39*, 1760.
190. Dionne, R.A.; Max, M.B.; Gordon, S.M.; et al. The substance P receptor antagonist CP-99,994 reduces acute postoperative pain. *Clin. Pharmacol. Ther*. **1998**, *64*, 562.
191. Hesketh, P.J.; Gralla, R.J.; Webb, R.T.; et al. Randomized Involvement of substance P and the NK-1 receptor 1747 123 Phase II study of the neurokinin 1 receptor antagonist CJ-11,974 in the control of cisplatin-induced emesis. *J. Clin. Oncol*. **1999**, *17*, 338.
192. Kramer, M.S.; Winokur, A.; Kelsey, J.; et al. Demonstration of the efficacy and safety of a novel substance P (NK-1) receptor antagonist in major depression. *Neuropsychopharmacology* **2004**, *29*, 385.
193. George, D.T.; Gilman, J.; Hersh, J.; et al. Neurokinin 1 receptor antagonism as a possible therapy for alcoholism. *Science* **2008**, *319*, 1536.
194. Monaco-Shawver, L.; Schwartz, L.; Tuluc, F.; et al. Substance P inhibits natural killer cell cytotoxicity through the neurokinin-1 receptor. *J. Leukoc. Biol*. **2011**, *89*, 113.
195. Manak, M.M.; Moshkoff, D.A.; Nguyen, L.T.; et al. Anti-HIV-1 activity of the neurokinin-1 receptor antagonist aprepitant and synergistic interactions with other antiretrovirals. *AIDS* **2010**, *24*, 2789.
196. Santini, D.; Vincenzi, B.; Guida, F.M.; et al. Aprepitant for management of severe pruritus related to biological cancer treatments: a pilot study. *Lancet Oncol*. **2012**, *13*, 1020.

197. Hill, R. NK1 (substance P) receptor antagonists - why are they not analgesic in humans? *Trends Pharmacol. Sci*. **2000**, *21*, 244.
198. Drugs used to treat Nausea/Vomiting Chemotherapy Induced. Dostęp online (02-03-2022): www.drugs.com/condition/nausea-vomiting-chemotherapy-induced.html
199. Jin, Y.; Wu, X.; Guan, Y.; et al. Efficacy and safety of aprepitant in the prevention of chemotherapy-induced nausea and vomiting: A pooled analysis. *Support. Care Cancer* **2012**, *20*, 1815.
200. Muñoz, M.; Coveñas, R. Safety of neurokinin-1 receptor antagonists. *Expert Opin. Drug Saf*. **2013**, *12*, 673.
201. Varty, G.B.; Cohen-Williams, M.E.; Morgan, C.A.; et al. The gerbil elevated plus-maze II: anxiolytic-like effects of selective neurokinin NK1 receptor antagonists. *Neuropsychopharmacology* **2002**, *27*, 371.
202. Harrison, T.; Williams, B.J.; Swain, C.J.; et al. Piperidine-ether based hNK1 antagonists 1: determination of the relative and absolute stereochemical requirements. *Bioorg. Med. Chem. Lett*. **1994**, *4*, 2545.
203. Varty, G.B.; Cohen-Williams, M.E.; Hunter, J.C. The antidepressant-like effects of neurokinin NK1 receptor antagonists in a gerbil tail suspension test. *Behav. Pharmacol*. **2003**, *14*, 873.
204. Rupniak, N.M.; Carlson, E.C.; Boyce, S.; et al. Enantioselective inhibition of the formalin paw late phase by the NK-1 receptor antagonist L-733,060 in gerbils. *Pain* **1996**, *67*, 189.
205. Castro-Obregón, S.; del Rio, G.; Chen, S.F.; et al. A ligand-receptor pair that triggers a non-apoptotic form of programmed cell death. *Cell Death Differ*. **2002**, *9*, 807.
206. Bang, R.; Biburger, M.; Neuhuber, W.L.; et al. Neurokinin-1 receptor antagonists protect mice from CD95- and tumor necrosis factor-alpha-mediated apoptotic liver damage. *J. Pharmacol. Exp. Ther*. **2004**, *308*, 1174.
207. Rittner, H.L.; Lux, C.; Labuz, D.; et al. Neurokinin-1 receptor antagonists inhibit the recruitment of opioid-containing leukocytes and impair peripheral antinociception. *Anesthesiology* **2007**, *107*, 1009.
208. Lang, K.; Drell, T.L.; Lindecke, A.; et al. Induction of a metastatogenic tumor cell type by neurotransmitters and its pharmacological inhibition by established drugs. *Int. J. Cancer*. **2004**, *112*, 231.
209. Zhang, H.; Kanduluru, A.K.; Desai, P.; et al. Synthesis and Evaluation of a Novel ^{64}Cu- and ^{67}Ga-Labeled Neurokinin 1 Receptor Antagonist for *in Vivo* Targeting of NK1R-Positive Tumor Xenografts. *Bioconjug. Chem.* **2018**, *29*, 1319.
210. Kanduluru, A.K.; Srinivasarao, M.; Wayua, C.; et al. Evaluation of a Neurokinin-1 Receptor–Targeted Technetium-99m Conjugate for Neuroendocrine Cancer Imaging. *Mol. Imaging Biol.* **2020**, *22*, 377.
211. MacLeod, A.M.; Merchant, K.J.; Cascieri, M.A.; et al. N-Acyl-L-tryptophan benzyl esters: potent substance P receptor antagonists. *J. Med. Chem.* **1993**, *36*, 2044.
212. Vergnano, A.M.; Salio, C.; Merighi, A. NK1 receptor activation leads to enhancement of inhibitory neurotransmission in spinal substantia gelatinosa neurons of mouse. *Pain* **2004**, *112*, 37.
213. Rahman, A.; Inoue, T.; Kamei, C. Role of substance P in allergic nasal symptoms in rats. *Eur. J. Pharmacol.* **2006**, *532*, 155.
214. Rahban, M.; Danyali, S.; Zaringhalam, J.; et al. Pharmacological blockade of neurokinin1 receptor restricts morphine-induced tolerance and hyperalgesia in the rat. *Scand. J. Pain* **2021**, *22*, 193.

215. Cascieri, M.A.; Ber, E.; Fong, T.M.; et al. Characterization of the binding and activity of a high affinity, pseudoirreversible morpholino tachykinin NK1 receptor antagonist. *Eur. J. Pharmacol*. **1997**, *325*, 253.
216. Product information. Emend (aprepitant). Merck, May 2003. Dostęp online (13-01-2022): www.merck.com/product/usa/pi_circulars/e/emend/emend_pi.pdf
217. Tattersall, F.D.; Rycroft, W.; Cumberbatch, M.; et al. The novel NK1 receptor antagonist MK-0869 (L-754,030) and its water soluble phosphoryl prodrug, L-758,298, inhibit acute and delayed cisplatin-induced emesis in ferrets. *Neuropharmacology* **2000**, *39*, 652.
218. Saito, H.; Yoshizawa, H.; Yoshimori, K.; et al. Efficacy and safety of single dose fosaprepitant in the prevention of chemotherapy-induced nausea and vomiting in patients receiving high-dose cisplatin: a multicentre, randomised, double-bind, placebo-controlled phase 3 trial. *Ann. Oncol*. **2013**, *24*, 1067.
219. Armstrong, D.M.; Pickel, V.M.; Joh, T.H.; et al. Immunocytochemical localization of catecholamine synthesizing enzymes and neuropeptides in the area postrema and medial nucleus tractus solitarius of rat brain. *J. Comp. Neurol*. **1981**, *196*, 505.
220. Majumdar, A.K.; Howard, L.; Goldberg, M.R.; et al. Pharmacokinetics of Aprepitant After Single and Multiple Oral Doses in Healthy Volunteers. *J. Clin. Pharmacol*. **2006**, *46*, 291.
221. Huskey, S.E.W.; Dean, B.J.; Doss, G.A.; et al. The metabolic disposition of aprepitant, a Substance P receptor antagonist, in rats and dogs. *Drug Metab. Dispos*. **2004**, *32*, 246.
222. Sanchez, R.I.; Wang, R.W.; Newton, D.J.; et al. Cytochrome P450 3A4 is the major enzyme involved in the metabolism of the substance P receptor antagonist aprepitant. *Drug Metab. Dispos*. **2004**, *32*, 1287.
223. Spitsin, S.; Tebas, P.; Barrett, J.S.; et al. Antiinflammatory effects of aprepitant coadministration with cART regimen containing ritonavir in HIV-infected adults. *JCI Insight* **2017**, *2*, e95893.
224. Liu, X.; Zhu, Y.; Zheng, W.; et al. Antagonism of NK-1R using aprepitant suppresses inflammatory response in rheumatoid arthritis fibroblast-like synoviocytes. *Artif. Cells Nanomed. Biotechnol*. **2019**, *47*, 1628.
225. Tebas, P.; Tuluc, F.; Barrett, J.S.; et al. A randomized, placebo controlled, double masked phase IB study evaluating the safety and antiviral activity of aprepitant, a neurokinin-1 receptor antagonist in HIV-1 infected adults. *PLoS One* **2011**, *6*, e24180.
226. Noronha, V.; Bhattacharjee, A.; Patil, V.M.; et al. Aprepitant for Cough Suppression in Advanced Lung Cancer: A Randomized Trial. *Chest* **2020**, *157*, 1647.
227. Zic, J.A.; Straka, B.T.; McGirt, L.Y.; et al. Aprepitant for the Treatment of Pruritus in Sézary Syndrome: A Randomized Crossover Clinical Trial. *JAMA Dermatol*. **2018**, *154*, 1221.
228. Kwatra, S.G.; Boozalis, E.; Huang, A.H.; et al. Proteomic and Phosphoproteomic Analysis Reveals that Neurokinin-1 Receptor (NK1R) Blockade with Aprepitant in Human Keratinocytes Activates a Distinct Subdomain of EGFR Signaling: Implications for the Anti-Pruritic Activity of NK1R Antagonists. *Medicines* **2019**, *6*, 114.
229. Reinhardt, R. Comparison of neurokinin-1 antagonist, L-745,030, to placebo, acetaminophen and ibuprofen in the dental pain model. *Clin. Pharmacol. Ther*. **1998**, *63*, 168.
230. Keller, M.; Montgomery, S.; Ball, W.; et al. Lack of efficacy of the substance p (neurokinin 1 receptor) antagonist aprepitant in the treatment of major depressive disorder. *Biol. Psychiatry* **2006**, *59*, 216.

231. Muñoz, M.; Crespo, J.C.; Crespo, J.P.; et al. Neurokinin-1 receptor antagonist aprepitant and radiotherapy, a successful combination therapy in a patient with lung cancer: A case report. *Mol. Clin. Oncol*. **2019**, *11*, 50.
232. Serafin, M.B.; Bottega, A.; da Rosa, T.F.; et al. Drug repositioning in oncology. *Am. J. Ther.* **2021**, *28*, e111.
233. Muñoz, M.; Gonzalez-Ortega, A.; Salinas-Martin, M.C.; et al. The neurokinin-1 receptor antagonist aprepitant is a promising candidate for the treatment of breast cancer. *Int. J. Oncol.* **2014**, *45*, 1658.
234. Bayati, S.; Bashash, D.; Ahmadian, S.; et al. Inhibition of tachykinin NK 1 receptor using aprepitant induces apoptotic cell death and G1 arrest through Akt/p53 axis in pre-B acute lymphoblastic leukemia cells. *Eur. J. Pharmacol*. **2016**, *791*, 274.
235. Ge, C.; Huang, H.; Huang, F.; et al. Neurokinin-1 receptor is an effective oxidative stress through mitochondrial calcium overload. *Proc. Natl. Acad. Sci. USA* **2019**, *116*, 19635.
236. Alfieri, A.B.; Cubeddu, L.X. Efectos de los antagonistas de los receptores NK1 y de la dexametasona sobre la inflamación neurogénica inducida por ciclofosfamida y por radiación X, en la rata. *Arch. Venez. Farmacol. Ter*. **2004**, *23*, 61.
237. Kast, R.E.; Ramiro, S.; Lladó, S.; et al. Antitumor action of temozolomide, ritonavir and aprepitant against human glioma cells. *J. Neurooncol*. **2016**, *126*, 425.
238. Bashash, D.; Safaroghli-Azar, A.; Bayati, S.; et al. Neurokinin-1 receptor (NK1R) inhibition sensitizes APL cells to anti-tumor effect of arsenic trioxide via restriction of NF-κB axis: Shedding new light on resistance to aprepitant. *Int. J. Biochem. Cell Biol*. **2018**, *103*, 105.
239. Robinson, P.; Kasembeli, M.; Bharadwaj, U.; et al. Substance P receptor signaling mediates doxorubicin-induced cardiomyocytes apoptosis and triple-negative breast cancer chemoresistance. *Biomed. Res. Int*. **2016**, *2016*, 1959270.
240. Henssen, A.G.; Odersky, A.; Szymansky, A.; et al. Targeting tachykinin receptors in neuroblastoma. *Oncotarget* **2017**, *8*, 430.
241. Wu, H.; Cheng, X.; Huang, F.; et al. Aprepitant sensitizes acute myeloid leukemia cells to the cytotoxic effects of cytosine arabinoside in vitro and in vivo. *Drug Des. Dev. Ther*. **2020**, *14*, 2413.
242. Un, H.; Ugan, R.A.; Kose, D.; et al. A novel effect of aprepitant: Protection for cisplatin-induced nephrotoxicity and hepatotoxicity. *Eur. J. Pharmacol*. **2020**, *880*, 173168.
243. Lee, M.; McCloskey, M.; Staples, S. Prolonged use of aprepitant in metastatic breast cancer and a reduction in CA153 tumour marker levels. *Int. J. Cancer Clin. Res*. **2016**, *3*, 071.
244. Halik, P.; Gniazdowska, E.; Koźmiński, P.; et al. In vitro NK1R affinity evaluation of novel radioconjugates based on peptide antagonist SPANTIDE I and Ga-68/Lu-177 theranostic like isotopes for glioma cancer. Podczas *Trends in Radiopharmaceuticals (ISTR-2019*). Materiały z międzynarodowego sympozjum. Program i streszczenia.
245. Spector, R.; Snodgrass, S.R.; Johanson, C.E. A balanced view of the cerebrospinal fluid composition and functions: Focus on adult humans. *Exp. Neurol*. **2015**, *273*, 57.